eIF2B bodies and their role in the integrated stress response

HODGSON, Rachel Elizabeth

eIF2B Bodies and their Role in the Integrated Stress Response

Rachel Elizabeth Hodgson

A thesis submitted in partial fulfilment of the requirements of Sheffield Hallam University for the degree of Doctor of Philosophy

June 2019

Candidate Declaration

I hereby declare that:

1. I have not been enrolled for another award of the University, or other academic or professional organisation, whilst undertaking my research degree.

2. None of the material contained in the thesis has been used in any other submission for an academic award.

3. I am aware of and understand the University's policy on plagiarism and certify that this thesis is my own work. The use of all published or other sources of material consulted have been properly and fully acknowledged.

4. The work undertaken towards the thesis has been conducted in accordance with the SHU Principles of Integrity in Research and the SHU Research Ethics Policy.

The word count of the thesis is 32,255

Name	Rachel Elizabeth Hodgson
Award	Doctor of Philosophy
Date of Submission	June 2019
Faculty	Health and Wellbeing
Director(s) of Studies	Dr Susan G. Campbell

Contents

List of Figures

Abbreviations

α	Alpha
β	Beta
δ	Delta
γ	Gamma
ε	Epsilon
µ	Micro (prefix)
AT	Acyl transferase
ATF4	Activating transcription factor 4
C. albicans	*Candida albicans*
CHOP	C/EBP homologous protein
CTPS	Cytidine triphosphate synthetase
dsRNA	Double-stranded RNA
eEF	Eukaryotic elongation factor
eIF	Eukaryotic initiation factor
ER	Endoplasmic reticulum
eRF	Eukaryotic release factor
FACs	Fluorescence-activated cell sorting
FRAP	Fluorescent recovery after photobleaching
G3BP	GTPase activating protein binding protein 1
GADD34	Growth arrest and DNA damage-inducible protein
GCN2	General amino acid control nonderepressible 2
GEF	Guanine nucleotide exchange factor

GS	Glutamine synthetase
GTP	Guanosine-5'-triphosphate
HRI	Heme-regulated inhibitor
ICC	Immunocytochemistry
IRES	internal ribosome entry sites
ISR	Integrated stress response
Met-tRNA$_i$	Methionylated initiator transfer RNA
mRNA	Messenger RNA
NT	Nucleotidyl transferases
PABP	Poly(A)-binding protein
P-bodies	Processing bodies
PERK	Protein kinase RNA-like endoplasmic reticulum kinase
Pi	Inorganic phosphate
PIC	Pre-initiation complex
PKR	Protein kinase R
RIPK1	Receptor-interacting serine/threonine-protein kinase 1
RNA	Ribonucleic acid
rRNA	Ribosomal ribonucleic acid
S. cerevisiae	*Saccharomyces cerevisiae*
S. pombe	*Schizosaccharomyces pombe*
SA	Sodium arsenite
SG	Stress granule
Tg	Thapsigargin

TIA1	T-cell intracellular antigen 1
uORF	Upstream open reading frame
UTR	Untranslated region
VWM	Vanishing white matter

Abstract

Eukaryotic initiation factor 2 (eIF2) is a G protein comprised of 3 subunits (α, β and γ) that is critical for translation. It is tightly regulated in the integrated stress response (ISR) via the phosphorylation of its α subunit following the induction of cellular stress. In its phosphorylated form eIF2α inhibits the guanine nucleotide exchange factor (GEF) eukaryotic initiation factor 2B (eIF2B), resulting in the attenuation of global protein synthesis. eIF2B is a multisubunit protein comprised of regulatory and catalytic subunits. The catalytic subunits are responsible for the GEF activity whereas the regulatory subunits mediate inhibition by phosphorylated eIF2α. Through studying the localisation of eIF2B subunits, cytoplasmic eIF2B bodies were identified in mammalian cells. A relationship between body size and the eIF2B subunits localising to them exists; larger bodies contain all subunits and smaller bodies contain predominantly catalytic subunits. eIF2 localises to eIF2B bodies and moves through these bodies in a manner that correlates with eIF2B GEF activity. Upon the induction of cellular stress phosphorylated eIF2α localises predominately to larger eIF2B bodies which contain regulatory subunits and a decrease in the movement of eIF2 through these bodies is observed. Interestingly, drugs that inhibit the ISR can rescue the movement of eIF2 through these eIF2B bodies, in a manner that correlates to cellular levels of phosphorylated eIF2α. In contrast, smaller eIF2B bodies, which contain predominately catalytic subunits, show increased movement of eIF2 during cellular stress. This increase in movement is accompanied by an increase in the localisation of eIF2Bδ to these bodies, suggesting the formation of a novel eIF2B subcomplex. This response is mimicked by ISR-inhibiting drugs, providing insight into their potential mechanisms of action. This study provides the first evidence that the composition and function of mammalian eIF2B bodies is regulated by the ISR and the drugs that control it.

Acknowledgements

I would like to take this opportunity to firstly thank my supervisor's Dr Susan Campbell and Dr Liz Allen, for the opportunity to work on this project. Your guidance and encouragement throughout the entirety of my PhD has been invaluable. It's been quite a journey and I am extremely grateful for all the support, thank you for always having an open door! I would also like to thank Dr Karl Norris for offering vast amounts of knowledge and for always being there to provide endless amounts of guidance, support and friendship.

I would like to thank the following people for their academic contributions. Prof. Mark Ashe and Prof. Graham Pavitt for their helpful discussions. Prof. Christine Le Maitre and Dr Lucy Crooks for their guidance on statistical analysis. Prof. David Ron for kindly gifting the CHO cells used in this thesis. Dr Noel Wortham for his advice on antibodies and for kindly gifting the pHM2Bε plasmid used in this thesis. Dr Nancy Kedersha for suggestions regarding antibodies.

I would like to give a special thanks and appreciation for all of those who have made working in the BMRC so enjoyable. I am grateful to all those who have given me help, advice, and motivation in the lab, but also for the friendship, great laughs and unforgettable memories outside of the lab.

Thank you to my friends and family for always supporting me.

I gratefully acknowledge the support for this work through a graduate teaching assistant PhD studentship from the Biomolecular sciences Research Centre at Sheffield Hallam University.

1. Introduction

1.1 General Introduction

Different cell types exhibit distinct gene expression profiles which are rapidly modulated in response to internal and external stimuli. Genes are transcribed into mRNA molecules in the nucleus and then transported to the cytoplasm where they are translated into proteins. The initiation step of translation is rate limiting and therefore modulation of this step provides a control point in gene expression. The protein eukaryotic initiation factor 2 (eIF2) in its active guanosine triphosphate (GTP) bound form is essential for translation initiation. Following subsequent rounds of translation eIF2B acts as a guanine nucleotide exchange factor (GEF) and is required to replenish eIF2-GTP within the cell (Panniers and Henshaw, 1983). Recognition of adverse stimuli by a number of cellular pathways can lead to the inhibition of eIF2B via a common pathway termed the integrated stress response (ISR). Tight control of eIF2B by the ISR is particularly important in allowing the cell to respond to adverse conditions that induce cellular stress.

In yeast eIF2B has been found to localise to cytoplasmic foci termed, eIF2B bodies (Campbell *et al*., 2005; Moon and Parker, 2018; Noree *et al*., 2010; Taylor *et al*., 2010). These foci appear to be sites of GEF activity that can be regulated by conditions of cellular stress (Campbell *et al*., 2005; Taylor *et al*., 2010). The localisation of eIF2B has not previously been investigated in mammalian cells. Mutations in mammalian eIF2B are causative of the neurodegenerative disease, leukoencephalopathy with vanishing white matter (VWM). The pathophysiology of VWM is unclear and therefore investigating the cellular localisation of eIF2B may provide a platform to better understand disease mechanisms. This thesis aims to characterise mammalian eIF2B localisation and explore the role of this localisation with respect to the ISR.

1.2 Translation

Eukaryotic genomes encode thousands of proteins and through the process of translation; the cell can rapidly control gene expression. Messenger RNA (mRNA) molecules are transcribed from genes and provide a template to synthesise a polypeptide chain complementary to the DNA sequence of the gene. The structure of a mRNA molecule is shown in Figure 1.1. Structurally the 5' end of a mRNA molecule encodes an untranslated region (5' UTR). The UTR serves as a ribosome binding site and can also contain upstream open reading frames (uORFs) for non-canonical methods of translation (Young and Wek, 2016). The far 5' nucleotide of the mRNA is bound to the mRNA by a triphosphate bond and methylated at position 7 (Shatkin, 1976). This nucleotide is referred to as the cap structure and is required for cap-dependent translation (Section 1.2.1.2.1). The coding sequence of the mRNA contains a number of codons that encode the amino-acid sequence for the protein and a start codon for the initiation of translation and a stop codon for termination. Following the coding region the mRNA has a 3' UTR which often contains binding sites for regulatory proteins (Barrett *et al*., 2012). A poly(A) tail (stretch of adenine bases) is added to the far 3' end of mature mRNA molecules, providing protection against degradation and also enhancing cap-dependent translation (Dreyfus and Régnier, 2002).

Through the process of translation mRNAs are selectively translated into proteins. Tight regulation of the translation pathway controls the cellular abundance of specific proteins to promote cellular homeostasis. Central to the process of translation is the ribosome. Ribosomes from all species consist of two subunits both of which are formed from numerous ribosomal proteins and ribosomal RNA molecules (Ramakrishnan, 2011). The complete 80S eukaryotic ribosome is formed from a smaller 40 S subunit, responsible for decoding the mRNA sequence and a larger 60 S subunit, which catalyses peptide bond formation (Doudna and Rath, 2002). The translation pathway can be divided into three stages: initiation, elongation and termination. During the initiation phase, the 80 S ribosome is assembled at the start codon of a target mRNA molecule, mediated by a number of eukaryotic initiation factors (eIFs) (Hinnebusch and Lorsch, 2012). During the elongation phase, the ribosome translocates each codon of the target mRNA molecule in turn (Doudna and Rath, 2002). Transfer ribonucleic acid (tRNA) molecules carrying amino acids selectively

interact with the ribosome through complementary binding of the tRNA anticodon and mRNA codons positioned within the ribosome (Dever and Green, 2012). The ribosome catalyses the formation of peptide bonds between the amino acids carried by the tRNAs (Doudna and Rath, 2002). As the ribosome translocates the mRNA a polypeptide chain is selectively synthesised. In the final step of translation, the termination step, the polypeptide chain is released from the ribosome and the translational machinery disassembles, ready to facilitate subsequent rounds of translation.

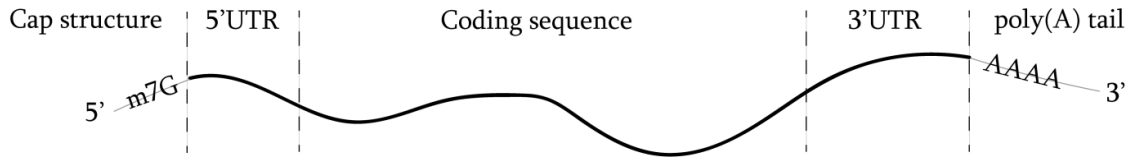

Figure 1.1 The structure of a mRNA molecule.
The sequence of a mRNA transcript can be divided into five sections. In a 5' to 3' direction these are: The cap structure, the 5' untranslated region (UTR), the coding sequence, the 3' UTR and the poly(A) tail. The coding sequence encodes a template for the amino acid sequence of a protein. The 5' and 3' UTR do not encode the protein sequence but are important for the regulation of the protein translation. The cap structure and the poly(A) tail protect the mRNA from degradation and facilitate its translation.

1.2.1 Translation initiation

The complex process by which ribosomes are recruited to the mRNA and the appropriate start codon is selected, is defined as translation initiation. In eukaryotes, the highly conserved heterotrimeric G-protein eIF2 is essential for this process. In its active GTP bound form, eIF2 binds to a methionyl initiator transfer RNA (Met-$tRNA_i$) molecule to form a ternary complex. The ternary complex is loaded onto the small (40S) ribosomal subunit facilitated by the binding of other eIFs, to form a 43S pre-initiation complex (PIC) (Hinnebusch and Lorsch, 2012). The PIC is recruited to the 5'-end of a target mRNA molecule, and scans the mRNA sequence for an appropriate start codon (Hinnebusch and Lorsch, 2012). During the scanning process, eIF2-GTP is hydrolysed, mediated by the GTPase-activating protein eIF5 (Huang *et al*., 1997). Upon start codon recognition eIF2-GDP is released in combination with eIF5, and the 60S ribosomal subunit interacts with the 40S ribosomal subunit. This initiation process generates a full 80S ribosome with an appropriately positioned Met-$tRNA_i$ at the start codon of a mRNA ready to enter the translation elongation phase (Hinnebusch and Lorsch, 2012).

1.2.1.1 Formation of the 43 S Preinitiation complex

In the first step of translation initiation, a ternary complex comprised of eIF2-GTP and a Met-$tRNA_i$ is loaded onto the 40 S ribosomal subunit to form a 43 S PIC (Hinnebusch and Lorsch, 2012). In its GTP-bound form, eIF2 has high affinity for Met-$tRNA_i$ and interacts to form the ternary complex (Erickson and Hannig, 1996; Kapp and Lorsch, 2004; Levin *et al*., 1973; Safer *et al*., 1975). eIF2 is comprised of three non-identical subunits, α, β and γ. The γ subunit of eIF2 binds the Met-$tRNA_i$ and the α and β subunits appear to stabilise this interaction (Naveau *et al*., 2010; Nika *et al*., 2001; Yatime *et al*., 2004).

The loading of the ternary complex onto the 40 S ribosomal subunit is facilitated by eIFs 1, 1A, 3 and 5. eIF1 and 1A induce a conformational change in the 40 S ribosomal subunit which promotes the association of the ternary complex (Passmore *et al*., 2007). Binding of eIF1 to the 40 S ribosomal subunit requires the presence of eIF3, and additionally binding of eIF1A to the 40 S ribosomal subunit requires the presence of both eIF1 and eIF3 (Majumdar *et al*., 2003). eIF5 has a role bridging the interaction between eIF2 and eIF3 (Asano *et al*., 2000). Interestingly, eIF1, 2, 3 and 5 have been

shown to form a stable multifactorial complex (MFC) complex in yeast (Asano *et al*., 2000) and more recently in mammalian cells (Sokabe *et al*., 2012). The rate in which the Met-tRNA$_i$ is delivered to the 40 S ribosomal subunit is independent of whether it is complexed with eIF2-GTP alone as a ternary complex (which interacts with eIF1, 3 and 5 already bound to the 40 S subunit) or in combination with eIF1, 3 and 5 as a MFC (Sokabe *et al*., 2012). The role of the MFC in the initiation of translation therefore appears to be of little significance for the formation of the 43 S PIC. Recent data has suggested the MFC may have a more apparent role in the assembly of the 80 S ribosome complex through promoting eIF2 release from the Met-tRNA$_i$ (Sokabe *et al*., 2012).

1.2.1.2 mRNA recruitment and scanning

1.2.1.2.1 Cap-dependent initiation

The 43 S PIC is loaded onto the 5' end of a target mRNA molecule facilitated by the cap complex, eIF4F, formed of eIF4E, eIF4A and eIF4G (Figure 1.2). The attachment of the ribosome is impeded by secondary structures in the mRNA 5' UTR. In order to facilitate the 43 S PIC binding to mRNAs with structured 5' UTRs, eIF4A exerts helicase activity to produce a single stranded binding site near the 5' cap of the mRNA (Rogers *et al*., 1999). eIF4A lacks RNA-binding domains and only weakly interacts with single stranded mRNA (Lorsch and Herschlag, 1998). eIF4E however can recognise and interact with the mRNA cap structure, and is responsible for recruiting eIF4A to the 5' UTR of the target mRNA (Rogers *et al*., 2001). This interaction of eIF4E with the mRNA cap is enhanced by eIF4G (Gross *et al*., 2003), which also acts as a scaffold protein orientating eIF4A in the correct position to unwind the mRNA structure (Hilbert *et al*., 2011; Oberer *et al*., 2005; Schutz *et al*., 2008). eIF4G also stabilises the binding of the 43 S PIC on to the mRNA molecule through interactions with eIF3 (Villa *et al*., 2013). Additionally, eIF4G can interact with the poly(A)-binding protein (PABP) present at the 3' end of a mRNA molecule (Tarun and Sachs, 1996) to produce a closed loop structure that is thought to enhance translation efficiency and ribosome re-initiation (Michel *et al*., 2000; Wells *et al*., 1998).

Once bound the 43 S PIC complex scans the mRNA in a 5' to 3' direction until a start codon is detected through complementarity to the anticodon of the Met-tRNA$_i$ (Figure

1.2). eIF1 and eIF1A promote a scanning-competent conformation of the 40 S ribosomal subunit (Passmore *et al*., 2007) and ATP-dependent helicase activity of eIF4A melts secondary structures of the mRNA allowing the 43 S PIC to translocate along it. The requirement of eIF4A is proportional to the degree of secondary structure (Jackson, 1991; Svitkin *et al*., 2001), and for moderately structured mRNA molecules eIF4B is required as a co-factor of eIF4A to stimulate its helicase activity (Dmitriev *et al*., 2003; Özeş *et al*., 2011; Rozovsky *et al*., 2008). In the case of highly stable secondary structures the helicase activity of eIF4A is not sufficient and the helicase DHX29 is required (Pisareva *et al*., 2008).

1.2.1.2.2 Cap-independent initiation

Although 95 % of mRNAs are translated via cap-dependent initiation (Merrick, 2004), cap-independent initiation also occurs in eukaryotic cells. Cap-independent initiation bypasses the requirement for cap-dependent ribosome scanning. It relies on the presence of internal ribosome entry sites (IRES) in the mRNA sequence that allow for the direct recruitment of the 40 S ribosome subunit to the vicinity of the start codon (Van Eden *et al*., 2004). The involvement of eIFs in cap-independent initiation varies between mRNA transcripts and it is believed that the secondary structures of IRES can facilitate interactions between the mRNA and the translational apparatus (Pisarev *et al*., 2005).

1.2.1.3 Start codon selection and 80 S ribosome assembly

The 43 S PIC scans the mRNA until a start codon, most commonly AUG, is detected through complementary binding of the Met-tRNA$_i$ anticodon (Figure 1.2). The α subunit of eIF2 and the 18 S ribosomal RNA (rRNA) component of the small 40 S ribosomal subunit, interact with specific nucleotides surrounding the start codon, increasing the efficiency for selection of start codons in optimal context (Kozak, 1986; Pisarev *et al*., 2006). During ribosome scanning eIF2-GTP is hydrolysed, promoted by the GTPase-activator protein eIF5 (Huang *et al*., 1997). The subsequent GDP and inorganic phosphate (Pi) molecules are not released from eIF2 keeping it in a scanning-competent conformation. Upon start codon selection, the 43 S PIC undergoes a large conformational change, eIF5 promotes the displacement of eIF1 (Algire *et al*., 2005; Maag *et al*., 2005; Nanda *et al*., 2009) and subsequently the Pi molecule from eIF2 is

released (Algire *et al*., 2005) (Figure 1.2). The conformation adopted by the 43 S PIC triggers scanning arrest. In its GDP-bound form eIF2 has reduced affinity for the Met-$tRNA_i$ (Erickson and Hannig, 1996; Kashiwagi *et al*., 2019) and this affinity is further reduced by the association of the PIC components eIF5 and eIF3 (Sokabe *et al*., 2012). eIF2-GDP is released from the 43 S PIC in complex with eIF5 (Algire *et al*., 2005; Singh *et al*., 2006), allowing for eIF5B-GTP to bind (Figure 1.2). eIF5B-GTP interacts with eIF1A (Marintchev *et al*., 2003) recruiting it to the 40 S ribosomal subunit where it accelerates the joining of the 60 S ribosomal subunit, stimulating the release of eIF1 and eIF3 (Unbehaun *et al*., 2004) and forming the complete 80 S ribosomal complex (Acker *et al*., 2006) (Figure 1.2). eIF5B hydrolyses GTP to induce a conformational change which is accompanied by the release of eIF5B and eIF1A (Figure 1.2), positioning the 80 S ribosomal subunit ready for translation elongation (Fringer *et al*., 2007).

1.2.1.4 Recycling of eIF2-GTP

In order for subsequent rounds of translation initiation to occur within the cell, eIF2-GTP must be replenished. eIF2 has a higher affinity for GDP (Erickson and Hannig, 1996), and thus the GEF, eukaryotic initiation factor 2B (eIF2B), is required for the recycling of eIF2-GDP to its GTP bound form (Figure 1.2). In yeast eIF2B acts as a dual functioning protein (Jennings *et al*., 2013). eIF2-GDP is released from the 43 S PIC in complex with eIF5, which functions as a GDP dissociation inhibitor (GDI) (Jennings and Pavitt, 2010). eIF2B acts as a GDI displacement factor (GDF) to release eIF2-GDP from eIF5 (Jennings *et al*., 2013), prior to performing its GEF activity. In mammalian cells the role of eIF2B as a GDF has not currently been evaluated however unlike in yeast, mammalian eIF5 does not appear to have GDI activity (Sokabe *et al*., 2012). The GEF activity of eIF2B is tightly regulated within the cell. The structure and role of eIF2B will be further reviewed in Section 1.4.

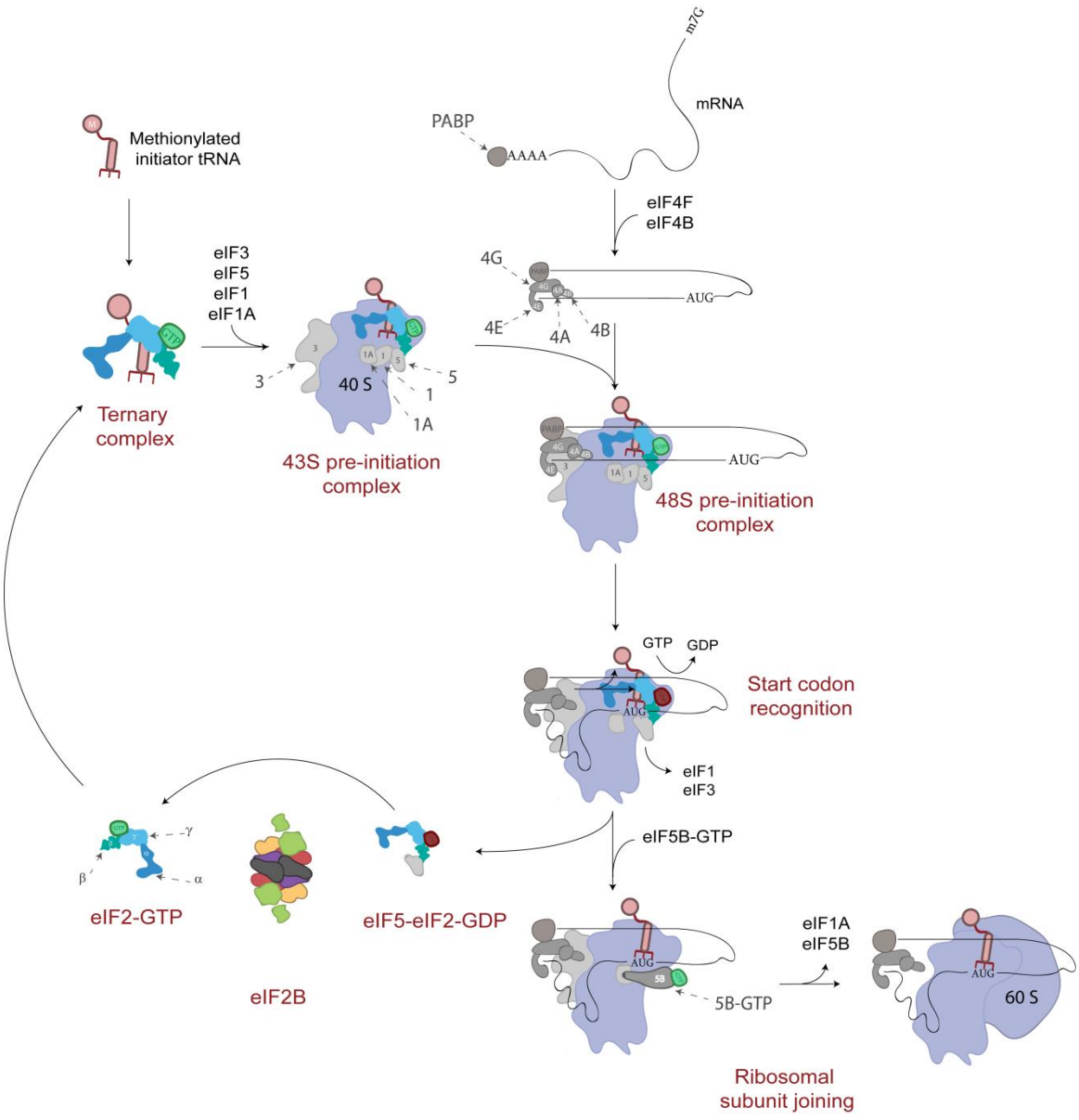

Figure 1.2 Translation initiation pathway.
A ternary complex formed of eIF2-GTP and a methionylated initiator tRNA, is recruited to the 40S ribosomal subunit by various eIFs to form a 43 S PIC. Facilitated by other eIFs, the 43 S PIC is loaded onto a target mRNA molecule and scans the mRNA sequence for a start codon. Upon recognition of a start codon, eIF2-GTP is hydrolysed and released in complex with eIF5. eIF5B accommodates the binding of the 60S ribosomal subunit to the 40S subunit forming the elongation ready 80S ribosome. eIF2-GDP-eIF5 is recycled to eIF2-GTP by eIF2B.

1.2.2 Translation elongation

During the elongation phase of translation, a nascent polypeptide chain complementary to the mRNA coding sequence is synthesised. This reaction is catalysed by the 80 S ribosome. Through a series of conformational changes mediated by eukaryotic elongation factors (eEFs), the 80 S ribosome facilitates the sequential joining of each amino acid in the chain. The process of translation elongation is highly conserved between eukaryotes and bacteria and mechanistic insights to this process have been largely generated in bacterial systems (Rodnina and Wintermeyer, 2009).

The 80S ribosome has three tRNA-binding sites, the A-site, the P-site and the E-site (Ben-Shem *et al*., 2011). Following translation initiation the 80S ribosome is positioned with the Met-tRNA$_i$ located in the P-site, stabilised through complementary binding of its anticodon to the start codon (Figure 1.3). In the first step of elongation, termed decoding, the ribosome selects a tRNA with an anticodon that is complementary to the second codon in the open reading frame which resides in the A site of the ribosome. The eukaryotic elongation factor 1A (eEF1A), in its GTP-bound form, delivers the aminoacyl-tRNA to the ribosomal A-site. Upon complementary base pairing of an aminoacyl-tRNA anticodon and the mRNA codon, eEF1A is hydrolysed, releasing the factor and depositing the aminoacyl-tRNA in the A-site (Figure 1.3) (Dever and Green, 2012). The peptidyl transferase centre of the large ribosomal subunit catalyses the rapid formation of a peptide bond between this aminoacyl-tRNA and the aminoacyl-tRNA located in the P-site of the ribosome (Beringer and Rodnina, 2007), transferring the growing peptidyl chain onto the A-site of the ribosome and leaving the deaminoacylated-tRNA in the P-site (Figure 1.3). The ribosome then undergoes a conformational rearrangement, rotating both subunits (Frank and Agrawal, 2000; Zhang *et al*., 2009), positioning the acceptor ends of the tRNA molecules currently located in the P-site and the A-site of the ribosome to the E-site and P-site respectively (Moazed and Noller, 1989; Munro *et al*., 2007). eEF2 in its GTP-bound form is responsible for stabilising this rotated conformation (Agirrezabala *et al*., 2008) (Figure 1.3). Through its hydrolysis, eEF2 promotes the translocation of the mRNA, positioning the third codon of the open reading frame in the A-site and the first and second codons accompanied by the bound tRNAs to the E-site and P-site respectively (Figure 1.3) (Ratje *et al*., 2010). The ribosome subunits then rotate back to their original

conformation (Gao *et al.,* 2009) ready for the next cycle of elongation. Through repetition of this process a polypeptide chain complementary to the mRNA coding sequence is synthesised.

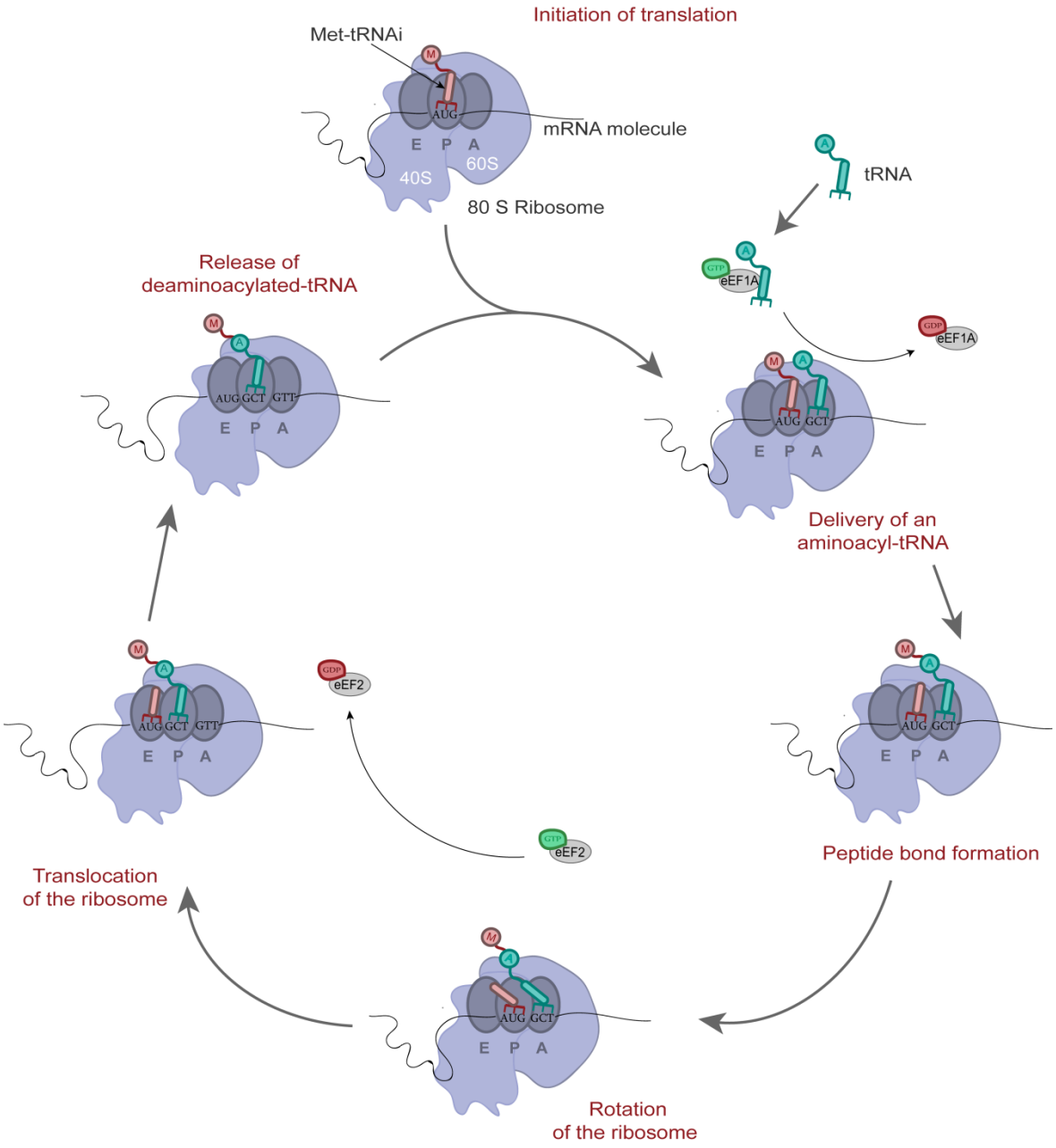

Figure 1.3 Translation elongation pathway.
Following translation initiation the Met-tRNA$_i$ is positioned in the ribosomal P site. eEF1A-GTP delivers a tRNA carrying a specific amino acid to the ribosomal A site where it binds through complementary binding of the tRNA anticodon to the mRNA codon. The 60S ribosomal subunit catalyses the formation of a peptide bond between the amino acid held in the P site and the A site. eEF2-GTP stimulates the translocation of the ribosome along the mRNA positioning the next codon of the mRNA sequence into the ribosomal A site. The tRNA is released from the E site and the process repeats until a stop codon is reached.

1.2.3 Translation termination and ribosome recycling

The ribosome continues to translocate along the mRNA catalysing the formation of the polypeptide chain until a stop codon, UAA, UGA, or UAG, enters the A site (Capone *et al*., 1986). Recognition of a stop codon triggers the release of the polypeptide chain and recycling of the ribosome for subsequent rounds of translation in a process mediated by the eukaryotic release factors (eRF), eRF1 and eEF3 (Zhouravleva *et al*., 1995).

eRF1 binds to eRF3-GTP and acts as a GTP dissociation inhibitor (Pisarev *et al*., 2006). eRF3 directs eRF1 to the ribosome (Bertram *et al*., 2000), and interaction with the ribosome promotes the hydrolysis of eRF3-GTP (Frolova *et al*., 1996). Hydrolysis of eRF3 induces conformational changes in eRF1, positioning eRF1 in the peptidyl transferase centre of the ribosome, coupling stop codon recognition and peptide release (Alkalaeva *et al*., 2006; Fan-Minogue *et al*., 2008). Once the completed polypeptide chain has been released, the 80S ribosome must dissociate from eRF1 (Pisarev *et al*., 2007), the mRNA and the de-acylated tRNA in order to initiate translation of other mRNA molecules. In some cases the ribosome may only partially dissociate, allowing for re-initiation of translation on the same mRNA transcript. This process relies upon the binding of eIF4F and PABP during initiation to bring the 5' and 3' ends of a mRNA into close proximity (Tarun and Sachs, 1996), and occurs most commonly for transcripts that contain short open reading frames upstream of the main coding sequence (Gunišová *et al*., 2018).

eRF1 and eRF3 have been shown to promote ribosomal subunit dissociation, however this occurs at a slow rate and is not sufficient to account for the rate at which a cell can reinitiate translation (Shoemaker *et al*., 2010). Translation initiation factors can mediate the recycling of the ribosome at specific concentrations of Mg^{2+} (Pisarev *et al*., 2007). Binding of eIF3 to the 40S ribosomal subunit promotes disassembly into the 60S subunit and the 40S subunit bound to the mRNA and de-acylated tRNA (Siridechadilok *et al*., 2005). eIF1 then induces release of the de-acylated tRNA, followed by eIF3 mediated dissociation of the mRNA (Pisarev *et al*., 2010). More recently the protein ABCE1 was identified to promote ribosome recycling and is important for facilitating the process in a wider range of Mg^{2+} concentrations (Barthelme *et al*., 2011; Pisarev *et al*., 2010).

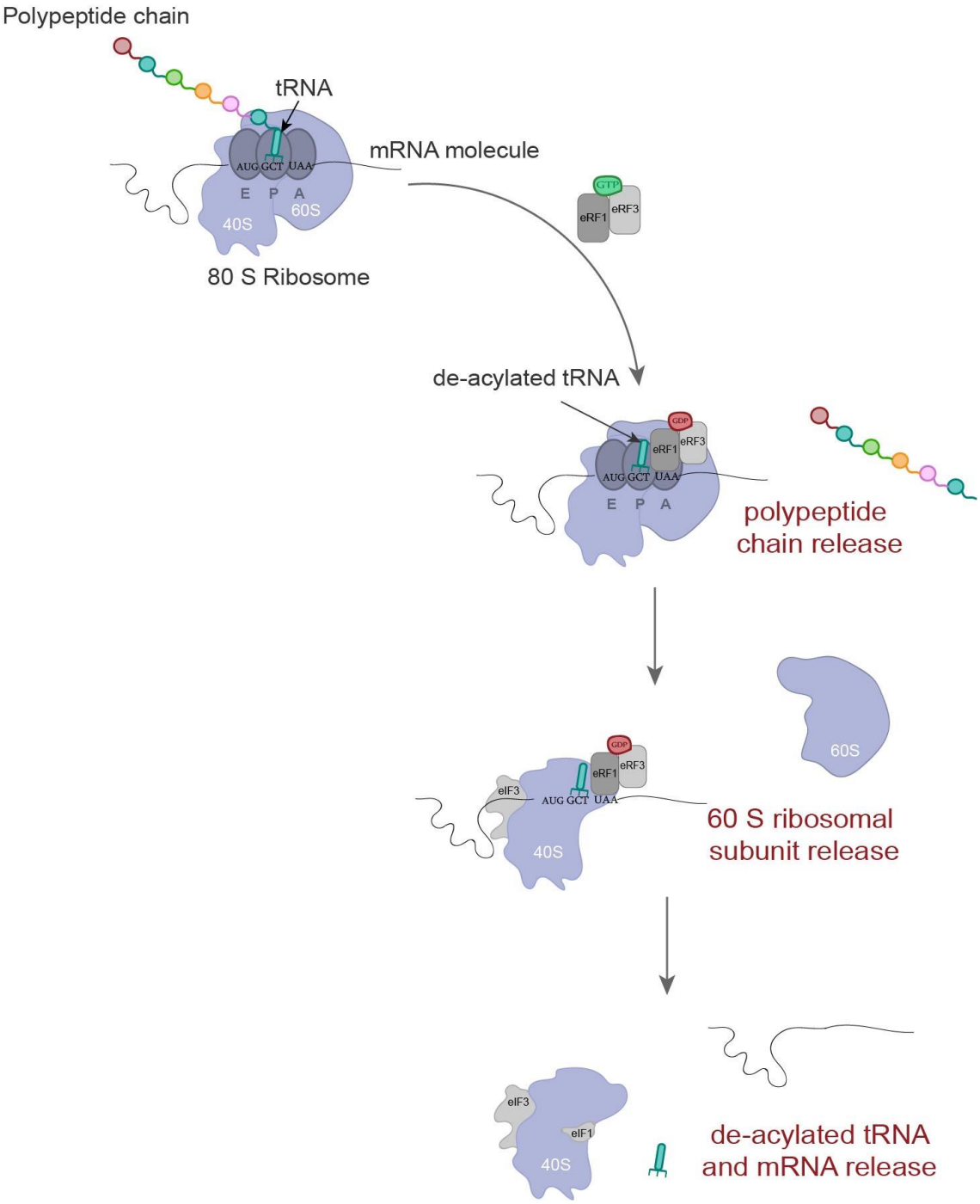

Figure 1.4 Translation termination and ribosome recycling pathway.
The presence of a stop codon in the ribosomal A site triggers termination of translation. eRF3-GTP directs eRF1 to the ribosomal A site. eRF3-GTP hydrolysis stimulates binding of eRF1 to the stop codon and subsequent release of the polypeptide chain. eIF3 binds the 40S ribosomal subunit and mediates the release of the 60S ribosomal subunit. eIF1 then mediates the release of the mRNA and tRNA molecule freeing the 40S ribosomal subunit.

1.3 Regulation of translation initiation during cellular stress

The process of translation involves a significant amount of cellular energy and therefore tight regulation is crucial in response to adverse cellular conditions. The cell must establish an impeccable balance between energy conservation and the synthesis of stress responsive proteins in order to restore cellular homeostasis. There are a number of pathways through which the cell can regulate translation initiation during cellular stress including, eIF4E-BP dephosphorylation (Patel *et al*., 2002) and eIF4G cleavage (Gradi *et al*., 1998; Svitkin *et al*., 1999). However, one of the best studied and most diverse mechanisms of translational control in response to cellular stress is the ISR; a series of stress sensing pathways that regulate translation through the common mechanism of eIF2 phosphorylation.

1.3.1 The integrated stress response

eIF2 plays a pivotal role in the initiation of translation and therefore serves as an important target for regulation. The core event of the ISR is the phosphorylation of eIF2α at serine residue 51 by stress-responsive eIF2α kinases, which leads to the inhibition of eIF2B. Once inhibited eIF2B cannot replenish eIF2-GTP within the cell and global translation is attenuated. Paradoxically, the translation of a number of stress-responsive proteins is upregulated, conserving energy and favouring homeostatic reprogramming.

1.3.1.1 Activation of the ISR and attenuation of global protein synthesis

Through control of the guanine nucleotide status of eIF2, global translation levels can be manipulated as part of the ISR. Under normal cellular conditions, in its GTP-bound form, eIF2 forms a ternary complex with a Met-tRNA$_i$. The ternary complex facilitates the delivery of the Met-tRNA$_i$ to the ribosome, and assists ribosomal translocation to an appropriate start codon, where complementary binding of the Met-tRNA$_i$ anticodon initiates translation. eIF2 is released in its inactive GDP-bound form, in combination with another initiator factor, eIF5. In order for subsequent rounds of translation to occur eIF2 must be released from eIF5 and replenished in its active GTP-bound form. This reaction is catalysed by eIF2B and therefore eIF2B provides a critical controlled point in the translation initiation pathway. A more detailed description of translation initiation can be found in Section 1.2.1. In response to various cellular stress stimuli,

stress-sensing pathways become activated and promote the induction of the ISR through the common down-stream mechanism of eIF2α phosphorylation (Brostrom and Brostrom, 1998; Dever *et al*., 1992). In its phosphorylated form eIF2 becomes a competitive inhibitor of eIF2B activity (Dever *et al*., 1995; Rowlands *et al*., 1988); subsequently levels of eIF2-GTP are depleted within the cell, leading to a global attenuation of protein synthesis (Figure 1.5). The precise mechanism of eIF2B inhibition by phosphorylated eIF2α is discussed in Section 1.4.3.1.

In yeast a single eIF2α kinase, GCN2 (general amino acid control nonderepressible 2), is responsible for phosphorylating eIF2α and inducing the ISR in response to amino acid deprivation in order to reduce the cellular demand for amino acids (Vazquez de Aldana *et al*., 1994) (Figure 1.5). GCN2 is highly conserved from yeast to mammalian cells (Castilho *et al*., 2014), however in mammalian cells three additional eIF2α kinases which phosphorylate the same single serine residue of eIF2α exist (Donnelly *et al*., 2013). These kinases are termed: PKR (protein kinase R), PERK (protein kinase RNA-like endoplasmic reticulum kinase), and HRI (heme-regulated inhibitor) (Castilho *et al*., 2014) (Figure 1.5). The mammalian eIF2α kinases share extensive homology in their catalytic domains, which contain a dimerization interface, crucial for kinase activation and catalytic function. Each kinase however harbours a unique regulatory domain that allows for activation of the ISR by a range of cellular stresses (Berlanga *et al*., 1998; Chen *et al*., 1991; Harding *et al*., 1999; Meurs *et al*., 1990; Shi *et al*., 1998). PKR is activated mainly by double-stranded RNA (dsRNA) during viral infection and promotes survival by reducing the translation of viral mRNAs (Clemens and Elia, 1997; Lemaire *et al*., 2008). PERK is principally activated in response to endoplasmic reticulum (ER) stress, commonly caused by the accumulation of unfolded proteins in the ER. PERK activation alleviates this stress by decreasing the level of proteins localising to the ER (Harding *et al*., 2000; Patil and Walter, 2001). Unlike the other kinase molecules which are globally expressed, HRI is predominately expressed in erythroid cells and protects the cell against toxic globin aggregates. When heme is unavailable to form hemoglobin, HRI mediates the downregulation of protein synthesis, decreasing the translation of globin and preventing the formation of toxic globin aggregates (Han 2001, Lu 2001). HRI has also been shown to be activated in non-erythroid cells in

response to arsenite induced oxidative stress and is required to promote cellular recovery through ISR signalling (McEwen *et al*., 2005).

In addition to natural stimuli, the ISR can be induced chemically. Two chemicals commonly used to induce the ISR for experimental studies are Thapsigargin (Tg) and sodium arsenite (SA) (Figure 1.5). Tg is a potent inducer of ER stress, it inhibits the sarcoplasmic/ER Ca^{2+} ATPase (SERCA) causing a decrease in ER calcium levels. Depleted calcium levels within the ER leads to the inactivation of calcium-dependent chaperones required for protein folding (Hebert and Molinari, 2007; Oslowski and Urano, 2011). The accumulation of misfolded proteins in the ER results in the activation of the eIF2α kinase, PERK. SA is a potent inducer of oxidative stress. Treatment of cells with SA increases intracellular levels of reactive oxygen species (ROS) (Chen *et al*., 1998). Increased levels of intracellular ROS result in the activation of the eIF2α kinase HRI (Han *et al*., 2001; McEwen *et al*., 2005).

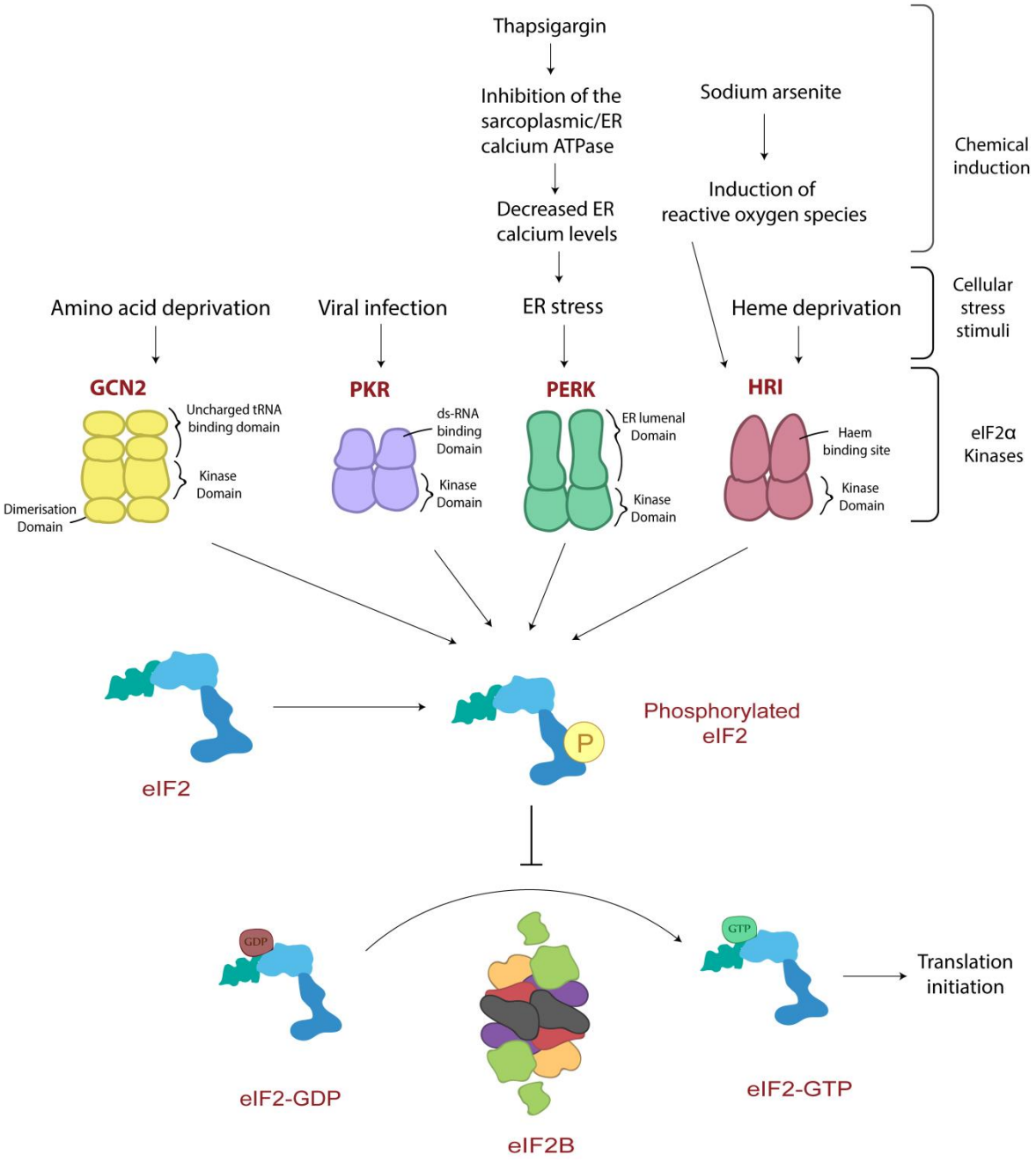

Figure 1.5 Activation of the ISR pathway.
In response to various cellular stress stimuli eIF2α kinase molecules are activated through dimerization. eIF2α kinase molecules phosphorylate the α subunit of eIF2. In its phosphorylated form, eIF2 is a competitive inhibitor of eIF2B activity preventing replenishment of eIF2-GTP within the cell and inhibiting translation initiation.

1.3.1.1.1 Formation of stress granules

Decreased levels of cellular eIF2-GTP leads to the formation of eIF2-GTP-deficient, and therefore non-productive preinitiation complexes. In the absence of productive preinitiation complexes, fewer ribosomes are loaded onto mRNA transcripts and as elongating ribosomes reach stop codons, global translation is down-regulated. Stalled complexes of mRNA molecules bound by non-productive preinitiation complexes can be recruited to large cytoplasmic granules, termed stress granules (SG) (Figure 1.6) (Kedersha *et al*., 1999; Kimball *et al*., 2003). In mammalian cells, SG assembly is mediated by RNA binding proteins including T-cell intracellular antigen 1 (TIA1), and GTPase activating protein binding protein 1 (G3BP) (Kedersha *et al*., 1999; Kimball *et al*., 2003). Through self-aggregation (Gilks *et al*., 2004; Tourrière *et al*., 2003), these RNA binding proteins promote the formation of a stable core structure containing mRNAs and non-productive preinitiation complexes, in addition to other proteins (Jain *et al*., 2016) . Recent evidence suggests that RNA-RNA interactions also promote the assembly of these core structures and contribute to their stability (Treeck *et al*., 2018). These core structures become rapidly surrounded by a more dynamic shell, formed through interactions of intrinsically disordered regions of RNA binding proteins (Jain *et al*., 2016). Studies have shown that SG components can rapidly shuttle through SGs, and it is suggested that the shell provides a scaffold for this dynamic exchange, with the transition of components between the core and shell modulated by numerous protein and RNA remodelling complexes (Buchan, 2014; Jain *et al*., 2016; Kedersha *et al*., 2000). It is currently believed that SGs provide a hub in which mRNAs can be sorted and then stored for translational re-initiation upon restoration of cellular homeostasis or instead be directed for decay (Anderson and Kedersha, 2006; Jain *et al*., 2016).

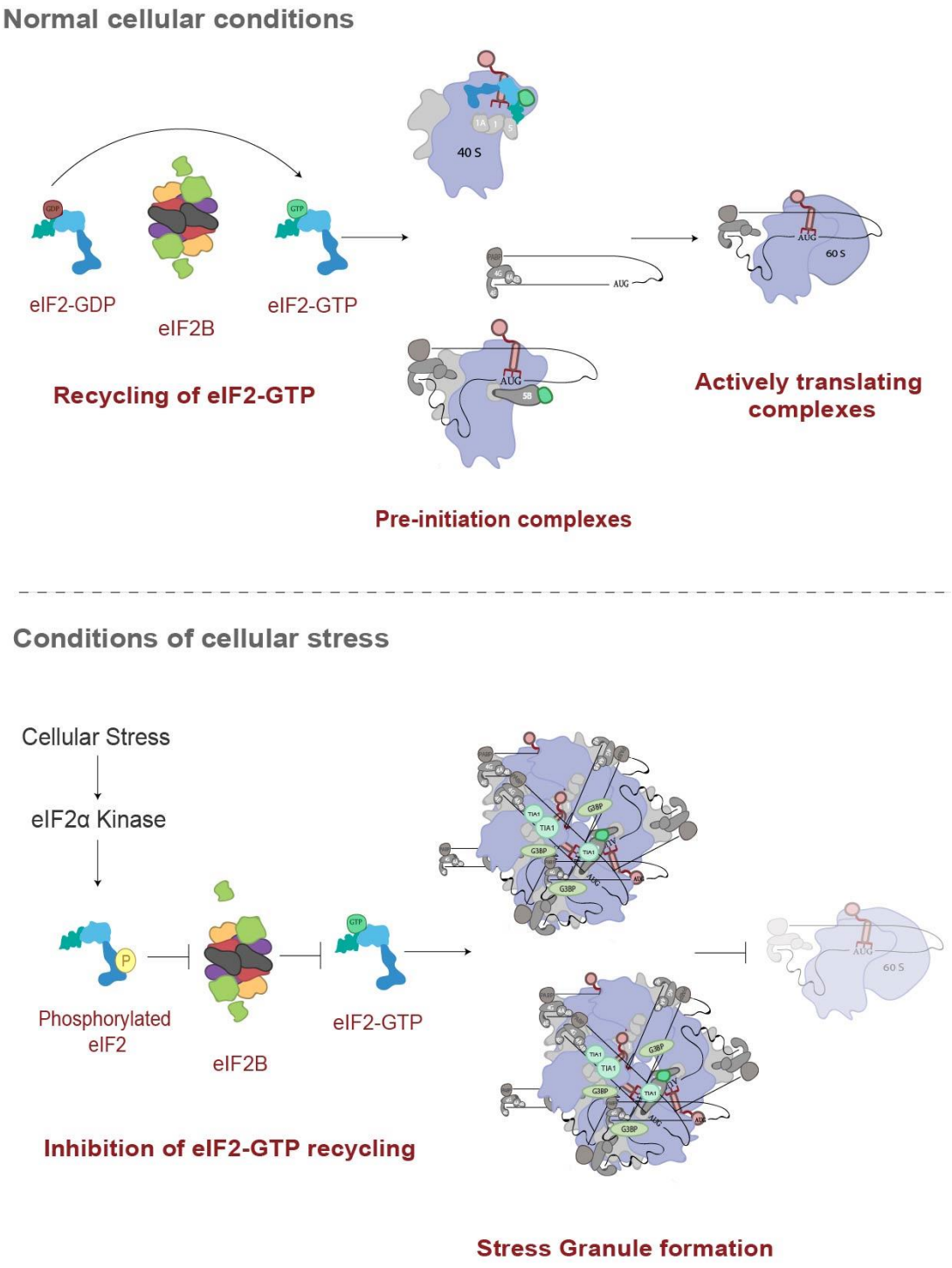

Figure 1.6 Stress granule formation pathway.
Under normal cellular conditions eIF2B recycles eIF2-GDP into its GTP-bound form. eIF2-GTP along with a number of other eIFs form pre-initiation complexes with target mRNA molecules and the 40S ribosomal subunit. Translation of these pre-initiation complexes is initiated through hydrolysis of eIF2-GTP which promotes binding of the large ribosomal subunit. In response to conditions of cellular stress, eIF2 is phosphorylated and becomes a competitive inhibitor of eIF2B activity, preventing eIF2-GTP recycling. Pre-initiation complexes form in the absence of eIF2-GTP. Joining of the large ribosome subunit is thus less favourable and translation becomes stalled. RNA binding proteins including G3BP and TIA1 mediate the aggregation of stalled pre-initiation complexes to form SGs.

1.3.1.2 Cellular recovery signalling

The length and severity of ISR induction determine the fate of a cell. During episodes of acute or short lived cellular stress, the ISR promotes cellular recovery signalling. However, in cases of severe or long lived cellular stress, where ISR signalling is unable to restore cellular homeostasis, the ISR can induce cell death signalling (Rutkowski *et al*., 2006). In addition to the down-regulation of global protein synthesis, the ISR induces translational up-regulation of specific mRNAs which mediate these signalling pathways. The translation of these mRNAs is most commonly regulated by the presence of upstream open reading frames (uORFs) in their 5' UTR. uORFs are generally inhibitory for the translation of a mRNA transcript under normal cellular conditions, however during episodes of cellular stress, they can promote the translation of a mRNA. Under normal cellular conditions the circularisation of a mRNA through interactions between eIF4F and PABP promotes re-initiation of the scanning ribosome. Upon stop codon recognition, the 60S ribosome dissociates whereas the 40S ribosome remains associated. Binding of a ternary complex to the scanning 40S ribosome allows for consecutive rounds of translation of the mRNA transcript. When ternary complexes are present in abundance, translation is initiated at uORFs, however when ternary complex levels are depleted, the scanning ribosome is unlikely to bind a ternary complex by the time it reaches a uORF. As the ribosome will continue to scan the transcript until a ternary complex joins, it is more likely the ribosome will bypass any uORFs and initiate translation at the coding ORF, in a process termed leaky scanning, as shown in Figure 1.7. *GCN4* in yeast was the first mRNA shown to be regulated by the ISR through the presence of uORFs (Mueller and Hinnebusch, 1986). Although there is no *GCN4* ortholog in mammalian cells, the best characterised mRNA regulated via this mechanism is the transcription factor Activating transcription factor 4 (*ATF4*). *ATF4* mRNA is ubiquitously expressed; however under normal cellular conditions protein levels are low (Harding *et al*., 2000; Vallejo *et al*., 1993). The human *ATF4* mRNA contains three uORFs (Harding *et al*., 2000) (Figure 1.7). Under normal cellular conditions, the first two uORFs which encode short polypeptides (3 amino acids and 12 amino acids in length respectively) are translated (Ameri and Harris, 2008). The up-stream uORFs in mammalian *ATF4* act as re-initiation uORFs; upon stop codon recognition, the 60S ribosome dissociates whereas the 40S ribosome remains

associated. When ternary complexes are readily available, the scanning 40 S ribosome acquires a new ternary complex in sufficient time to reinitiate translation at the next uORF. The final uORF sequence overlaps with the coding sequence of ATF4 in an out-of-frame manner and therefore the translation of uORF3 inhibits the translation of ATF4 (Figure 1.7) (Lu *et al*., 2004b; Vattem and Wek, 2004).

ATF4 can activate pro-survival mechanisms within the cell through a number of different pathways. Both PERK and GCN2 induced phosphorylation of eIF2α have been shown to induce ATF4 mediated autophagy (B'chir *et al*., 2013). Autophagy is a highly conserved cellular process that serves to recycle cytoplasmic materials in order to maintain cellular energy levels, metabolism and levels of amino acids (Mizushima and Komatsu, 2011). Additionally, PERK induced ATF4 signalling can alleviate ER stress that has been induced by the accumulation of unfolded proteins in the ER. ATF4 signalling activates two distinct signalling pathways, mediated by ATF6 and IRE1. ATF6 increases the ER protein folding capacity whereas IRE1 induces mRNA decay factors, reducing the protein folding load (Ron and Walter, 2011). If ISR signalling leads to the restoration of cellular homeostasis, ATF4-mediated activation of the transcription factor C/EBP homologous protein (CHOP), can contribute to the restoration of global translation. CHOP induces the transcription of Growth arrest and DNA damage-inducible protein (*GADD34*), an eIF2α phosphatase regulatory subunit which contributes to the dephosphorylation of eIF2α (Brush *et al*., 2003). In cases of severe cellular stress where the pro-survival mechanisms induced by the ISR are unsuccessful in restoring homeostasis, the ISR promotes cell death signalling. One of the best studied mechanisms of ISR-induced cell death also involves ATF4-mediated activation of CHOP. CHOP has been shown to induce apoptosis via a number of mechanisms including, repression of anti-apoptotic proteins (McCullough *et al*., 2001) and upregulation of death receptors (Yamaguchi and Wang, 2004). Hence ATF4 and CHOP have extensive roles in the ISR and function as common mediators to produce tailored responses, both pro- and anti-survival dependent on the cellular stress stimuli.

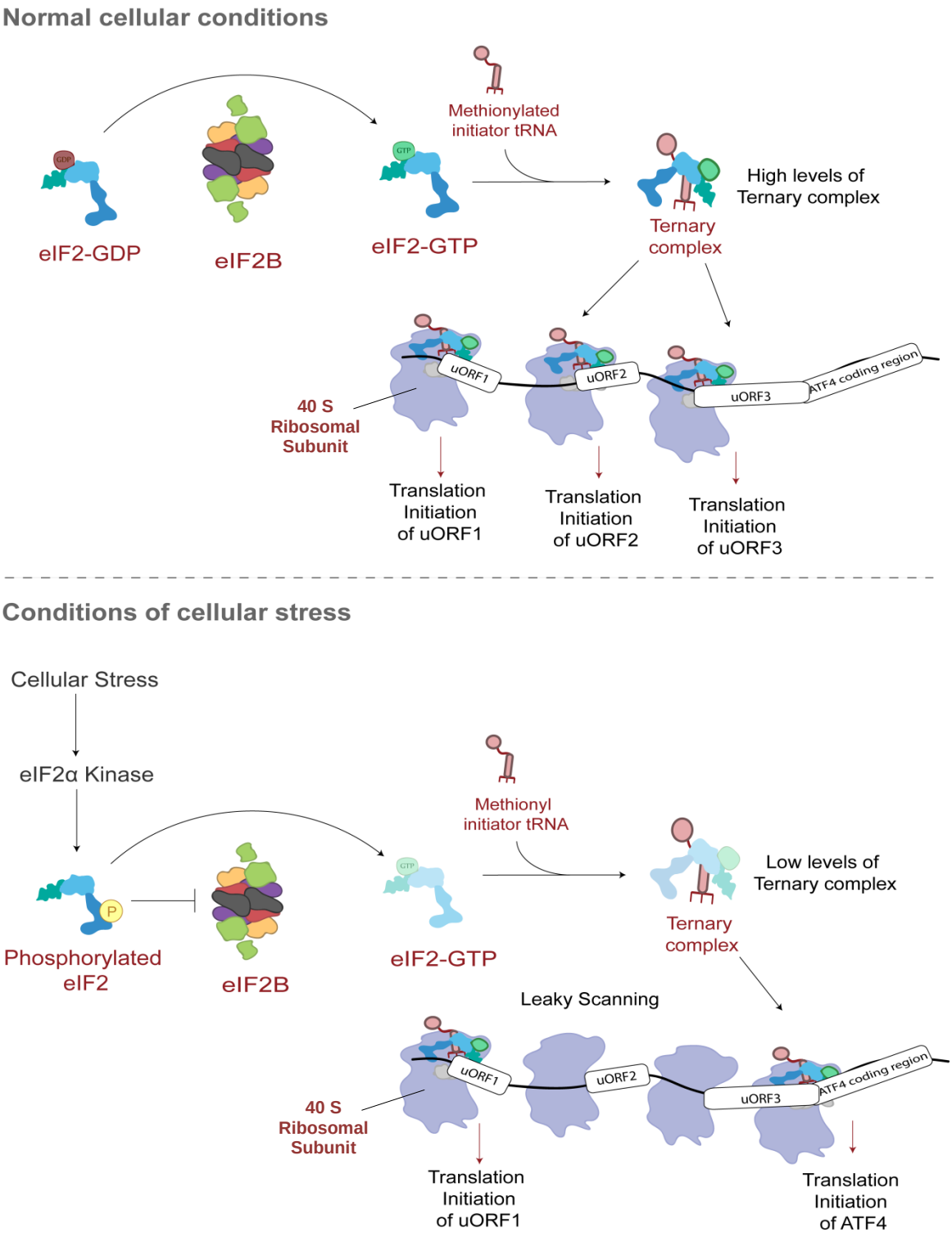

Figure 1.7 Regulation of ATF4 expression by Leaky Scanning.
ATF4 expression is regulated by the presence of three uORFs. Under normal cellular conditions levels of ternary complex are abundant within the cell. Scanning ribosomes readily associate with a ternary complex, initiating translation at the uORFs of ATF4. In response to conditions of cellular stress, levels of ternary complex are reduced within the cell and scanning ribosomes more commonly reach the coding region of ATF4 before associating with a ternary complex.

1.3.2 Small molecule modulation of the ISR

The ISR provides a central network for maintaining cellular homeostasis and therefore the dysregulation of ISR signalling has numerous pathological consequences and has been linked to conditions such as: cancer, diabetes, cardiovascular disease and neurodegeneration (Bi *et al*., 2005; Eizirik *et al*., 2008; Prahlad and Morimoto, 2009; Santos-Ribeiro *et al*., 2018). The ISR can induce both cell survival signalling and cell death signalling and maintaining a balance between these two signalling pathways is crucial. The phosphorylation of eIF2 is the core event through which all signalling pathways that stimulate the ISR converge, and therefore is an appealing therapeutic target.

1.3.2.1 GSK2606414

In neurodegenerative diseases, both ISR signalling enhancers and inhibitors can be neuroprotective, dependent on the underlying molecular mechanisms of the disease. Sephin 1, which indirectly prevents eIF2α dephosphorylation through the inhibition of GADD34, delays the onset of clinical symptoms in multiple sclerosis mouse models (Chen *et al*., 2019). Similarly the upregulation of PERK has also been shown to prevent clinical symptoms (Lin *et al*., 2007). In multiple sclerosis, the translation of ISR-responsive-proteins reduces the cytotoxic impact of inflammation on oligodendrocytes reducing disease associated oligodendrocyte loss (Chen *et al*., 2019). Somewhat paradoxically, PERK inhibition can also reduce clinical symptoms of neurodegenerative disease. Increased levels of PERK and phosphorylated eIF2α have been documented in Parkinson's disease patients (Hoozemans *et al*., 2007). This is hardly surprising as the key pathological hallmark of Parkinson's is the aggregation of misfolded α-synuclein proteins into abnormal cellular deposits, termed Lewy bodies (Power *et al*., 2017). Although ISR-induced PERK signalling can be protective in reducing the load of misfolded proteins, chronic PERK activation (as in Parkinson's) prevents global translation and stimulates cell death. Treatment of Parkinson's disease mice with the PERK inhibitor GSK2606414 promotes survival of dopaminergic neurons and improves motor function, likely through restoring levels of synaptic proteins (Mercado *et al*., 2018).

Over the last decade, unfolded proteins in the brains of patients suffering from neurodegenerative or memory compromising diseases has been increasingly

documented (Scheper and Hoozemans, 2015). As a result, pharmaceutical modulation of PERK has gained significant interest over the last few years. In addition to Parkinson's disease, GSK2606414 also appears promising in preventing neurodegeneration in prion-disease, frontotemporal dementia and Marinesco-Sjögren syndrome (Grande *et al*., 2018; Moreno *et al*., 2013; Radford *et al*., 2015). GSK2606414 however has poor pharmacokinetic properties. The specificity of GSK2606414 is limited with recent studies demonstrating it also inhibits Receptor-interacting serine/threonine-protein kinase 1 (RIPK1), a kinase involved in inflammatory signalling (Rojas-Rivera *et al*., 2017). Furthermore, in mouse models, GSK2606414 induces pancreatic toxicity (Moreno *et al.*, 2013), likely due to pancreatic cells requiring some level of ISR induction to regulate high levels of protein synthesis for their endocrine function. These results highlight the requirement of tailored ISR targeting in different cell types.

1.3.2.2 ISRIB

Recently the small molecule ISRIB (ISR InhiBitor) was identified in a cell-based screen for inhibitors of PERK activity (Sidrauski *et al*., 2013). ISRIB reverses phosphorylated eIF2α induced translational repression (Halliday *et al*., 2015; Sidrauski *et al*., 2013; Sidrauski *et al*., 2015a), through restoration of eIF2B activity (Sekine *et al*., 2015; Sidrauski *et al*., 2015b). The mechanisms through which ISRIB enhances eIF2B activity will be discussed further in Section 1.4.3.2. Like GSK2606414, ISRIB is neuroprotective (Sidrauski *et al*., 2013), however it presents as a more promising therapeutic as it does not induce pancreatic toxicity (Halliday *et al.*, 2015). This is likely due to the fact ISRIB only has a defined window of activation, and above a certain threshold of eIF2α phosphorylation ISRIB no longer inhibits the ISR (Rabouw *et al*., 2019; Sidrauski *et al*., 2015a). This mechanism allows ISRIB to prevent low levels of ISR induction which may contribute to neurodegeneration, while retaining the cell's ability to promote the cytoprotective effects of ISR activation in response to higher levels of cellular stress.

1.3.2.3 DBM and Trazodone

Similarly to ISRIB, the FDA-approved drugs dibenzoylmethane (DBM) and trazodone are also able to partially reverse stress-induced translational repression (Halliday *et al*., 2017). The mechanism though which these drugs reverse the effects of the ISR is

currently unknown. Future studies into the mechanisms of these drugs could improve their therapeutic potential for neurological disease.

1.4 eukaryotic Initiation Factor 2B

eIF2B is the guanine nucleotide exchange factor for eIF2 and therefore plays a fundamental role in the initiation of translation (described in Section 1.2.1). Although functionally similar to other guanine nucleotide exchange factors, eIF2B exhibits a greater level of complexity within its quaternary structure. It is composed of five non-identical subunits, termed α through to ε, encoded in human cells by the genes EIF2B1-5 respectively. In its native form eIF2B exists as a heterodecamer composed of two copies of each of its five subunits (Gordiyenko *et al*., 2014; Wortham *et al*., 2014), however within mammalian cells, eIF2B has also been documented to form sub-complexes which contain varying degrees of the individual eIF2B subunits (Liu *et al*., 2011; Wortham *et al*., 2014). The γ and ε subunits catalyse the guanine nucleotide exchange activity of eIF2B, whereas the α, β and δ subunits are required to regulate this activity in response to various cellular signals (Kimball *et al*., 1998; Pavitt *et al*., 1997; Pavitt *et al*., 1998; Williams *et al*., 2001). Through its regulation, eIF2B provides a critical controlled point in the translation initiation pathway such that in response to adverse conditions the cell can down-regulate global translation to preserve energy. In yeast eIF2B localises to cytoplasmic bodies, termed eIF2B bodies. These foci represent sites where eIF2B catalytic activity occurs and is also regulated (Campbell *et al.,* 2005). The cytoplasmic organisation of mammalian eIF2B complexes has not previously been investigated.

1.4.1 eIF2B subunit function

The eIF2B catalytic subunits, eIF2Bε and eIF2Bγ, are responsible for the GEF activity of eIF2B. The C terminal domain of eIF2Bε facilitates binding of eIF2 and through its HEAT domain can catalyse eIF2 nucleotide exchange; however the rate of this exchange is greatly enhanced through joining of the other eIF2B subunits (Gomez and Pavitt, 2000). eIF2Bγ enhances eIF2B activity through binding to GTP (Williams *et al.* 2001; Gordiyenko *et al.* 2014), but also by facilitating the displacement of eIF5 from eIF2-GDP to allow for guanine nucleotide exchange, following the initiation of translation (Jennings and Pavitt, 2014). The eIF2B regulatory subunits are responsible for mediating levels of eIF2B activity, dependent on the cellular environment. As eIF2 has a higher affinity for GDP (Erickson and Hannig, 1996) the level of guanine nucleotide exchange activity of eIF2B within the cell can determine global translation rates. In response to conditions of cellular stress eIF2 becomes phosphorylated, converting eIF2 from a substrate, to a competitive inhibitor of eIF2B GEF activity, stimulating the ISR (Dever *et al*., 1995; Rowlands *et al*., 1988) (Section 1.3.1). This phosphorylation induced inhibition is conferred by the eIF2B regulatory subunits. eIF2Bα in particular is required to confer this inhibition however mutational analysis of eIF2Bβ and eIF2Bδ suggests these subunits also contribute (Dev *et al*., 2010; Dever *et al*., 1993; Elsby *et al*., 2011; Fabian *et al*., 1997; Hannig *et al*., 1990; Kimball *et al*., 1998; Krishnamoorthy *et al*., 2001; Pavitt *et al*., 1997; Siekierka *et al*., 1982).

1.4.2 eIF2B structural arrangement

Prior to 2014, eIF2B was believed to be a pentameric complex comprised of one copy of each of its subunits, however mass spectrometry has revealed that eIF2B is actually a decameric complex comprised of two copies of each of its subunits (Gordiyenko *et al*., 2014; Wortham *et al*., 2014). The crystal structure of decameric eIF2B, solved for *Schizosaccharomyces pombe* (*S. pombe*) (Kashiwagi *et al*., 2016) and later solved for mammalian cells (Tsai *et al*., 2018; Zyryanova *et al*., 2018), revealed a central core composed of a hexameric arrangement of two copies of each of the regulatory subunits, flanked at opposite sides by a heterodimer of the catalytic subunits (**Figure 1.8**). Expression of eIF2Bγ is required to stabilise the expression of eIF2Bε within the cell and the formation of a heterodimeric complex of these two subunits is believed to be the first step in decameric formation (Figure 1.9) (Wang *et al*., 2012; Wortham and

Proud, 2015). eIF2Bγ and eIF2Bε contain homologous domains with sequence similarity to nucleotidyl transferases (NT) and acyl transferases (AT) (Figure 1.10) (Koonin, 1995). Genetic manipulation of these domains in mammalian systems has revealed a requirement for the NT-like domain of both proteins to facilitate their binding, and also the binding of the regulatory subunits. The AT-like domain of eIF2Bε also facilitates association with the regulatory subunits; however the AT-like domain of eIF2Bγ is not required (Wang *et al*., 2012). The regulatory subunits of eIF2B reside within the centre of the decamer (**Figure 1.8**). It has been proposed that first a heterodimer of eIF2Bβ and eIF2Bδ bind the catalytic heterodimer, through interactions between eIF2Bβ and eIF2Bε, and eIF2Bδ and eIF2Bγ to form a tetrameric subcomplex (Figure 1.9). The decamer is completed through the joining of two tetrameric complexes stabilised by a homodimer of eIF2Bα (Figure 1.9) (Wortham and Proud, 2015; Wortham *et al*., 2016). Studies in yeast first revealed that the eIF2B regulatory subunits share high sequence homology, particularly in their C terminal domains (Figure 1.10) (Bushman *et al*., 1993; Paddon *et al*., 1989) which are highly conserved from yeast to mammalian cells (Price *et al*., 1996). The hydrophobicity of the C terminal domains facilitates the dimerization of eIF2Bα subunits to form homodimers, and the dimerization of eIF2Bβ and eIF2Bδ to form heterodimers (Bogorad *et al*., 2014; Kuhle *et al*., 2015). An eIF2Bα homodimer and two eIF2B(βδ) heterodimers form a hexameric structure within the decamer, facilitated by the arrangement of the C terminal domains into the decameric core (Kuhle *et al*., 2015). In this arrangement the N terminal domains are accessible for interactions with eIF2α (**Figure 1.8**) (Kashiwagi *et al*., 2016; Tsai *et al*., 2018; Zyryanova *et al*., 2018).

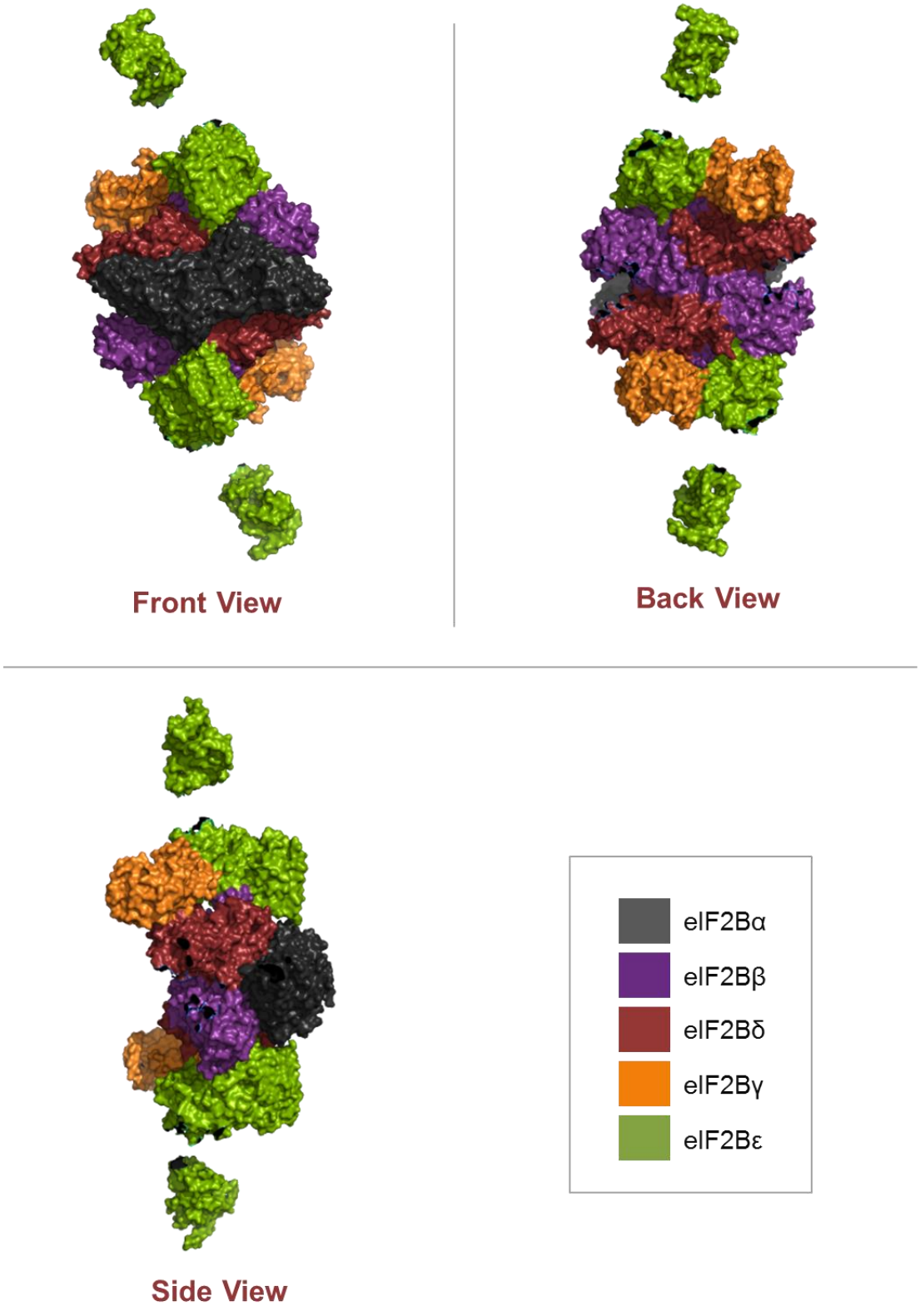

Figure 1.8 The crystal structure of mammalian eIF2B.
The structure was solved by Kenner *et al.* (2019) PDB code 6O81 and was drawn here using PYMOL (DeLano, 2002). In its native conformation eIF2B exists as a decamer comprised of two copies of each of its 5 subunits. Two copies of each of the regulatory subunits (α, β, and δ) reside in the centre of the decamer, forming a hexameric regulatory core. The core is flanked on either side by a heterodimer of the catalytic subunits (γ and ε).

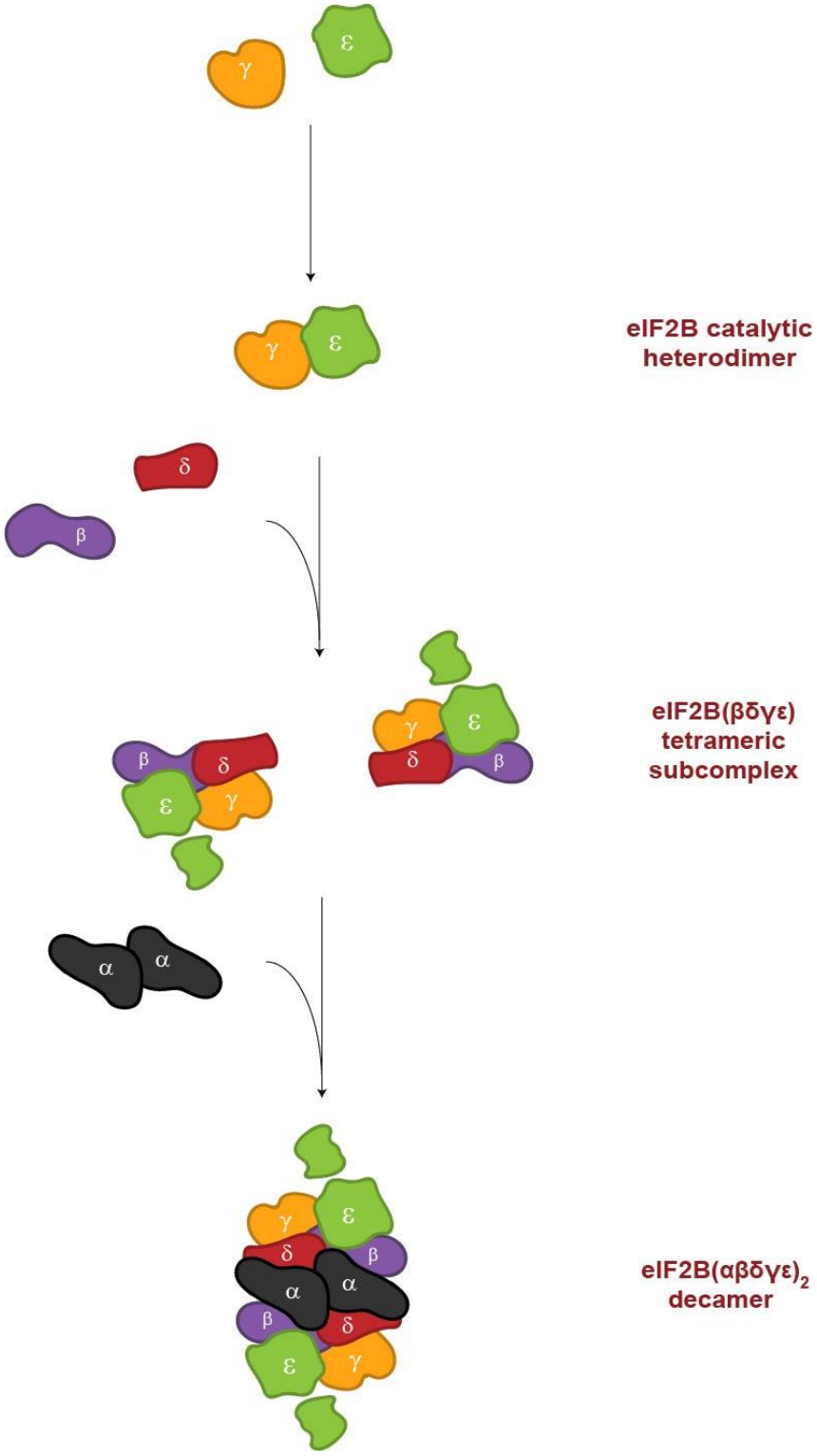

Figure 1.9 Schematic of eIF2B decamer assembly.
A model for the assembly of decameric eIF2B was proposed by Wortham *et al.,* 2015. eIF2Bε and eIF2Bγ subunits first bind to form a catalytic heterodimer. eIF2Bβ and eIF2Bδ subunits then bind the eIF2B catalytic heterodimer to form an eIF2B tetrameric subcomplex. Two eIF2B tetrameric subcomplexes are then bound by an eIF2Bα homodimer to complete the decameric conformation.

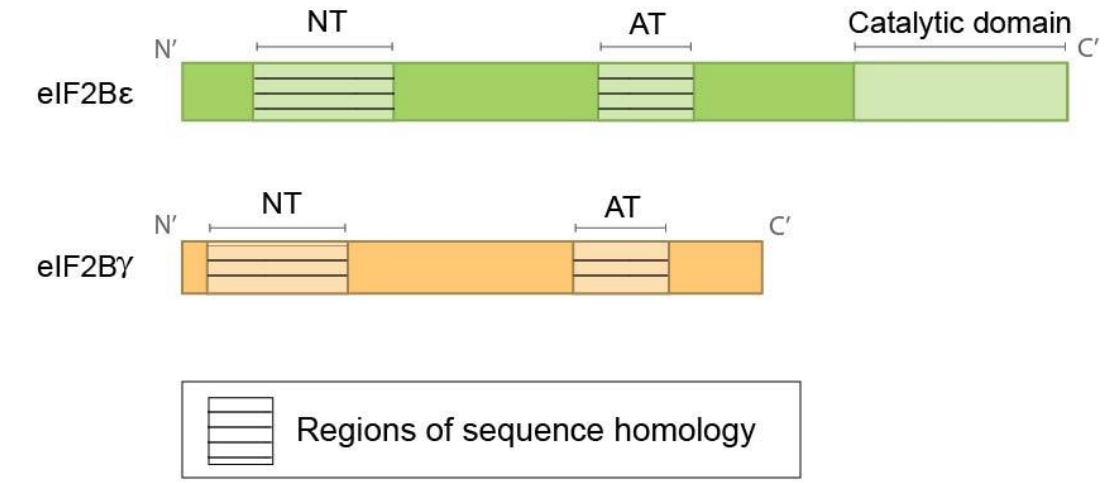

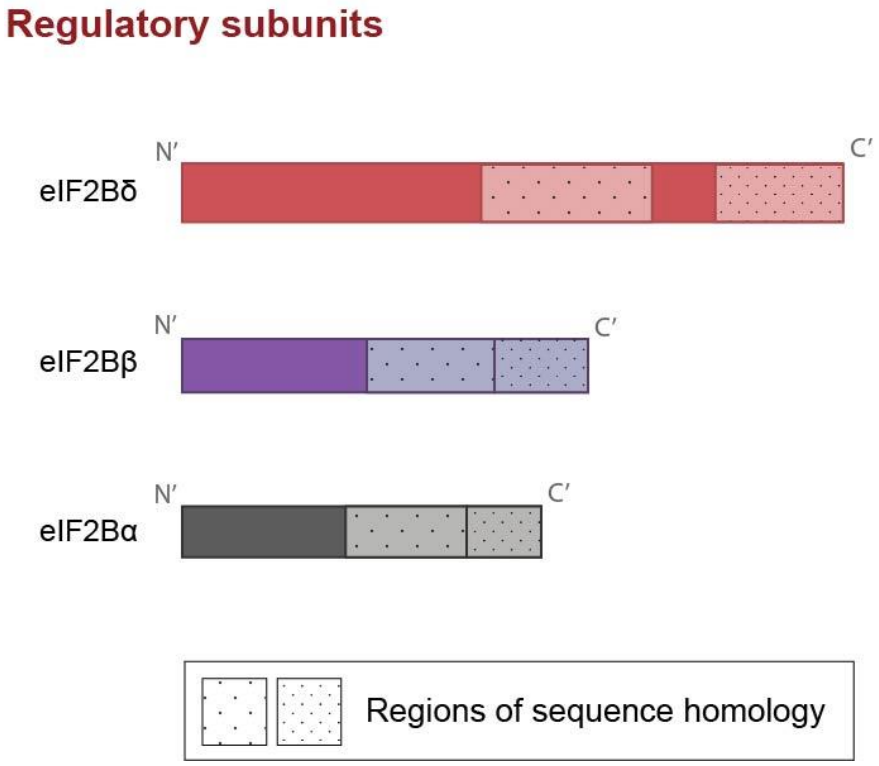

Figure 1.10 Schematic representation of regions of sequence homology within the eIF2B subunits. The catalytic subunits of eIF2B share domains of high sequence homology with each other, but also with nucleotidyl transferases (NT) and acyl transferases (AT). The regulatory subunits of eIF2B share domains of high sequence homology within their C terminal domains.

1.4.2.1 eIF2B subcomplexes

In mammalian cells eIF2B(βδγε) tetrameric subcomplexes have been shown to exist (Figure 1.11) and *in vitro* GEF assays suggest they function at approximately 50 % the activity of the decameric complex (Liu *et al*., 2011; Wortham *et al*., 2014). Additionally, functional eIF2B(γε) catalytic subcomplexes have been identified in yeast and mammalian cells (Figure 1.11) and *in vitro* GEF assays suggest they harbour approximately 20 % of the activity of the decameric complex (Liu *et al*., 2011; Pavitt *et al*., 1998). Whether these subcomplexes are present as intermediates in decamer formation or are themselves functionally important complexes in cellular regulation is unknown. Due to the requirement of the eIF2B regulatory subunits to mediate the inhibitory effects of phosphorylated eIF2α, the presence of subcomplexes harbouring different arrangements of subunits could facilitate different responses to cellular stress. This could perhaps provide a highly controlled level of eIF2B regulation within the cell.

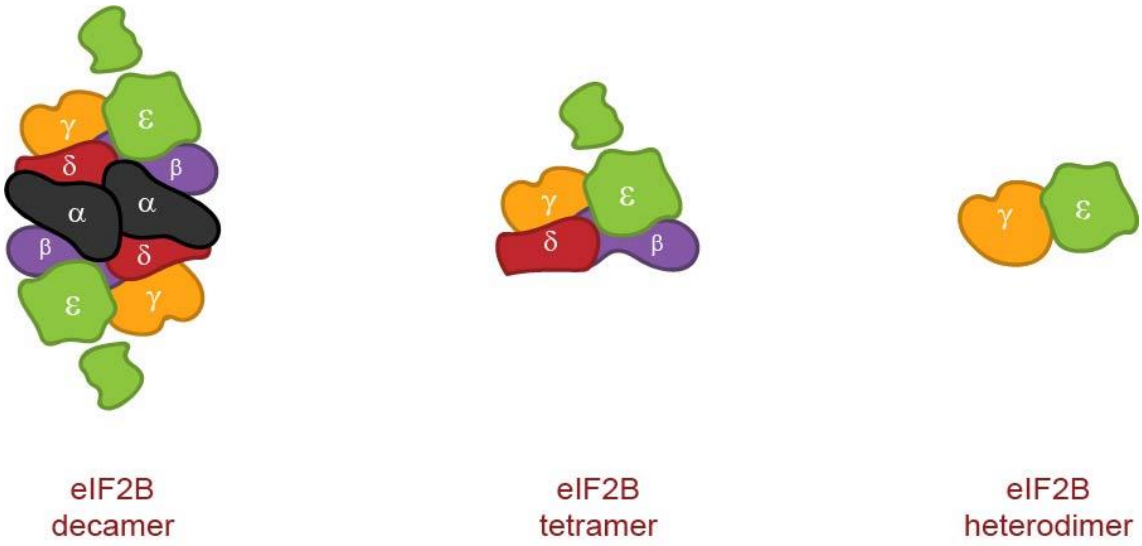

Figure 1.11 eIF2B complexes identified in mammalian cells.
eIF2B forms a decameric complex in its native form composed of two copies of each of its five subunits. eIF2B has also been shown to form tetrameric complexes that contain one copy of each subunit except for the α subunit and heterodimers of one copy of each of the catalytic subunits; γ and ε.

1.4.3 eIF2B mediated regulation of translation initiation

1.4.3.1 Regulation by phosphorylated eIF2α

The initiation step of the translation pathway is rate limiting and therefore the inhibition of eIF2B by phosphorylated eIF2α (serine residue 51) provides an important mechanism through which translation can be controlled. Levels of eIF2B within the cell are lower than eIF2 and thus even partial phosphorylation is sufficient for the down-regulation of protein synthesis. Although phosphorylated eIF2α has been known to inhibit eIF2B since 1982 (Siekierka *et al*., 1982), the exact mechanism through which phosphorylated eIF2 induces this inhibition has remained largely unknown. Recent structural studies have solved structures of eIF2B bound to both phosphorylated and non-phosphorylated eIF2α, providing the first insight into this precise mechanism (Adomavicius *et al*., 2019; Bogorad *et al*., 2017; Gordiyenko *et al*., 2018; Kashiwagi *et al*., 2019; Kenner *et al*., 2019). Although the structure of eIF2B is highly conserved (Kashiwagi *et al*., 2016; Tsai *et al*., 2018; Zyryanova *et al*., 2018), phosphorylated eIF2α appears to inhibit eIF2B via distinct mechanisms within yeast and mammalian cells.

In yeast, both phosphorylated and non-phosphorylated eIF2α share a binding pocket (Figure 1.12). eIF2α binds to the C terminal domains of eIF2Bα and eIF2Bδ and has minor contacts with eIF2Bβ. This binding positions eIF2β and eIF2γ in close proximity to the catalytic domain of eIF2B, facilitating nucleotide exchange. Upon phosphorylation of eIF2α, conformational changes in the structure of eIF2α surrounding the phosphorylation site are believed to enhance the binding of eIF2α to eIF2Bα and eIF2Bδ. This results in a conformational change in eIF2B that displaces the catalytic domain from its original close proximity to eIF2β and eIF2γ inhibiting nucleotide exchange (Adomavicius *et al*., 2019; Gordiyenko *et al*., 2018). Similarly to yeast two molecules of eIF2 are able to bind mammalian eIF2B, however the binding site of eIF2 is not conserved from yeast to mammalian eIF2B. Mammalian eIF2α binds to decameric eIF2B by bridging across the two eIF2B(βδγε) tetrameric arrangements, binding to eIF2Bβ resident within one eIF2B(βδγε) tetramer of the decamer and eIF2Bδ resident within the opposite eIF2B(βδγε) tetramer (Figure 1.12). This arrangement positions eIF2γ in an orientation appropriate for catalytic exchange by eIF2Bε (Kenner *et al*., 2019). In yeast eIF2α interacts with each eIF2B(βδγε) tetramer independently, and the main contact between eIF2α and eIF2B is mediated by eIF2Bα (Adomavicius *et*

al., 2019; Kenner *et al*., 2019). Furthermore, unlike in yeast, in mammalian cells there is no overlap between the binding sites of eIF2α in its unphosphorylated and phosphorylated forms. Phosphorylation of eIF2α induces N terminal refolding, exposing hydrophobic residues that facilitate interactions with eIF2Bα and eIF2Bδ (figure 1.12). Binding of phosphorylated eIF2α to eIF2Bα and eIF2Bδ is non-productive for eIF2B GEF activity and blocks the binding site for non-phosphorylated eIF2, inhibiting eIF2B GEF activity (Kenner *et al*., 2019).

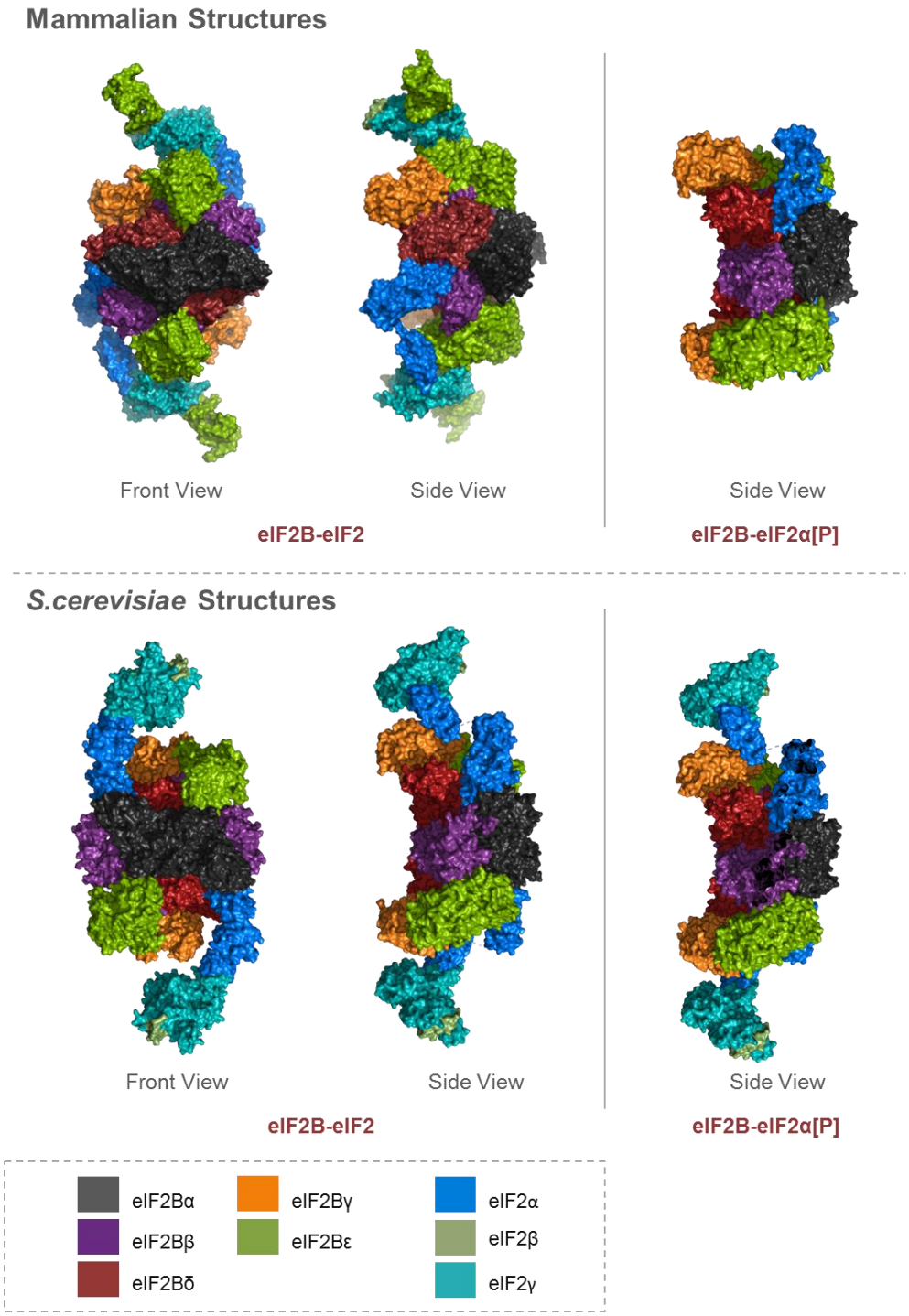

Figure 1.12 Crystal structures of mammalian and *S. cerevisiae* eIF2B bound to eIF2 and eIF2α[P]. The mammalian structure was solved by Kenner *et al.* (2019) PDB code 6O81 and the *S. cerevisiae* structure was solved by Adomavicius *et al.* (2019) PDB code 6I3M. The structures here were drawn using PYMOL (DeLano, 2002). eIF2B is comprised of two eIF2B(βδγε) tetramers stabilised by an eIF2Bα homodimer. The binding pocket for mammalian eIF2 is formed by residues of eIF2Bδ and residues of eIF2Bβ present in opposite eIF2B(βδγε) tetramers. In its phosphorylated form the binding pocket for eIF2 is comprised of residues present in eIF2Bδ and eIF2Bα. The binding pocket of *S.cerevisiae* eIF2 is formed mainly from residues of eIF2Bα and eIF2Bδ. In its phosphorylated form eIF2 also binds to eIF2B through this binding pocket.

1.4.3.2 Regulation of eIF2B through binding of ISRIB

The small molecule ISRIB was recently identified to reverse ISR-induced translational repression through restoration of eIF2B activity and appears to be a promising therapeutic, as discussed in Section 1.3.2.2. ISRIB is a small molecule that restores eIF2B activity through bridging two eIF2B(βδγε) tetramers to promote decamer formation (Sidrauski *et al*., 2015b; Tsai *et al*., 2018; Zyryanova *et al*., 2018) (Figure 1.10). ISRIB binds between the N termini of eIF2Bδ and eIF2Bβ within the tetrameric structure, as ISRIB is a symmetrical molecule it can bind two tetramers in this way promoting the stabilisation of two tetramers to form an eIF2B$(\beta\delta\gamma\varepsilon)_2$ octamer (Tsai *et al.*, 2018; Zyryanova *et al.*, 2018). The interface formed between the two eIF2B tetramers favours the binding of eIF2Bα homodimers when compared to single tetramers. Through stabilising this tetrameric interface, ISRIB promotes decameric formation (Tsai *et al.*, 2018). The presence of ISRIB does not disrupt binding of phosphorylated eIF2 and consequently phosphorylated eIF2α is still capable of inhibiting eIF2B in the presence of ISRIB. The ability of ISRIB to restore translation within a cell is dependent on the levels of phosphorylated eIF2. In the absence of phosphorylated eIF2 ISRIB does not enhance eIF2B activity, however during episodes of mild cellular stress, associated with moderate phosphorylation of eIF2, ISRIB is able to enhance eIF2B activity (Rabouw *et al*., 2019; Sidrauski *et al*., 2015a). This is likely through stabilising the decameric conformation of eIF2B to increase the overall level of eIF2B activity within the cell. Decameric eIF2B harbours two eIF2 binding sights and is approximately twice as efficient at performing GEF activity when compared to tetrameric eIF2B which harbours only one eIF2 binding site (Kenner *et al*., 2019; Liu *et al*., 2011). During episodes of extreme cellular stress, associated with high levels of phosphorylated eIF2, ISRIB is no longer capable of rescuing eIF2B activity (Rabouw *et al*., 2019; Sidrauski *et al*., 2015a). This is likely a consequence of the stabilised decameric complexes of eIF2B becoming saturated by the high level of phosphorylated eIF2 present within the cell when compared to non-phosphorylated eIF2.

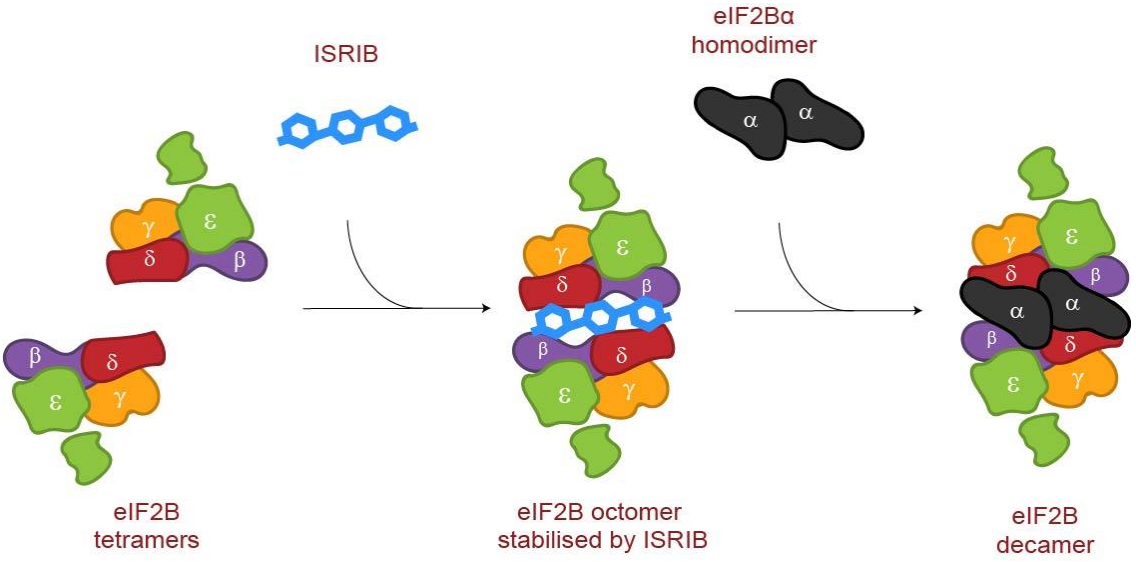

Figure 1.13 ISRIB promotes eIF2B decameric assembly.
ISRIB binds to eIF2Bβ and δ subunits within two distinct eIF2B(βδγε) tetramers, stabilising the binding of the two tetramers and forming an eIF2B$(\beta\delta\gamma\varepsilon)_2$ octamer. The octameric conformation of eIF2B favours the binding of an eIF2Bα homodimer, promoting the assembly of the eIF2B decamer.

1.4.4 Cellular localisation of eIF2B

In yeast eIF2B has been shown to localise to cytoplasmic foci which have been termed eIF2B bodies (Campbell *et al*., 2005; Moon and Parker, 2018; Noree *et al*., 2010; Taylor *et al*., 2010). eIF2B bodies are cytoplasmic granules formed of accumulations of eIF2B and eIF2. Morphologically eIF2B bodies commonly exist as a filamentous-like structure (Campbell *et al*., 2005; Noree *et al*., 2010). This morphology appears common in yeast with a number of other enzymes also documented to localise to filaments, including glutamine synthetase (GS) and Cytidine triphosphate synthetase (CTPS) (Noree *et al*., 2010). Studies investigating the filamentous nature of GS and CTPS synthase have linked this localisation to enzyme inactivation and adverse cellular conditions (Noree *et al*., 2014; Petrovska *et al*., 2014). eIF2B bodies however appear somewhat different to these filamentous structures. Campbell *et al.,* (2005) demonstrated that eIF2 dynamically interacted with the eIF2B body at a rate that correlated with eIF2B GEF activity, suggesting that eIF2B bodies are sites of enzyme activity.

1.5 Vanishing White Matter disease

The importance of eIF2B function within the cell is highlighted by the fact that mutations in any of the five subunits of eIF2B lead to the fatal neurological disorder, leukoencephalopathy with vanishing white matter (VWM). VWM is also known as childhood ataxia with central nervous system hypomyelination (CACH), and although it is a rare disease it is regarded as the most prevalent childhood leukodystrophy and is associated with a very poor prognosis (Bugiani *et al*., 2010). Clinically the disease is characterised by a mutation in any of the five subunits of eIF2B accompanied by chronic degradation of the cerebral white matter. The affected white matter appears thinned and porous due to dispersal by vacuoles and MRI imaging reveals cerebrospinal fluid filled areas where white matter has been largely degraded (van der Knaap *et al*., 1998). Phenotypically, symptoms and disease progression vary dramatically. This is likely due to the genetic complexity of VWM with currently around 200 mutations, across the 5 eIF2B subunits, characterised as causative of VWM according to the Human Gene Mutation Database. There is no cure for VWM and elucidating common pathophysiological mechanisms across the broad spectrum of causative mutations remains difficult.

1.5.1 Patient symptoms and clinical progression

VWM disease has a wide clinical spectrum and the severity of disease appears to inversely correlate with age of onset (Hamilton *et al*., 2018). In classical cases of VWM, disease onset occurs in childhood and is symptomatically characterised by cerebellar ataxia, spasticity, mild mental decline and less commonly loss of vision and epilepsy (Hanefeld *et al*., 1993; Schiffmann *et al*., 1994; van der Knaap *et al*., 1997). In addition to neurological symptoms some patients also present with ovarioleukodystrophy (Boltshauser *et al*., 2002; Hamilton *et al*., 2018; van der Knaap *et al*., 2006). Exposure to stressful episodes including, fever, head trauma and acute fright can cause disease onset and can also contribute to episodes of rapid neurological deterioration, which influence disease progression. During these episodes patient motor function rapidly declines and recovery is usually incomplete. Patient prognosis is poor with severe episodes commonly resulting in comas which are often fatal (Maletkovic *et al*., 2008; van der Knaap *et al*., 1998).

Milder cases of VWM appear to be associated with onset in adolescence or adulthood, where episodes of rapid deterioration are less prominent but cognitive problems are more apparent (Hamilton *et al*., 2018; Labauge *et al*., 2009; Van Der Knaap *et al*., 2004). Early infantile and antenatal cases of VWM are associated with severe disability and higher mortality (Francalanci *et al*., 2001; Hamilton *et al*., 2018). In these early onset cases of VWM involvement of organs other than the brain and ovaries have been documented and patients often suffer symptoms including, cataracts, pancreatitis and kidney hypoplasia (van der Knaap *et al*., 2003).

1.5.2 Pathophysiology and genotype-phenotype link

VWM is a genetically complex disease. It is caused by autosomal recessive mutations, most commonly missense mutations that may exist in homozygous or heterozygous states (Pavitt and Proud, 2009). Frameshift and nonsense mutations occur less frequently (Li *et al*., 2004) and have never been observed in the homozygous state likely due to their association with severe VWM phenotypes (Pavitt and Proud, 2009). Figure 1.14, adapted from Shimada *et al.,* (2015), demonstrates the distribution of over 100 characterised VWM mutations across the genes ecoding the eIF2B subunits. Mutations arise most frequently in *EIF2B5* (encoding eIF2Bε), dispersed across the gene but largely sparing the 3' end which encodes the catalytic domain of eIF2B; mutations in this region would likely be fatal (Gomez and Pavitt, 2000; Gomez *et al*., 2002). eIF2Bγ shares high sequence homology with eIF2Bε and mutations occuring in *EIF2B3* (encoding eIF2Bγ), generally cluster around areas of sequence homology to *EIF2B5*. Additionally, mutations affecting the regulatory subunits also appear to cluster in regions of homology. The regulatory subunits of eIF2B (α,β and δ) share high sequence homology in their C terminal domains. VWM mutations identified in *EIF2B1, EIF2B2 and EIF2B4* (encoding eIF2B α,β and δ respectively) in general cluster towards the 3' portion of the genes.

Biochemical analyses have investigated the functional effects of VWM mutations on eIF2B. Some mutations destabilise interactions between eIF2B subunits affecting complex formation, whereas other mutations affect the GEF activity of eIF2B either directly or indirectly through impairing eIF2 binding (de Almeida *et al*., 2013; Fogli and Boespflug-Tanguy, 2006; Li *et al*., 2004; Richardson *et al*., 2004; Scheper *et al*., 2006; Wortham and Proud, 2015). The recent discovery of ISRIB appears a promising avenue

in the treatment of VWM mutations that destabilise the decameric conformation of eIF2B (Liang Wong *et al*., 2018; Tsai *et al*., 2018; Zyryanova *et al*., 2018). The small molecule 2BAct has recently been derived from ISRIB and has similar effects to ISRIB on eIF2B activity but improved pharmacodynamic properties. 2BAct prevents disease phenotypes in a VWM mouse models harbouring a mutation which effects eIF2B complex formation (eIF2Bε R191H mutation - R195H in humans) (Wong *et al*., 2019), demonstrating therapeutic potential for 2BAct in the treatment of eIF2B complex destabilising VWM mutants. Mutations have also been identified that affect neither complex formation nor eIF2B activity *in vitro* but cause some of the most severe forms of VWM *in vivo* (Liu *et al*., 2011; Wortham and Proud, 2015). The mechanisms of these mutations remain elusive and therefore the development of treatments for these particular mutations is difficult.

Although eIF2B is a global regulator of protein synthesis, glial cells appear to be selectively vulnerable to eIF2B mutations, and VWM disease presents with populations of immature astrocytes and an increased number of oligodendrocyte progenitor cells (Dooves *et al*., 2016). Patient glial cells commonly exhibit an elevated ISR (Abbink *et al*., 2018; van der Voorn *et al*., 2005; van Kollenburg *et al*., 2006) and PERK induced induction of the ISR in mouse models has been found to recreate this glial cell phenotype (Lin *et al*., 2014). Primary fibroblast cells isolated from VWM disease patients have been shown to have a heightened stress response, characterised by a hyper-induction of the downstream ISR transcription factor ATF4, whereas patient lymphoblast cells appear to maintain normal levels of ATF4 induction following exposure to stress (Horzinski *et al*., 2010; Kantor *et al*., 2005). Although the exact role of the ISR is unclear in VWM pathophysiology these data suggest it may be linked to the tissue-specificity of VWM and is a key area for future research.

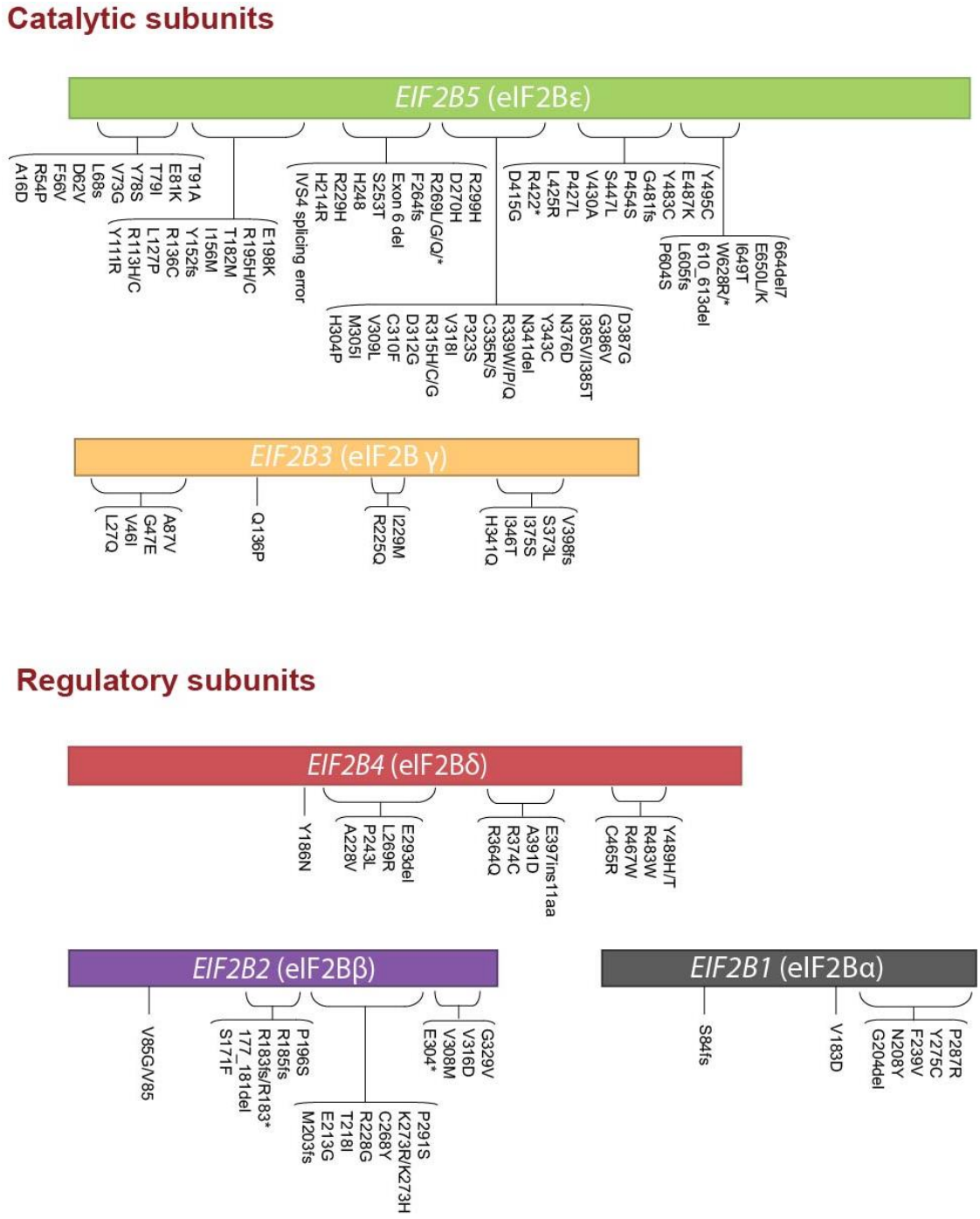

Figure 1.14 The distribution VWM mutations across the genes encoding the 5 eIF2B subunits adapted from Shimada *et al.,* (2015).

VWM mutations have been identified across all 5 subunits of eIF2B. Mutations most frequently occur in *EIF2B5* and reside throughout the gene, except for the 3' domain which is mostly spared. Mutations in *EIF2B3* most commonly cluster within areas of the 5' and 3' ends of the gene which have high sequence homology to *EIF2B5*. Mutations in the genes encoding the regulatory eIF2B subunits, *EIF2B1, EIF2B2* and *EIF2B4* rarely occur within the 5' sequences of the genes and cluster more within the central region and the 3' end of the genes.

1.6 Project overview

The functional localisation of eIF2B has not previously been investigated in mammalian cells. This thesis aims to elucidate localisation patterns of eIF2B in mammalian cells and determine the functional significance of this localisation under normal cellular conditions and during conditions of cellular stress. Currently the pathophysiology of VWM remains elusive, with the functional impact that mutations have on eIF2B, correlating poorly with disease severity and progression. It could be hypothesised that the localisation of eIF2B within a cell may contribute to VWM pathology. This study aims to characterise eIF2B localisation in cells affect by VWM pathology and explore the function of eIF2B localisation during conditions of cellular stress.

The cellular localisation of eIF2B will be investigated under normal cellular conditions in cell types linked to VWM pathology. In yeast eIF2B localises to cytoplasmic bodies, termed eIF2B bodies. Here we aim to determine if eIF2B bodies exist in mammalian cells. It can be hypothesised that eIF2B will localise to eIF2B bodies in mammalian cells. In order to observe mammalian eIF2B localisation, a plasmid encoding a fluorescently tagged eIF2B subunit will be transiently expressed in mammalian cells and the phenotypic localisation of the eIF2B subunit will be visualised by confocal microscopy. ICC will be used to study the localisation of the other 4 subunits of eIF2B in relation to the fluorescently tagged subunit.

If eIF2B is found to localise to cytoplasmic bodies in mammalian cells the relationship of eIF2 and the eIF2B body will be investigated. In yeast eIF2 exists as a mobile component of the eIF2B body and this mobility is manipulated by the modulation of eIF2B GEF activity. It is hypothesised that eIF2 will form a mobile component of eIF2B bodies and we aim to determine if the mobility will correlate to the activity of eIF2B within the cell. Fluorescent recovery after photobleaching (FRAP) analysis will be used as a tool to analyse the movement of eIF2 within eIF2B bodies and treatments with Tg and SA will be used to induce cellular stress as a method to decrease eIF2B activity within the cell.

In recent years several small molecules have been found to relieve cellular stress induced translational repression (Sidrauski *et al.* 2015a; Halliday *et al.* 2017). If the dynamics between eIF2 and mammalian eIF2B bodies are found to be altered during

conditions of cellular stress, the impact of these molecules on eIF2B body dynamics will be assessed. To determine if this event occurs FRAP analysis will be used to investigate the movement of eIF2 within the eIF2B bodies. Transient expression of a fluorescently tagged eIF2B subunit coupled with ICC will be used to study eIF2B subunit distribution patterns.

2. Materials and Methods

2.1 Cell culture

2.1.1 Cell culture conditions

U373 astrocytoma cells were cultured in Minimum Essential Medium (MEM), supplemented with 10 % (v/v) Fetal Bovine Serum (FBS), 1 % (w/v) non-essential amino acids, 1 % (w/v) sodium pyruvate, 1 % (w/v) glutamine and 1 % (w/v) penicillin/streptomycin, all purchased from Life Technologies Co. (New York, USA). Primary human astrocytes were cultured in Astrocyte Medium (AM) supplemented with 10 % (v/v) FBS, 1 % (v/v) astrocyte growth supplement and 1 % (w/v) penicillin/streptomycin, all purchased from ScienCell Research Laboratories (Buckingham, UK). MG-63 cells were cultured in Roswell Park Memorial Institute medium (RPMI) supplemented with 10 % (v/v) FBS and 1 % (w/v) penicillin/streptomycin. HEK293 and HepG2 cells were cultured in Dulbecco's Modified Eagle's Medium (DMEM) supplemented with 10 % FBS (v/v) and 1 % (w/v) penicillin/streptomycin. CHO-C30 cells and CHO-C30 cells harbouring the L180F mutation within the eIF2B4 gene (Sekine *et al.,* 2015) were a kind gift from Prof D Ron (Cambridge Institute for Medical Research). Cells were cultured in Nutrient Mixture F12 Ham medium (Sigma, Dorset, UK) supplemented with 10 % Fetal calf serum (FetalClone II, Thermo) and 1 % (w/v) penicillin/streptomycin, (Life Technologies Co. (New York, USA)). All cells were maintained at 37°C under 5 % CO_2 and were routinely tested for contamination with MycoAlert™ Mycoplasma Detection Kit purchased from Lonza (Slough, UK).

2.1.2 Transient transfections

One day prior to transfection, primary human astrocytes or CHO cells were seeded at a density of 1 x 10^5 cells, and all other cells were seeded at a density of 8 x 10^4 cells in a 6-well plate or fluorodish. Transfections were performed by chemical transfection with 1 mg mL^{-1} polyethylenimine (PEI) (Sigma, Dorset, UK). 1-3 µg of plasmid DNA was diluted in 100 µL of serum and antibiotic free cell culture medium. Diluted DNA was mixed with PEI and incubated at room temperature for 10 minutes. The volume of PEI used was based on a 3:1 ratio of PEI (µL):plasmid DNA (µg). 600 µL of antibiotic free cell culture media was added to the transfection mix, and the total volume added to

the cells. Cells were incubated at 37 °C for 23 hours, with an additional 2 mL of antibiotic free media added at the 2.5 hour time point. Cell culture media was changed to complete media and cells were incubated at 37 °C for 24 to 48 hours prior to imaging.

2.1.3 Cell treatments

To induce cellular stress, cells were treated with 1 µM Tg for 1 hour, or 125 µM SA for 30 minutes or 500 µM SA for 1 hour (all purchased from Sigma, Dorset, UK). For drug treatments, cells were treated with 200 nM ISRIB, 20 µM DBM or 20 µM Trazodone for 1 hour (all purchased from Sigma, Dorset, UK).

2.2 Plasmids

pCMV6-AC-GFP plasmid vectors encoding, *EIF2B5* or *EIF2S1* were purchased from Origene (Rockville, Maryland, USA). The coding ORF of *EIF2B5* from the pCMV6-AC-GFP vector was cloned into a pCMV6-AC-RFP vector (Origene). The construct was verified by sequencing. The coding ORF of the *EIF2S1* pCMV6-AC-GFP plasmid was mutated using site directed mutagenesis to generate an S51A mutation. The construct was verified by sequencing. pHM2Bε was a kind gift from Dr N Wortham, The University of Southampton.

2.2.1 Site directed mutagenesis

Site directed mutagenesis was performed using a QuikChange II Site-Directed Mutagenesis Kit (Agilent, Stockport, UK) in accordance with manufacturer's instructions. In order to increase the efficiency of bacterial transformations with mutagenic plasmid DNA, an extra step was performed. Following the *Dpn*I digestion step, reactions were concentrated to 1/5 th of their original volume by ethanol precipitation. 3 M sodium acetate was diluted 1 in 20 in ice cold 100 % (v/v) ethanol (-20 °C) and added to the reactions. The reaction mixtures were incubated at -20 °C for 1 hour and the DNA was then pelleted by centrifugation at 17000 *x g* for 15 minutes. The supernatant was removed, and the DNA was washed once in cold 70 % (v/v) ethanol before being centrifuged again for a further 5 minutes. The supernatant was removed, and the pell*et* allowed to air dry at room temperature for 10 minutes. The DNA was then resuspended in sterile dH_2O to 1/5th the total volume of the original reaction

volume. DNA was stored at 4 °C until transformation following the manufacturer's instructions.

2.2.2 Generating chemically competent *E.coli*

XL 10-Gold ultracompetent cells (Fisher Scientific, Loughborough, UK) were inoculated in Lysogeny broth (LB) (Sigma, Dorset, UK) and incubated in a shaking incubator at 37 °C overnight. The following morning the overnight culture was diluted 1 in 100 in LB. Cells were grown to an optical density at 600 nm (OD_{600nm}) of between 0.5 and 0.7 and then incubated for 15 minutes on ice. Cells were pelleted at 4000 rpm for 5 minutes at 4 °C and then resuspended in TBF I buffer (0.03 M potassium acetate, 0.05 M manganese chloride tetrahydrate, 0.01 M potassium chloride, 0.008 M calcium chloride tetrahydrate, 15 % (v/v) glycerol) and incubated for 1 hour on ice. Cells were then pelleted at 4000 rpm for 5 minutes at 4 °C and then resuspended in TBF II buffer (0.001 M 3-(*N*-morpholino)propanesulfonic acid, 0.001 M potassium chloride, 0.06 M calcium chloride tetrahydrate, 15 % (v/v) glycerol). Cells were aliquoted, flash frozen in liquid nitrogen and stored at - 80 °C.

2.2.3 Bacterial Transformation

Plasmid constructs were amplified by bacterial transformation. Competent *Escherichia coli* (*E.coli*) (-80 °C) were defrosted on ice for 30 minutes prior to transformation. Competent DH5α cells (generated in Section 2.2.2) were used to transform *EIF2S1* pCMV6-AC-GFP for site directed mutagenesis, and competent JM109 cells (Promega, Southampton, UK) were used for all other plasmid transformations. 1 µL of plasmid DNA was added to 50 µL competent *E.coli* and incubated on ice for 1 hour. Following incubation cells were heat shocked at 42 °C for 90 seconds. Transformations were then incubated on ice for 2 minutes prior to plating on LB Agar plates containing 50 mg mL^{-1} carbenicillin, which were then incubated at 37 °C overnight.

2.2.4 Extracting plasmid DNA from transformed *E.coli*

Transformed bacteria were inoculated in LB containing 50 mg mL^{-1} carbenicillin and incubated in a shaking incubator at 37 °C overnight. Plasmid DNA was extracted from cultures using a GeneJET plasmid Miniprep kit (Fisher Scientific, Loughborough, UK) according to the manufacturers instructions. The concentration of the purified plasmids was determined using a NanoDrop 1000 Spectrophotometer.

2.3 Protein analysis

2.3.1 Extraction of protein from cultured cells

Culture media was removed, and cells were washed with phosphate buffered saline (PBS) (Sigma, Dorset UK). Cells were lysed in Cell Lytic M containing 1 % (v/v) protease inhibitor cocktail (Sigma, Dorset, UK), for 15 mins shaking at room temperature. Cell extracts were harvested by scraping flasks with a cell scraper. Cellular debris was pelleted by centrifugation at 12,000 *x g* for 12 minutes at 4 °C. Protein extracts were either subject to dot blot analysis or, for western blot analysis, the concentration of the extracts were quantified.

2.3.2 Dot blot analysis

For dot blot analysis 1 µL of protein sample was applied to a nitrocellulose membrane and allowed to air dry. Membranes were blocked in Tris-buffered saline supplemented with 0.1 % (v/v) Tween 20 (TBST) and 5 % (w/v) nonfat milk (Premier Foods, London, UK) for 1 hour. Primary antibodies were diluted in block solution and incubated with membranes overnight at 4 °C. The following antibodies were used: eIF2Bε (1:500 dilution, ARP61329_P050; Aviva Systems Biology, San Diego, USA), eIF2Bγ (1:500 dilution, sc-137248; Santa Cruz, California, USA), eIF2Bδ (1:100 dilution, sc-271332; Santa Cruz Biotechnology, California, USA) and β-actin (1:1000 dilution, ab8224, Abcam, Cambridge, UK). Membranes were then washed in TBST and incubated for 1 hour with appropriate LiCor secondary antibodies diluted 1:10,000 in 5 % (w/v) nonfat milk in TBST. Dot blots were visualised on a LiCor Odyssey Scanner with Image Studio Lite software.

2.3.3 Quantification of protein extracts

Protein extracts were subject to a Bicinchoninic Acid (BCA) protein assay to determine the protein concentration for western blot analysis. Bovine Serum Albumin (BSA) (Sigma, Dorset, UK) was diluted in Cell Lytic M to generate a set of protein standards ranging from 0.1 mg mL^{-1} to 4 mg mL^{-1}. Protein samples and standards were incubated in a 96-well plate with BCA reagent (0.4 % (w/v) copper sulphate in BCA) at 1:20 ratio for 30 minutes. The absorbance was determined using a Victor^2 1420 multi-label counter (Wallac) at a wavelength of 570 nm.

2.3.4 Concentrating protein samples

For western blot analysis protein samples were concentrated using 10 kDa MWCO Viva spin 2 columns (Fischer Scientific, Loughborough, UK), in accordance with the manufacturer's instructions.

2.3.5 Western blot analysis

Concentrated protein extracts were diluted in 4 x SDS-PAGE sample buffer (Expedeon, Swavesey, UK) and incubated at 95 °C for 4 minutes. 60 µg of total protein was resolved on a 10 % polyacrylamide gel, and electroblotted onto nitrocellulose membrane. Membranes were blocked in TBST supplemented with either 5 % (w/v) nonfat milk or 5 % (w/v) BSA for 1 hour. Primary antibodies were diluted in block solution and incubated with membranes overnight. The following antibodies were used: eIF2Bε (1:500 dilution, ARP61329_P050; Aviva Systems Biology, San Diego, USA), eIF2α (1:100 dilution, sc-11386; Santa Cruz Biotechnology, California, USA) and phospho-eIF2α (ser51) (1:1000 dilution, 44728G, Invitrogen, Fisher Scientific). In order to quantify levels of proteins detected by western blot a β-actin antibody (1:1000 dilution, ab8224, Abcam, Cambridge, UK) was used as a loading control. Following primary antibody incubations, membranes were then washed with TBST, and then incubated for 1 hour with appropriate LiCor secondary antibodies diluted 1:10,000 in block solution (goat-anti-rabbit IRDye 680RD P/N 925-68071 and goat-anti-mouse IRDye 800CW P/N 925-32210) (LiCor, Cambridge, UK). Following secondary antibody incubations, membranes were washed with TBST and then visualised on a LiCor Odyssey Scanner with Image Studio Lite software.

2.3.6 Puromycin incorporation assays

For puromycin incorporation assays, cells were seeded at a density of 6.7 x 10^5 cells in T75 flasks. One day later, culture media was replaced with fresh media. Cells were then either untreated or treated as outlined in Section 2.1.3. For puromycin labelling, cells were incubated with 91 µM puromycin (Fisher Scientific, Loughborough, UK) and 208 µM emetine (Sigma, Dorset, UK) for 5 minutes. Cells were then washed twice in ice cold PBS containing 355 µM cycloheximide (Sigma, Dorset, UK) and protein extracts were prepared as outlined in Section 2.3.1. Western blot analysis was performed on protein extracts as outlined in Section 2.3.5. For detection of puromycin, a primary puromycinylated protein antibody (1:500 dilution, clone 12D10, MABE343, Millipore,

Watford, UK) was used. In order to quantify levels of puromycin a primary antibody for β-actin (1:2000 dilution, ab8227, Abcam, Cambridge, UK) was used as a loading control.

2.4 Immunocytochemistry

Cells were grown on coverslips in 6 well plates and transfected as described in Section 2.1.2. Cells were fixed in ice cold methanol (Fischer Scientific, Loughborough, UK) at -20 °C for 15 minutes. Following fixation, cells were washed with PBS supplemented with 0.5 % (v/v) Tween 20 (PBST), and then blocked in PBS supplemented with 1 % (w/v) BSA. Cells were then washed with PBST, and probed with primary antibodies diluted in PBS supplemented with 1 % (w/v) BSA, overnight at 4 °C. The following antibodies were used: eIF2Bα (1:25 dilution, 18010-1-AP; Proteintech, Manchester, UK), eIF2Bβ (1:25 dilution, 11034-1-AP; Proteintech, Manchester, UK), eIF2Bδ (1:50 dilution, sc-271332; Santa Cruz Biotechnology, California, USA), eIF2Bγ (1:50 dilution, sc-137248; Santa Cruz, California, USA), eIF2Bγ (1:100 dilution, 11296-2-AP, Proteintech, Manchester, UK), eIF2Bε (1:500 dilution, ARP61329_P050; Aviva Systems Biology, San Diego, USA), eIF2α (1:20 dilution, FL-315 sc-11386; Santa Cruz Biotechnology, California, USA), phospho-eIF2α (ser51) (1:100 dilution, ab32157; Abcam, Cambridge, UK), myc (1:100 diltuion, ab18185, Abcam, Cambridge, UK), G3BP (1:100 dilution, ab56574, Abcam, Cambridge, UK), eIF3b (1:100 dilution, ab40799, Abcam, Cambridge, UK), polyubiquitinylated conjugates; FK1 (1:100 dilution, BML-PW8805, Enzo Life Sciences, Exeter, UK). Following primary antibody incubation, cells were washed with PBST and then probed with an appropriate AlexaFLuor conjugated secondary antibody (Fisher Scientific, Loughborough, UK), diluted in PBS supplemented with 1 % (w/v) BSA, for 1 hour at room temperature. Cells were then washed with PBST and mounted using VECTASHIELD HardSet Antifade Mounting Medium with DAPI (Vector Laboratories, California, USA). Cells were viewed on a Zeiss LSM 510 or Zeiss LSM 800 confocal microscope.

2.5 Confocal Microscopy

2.5.1 Zeiss LSM 510

The LSM 510 confocal was used with Zeiss 2009 software. All samples were imaged using a 40 X plan-apochromat oil objective. In order to image fluorophores excited at

488 nm and 568 nm, an argon laser with a maximum output of 25 mW at 55 % laser transmission was used. Fluorophores excited at 633 nm were imaged using a HeNe laser with a maximum output at 5mW at 100 % laser transmission.

2.5.2 Zeiss LSM 800

The LSM 800 confocal was used with Zen Blue software. All samples were imaged using a 40 X plan-apochromat oil objective, except in the case of Airyscan super resolution imaging where a 63 X plan-apochromat oil objective was used. To image DAPI staining a 405 nm diode laser with a maximum output of 5 mW was used. For imaging of fluorophores excited at 488 nm, a 488 nm diode laser with a maximum output of 10 mW was used. In order to image fluorophores excited at 633 nm, a 640 nm diode laser with a maximum output of 5 mW was used. All lasers were used at 0.2 % laser transmission.

2.5.3 FRAP analysis

2.5.3.1 Imaging

FRAP experiments performed for Chapter 3, Chapter 4 and Section 5.2.5 of Chapter 5 were carried out on the LSM 510 confocal microscope. Bleaching was carried out with 23 iterations at 100 % laser power (488 nm argon laser). An image was captured before bleaching and then after bleaching, 12 images were captured for 589.82 msec. For Chapter 3 FRAP experiments, a 600 msec interval between images was carried out. These timings were optimised to better represent the recovery period. For the FRAP experiments performed for Chapter 4 and Chapter 5, Section 5.2.5, images were captured without an interval. FRAP experiments performed for all other sections of Chapter 5 were carried out on the LSM 800. Bleaching was carried out with 23 iterations at 100 % laser power (488 nm diode laser). An image was captured before bleaching and then after bleaching, 48 images were captured for 118 msec, with no interval between images.

2.5.3.2 Analysis

Pre-bleach, bleach and recovery images from each experiment were analysed in accordance to the methodology by Campbell and Ashe (2007). FRAP curves were fitted using GraphPad Prism software. The data was entered into a XY table and plotted. The

data was fitted to a one phase association model (below) where 'y_0' is the y value when x is zero, 'Plateau' is the y value at infinite values of x and 'K' is the rate constant. The data was fitted using nonlinear regression.

$$y = y_0 + (Plateu - y_0).(1 - e^{(-K.x)})$$

The percentage of eIF2 recovery was determined as the mobile phase of the recovery curve represented as the plateau of the FRAP recovery curves.

2.6 Analysing populations of eIF2B bodies

2.6.1 Calculating percentages of different sized bodies

Using confocal microscopy, different size populations of eIF2B bodies were observed. In order to categorise these bodies by size, Image J software was used to measure the area of the bodies. Scale bars were used to set the number of pixels per µm and the freehand line tool was used to draw around the eIF2B bodies in order to calculate the area. Three categories were determined, large bodies; ≥10 µm^2, medium bodies; ≥ 3 µm^2 ≤ 9.99 µm^2 and small bodies ≤ 2.99 µm^2. Having determined the size categories for the different populations of eIF2B bodies, counts were performed by eye using the images of each sized body that had been measured on image J as a reference. In order to minimise human error, for all counts at least 50 cells were analysed and counts were performed blind. For each experiment, the number of bodies that had been counted were converted into percentages and graphs were plotted using GraphPad Prism software.

2.6.2 Determining co-localisation of antibody staining with eIF2B bodies

eIF2B bodies were counted as described in Section 2.6.1. eIF2B bodies were classed as positive for co-localisation when the eIF2B body signal and antibody signal overlapped completely.

2.7 Statistical analysis

In order to determine statistically significant differences within the groups of data presented in this thesis, all data was first subject to a shapiro wilk test for normality. Data was considered parametric when $p < 0.05$. All groups of data were found to be non-parametric. For the comparison of three or more groups of data a Kruskal-Wallis

test was performed followed by a Conover Inman post-hoc test, using StatsDirect Statistical Analysis software. Differences in data were considered significant when $p < 0.05$.

3. Cellular localisation of mammalian eIF2B subunits

3.1 Introduction

The cytoplasm of a cell is highly organised and contains numerous intracellular structures. The process of translating protein is highly energy consuming and thus requires tight regulation within the cell. The accumulation and concentration of specific cellular components at precise foci allows for compartmentalisation of the various biochemical reactions that take place in the cytosol, allowing cells to function in an energy efficient manner. A number of translation associated factors have been well documented to accumulate into cytoplasmic granules, and these granules can function as sites of translational control.

Under normal cellular conditions the translation of mRNA transcripts is initiated following the recruitment of the 80 S ribosome to an appropriate start codon, in a process facilitated by a number of eIFs (Chapter 1, Section 1.2.1). In response to conditions of cellular stress, global translation is downregulated to preserve energy and the translation of specific stress responsive mRNAs is upregulated to promote homeostasis in a process known as the ISR (Chapter 1, Section 1.3.1). One of the best characterised classes of translation factor containing granules are SGs and the assembly of SGs is driven by the ISR. The ISR is activated by the phosphorylation of eIF2α at serine 51, by a family of eIF2α kinases that serve as sensors to environmental stress (Donnelly *et al*., 2013). This phosphorylation of eIF2 results in the inhibition of eIF2B activity. eIF2B acts as a GEF for eIF2 and is required within the cell to restore levels of eIF2-GTP following successive rounds of translation (Chapter 1, Section 1.4). eIF2-GTP is required for efficient recruitment of the 80 S ribosome to an appropriate start codon and thus the reduced availability of eIF2-GTP stalls translation initiation within the cell. Preinitiation complexes and their associated mRNA transcripts are assembled into SGs (Kedersha *et al*., 2002) by specific RNA-binding proteins including G3BP (Tourrière *et al*., 2003) (Chapter 1, Section 1.3.1.1.1). SGs function as a reservoir of partly translated mRNA molecules that can return to the translating pool upon restoration of cellular homeostasis (Kedersha and Anderson, 2002). In cases where high levels of cellular stress remain, mRNA transcripts are degraded by the cell. P-bodies are another class of cytoplasmic granule that contain translation associated factors. Like SGs, P-bodies form during conditions of cellular stress (although

phosphorylation of eIF2α is not necessary) and contain translationally repressed mRNAs. P-bodies however also contain mRNA decay machinery and were initially hypothesised to be cellular sites of mRNA decay (Kedersha *et al*., 2005; Sheth and Parker, 2003). More recent studies have challenged this hypothesis through demonstrating that mRNA molecules present in P-bodies can return to the translating pool (Brengues *et al*., 2005) and that mRNA decay can occur in the absence of P-bodies (Decker *et al*., 2007; Eulalio *et al*., 2007). The exact role of P-bodies is still unclear, but it is currently hypothesised they function as storage granules (Luo *et al*., 2018).

eIF2B bodies are another class of translation associated cytoplasmic granules that have been shown to exist in yeast (Campbell, Hoyle and Ashe, 2005; Noree *et al.*, 2010; Taylor *et al.*, 2010; Moon and Parker, 2018). eIF2B bodies are less well characterised when compared to SGs and currently eIF2B and eIF2 are the only known components (Campbell *et al*., 2005; Noree *et al*., 2010; Taylor *et al*., 2010). The Ashe lab group first identified eIF2B bodies in *Saccharomyces cerevisiae* (*S*. c*erevisiae*) and demonstrated that eIF2B is a stable component of the body whereas the association of eIF2 is dynamic (Campbell *et al*., 2005). Furthermore, eIF2 moves through the bodies at a rate that correlates to eIF2B GEF activity suggesting that the bodies are sites of eIF2 guanine nucleotide exchange (Campbell *et al*., 2005). It was predicted that if these bodies were sites of eIF2B GEF activity they may have an important role in translation initiation. Seemingly it was demonstrated that eIF2B bodies exist in readily translating cells, and that inhibition of translation resulted in the dispersal of the eIF2B bodies (Campbell *et al*., 2005). A more recent study from the Parker group demonstrated eIF2B body assembly to only occur in response to cellular stress conditions in *S*.c*erevisiae* (Moon and Parker, 2018). These results are very much contradictory and further research into the role of eIF2B bodies during conditions of cellular stress may provide a clearer insight into their role.

Mutations in eIF2B lead to the neurological disorder VWM (Leegwater *et al*., 2001; van der Knaap *et al*., 2002). The functional impact of eIF2B mutations correlate poorly with the severity of the patient phenotype (Liu *et al*., 2011) (Chapter 1, Section 1.5.2). eIF2B bodies are yet to be characterised in higher eukaryotes. Characterising the cellular localisation of eIF2B could offer further insight into the possible disease mechanisms of VWM. This chapter aims to explore eIF2B localisation patterns in mammalian cells. The

pathological effects of VWM are predominately observed within patient glial cells and therefore these cell types are of particular interest for exploring eIF2B localisation. The ε subunit of eIF2B has previously been documented to localise to SGs (Kimball *et al*., 2003) and therefore eIF2B localisation in relation to SGs and P-bodies will also be explored.

It can be hypothesised that as in yeast, eIF2B will localise to discrete cytoplasmic bodies in mammalian cells. In order to determine if eIF2B localises to cytoplasmic bodies in mammalian cells, a plasmid encoding eIF2Bε C-terminally tagged with GFP will be expressed in the glial cell line U373 (astrocytoma cells). The cellular localisation of the eIF2Bε-GFP construct will be analysed by confocal microscopy. To determine the localisation of the other eIF2B subunits in relation to eIF2Bε-GFP, cells expressing eIF2Bε-GFP will be fixed and ICC will be performed using primary antibodies directed against the other eIF2B subunits. Primary antibody signals will be detected by fluorescently tagged secondary antibodies and the localisation of these signals analysed by confocal microscopy. In order to investigate eIF2B localisation in relation to SGs and P-bodies, cells expressing eIF2Bε-GFP will be fixed and ICC will be performed using primary antibodies directed against key components of SGs and P-bodies. Primary antibody signals will be detected by fluorescently tagged secondary antibodies and the localisation of these antibody signals analysed by confocal microscopy.

3.2 Results

3.2.1 Transiently expressed eIF2Bε localises to a heterogeneous population of different sized cytoplasmic bodies in mammalian cells

In order to study the cellular localisation of mammalian eIF2B in live cells, eIF2Bε bearing a C-terminal GFP tag was transiently transfected into the astrocytoma cell line, U373. This cell line was chosen as glial cells are the cell type predominately affected in VWM (Bugiani *et al*., 2018; Dooves *et al*., 2016). Western blot analysis was used to confirm the expression of the eIF2Bε-GFP construct (Figure 3.1A). Expression of eIF2Bε has been shown to stabilise expression levels of eIF2Bγ within the cell (Wortham *et al*., 2016). To provide an indication as to whether the overexpression of eIF2Bε-GFP affected expression levels of eIF2Bγ dot blot analysis was performed on transfected and untransfected cells. Normalisation of the dot blot signal indicated that eIF2Bγ expression was not increased in transfected cells (Figure 3.1B). Confocal analysis of cells expressing eIF2Bε-GFP revealed that eIF2Bε-GFP either adopted a dispersed cytoplasmic localisation (11 % of cells) or localised to cytoplasmic bodies which were termed eIF2B bodies (89 % of cells) (Figure 3.2). The size and abundance of the eIF2B bodies within individual cells varied. To better understand the pattern of eIF2Bε-GFP localisation, the eIF2B bodies were classified by size: large (≥10 μm^2), medium (≥ 3 μm^2 ≤ 9.99 μm^2) or small (≤ 2.99 μm^2). Cells exhibiting 4 phenotypes for eIF2Bε-GFP localisation were observed: eIF2Bε-GFP localised to only large (Figure 3.2B i), only medium (Figure 3.2B ii) or only small (Figure 3.2B iii) or a mixture of large medium or small eIF2B bodies (Figure 3.2B iv). To determine the abundance of these different localisation phenotypes counts were carried out across 100 cells expressing eIF2Bε-GFP (Figure 3.2C i). Cells displaying eIF2Bε-GFP localised to a mixture of large, medium or small eIF2B bodies were the predominant phenotype (60 %), and contained on average 1 large, 2 medium and >15 small eIF2B bodies (Figure 3.2C ii). The second most frequent phenotype was cells displaying eIF2Bε-GFP localised to only small eIF2B bodies (25 %). Cells displaying eIF2Bε-GFP localised to only medium eIF2B bodies were less frequent again (4 %), and cells that displayed eIF2Bε-GFP localised to only large eIF2B bodies were the least frequent (1 %).

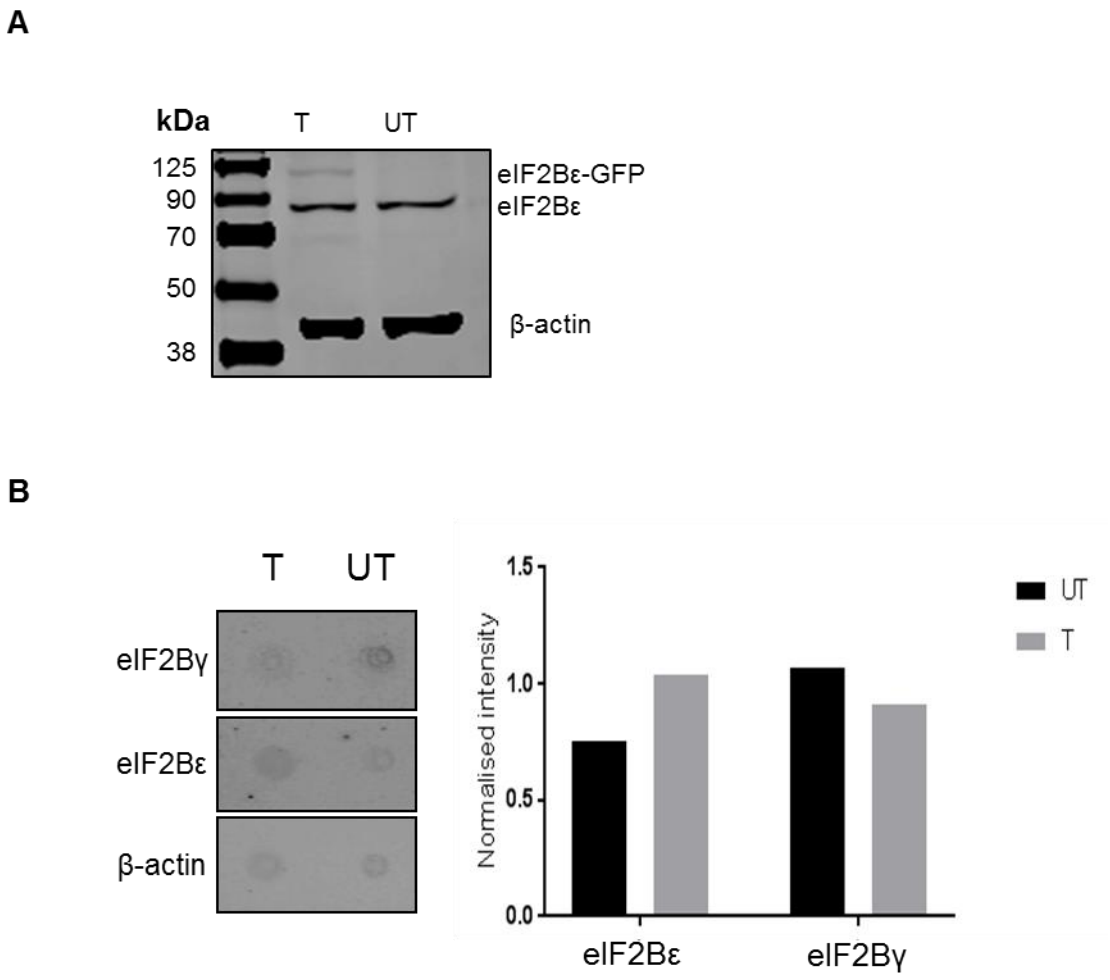

Figure 3.1 Expression levels of eIF2Bε-GFP in U373 cells and its influence on eIF2Bγ expression levels.

(A) Western blot analysis of eIF2Bε expression in U373 cells, untransfected or transfected with eIF2Bε-GFP. β-actin has been included as a loading control. (B) U373 cells transfected with eIF2Bε-GFP were sorted into transfected and non-transfected populations by fluorescence-activated cell sorting (FACs). Expression levels of eIF2Bε and eIF2Bγ were examined by dot blot analysis.

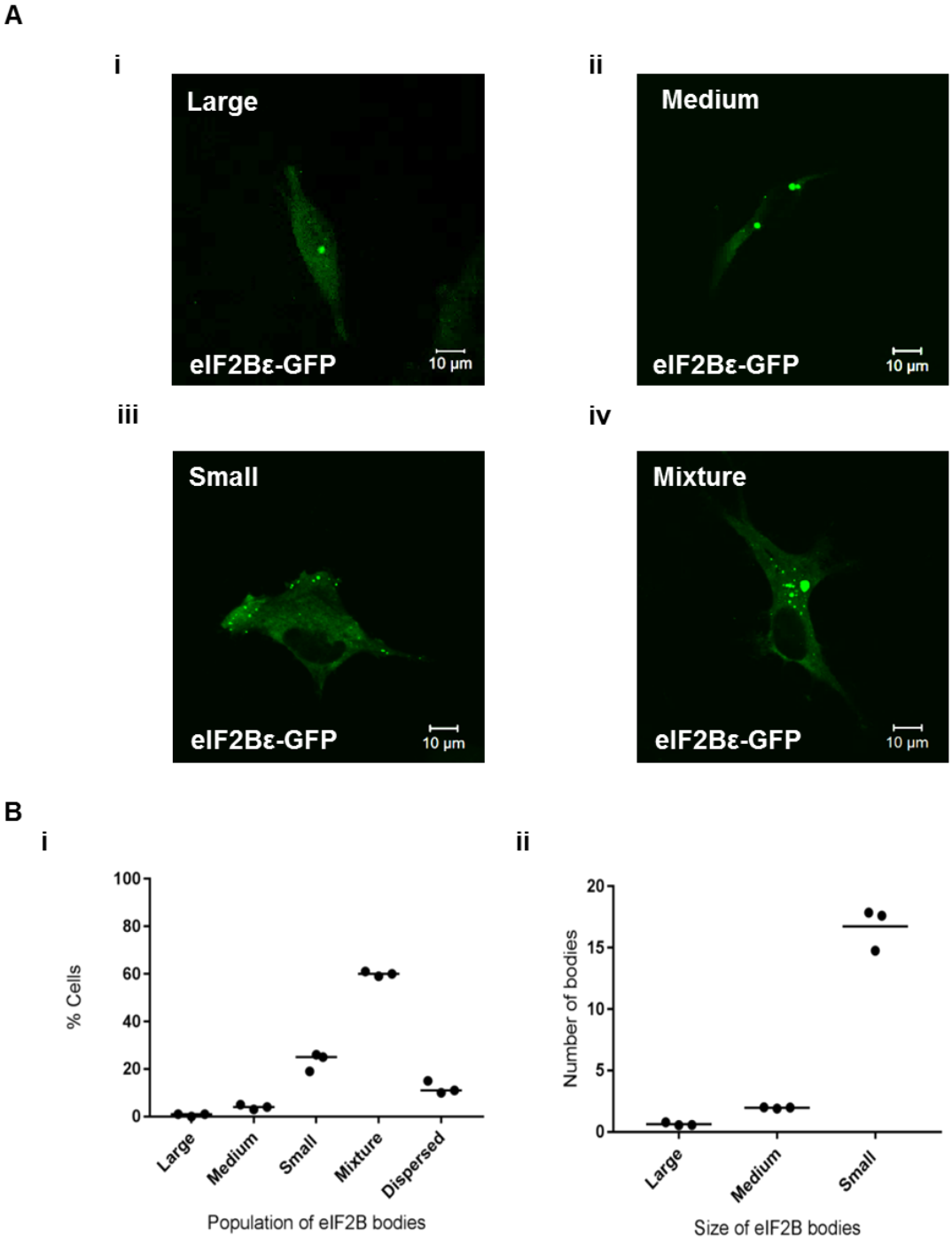

Figure 3.2 eIF2Bε-GFP expressed in U373 cells localises to cytoplasmic bodies.
(A) Live cell confocal images of U373 cells expressing eIF2Bε-GFP localised to (i) only large (≥10 µm^2), (ii) only medium (≥ 3 µm^2 ≤ 9.99 µm^2), (iii) only small (≤ 2.99 µm^2), or (iv) a mixture of large, medium or small eIF2B bodies. (B) (i) The median percentage of cells, in a population of 100 cells, expressing eIF2Bε-GFP dispersed throughout the cytoplasm or localised to only large, only medium, only small or a mixture of large, medium or small eIF2B bodies (n=3), (ii) within the population of cells containing a mixture of large, medium or small eIF2B bodies, the mean number of large, medium and small eIF2B bodies.

3.2.2 The GFP tag is not responsible for the observed localisation of eIF2Bε-GFP to cytoplasmic bodies

In order to ensure that the observed localisation of eIF2Bε-GFP was not caused by aggregation of the GFP tag, localisation of transiently expressed eIF2Bε with an alternative C-terminal tag (myc-tag) was also observed in U373 cells. U373 cells were transiently transfected with eIF2Bε-myc, fixed in methanol and immunocytochemistry (ICC) was performed with an anti-myc-tag antibody. Confocal microscopy revealed that similarly to eIF2Bε-GFP (Figure 3.2), eIF2Bε-myc was either dispersed within the cytoplasm of cells or localised to cytoplasmic bodies (Figure 3.3). The cytoplasmic bodies varied in size and number between cells and populations of cells with eIF2Bε-myc localised to only large (≥10 μm^2) (Figure 3.3A i), only medium (≥ 3 μm^2 ≤ 9.99 μm^2) (Figure 3.3A ii), only small (≤ 2.99 μm^2) (Figure 3.3A iii) or a mixture of large, medium or small (Figure 3.3A iv) eIF2B bodies were observed. Counts were carried out across a population of 50 transfected cells to determine the percentage of each of the observed localisation phenotypes (Figure 3.3B i). eIF2Bε-myc was dispersed throughout the cytoplasm in 34 % of cells. In the remaining 66 % of cells eIF2Bε-myc localised to eIF2B bodies and showed a similar localisation pattern to that observed for eIF2Bε-GFP. 34% of cells contained a mixture of large, medium or small eIF2B bodies, and on average these cells contained 0 large, 2 medium and 13 small eIF2B bodies (Figure 3.3B ii). 22 % of cells contained only small eIF2B bodies, 8 % of cells contained only medium eIF2B bodies and 2 % of cells contained only large eIF2B bodies.

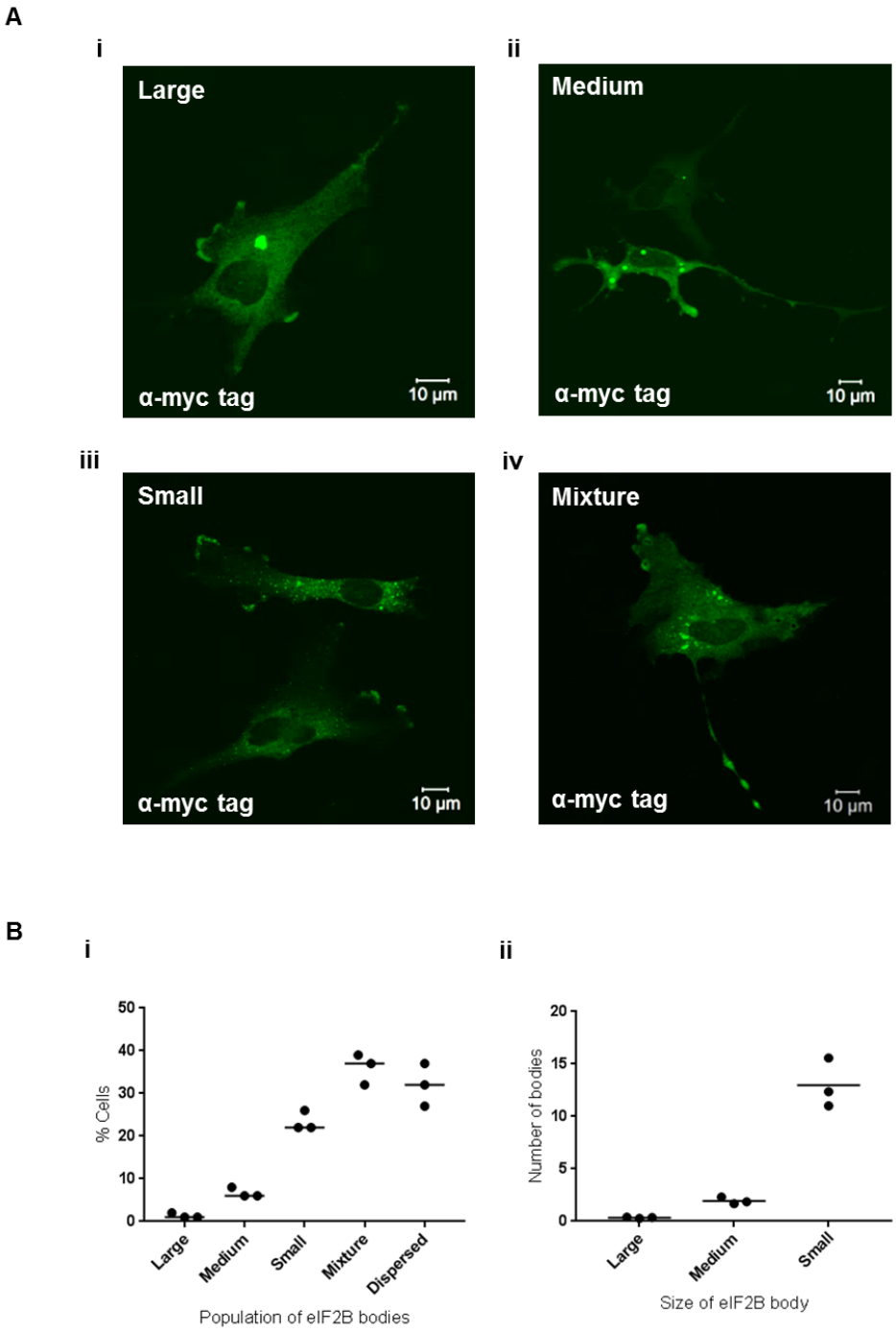

Figure 3.3 eIF2Bε-myc expressed in U373 cells localises to cytoplasmic bodies and shows a similar localisation pattern to eIF2Bε-GFP expressed in U373 cells.
U373 cells were transfected with eIF2Bε-myc, fixed in methanol and subjected to ICC with a primary anti-myc-tag antibody. Antibody staining was visualised using an appropriate secondary antibody conjugated to Alexa Fluor 488. (A) Confocal images of U373 cells expressing eIF2Bε-myc, (i) showing localisation to only large (≥10 µm^2), (ii) only medium (≥ 3 µm^2 ≤ 9.99 µm^2), (iii) only small (≤ 2.99 µm^2), or (iv) a mixture of large, medium or small eIF2B bodies. (B) (i) The median percentage of cells, in a population of 100 cells, exhibiting eIF2Bε-myc dispersed throughout the cytoplasm or localised to, only large, only medium, only small, or a mixture of different sized eIF2B bodies (n=3), (ii) within the population of cells containing a mixture of different sized eIF2B bodies, the mean number of large, medium and small eIF2B bodies is shown.

3.2.3 Endogenous eIF2B subunits localise to cytoplasmic bodies in mammalian cells

In order to confirm the observed localisation of eIF2B to cytoplasmic bodies was not a result of the eIF2Bε overexpression, the cellular localisation of endogenous eIF2B subunits was investigated. U373 cells were fixed in methanol and ICC was carried out individually for each of the five subunits of eIF2B. All subunits of eIF2B were found to localise to cytoplasmic bodies, of varying size and number (Figure 3.4).

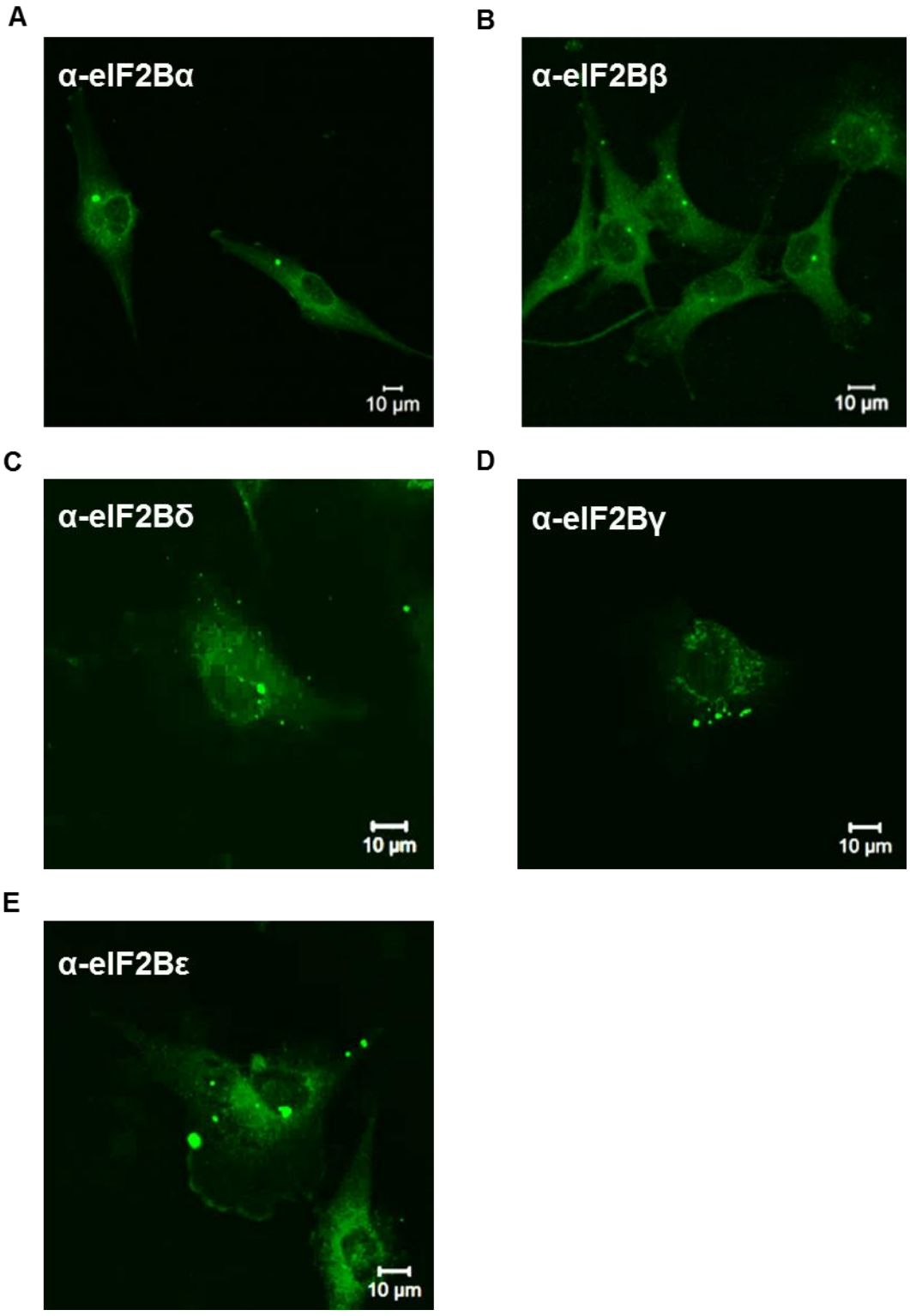

Figure 3.4 Confocal images of endogenous eIF2B subunits localising to cytoplasmic bodies in U373 cells.

U373 cells were fixed in methanol and subject to ICC with (A) anti-eIF2Bα, (B) anti-eIF2Bβ, (C) anti-eIF2Bδ, (D) anti-eIF2Bγ or (E) anti-eIF2Bε. Primary antibodies were visualised using appropriate secondary antibodies conjugated to Alexa Fluor 488 and imaged using confocal microscopy.

3.2.4 eIF2Bε-GFP bodies do not co-localise with polyubiquitin

Overexpression of proteins can become toxic to the cell. If protein levels reach a toxic level the cell may direct these proteins into cytoplasmic aggregates which are targeted for degradation by the proteasome (Bolognesi and Lehner, 2018). Due to the large size of the observed eIF2Bε-GFP bodies (sometimes ≥ 10 μM^2) it was important to ensure that these bodies were not aggregates of protein targeted for degradation. The cell targets proteins for degradation by tagging the proteins with ubiquitin. While ubiquitination can target proteins for a number of functions, only the addition of poly-ubiquitin directs proteins for degradation by the proteasome (Kleiger and Mayor 2014). In order to provide an insight as to whether the eIF2Bε-GFP bodies observed in this study were polyubiquitinated immunofluorescence analysis was performed. U373 cells expressing eIF2Bε-GFP were fixed in methanol and ICC was performed using a poly-ubiquitin FK1 antibody (Danielson and Hope, 2013). eIF2B bodies did not co-localise with the poly-ubiquitin antibody signal suggesting that they are not protein aggregates targeted for degradation (Figure 3.5).

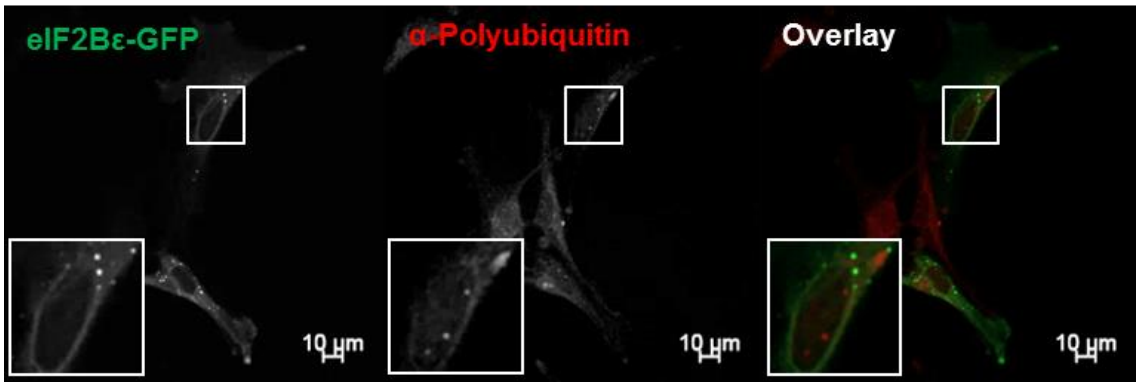

Figure 3.5 eIF2B bodies do not co-localise with poly-ubiquitin.
Confocal images of U373 cells transfected with eIF2Bε-GFP, fixed in methanol and subject to ICC with a primary anti-poly-ubiquitin antibody. Primary antibody signals were visualised using an appropriate Alexa Fluor 633 conjugated secondary antibody.

3.2.5 eIF2Bε-GFP bodies are distinct from stress granules and P-bodies

Previously eIF2Bε has been shown to localise to SGs in mammalian cells (Kimball *et al*., 2003). It was therefore important to determine whether the eIF2Bε-GFP bodies identified in this study were spatially discrete from SGs. Additionally, P-bodies are another class of cytoplasmic granule that contain translation associated factors (Luo *et al*., 2018). Although eIF2B has not previously been associated with P-bodies, the localisation of P-bodies was also analysed to determine if any co-localisation existed between P-bodies and the eIF2Bε-GFP bodies identified. U373 cells expressing eIF2Bε-GFP were exposed to either ER stress, through treatment with Tg, or to oxidative stress, through treatment with SA, in order to induce SG or P-body assembly. Cells were then fixed in methanol and subject to ICC with primary antibodies to SG and P-body specific markers. Confocal microscopy confirmed that eIF2B bodies are spatially distinct from G3BP containing SGs (Figure 3.6), eIF3B containing SGs (Figure 3.7) and GW182 containing P-bodies (Figure 3.8).

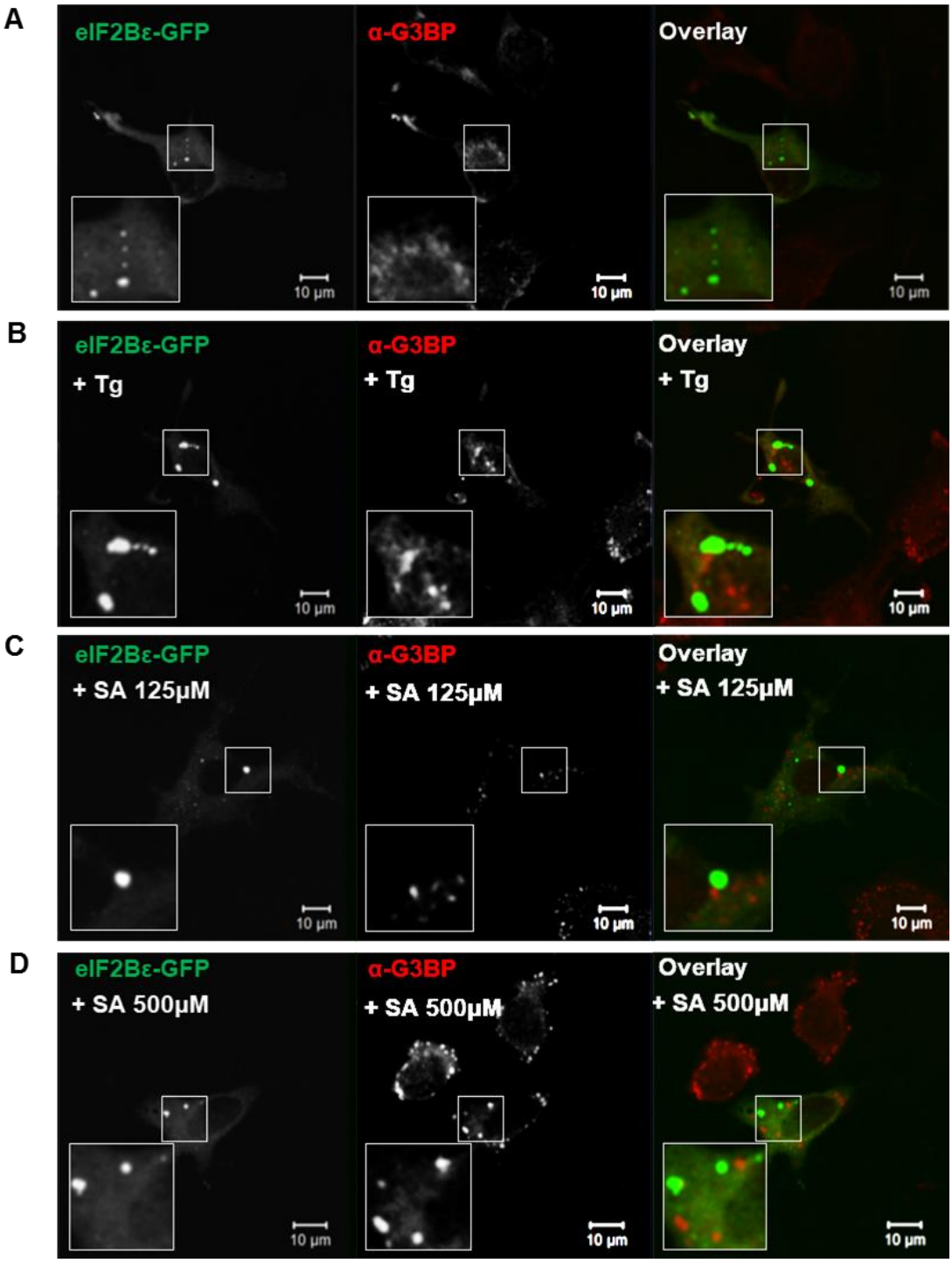

Figure 3.6 eIF2Bε-GFP bodies do not co-localise with G3BP containing stress granules. U373 cells were transfected with eIF2Bε-GFP and either (A) untreated, or treated with (B) 1 µM Tg, (C) 125 µM SA or (D) 500 µM SA. Cells were fixed in methanol, and subject to ICC with a primary anti-G3BP antibody. The anti-G3BP antibody was visualised using an appropriate Alexa Fluor 633 conjugated secondary antibody and imaged using confocal microscopy.

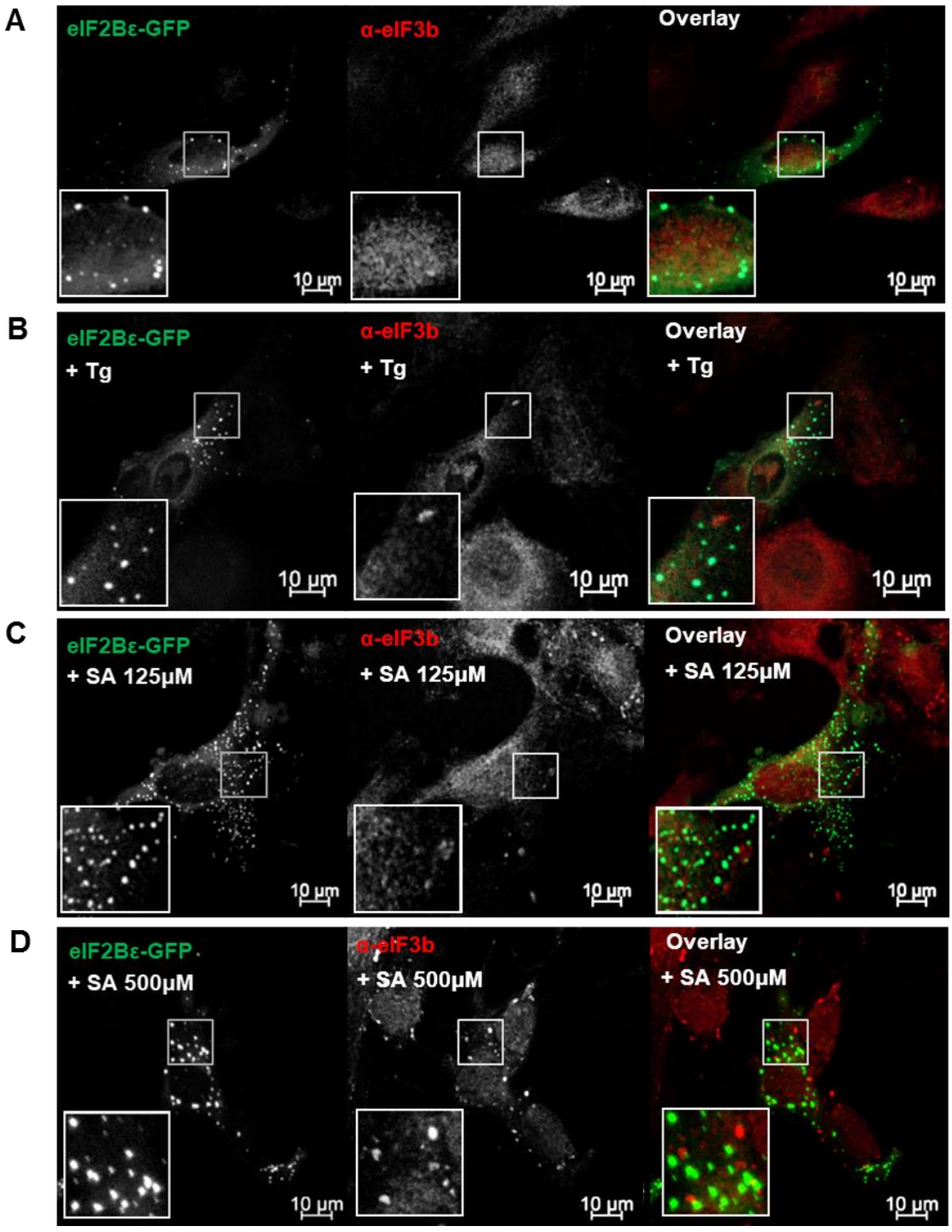

Figure 3.7 eIF2Bε-GFP bodies do not co-localise with eIF3b containing SGs.
U373 cells were transfected with eIF2Bε-GFP and either (A) untreated, or treated with (B) 1 μM Tg, (C) 125 μM SA or (D) 500 μM SA. Cells were fixed in methanol, and subject to ICC with a primary anti-eIF3b antibody. The anti-eIF3b antibody was visualised using an appropriate Alexa Fluor 633 conjugated secondary antibody and imaged using confocal microscopy.

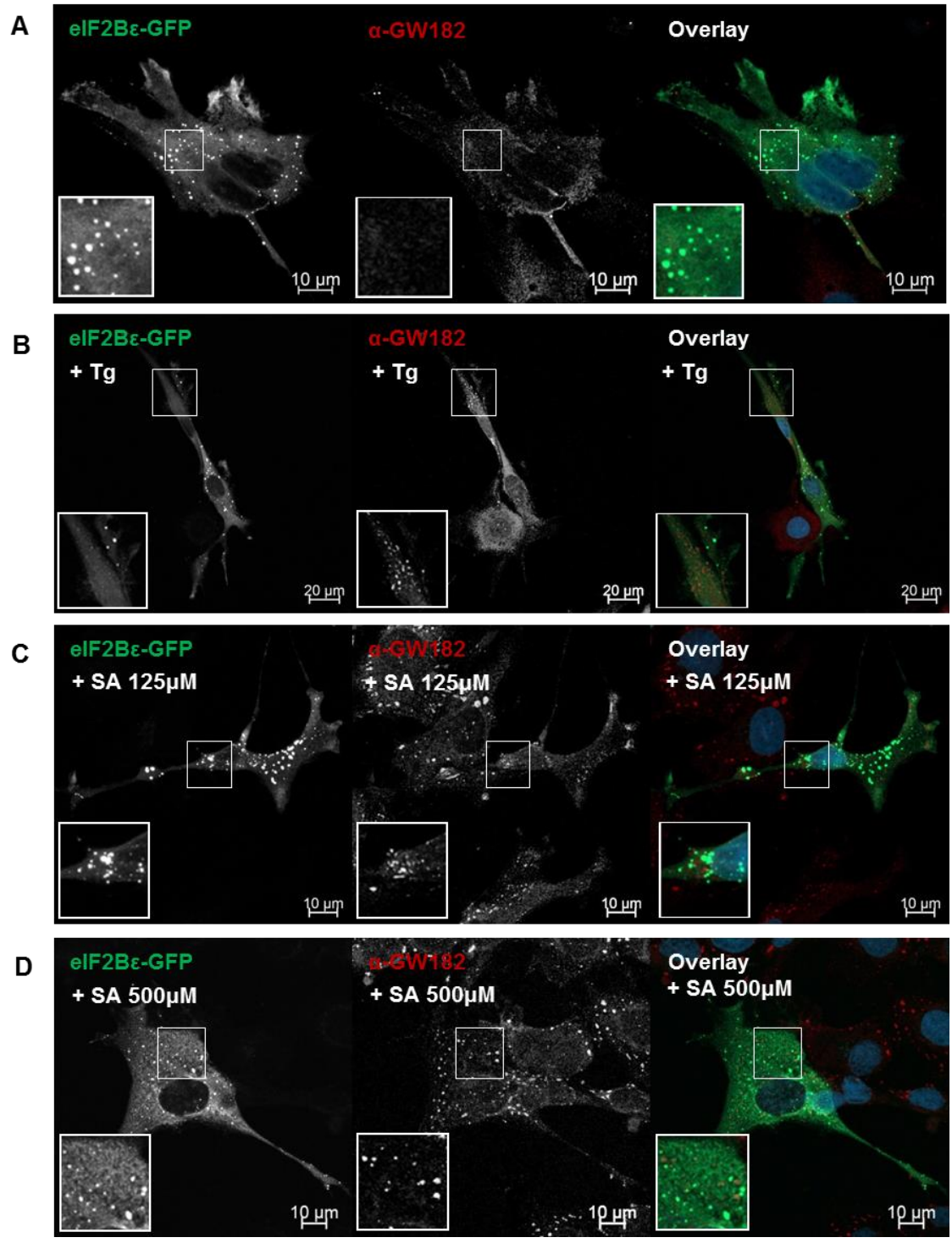

Figure 3.8 eIF2Bε-GFP bodies do not co-localise with GW182 containing P-bodies. U373 cells were transfected with eIF2Bε-GFP and either (A) untreated, or treated with (B) 1 μM Tg, (C) 125 μM SA or (D) 500 μM SA. Cells were fixed in methanol, and subject to ICC with a primary anti-GW182 antibody. The anti-GW182 antibody was visualised using appropriate Alexa Fluor 633 conjugated secondary antibody and imaged using confocal microscopy.

3.2.6 eIF2Bε-GFP localises to cytoplasmic bodies in primary human astrocytes

Studying the cellular localisation of eIF2B may provide a tool to assess the functional impact that VWM mutations have on eIF2B function. Astrocytes are one of the main cell types affected by VWM (Bugiani *et al*., 2018; Dooves *et al*., 2016). Having determined that transiently expressed eIF2Bε localises to eIF2B bodies in the human astrocytoma cell line, U373, the cellular localisation of eIF2Bε in primary human astrocytes was investigated. eIF2Bε-GFP was transiently transfected into primary human astrocytes and the localisation was observed by confocal microscopy. eIF2Bε-GFP was found to either localise to a number of different sized eIF2B bodies (75 % of cells) or remain dispersed throughout the cell cytoplasm (15 % of cells) (Figure 3.9). To better characterise the localisation of eIF2Bε-GFP to eIF2B bodies, counts were carried out to determine the percentage of cells that displayed eIF2Bε-GFP localised to only large (≥10 μm^2), only medium (≥ 3 μm^2 ≤ 9.99 μm^2), only small (≤ 2.99 μm^2) or a mixture of large, medium or small eIF2B bodies (Figure 3.9B i). Cells displaying eIF2Bε-GFP localised to only small eIF2B bodies were found to be the predominant phenotype (41 % of cells). Cells displaying eIF2Bε-GFP localised to a mixture of different sized eIF2B bodies were the second most frequent phenotype (35 % of cells), with cells on average containing contained 1 large, 1 medium and 25 small eIF2B bodies (Figure 3.9B ii). Cells displaying eIF2Bε-GFP localised to only medium eIF2B bodies were the third most frequent phenotype (8 % of cells) and cells that displayed eIF2Bε-GFP localised to only large eIF2B bodies were the least frequent phenotype (5 % of cells).

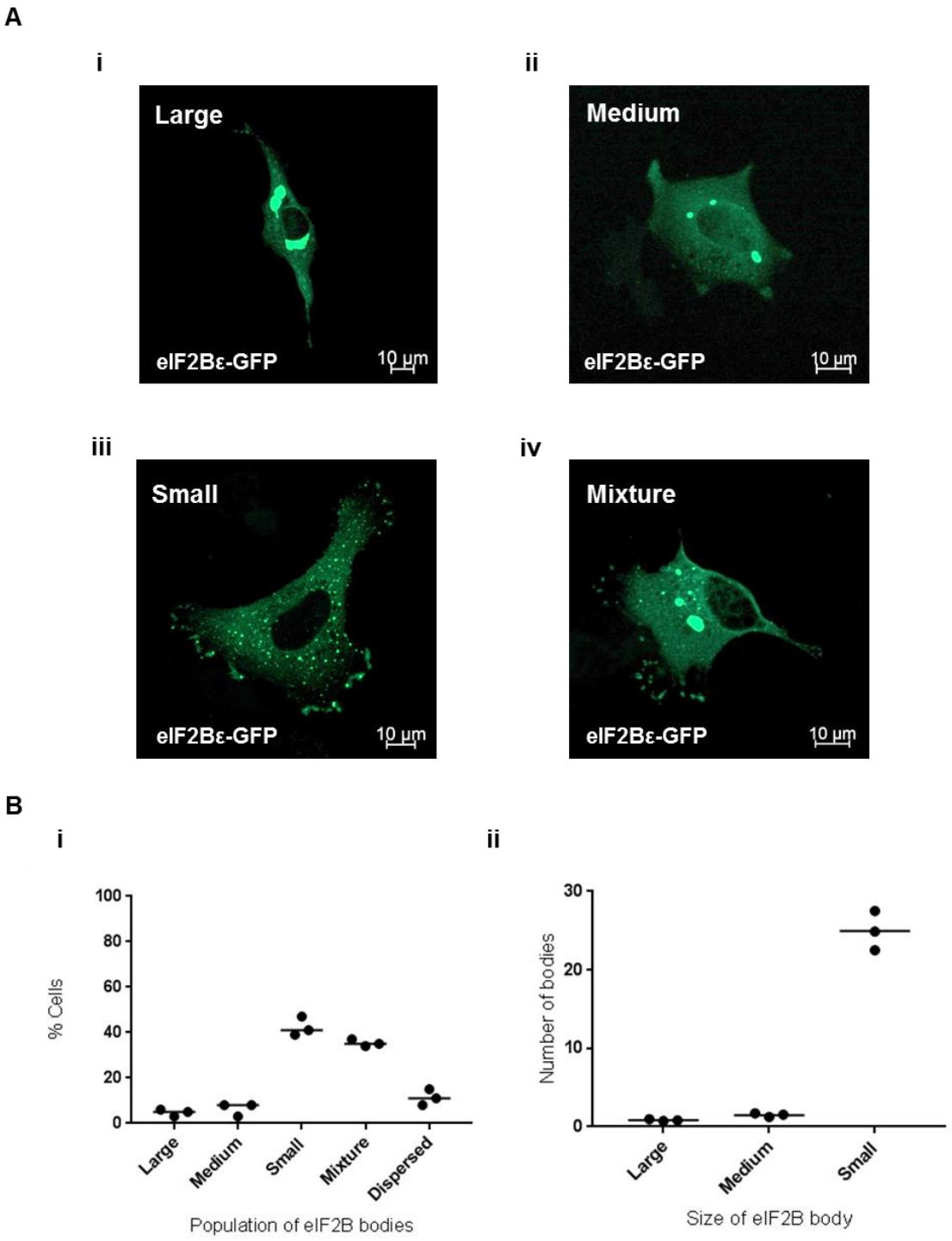

Figure 3.9 eIF2Bε-GFP localises to cytoplasmic bodies in primary human astrocytes. (A) Live cell confocal images of primary astrocyte cells transiently expressing eIF2Bε-GFP, (i) showing localisation to only large (≥10 µm^2), (ii) only medium (≥ 3 µm^2 ≤ 9.99 µm^2), (iii) only small (≤ 2.99 µm^2), and (iv) a mixture of large, medium or small eIF2B bodies. (B) (i) The median percentage of cells, in a population of 100 cells, exhibiting eIF2Bε-GFP dispersed throughput the cytoplasm or, localised to only large, only medium, only small or a mixture of different sized eIF2B bodies (n=3), (ii) within the population of cells containing a mixture of different sized eIF2B bodies, the mean number of large, medium and small eIF2B bodies.

3.2.7 eIF2Bε-GFP localises to cytoplasmic bodies in various mammalian cell lines

Mutations in eIF2B have been shown to have different effects on the function of eIF2B dependent upon the cell type they are expressed in (Horzinski *et al*., 2010; Kantor *et al*., 2005). In order to determine if eIF2B bodies were a specific feature of astrocytic cells or a general feature of mammalian cells, the cellular localisation of eIF2Bε-GFP in various human cell lines was investigated. eIF2Bε-GFP was transiently expressed in liver hepatocellular carcinoma cells (HepG2), human osteosarcoma cells (MG-63), and human embryonic kidney cells (HEK293) and the cellular localisation was observed using confocal microscopy. Similarly to the localisation patterns observed in astrocytic cells, for each of the cell lines analysed, eIF2Bε-GFP was either dispersed throughout the cytoplasm (40 % of cells for HepG2, 36 % of cells for MG-63 and 46 % of cells for HEK293) or localised to a number of different sized eIF2B bodies (60 % of cells for HepG2, 64 % of cells for MG-63 and 54 % of cells for HEK293) (Figure 3.10). To better characterise the localisation of eIF2Bε-GFP to different sized eIF2B bodies within these cell lines, counts were performed. Within a population of 100 cells, the percentage of cells displaying eIF2Bε-GFP localised to only large (≥10 μm^2), only medium (≥ 3 μm^2 ≤ 9.99 μm^2), only small (≤ 2.99 μm^2) or a mixture of large, medium or small eIF2B bodies was determined. For all cell lines similar trends were observed. Cells displaying a mixture of large, medium or small eIF2B bodies was found to be the most frequently observed phenotype for each cell line (30 % for HepG2, 28 % for MG-63 and 28% for HEK293). In the case of HepG2 cells, cells displaying only small eIF2B bodies were equally as frequent (30 % of cells). For MG-63 and HEK293 cells, cells displaying only small eIF2B bodies presented as a less frequent phenotype (26 % and 22 % of cells respectively). For HEK293 cells, 6 % of cells displayed eIF2Bε-GFP localised to only medium eIF2B bodies and 2 % displayed eIF2Bε-GFP localised to only large eIF2B bodies. Cells displaying eIF2Bε-GFP localised to only large, or only medium, eIF2B bodies were not observed for HepG2 and MG-63 cells.

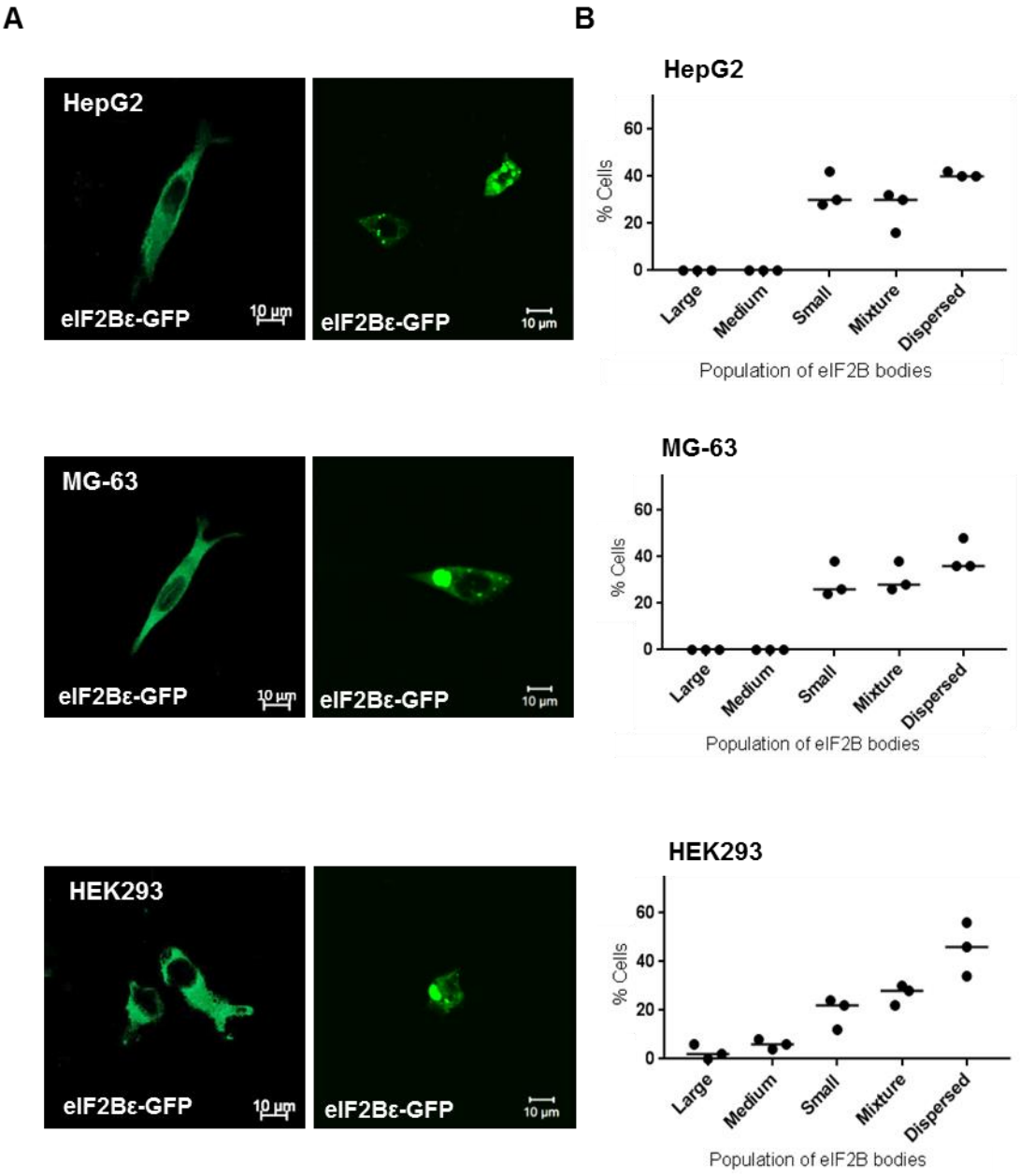

Figure 3.10 eIF2Bε-GFP localises to cytoplasmic bodies in mammalian cell lines.
(A) HepG2, MG-63 and HEK293 cells expressing eIF2Bε-GFP were observed via confocal microscopy and representative images are displayed in the panels. (B) The median percentage of cells, in a population of 100 cells, displaying eIF2Bε-GFP dispersed throughout the cytoplasm, or localised to only large (≥10 µm^2), only medium (≥ 3 µm^2 ≤ 9.99 µm^2), only small (≤ 2.99 µm^2) or a mixture of large, medium or small eIF2B bodies (n=3).

3.2.1 eIF2B(α-γ) subunits display unique localisation patterns to different sized eIF2Bε-GFP bodies in mammalian cells

Having shown that transiently expressed eIF2Bε-GFP localised to cytoplasmic bodies in mammalian cells, it was important to determine if the other subunits of eIF2B also localised to these foci. U373 cells expressing eIF2Bε-GFP were fixed in methanol and subjected to ICC with antibodies against eIF2Bα, β, δ and γ subunits individually.

Confocal microscopy revealed that eIF2Bα, β, δ and γ antibody signals co-localised with a proportion of eIF2Bε-GFP bodies (Figure 3.11). To better characterise the degree of co-localisation between eIF2Bα, β, δ or γ antibody signals and eIF2Bε-GFP bodies, counts were performed. Firstly, within a population of 50 cells, the percentage of cells that showed antibody signal co-localised to at least one eIF2Bε-GFP body was determined for each eIF2B subunit independently (Figure 3.12A). These cells were classified as displaying a degree of co-localisation between antibody signal and eIF2Bε-GFP bodies. For eIF2Bα, 52 % of cells displayed a degree of co-localisation. For eIF2Bβ, 66 % of cells displayed a degree of co-localisation. For eIF2Bδ, 78 % of cells displayed a degree of co-localisation and for eIF2Bγ 98 % of cells displayed a degree of co-localisation. The degree of co-localisation varied between subunits. This raised the question, could the size of the eIF2Bε-GFP bodies correlate with the eIF2B subunits present. To investigate this, counts were performed within the population of cells that had been found to display a degree of co-localisation between antibody signal and eIF2Bε-GFP bodies. The percentage of each sized eIF2B body (large, medium and small) that had an antibody signal co-localised was determined for each eIF2B subunit (α, β, δ, γ) (Figure 3.12B). For large eIF2Bε-GFP bodies, eIF2Bα co-localised with 87 %, eIF2Bβ co-localised with 88 %, eIF2Bδ co-localised with 94 % and eIF2Bγ co-localised with 100 %. For medium eIF2Bε-GFP bodies, eIF2Bα co-localised with 36 %, eIF2Bβ co-localised with 51 %, eIF2Bδ co-localised with 74 % and eIF2Bγ co-localised with 89 %. For small eIF2Bε-GFP bodies, eIF2Bα co-localised with 0 %, eIF2Bβ co-localised with 1 %, eIF2Bδ co-localised with 14 % and eIF2Bγ co-localised with 65 %.

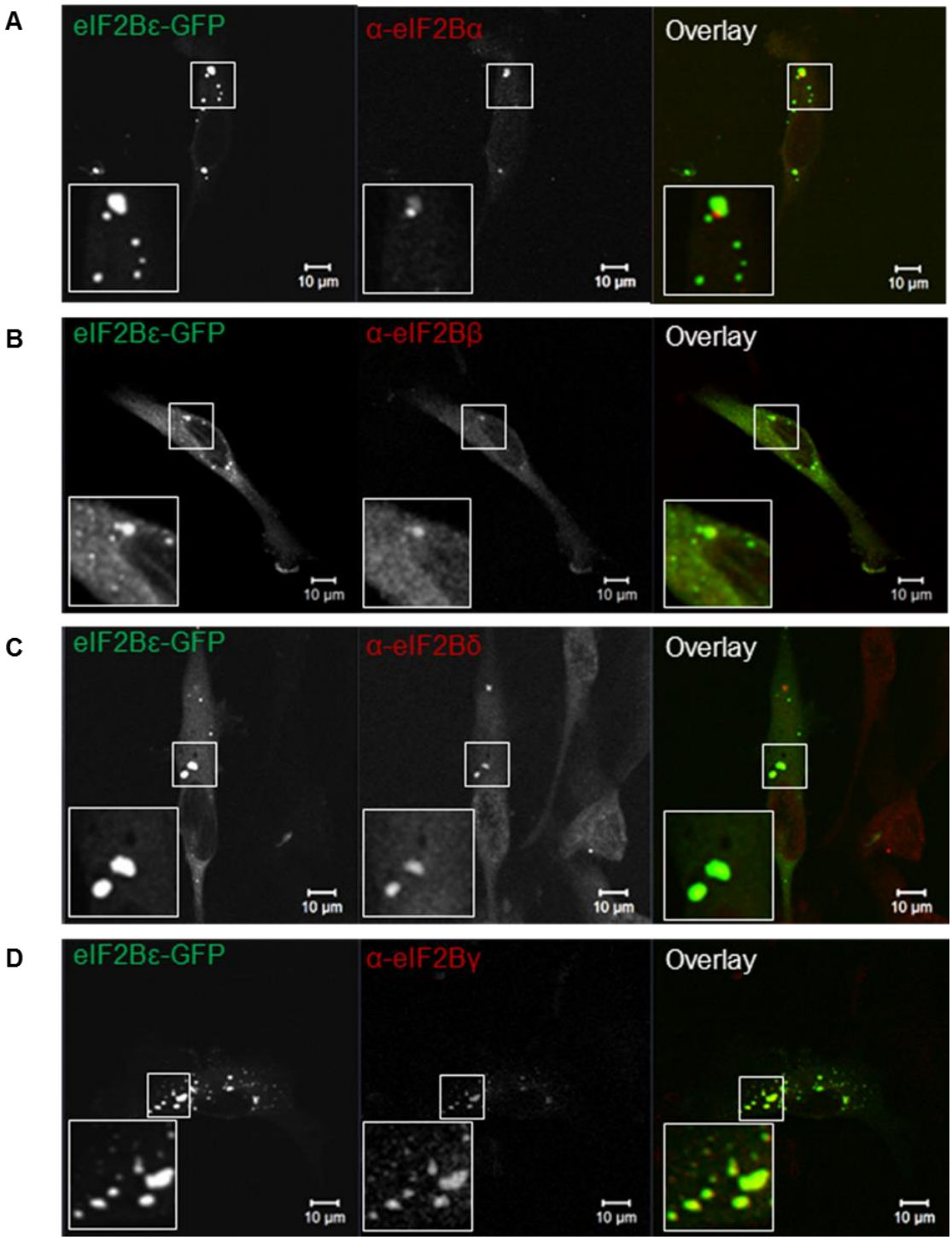

Figure 3.11 eIF2B(α-γ) subunits co-localise with eIF2Bε-GFP bodies.
Confocal images of U373 cells transfected with eIF2Bε-GFP, fixed in methanol and subject to ICC with primary (A) anti-eIF2Bα, (B) anti-eIF2Bβ, (C) anti-eIF2Bδ and (D) anti-eIF2Bγ antibodies. All antibodies were visualised using appropriate secondary antibodies conjugated to Alexa Fluor 568.

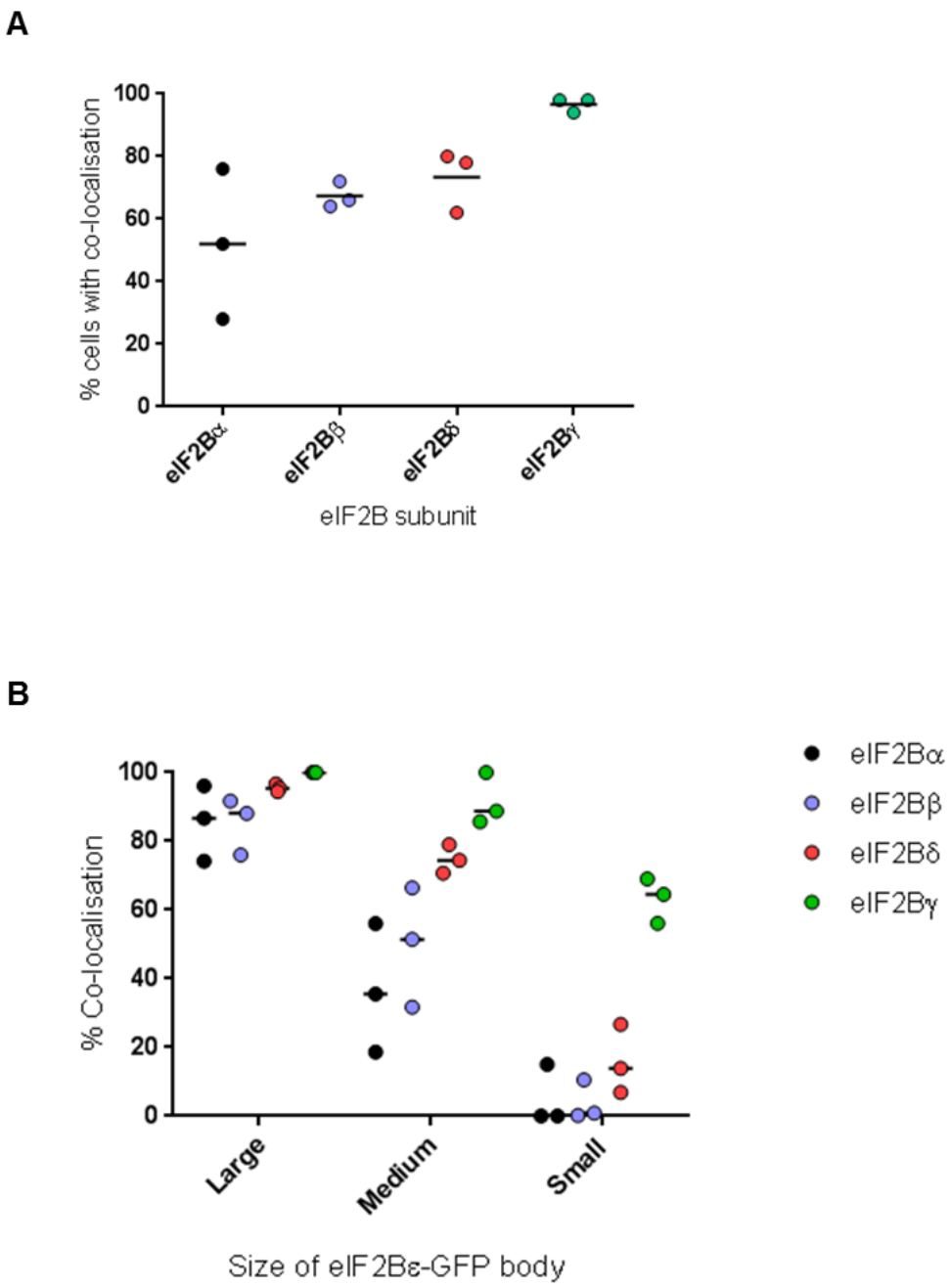

Figure 3.12 The degree to which eIF2B(α-γ) subunits co-localise with eIF2Bε-GFP bodies varies between different sized bodies.
U373 cells were transfected with eIF2Bε-GFP, fixed in methanol and subject to ICC with primary anti-eIF2Bα, anti-eIF2Bβ, anti-eIF2Bδ or anti-eIF2Bγ antibodies. All primary antibodies were visualised using appropriate secondary antibodies conjugated to Alexa Fluor 568. (A) For eIF2Bα, eIF2Bβ, eIF2Bδ or eIF2Bγ subunits, the percentage of cells with antibody signal co-localising to at least one eIF2Bε-GFP body; these cells were classified as displaying a degree of co-localisation (n = 3 counts of 50 cells). (B) For each eIF2B subunit (α-γ), within the population of cells that showed a degree of co-localisation, the median percentage of co-localisation between antibody signal and large, medium or small eIF2Bε-GFP bodies, (n=3 counts of 50 cells).

3.3 Discussion

Previous work in the yeasts *S. cerevisiae* and *Candida albicans* (*C. albicans*) has shown that eIF2B localises to cytoplasmic foci that have been termed eIF2B bodies (Campbell *et al*., 2005; Egbe *et al*., 2015). The cellular localisation of mammalian eIF2B has not previously been investigated. Understanding the function of mammalian eIF2B localisation could be a potential tool to provide further insights into the mechanisms of VWM disease. In the present study the cellular localisation of eIF2B has been analysed in U373 cells, a cell type linked to the phenotypic effects of VWM disease (Bugiani *et al*., 2018; Dooves *et al*., 2016). The ε subunit of eIF2B bearing a C-terminal GFP tag was transiently expressed in U373 cells to analyse eIF2B localisation in live cells. To confirm that this localisation was not a result of the eIF2Bε overexpression or self-aggregation of the GFP tag, ICC was used to analyse the localisation of endogenous eIF2B subunits. The data presented here demonstrates that as in yeast (Campbell *et al*., 2005; Noree *et al*., 2010) all 5 subunits of mammalian eIF2B localise to cytoplasmic foci (Figure 3.4), however this localisation appears to be more complex in mammalian cells. In yeast eIF2B has been shown to localise to a single cytoplasmic body, whereas the data presented here shows mammalian eIF2B localising to a number of different sized cytoplasmic bodies (Figure 3.4). These mammalian eIF2B bodies were present under normal cellular conditions. The cellular conditions under which eIF2B localises to cytoplasmic bodies within yeast has been debated. eIF2B bodies have been documented under normal growth conditions (Campbell *et al*., 2005; Noree *et al*., 2010) however other studies have documented that eIF2B bodies only form in response to conditions of cellular stress (Moon and Parker, 2018). The data presented here suggests that cellular stress is not required to stimulate mammalian eIF2B body assembly (Figure 3.4).

To better characterise the localisation of mammalian eIF2B bodies, the bodies were classified by size and counts performed to determine the average number of bodies present within cells for each size category. eIF2B bodies ≥10 μm^2 were classified as large, bodies ≥ 3 μm^2 ≤ 9.99 μm^2 were classified as medium and bodies ≤ 2.99 μm^2 were classified as small. On average eIF2Bε-GFP localised to 1 large, 2 medium and > 15 small eIF2B bodies in U373 cells (Figure 3.2). eIF2Bε-GFP was also expressed in primary human astrocytes (Figure 3.9). The distribution of different sized eIF2B bodies

was found to differ between U373 astrocytoma cells and primary human astrocytes, with the primary astrocytes harbouring higher numbers of small eIF2B bodies. The functional relevance of these different sized bodies is further explored in Chapter 4. In order to determine if this localisation was a specific feature of astrocytes, eIF2Bε-GFP was expressed in HepG2, MG-63, and HEK293 cells. eIF2Bε-GFP localised to different sized cytoplasmic foci in all three cell lines (Figure 3.10) demonstrating that eIF2B bodies are not a specific feature of astrocytes.

Having shown that eIF2B localises to cytoplasmic bodies in mammalian cells it was important to determine whether these foci were distinct from other well-known translation-associated granules. SGs are one of the best characterised translation-associated granules. They consist primarily of stalled 48S preinitiation complexes. eIF2Bε was shown to co-localise with SGs in embryonic mouse cells (Kimball *et al*., 2003) however more recent studies in yeast suggest eIF2B localises to foci distinct from SGs (Moon and Parker, 2018). In keeping with this, the data presented here demonstrates that mammalian eIF2B bodies are spatially discrete from SGs (Figure 3.6, Figure 3.7). P-bodies are another class of cytoplasmic granule to which translational machinery has been documented to localise. The data presented here shows eIF2B bodies are also spatially discrete from P-bodies (Figure 3.8), supporting eIF2B bodies are a unique cytoplasmic assembly.

In its native form eIF2B exists as a heterodecamer (Gordiyenko *et al*., 2014; Kashiwagi *et al*., 2016; Kashiwagi *et al*., 2017; Wortham *et al*., 2014), however subcomplexes of eIF2B have also been found to exist in mammalian cells, namely eIF2B(βδγε) tetramers and eIF2B(γε) heterodimers (Wortham *et al*., 2014). The data presented in this study highlight an increased complexity of the localisation of eIF2B within mammalian cells when compared to yeast. In yeast all five eIF2B subunits have been shown to localise to a single cytoplasmic body (Campbell *et al*., 2005; Noree *et al*., 2010). It was hypothesised that the increased number of eIF2B bodies within mammalian cells observed in this study may be linked to the presence of eIF2B subcomplexes. Indeed, a relationship between eIF2B body size and the eIF2B subunits present was observed in U373 cells. All subunits of eIF2B were found to localise to large and medium sized eIF2B bodies to some degree, supporting that eIF2B decameric or tetrameric complexes may reside within these foci. However, for small eIF2B bodies only the

catalytic eIF2B subunits predominately localised indicating that eIF2B heterodimers may makeup small eIF2B bodies (Figure 3.12). The GEF activity of eIF2B heterodimers is not regulated by cellular stress, due to the absence of eIF2B regulatory subunits which are required to confer stress sensitivity (Elsby *et al*., 2011; Fabian *et al*., 1997; Krishnamoorthy *et al*., 2001; Pavitt *et al*., 1998). Additionally *in vitro* biochemical assays have shown subcomplexes of eIF2B have reduced activity when compared to the full complex containing all five subunits (Liu *et al*., 2011). It could therefore be hypothesised that the different sized populations of eIF2B bodies identified here may function differently within the cell, and this may be important to the regulation of eIF2B activity.

4. Functionality of mammalian eIF2B bodies

4.1 Introduction

The most well studied mechanism of eIF2B regulation is the integrated stress response (ISR); an adaptive pathway highly conserved amongst eukaryotes (Chapter 1, Section 1.3.1). The core event in the ISR is the phosphorylation of eIF2α at serine 51, stimulated by stress-responsive eIF2α kinases (Wek *et al*., 2006). In mammalian cells there are four eIF2α kinases and although these kinases share homologous catalytic domains for the phosphorylation of eIF2α, they each have unique regulatory domains stimulated by distinct environmental or physiological stresses. Phosphorylation of eIF2α converts it from a substrate to a competitive inhibitor of eIF2B (Dever *et al*., 1995; Rowlands *et al*., 1988) preventing 5' cap-dependent translation, and thus leading to the downregulation of global protein synthesis. Paradoxically, the translation of a subset of ISR-responsive mRNAs that contain short upstream open reading frames (uORF) or internal ribosome entry sites (IRES) are upregulated (Chapter 1, Section 1.3.1.2) (Palam *et al*., 2011; Vattem and Wek, 2004). Increased translation of these mRNAs promotes pro-survival mechanisms to alleviate the cellular stress and restore homeostasis. However, in cases of long-term exposure or induction of chronic stress the ISR promotes translation of mRNAs involved in cell death signalling (Pakos-Zebrucka *et al*., 2016).

eIF2B exists as a decamer with hexameric regulatory core, comprised of two copies of each of the regulatory subunits; eIF2Bα, eIF2Bβ and eIF2Bδ. The catalytic activity of eIF2B is carried out by two heterodimers of eIF2Bγ and ε subunits which reside upon opposite sides of the hexameric core (Kashiwagi *et al*., 2016; Tsai *et al*., 2018; Zyryanova *et al*., 2018). The stress-induced inhibition of eIF2B by phosphorylated eIF2α is mediated by the eIF2B regulatory subunits (Dever *et al*., 1993; Fabian *et al*., 1997; Hannig *et al*., 1990; Kimball *et al*., 1998; Pavitt *et al*., 1997) (Chapter 1, Section 1.4.3.1). Under normal cellular conditions, eIF2Bε interacts with eIF2γ and catalyses the release of GDP. This reaction is further catalysed by interactions between eIF2α and the β and δ subunits of eIF2B (Kashiwagi *et al*., 2019; Kenner *et al*., 2019). In mammalian cells stress-induced phosphorylation of eIF2α induces a conformational rearrangement that alters the eIF2 binding site (Kashiwagi *et al*., 2019; Kenner *et al*., 2019). In its phosphorylated form eIF2α binds to the α and δ subunits of eIF2B (Kashiwagi *et al*.,

2019; Kenner *et al*., 2019). This conformation results in eIF2γ docking onto the γ subunit of eIF2B, preventing eIF2Bε from catalysing GDP release.

In yeast eIF2 shuttles through eIF2B bodies at a rate that correlates to the GEF activity of eIF2B. Stimulation of the ISR through phosphorylation of eIF2α decreases the rate eIF2 shuttles through the bodies suggesting that they are sites where eIF2B GEF activity can be regulated (Campbell *et al*., 2005; Egbe *et al*., 2015). The function of mammalian eIF2B bodies has not yet been investigated. In recent years phosphorylation of eIF2α and dysregulation of the ISR have emerged as common pathways in several neurodegenerative diseases including; Alzheimer's (Ma *et al*., 2013), schizophrenia (Trinh *et al*., 2012), amyotrophic lateral sclerosis (Kim *et al*., 2014) and VWM (Abbink *et al*., 2018; van der Voorn *et al*., 2005). Understanding how the activity of mammalian eIF2B bodies is regulated could provide a platform to better understand the pathological mechanisms of neurodegenerative disease.

This chapter aimed to determine the functional relationship between eIF2 and the mammalian eIF2B bodies identified in Chapter 3, both under normal cellular conditions and during the ISR. It was hypothesised that eIF2 would localise to the eIF2B bodies and that as in yeast, these bodies would be sites of eIF2B regulation. The localisation of eIF2 will be investigated using ICC techniques on cells expressing eIF2Bε-GFP bodies. To determine the dynamics between eIF2B and any eIF2 that localises to eIF2B bodies, FRAP analysis will be performed. In yeast the movement of eIF2 through eIF2B bodies correlated to eIF2B regulation, it was therefore hypothesised eIF2 would be mobile within mammalian eIF2B bodies and this movement would be affected by cellular stress. The movement of eIF2B within eIF2B bodies will be analysed in cells expressing eIF2Bε-GFP. For the assessment of eIF2 movement within eIF2B bodies, cells expressing the alpha subunit of eIF2, GFP tagged, will be used. eIF2Bε tagged with RFP will also be co-expressed in these cells to mark eIF2B bodies as this subunit is known localise to SGs. FRAP analysis will be performed on GFP tagged proteins only. This is due to high levels of background generated when using RFP fluorophores for FRAP experiments. In order to analyse the relationship between eIF2 and eIF2B bodies during cellular stress, two different inducers of the ISR will be used; Tg, an inducer of ER stress and SA, an inducer of oxidative stress.

4.2 Results

4.2.1 eIF2 localises to eIF2B bodies

In yeast eIF2 has been shown to co-localise to eIF2B bodies (Campbell *et al*., 2005; Noree *et al*., 2010). In order to determine if eIF2 localises to eIF2B bodies in mammalian cells, U373 cells transiently expressing eIF2Bε-GFP were fixed in methanol and ICC was carried out to visualise the cellular localisation of eIF2α.

Confocal microscopy demonstrated that eIF2α co-localises with all mammalian eIF2Bε-GFP bodies, independent of size (Figure 4.1A). Super-resolution microscopy of these bodies highlighted in greater detail that eIF2α and eIF2Bε-GFP co-localised. The close proximity of these two protein complexes suggests that the proteins may be interacting (Sekar and Periasamy, 2003).

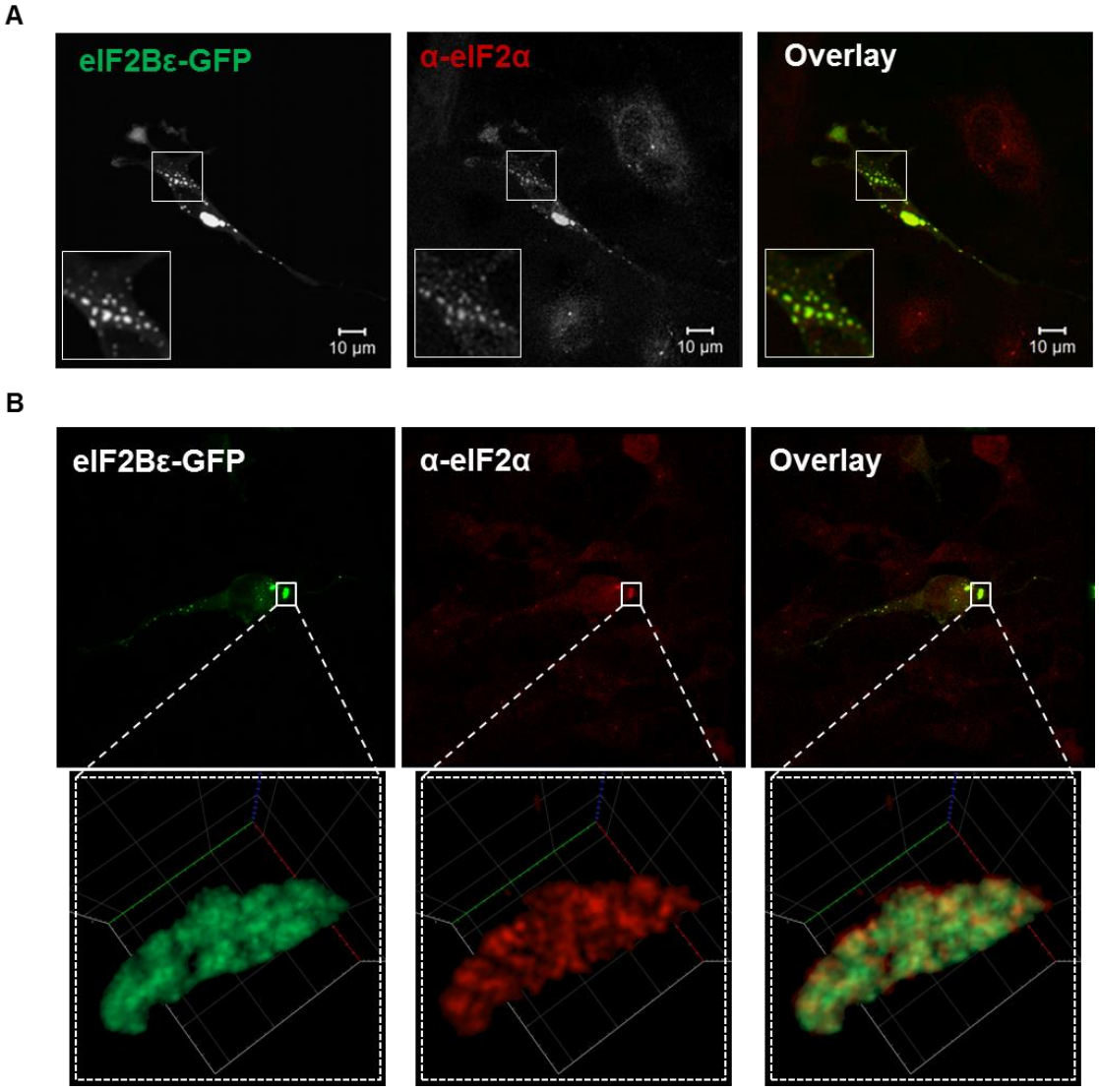

Figure 4.1 eIF2α co-localises with eIF2B bodies.
U373 cells were transfected with eIF2Bε-GFP, fixed in methanol and subject to ICC with a primary anti-eIF2α antibody. Primary antibody signal was visualised using an appropriate Alexa Fluor 568 conjugated secondary antibody. (A) Confocal images of eIF2α localised to eIF2Bε-GFP bodies. (B) Airyscan Super-resolution images of eIF2α localised to an eIF2Bε-GFP body captured on a Zeiss LSM 800 Confocal.

4.2.2 eIF2 can rapidly shuttle into eIF2B bodies

In yeast, the movement of eIF2 through eIF2B bodies correlates with eIF2B GEF activity, with many conditions or scenarios that reduce GEF activity leading to reduced eIF2 mobility (Campbell *et al*., 2005; Singh *et al*., 2011; Taylor *et al*., 2010). To assess the dynamics between eIF2 and eIF2B bodies in mammalian cells, fluorescent recovery after photobleaching (FRAP) was carried out. FRAP analysis can be used to measure the movement of fluorescently tagged proteins into a region of interest within the cell. This technique utilises the fact that photobleaching of fluorophores is irreversible and has no impact upon protein function. As outlined in Figure 4.2, a region of interest containing fluorescently tagged protein is selected and bleached (in this case an eIF2B body). The bleached region is then analysed over time to measure any recovery of fluorescence and this is plotted as a FRAP recovery curve. As bleaching of a fluorophore is irreversible the only way recovery of fluorescence can occur is if fluorescently tagged protein from another region of the cell moves into the region of interest.

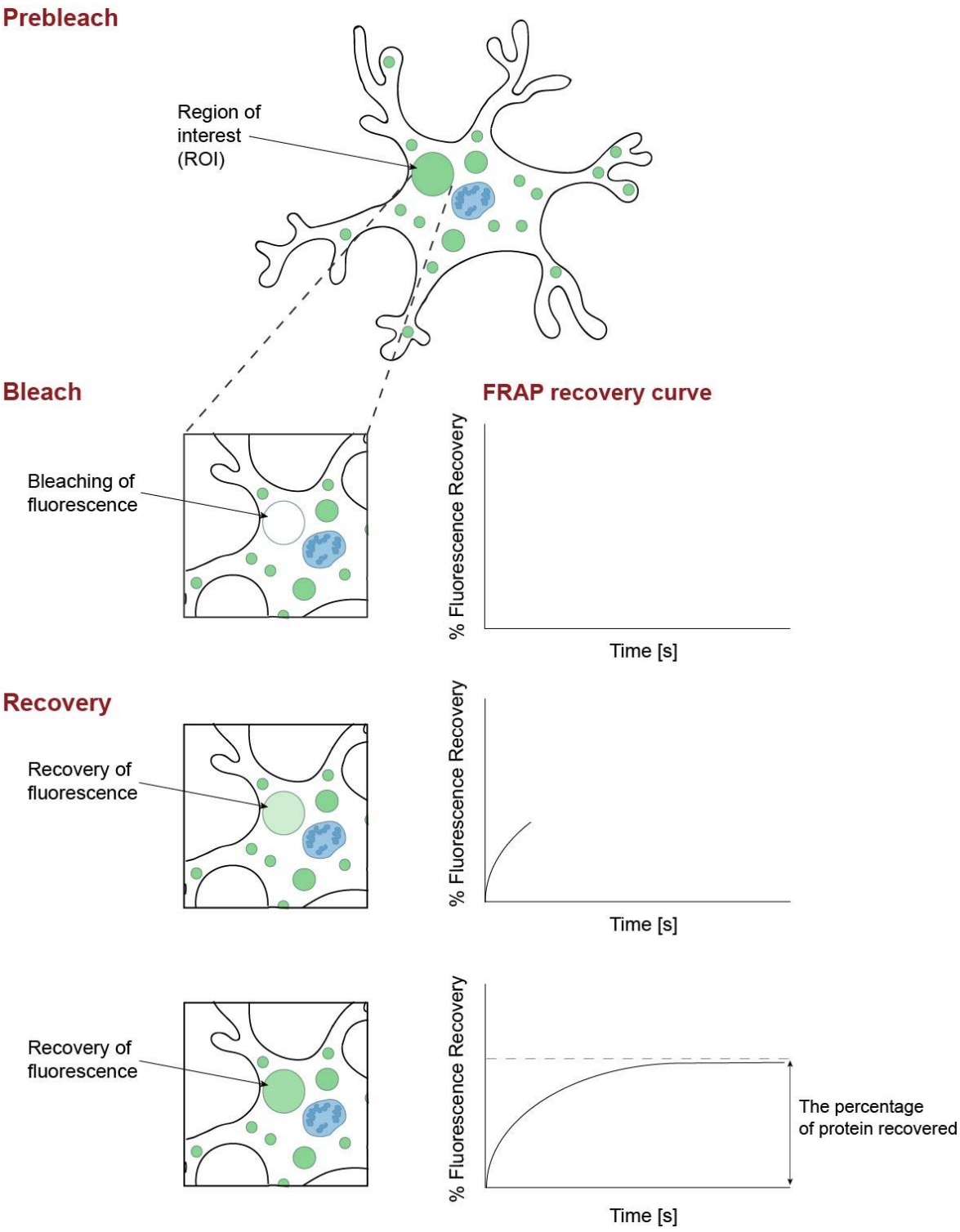

Figure 4.2 Fluorescence recovery after photobleaching technique.
A region of interest (ROI) containing a fluorescently tagged protein is selected. Using confocal microscopy, the fluorophores present within the ROI can be bleached. Over time images are taken of the ROI and the intensity of fluorescence signal within the ROI of interest is measured. The intensity of fluorescence signal can be normalised against the intensity of the pre-bleach fluorescence signal. This percentage of fluorescence recovery is plotted against the time the image was taken to generate a FRAP recovery curve. The total percentage of protein recovery is calculated as the plateau of the FRAP recovery curve.

U373 cells were transfected with eIF2Bε-GFP or eIF2α-GFP and eIF2Bε-RFP (to mark the eIF2B body) and FRAP analysis was carried out on large, medium and small eIF2B bodies. Following photobleaching eIF2Bε-GFP did not recover to any size eIF2B body, demonstrating that eIF2B is a resident component of eIF2B bodies (Figure 4.3). eIF2 however was found to recover to all sized eIF2B bodies following photobleaching indicating that eIF2 is a mobile component of the eIF2B bodies (Figure 4.3).

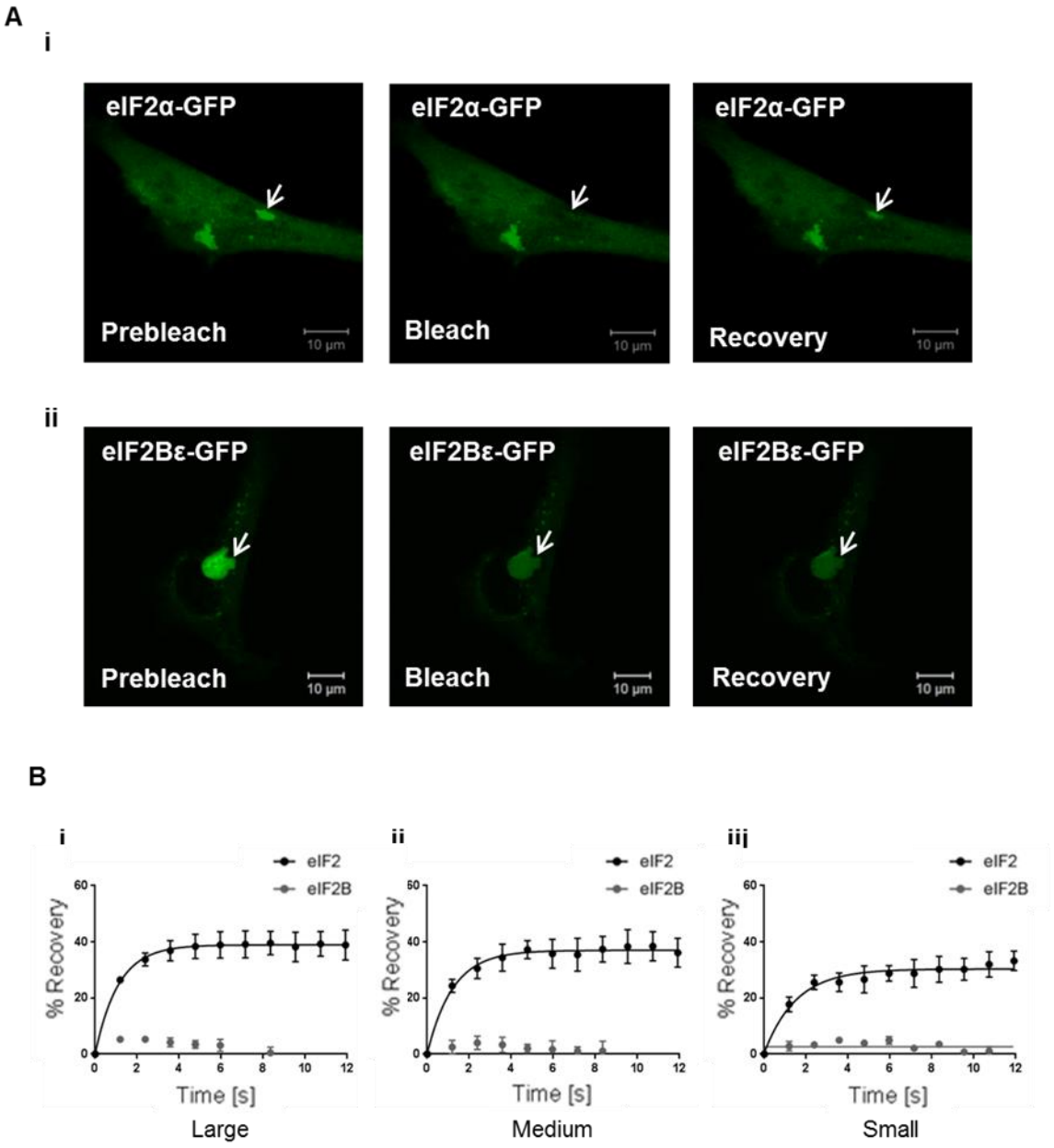

Figure 4.3 eIF2α-GFP is mobile within eIF2B bodies.
(A) FRAP analysis was carried out on the GFP fluorophore in U373 cells transiently expressing (i) eIF2α-GFP or (ii) eIF2Bε-GFP in addition to eIF2Bε-RFP to mark the eIF2B body. Panels show representative prebleach, bleach and recovery images. (B) Normalised FRAP curves for eIF2α-GFP and eIF2Bε-GFP recovery to (i) Large, (ii) Medium and (iii) Small eIF2B bodies. FRAP analysis was performed on 10 bodies (n=3). The percentage recovery is presented as mean ± s.e.m.

4.2.3 Phosphorylated eIF2α localises to eIF2B bodies during conditions of cellular stress

In response to various stress conditions, protein kinases phosphorylate eIF2α at serine 51, converting it from a substrate into a competitive inhibitor of eIF2B GEF activity (Dever *et al*., 1995; Rowlands *et al*., 1988). In yeast the movement of eIF2 through eIF2B bodies is decreased in response to cellular stress, suggesting the bodies are sites of eIF2B GEF activity (Campbell *et al*., 2005). Having shown that eIF2 is mobile within mammalian eIF2B bodies, the impact of cellular stress on this movement was investigated to determine if, as in yeast, the movement of eIF2 through mammalian eIF2B bodies correlates with levels of eIF2B GEF activity.

Phosphorylated eIF2α tightly binds to eIF2B and induces a conformational change which is unfavourable for performing GEF activity (Kenner *et al*., 2019). If phosphorylated eIF2α inhibits the GEF activity of eIF2B bodies, it would be expected that phosphorylated eIF2α would localise to the eIF2B bodies. The localisation of stress induced phosphorylated eIF2α in relation to eIF2B bodies was investigated. Two different cellular stress stimuli were used to induce eIF2α phosphorylation; Tg (1 μM), an ER stress, and SA, an oxidative stress at a lower and higher concentration (125 μM and 500 μM). The levels of phosphorylated eIF2α induced by Tg treatment and treatment with SA, at the two different concentrations, were analysed by western blot (Figure 4.4A). Under normal condtions cells had low levels of phosphorylated eIF2α present. All stress treatments induced a significant increase in levels of phosphorylated eIF2α, with Tg treatment inducing the lowest levels and the higher SA concentration (500 μM) inducing the highest levels. A puromycin incorporation assay was used to measure levels of global protein synthesis in response to Tg (1 μM) and SA (500 μM) stress treatments (Figure 4.4B). Global protein synthesis was found to decrease in a manner inversely correlating to levels of phosphorylaed eIF2α.

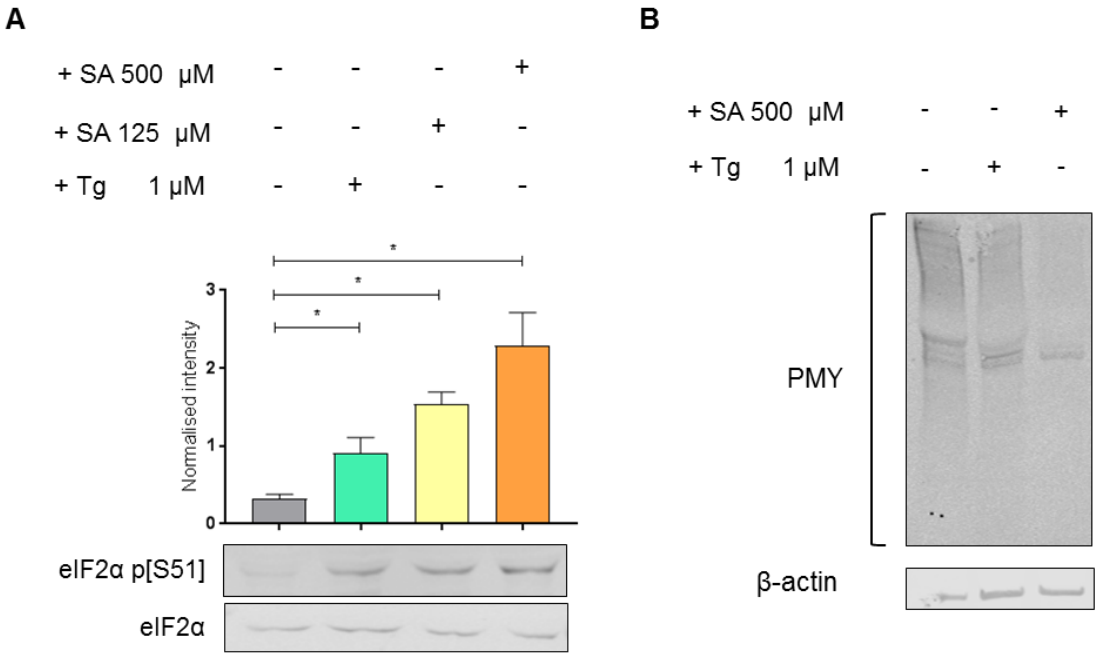

Figure 4.4 Thapsigargin and sodium arsenite treatments induce eIF2α phosphorylation (serine 51) and decrease protein synthesis.
(A) Western blot analysis of the expression level of total eIF2α and eIF2α phosphorylated at serine 51 (p[S51]) in U373 cells treated with 1 µM Tg , 125 µM SA or 500 µM SA to induce cellular stress. Levels of eIF2α p[S51] were normalised to levels of total eIF2α and presented as mean ± SD (n=3). P-values are derived from a Kruskal-Wallis test ($p = 0.0156$), followed by a Conover-Inman analysis; * $p \leq 0.05$. (B) Puromycin incorporation assays were carried out on U373 cells, either untreated or treated with 1 µM Tg or 500 µM SA, β-actin was used as a loading control (n=1).

Having determined that Tg and SA treatments induced phosphorylation of eIF2α, the cellular localisation of phosphorylated eIF2α was investigated following these treatments. eIF2B complexes containing the regulatory subunits are known to display a higher affinity for eIF2 when present in its phosphorylated form (Kashiwagi *et al*., 2017; Pavitt *et al*., 1998). As the regulatory subunits of eIF2B were found to predominately localise to the large and medium eIF2B bodies (Figure 3.12) it was hypothesised that phosphorylated eIF2α would predominately localise to these bodies. In order to explore this hypothesis, U373 cells transiently expressing eIF2Bε-GFP were subject to treatment with Tg (1 µM) and SA at two different concentrations (125 µM and 500 µM). The cells were fixed in methanol and ICC was carried out to visualise the cellular localisation of phosphorylated eIF2α. Confocal microscopy revealed that phosphorylated eIF2α localised to a proportion of eIF2B bodies following treatment with Tg and SA at both concentrations (Figure 4.5). Super-resolution microscopy highlighted phosphorylated eIF2α localised to an eIF2B body in cells treated with the higher concentration of SA (500 µM) (Figure 4.6).

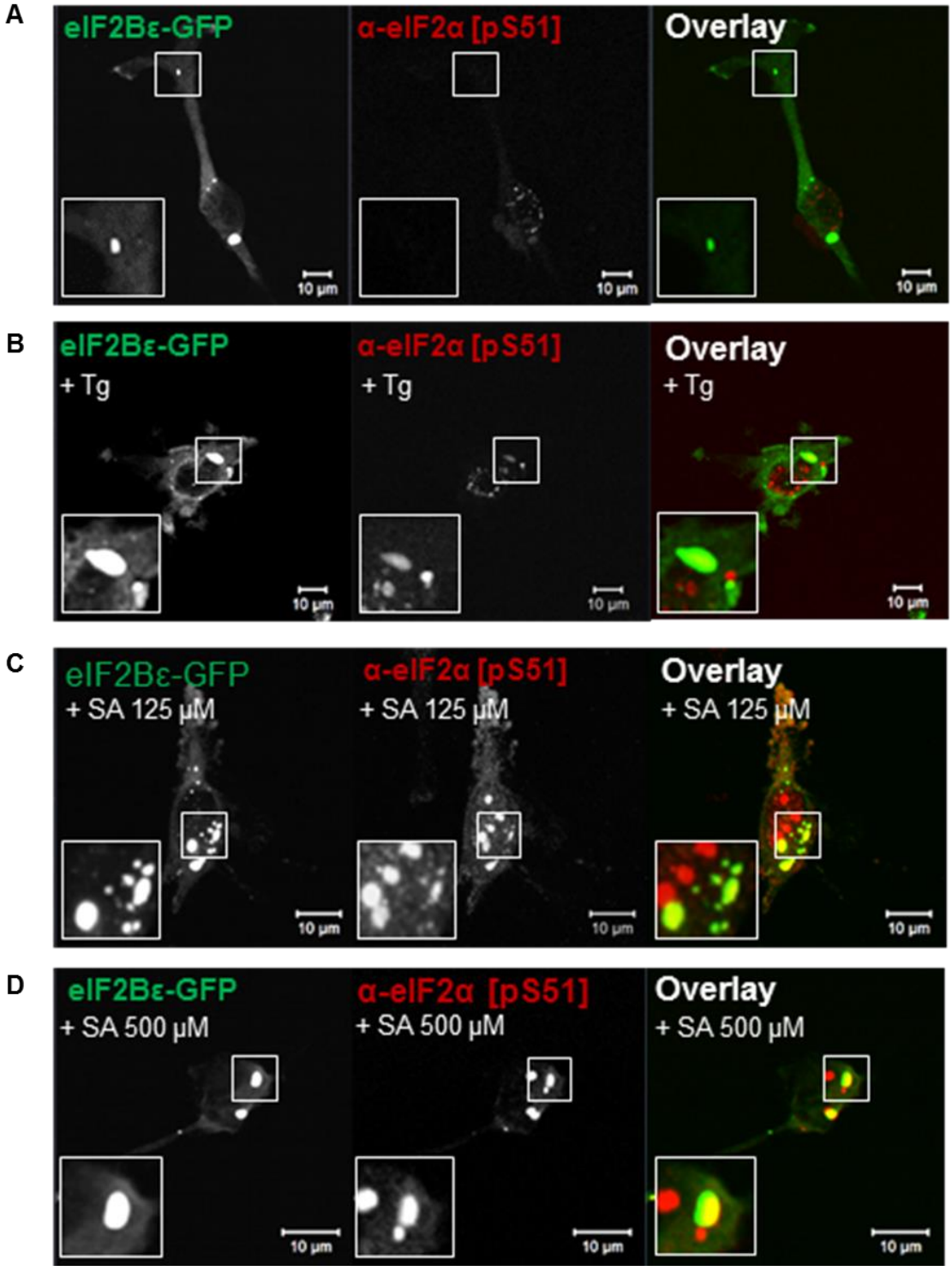

Figure 4.5 Phosphorylated eIF2α localises to eIF2B bodies.
Confocal microscopy images of U373 cells, transfected with eIF2Bε-GFP and either (A) untreated or treated with (B) 1 µM Tg, (C) 125 µM SA or (D) 500 µM SA. Cells were fixed in methanol, and subject to ICC with a primary anti-eIF2α p[S51] antibody. The anti-eIF2α p[S51] antibody was visualised using an appropriate Alexa Fluor 568 conjugated secondary antibody.

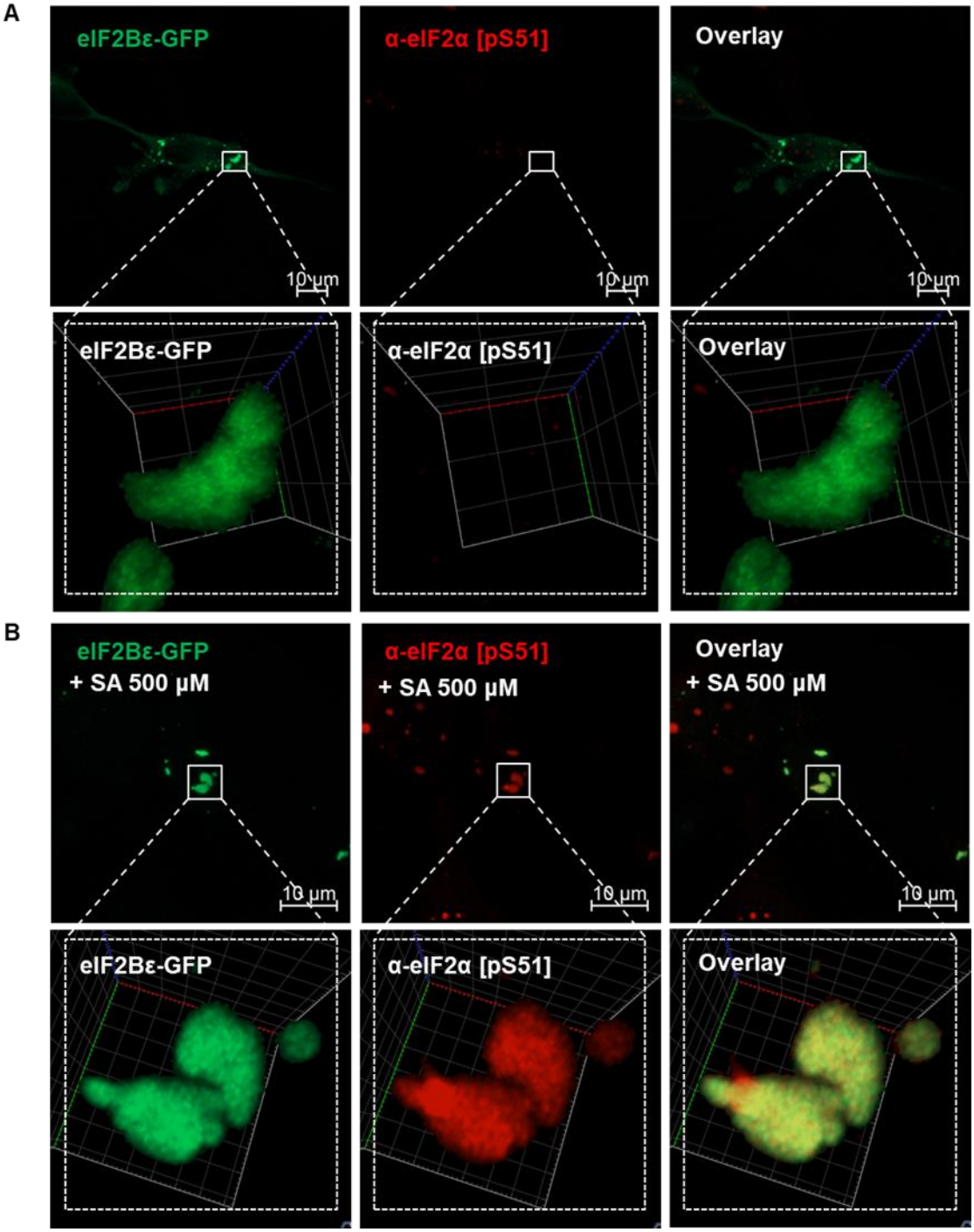

Figure 4.6 Super-resolution microscopy of phosphorylated eIF2α co-localised to eIF2B bodies.

U373 cells were transfected with eIF2Bε-GFP, and either (A) untreated or (B) treated with 500 µM SA. Cells were fixed in methanol, and subject to ICC with a primary anti-eIF2α p[S51] antibody. The anti-eIF2α p[S51] antibody was visualised using an appropriate Alexa Fluor 568 conjugated secondary antibody and imaged using the Airy scan super-resolution functionality on a Zeiss LSM 800 confocal microscope.

To better characterise the proportion of eIF2B bodies that phosphorylated eIF2α localised to following treatment with Tg (1 μM), SA (125 μM) or SA (500 μM), counts were carried out (Figure 4.7). As hypothesised a significantly higher proportion of large and medium eIF2B bodies had phosphorylated eIF2α localised to them when compared to small eIF2B bodies. This is consistent with eIF2B complexes containing the regulatory subunits having a higher affinity for eIF2 in its phosphorylated form (Kashiwagi *et al*., 2017; Pavitt *et al*., 1998). In untreated cells, phosphorylated eIF2α localised to 2 % of small eIF2B bodies, and 20 % of large and medium bodies. Induction of cellular stress through treatment with Tg (1 μM) lead to an increase in the percentage of large and medium bodies that phosphorylated eIF2α localised to (35 %), however no significant difference in the percentage of small bodies to which phosphorylated eIF2α localised was observed. Induction of higher levels of eIF2α phosphorylation through treatment with SA induced a greater increase in the percentage of large and medium eIF2B bodies to which phosphorylated eIF2α localised. In cells treated with 125 μM SA, phosphorylated eIF2α localised to 71 % of large and medium bodies and in cells treated with 500 μM SA, phosphorylated eIF2α localised to 68 % of large and medium bodies. A significant increase in localisation of phoshorylated eIF2α to small bodies was also observed under these SA treatments. In cells treated with 125 μM SA phosphorylated eIF2α localised to 13 % of small bodies and in cells treated with 500 μM SA, phoshorylated eIF2α localised to 27 % of small bodies.

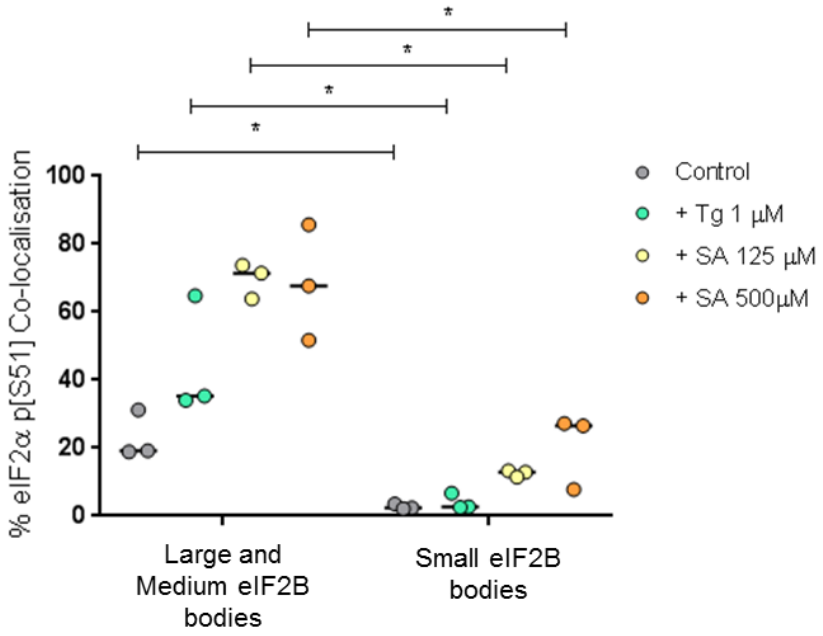

Figure 4.7 Phosphorylated eIF2α localises to eIF2B bodies in a size-dependent manner.

U373 cells expressing eIF2Bε-GFP were fixed in methanol and subject to ICC with an anti- eIF2α p[S51] antibody. The median percentage of anti-eIF2α p[S51] co-localised to large and medium or small eIF2Bε-GFP bodies was determined in a population of 50 cells (n=3). P-values are derived from a Kruskal-Wallis test (P = 0.0011), followed by a Conover-Inman analysis; * $p \leq 0.05$.

4.2.4 The movement of eIF2 into large and medium eIF2B bodies is impaired during cellular stress

Binding of phosphorylated eIF2α sequesters eIF2B GEF activity (Pavitt *et al*., 1998; Ramaiah *et al*., 1994). It was therefore hypothesised that the increased presence of phosphorylated eIF2α localised to large and medium bodies during cellular stress would reduce the GEF activity of eIF2B within these bodies. In yeast, the movement of eIF2 through eIF2B bodies correlates to eIF2B activity (Campbell *et al*., 2005; Taylor *et al*., 2010). FRAP analysis was used to measure the movement of eIF2 through large and medium eIF2B bodies during cellular stress as an indirect measure of eIF2B activity. FRAP analysis was carried out on eIF2α-GFP localised to large and medium eIF2B bodies in U373 cells (marked by the expression of eIF2Bε-RFP), either untreated as a control, or treated with Tg (1 μM) or SA (125 μM and 500 μM) to induce cellular stress. A significant decrease in the recovery of eIF2 to large and medium eIF2B bodies was observed following all stress treatments (Figure 4.8). The greatest decrease in recovery was observed for the higher concentration of SA (500 μM) (21 %) (Figure 4.8) followed by the lower concentration of SA (125 μM) (14 % decrease), and then Tg (1 μM) (8 % decrease). Interestingly the observed decrease in eIF2 movement following these three treatments inversely correlated to the levels of phosphorylated eIF2α induced by these treatments (Figure 4.4A).

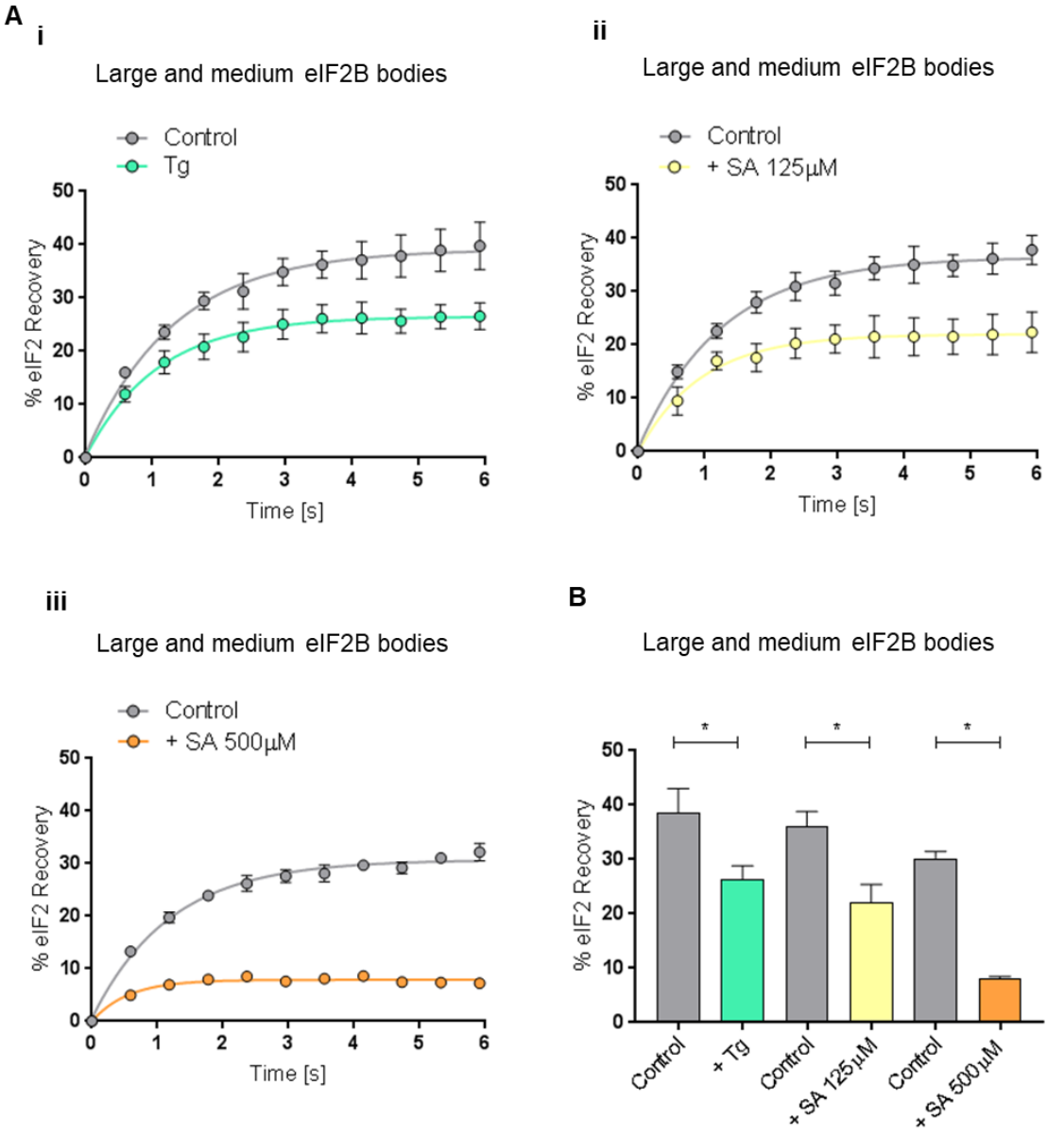

Figure 4.8 Conditions of cellular stress decrease the movement of eIF2 through large and medium eIF2B bodies.

FRAP analysis was carried out on eIF2α-GFP localised to large and medium eIF2B bodies in U373 cells transfected with eIF2α-GFP, and eIF2Bε-RFP to mark the eIF2B bodies. (A) Normalised FRAP recovery curves were plotted for cells treated with (i) 1 µM Tg, (ii) 125 µM SA or (iii) 500 µM SA to induce cellular stress. (B) The mean ±s.e.m percentage of eIF2α-GFP recovery was determined from the normalised FRAP recovery curves. FRAP analysis was performed on 10 bodies (n=3). P-values are derived from a Kruskal-Wallis test (P = 0.021), followed by a Conover-Inman analysis; * $p \leq 0.05$.

In order to confirm that the phosphorylation of eIF2α was responsible for the observed reduction in the movement of eIF2 through the large and medium eIF2B bodies, FRAP analysis was performed with an eIF2α mutant where serine 51 is replaced by Alanine (eIF2α S51A). This mutant cannot be phosphorylated, as confirmed by western blot (Figure 4.9A). FRAP analysis following stress treatment with the higher concentration of SA (500 μM) revealed that the eIF2α S51A mutant could move through large and medium eIF2B bodies (marked by the expression of eIF2Bε-RFP), while the movement of wild type (wt) eIF2α was severely reduced (Figure 4.9B). These data suggest that the movement of eIF2 through large and medium eIF2B bodies is specifically influenced by eIF2α phosphorylation.

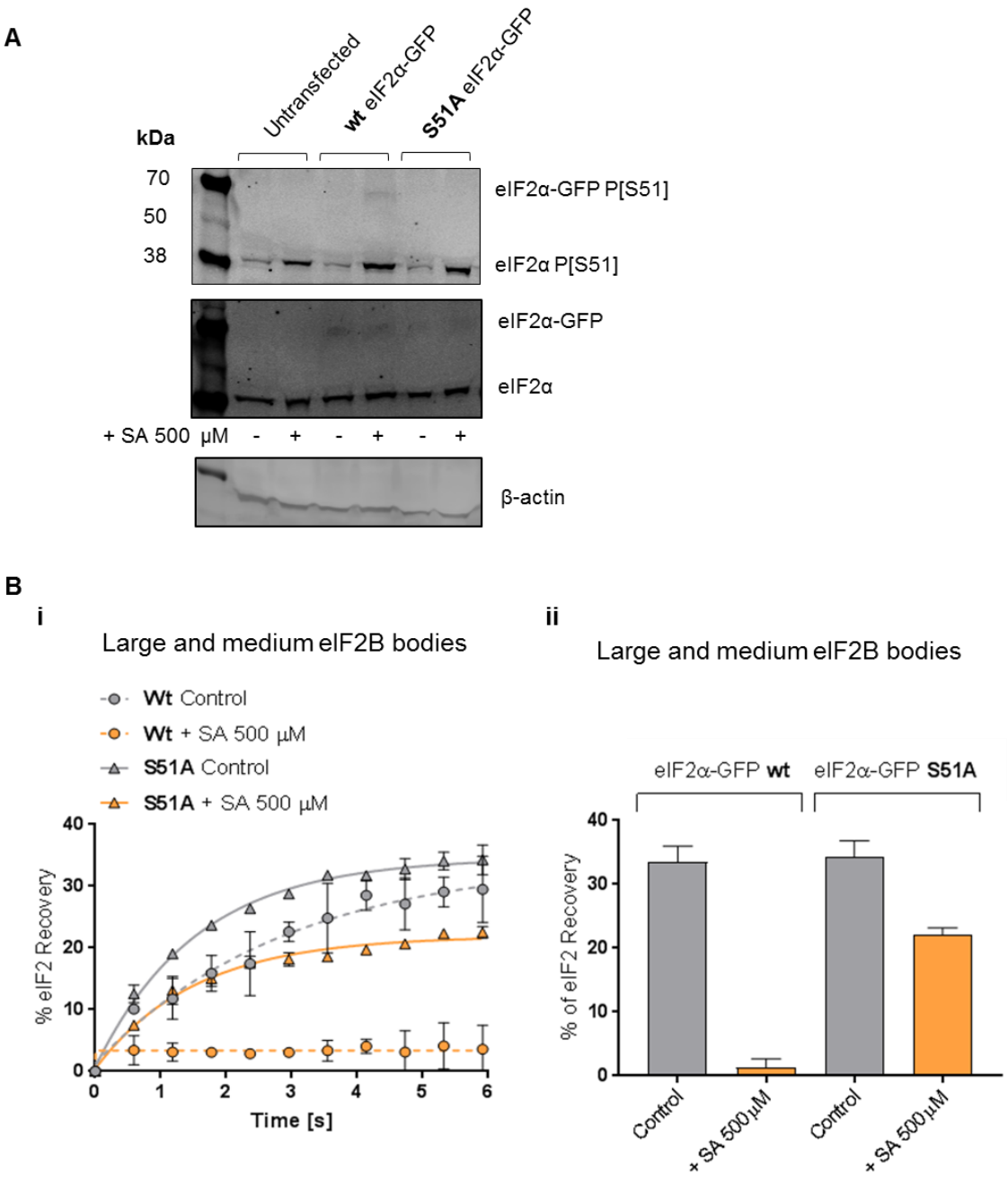

Figure 4.9 eIF2α S51A moves through large and medium eIF2B bodies during SA induced cellular stress.

U373 cells were transfected with either wt eIF2α-GFP or mutant eIF2α-GFP (S51A). Cells were either untreated of subject to treatment with SA (500 µM) to induce cellular stress. (A) Western blot analysis was performed to determine the phosphorylation status of wt eIF2α-GFP and mutant eIF2α-GFP (S51A). (B) FRAP analysis was carried out for wt and mutant (S51A) eIF2α-GFP localised to large and medium eIF2B bodies in the presence and absence of 500 µM SA. FRAP analysis was performed on 10 bodies (n=2) and (i) plotted as normalised FRAP recovery curves. (ii) The mean ± s.e.m percentage of eIF2α-GFP recovery was determined from the normalised FRAP recovery curves.

4.2.5 The movement of eIF2 into small eIF2B bodies is increased during cellular stress but is dependent on levels of eIF2α phosphorylation

The movement of eIF2 through large and medium eIF2B bodies decreased in the presence of phosphorylated eIF2α (Figure 4.8). The regulatory subunits of eIF2B are required to mediate phosphorylated eIF2α induced inhibition of eIF2B (Krishnamoorthy *et al*., 2001; Pavitt *et al*., 1997) and it was hypothesised that as the regulatory subunits localised to the large and medium eIF2B bodies (Figure 3.12) these were responsible for this decreased movement of eIF2. The small eIF2B bodies identified in this study primarily presented with only eIF2B catalytic subunits (eIF2Bγ and eIF2Bε) localised to them, with less than 15 % presenting with regulatory subunits also co-localised (Figure 3.12). It was therefore hypothesised that the movement of eIF2 through these bodies would not be downregulated by cellular stress treatments. FRAP analysis was carried out on eIF2α-GFP localised to small eIF2B bodies in U373 cells (marked by the expression of eIF2Bε-RFP), either untreated as a control, or treated with Tg (1 μM) or SA (125 μM and 500 μM) to induce cellular stress. Surprisingly, treatment with both Tg (1 μM) and the lower concentration of SA (125 μM) significantly increased the movement of eIF2α-GFP into these bodies (Figure 4.10A i and ii) and B). In contrast, a decrease in the percentage recovery of eIF2 was observed for the higher concentration of SA (500 μM) (Figure 4.10A iii and B).

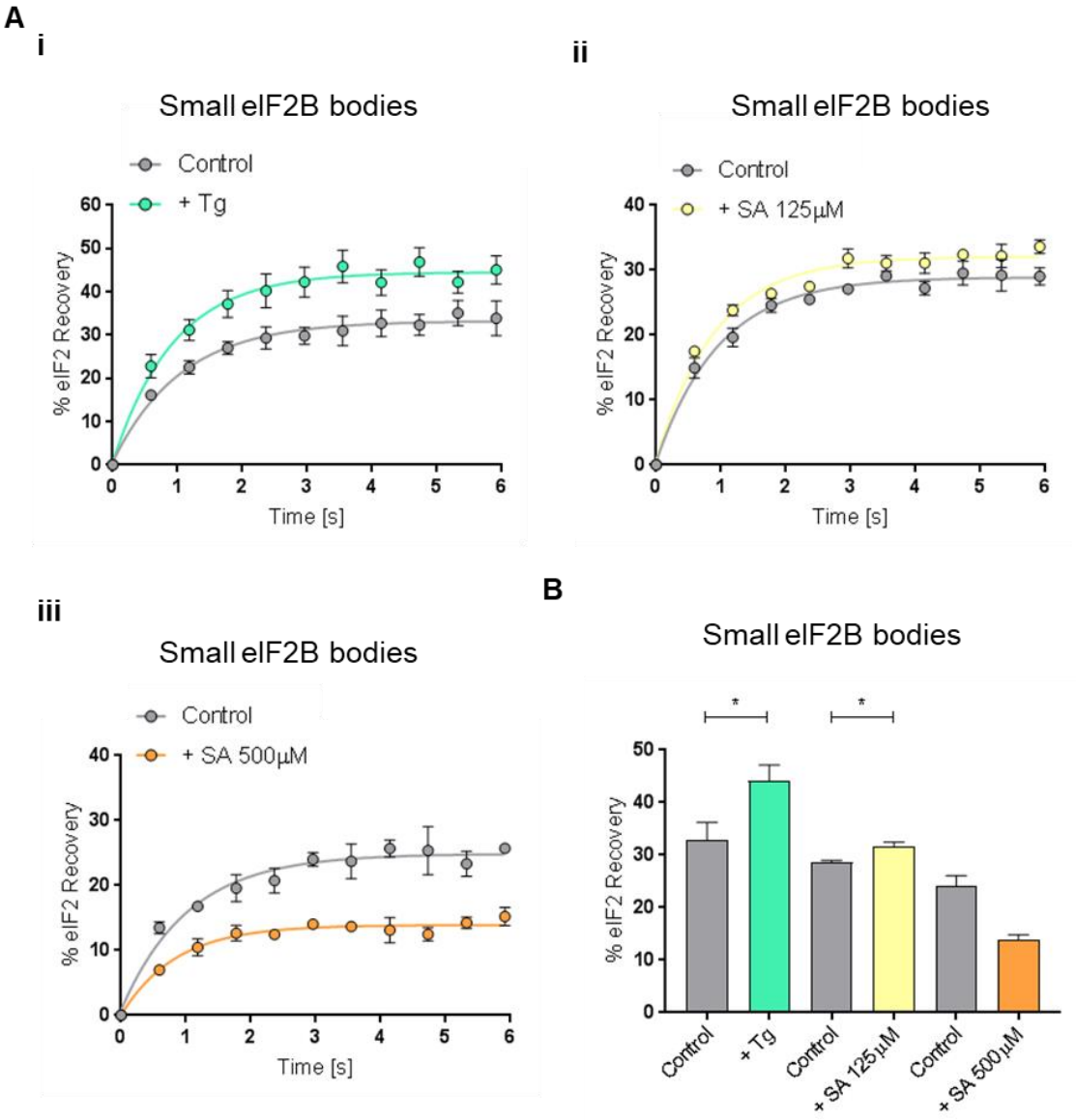

Figure 4.10 Cellular stress modulates the movement of eIF2 through small eIF2B bodies.

FRAP analysis was carried out on eIF2α-GFP localised to small eIF2B bodies in U373 cells transfected with eIF2α-GFP and eIF2Bε-RFP to mark the eIF2B bodies. Cells were treated with (i) 1 µM Tg, (ii) 125 µM SA or (iii) 500 µM. FRAP analysis was performed on 10 bodies (n=3) and plotted as normalised FRAP recovery curves. (B) The mean ± s.e.m percentage of eIF2α-GFP recovery was determined from the normalised FRAP recovery curves. P-values were derived from a Kruskal-Wallis test (P = 0.0082), followed by a Conover-Inman analysis; * $p \leq 0.05$.

4.2.6 Localisation of eIF2Bδ to small eIF2B bodies increases during cellular stress

The movement of eIF2 through small eIF2B bodies in the presence of low levels of phosphorylated eIF2α (Figure 4.10), suggests the GEF activity within these bodies is increased under these conditions. Increased GEF activity of eIF2B has been linked to subunit composition, specifically the presence of regulatory subunits (Dev *et al*., 2010; Fabian *et al*., 1997; Liu *et al*., 2011; Williams *et al*., 2001). To address whether the stress treatments had any impact upon the localisation of regulatory subunits within the small eIF2B bodies, U373 cells transfected with eIF2Bε-GFP were either untreated, or treated with Tg (1 μM) or SA (125 μM and 500 μM). Cells were then fixed in methanol and subject to ICC with antibodies to the eIF2B regulatory subunits. Interestingly, for all stress treatments, the percentage of eIF2Bδ co-localising to small eIF2B bodies increased by over 40 %, however no increase in the percentage co-localisation of eIF2Bα or eIF2Bβ to small eIF2B bodies was observed (Figure 4.11).

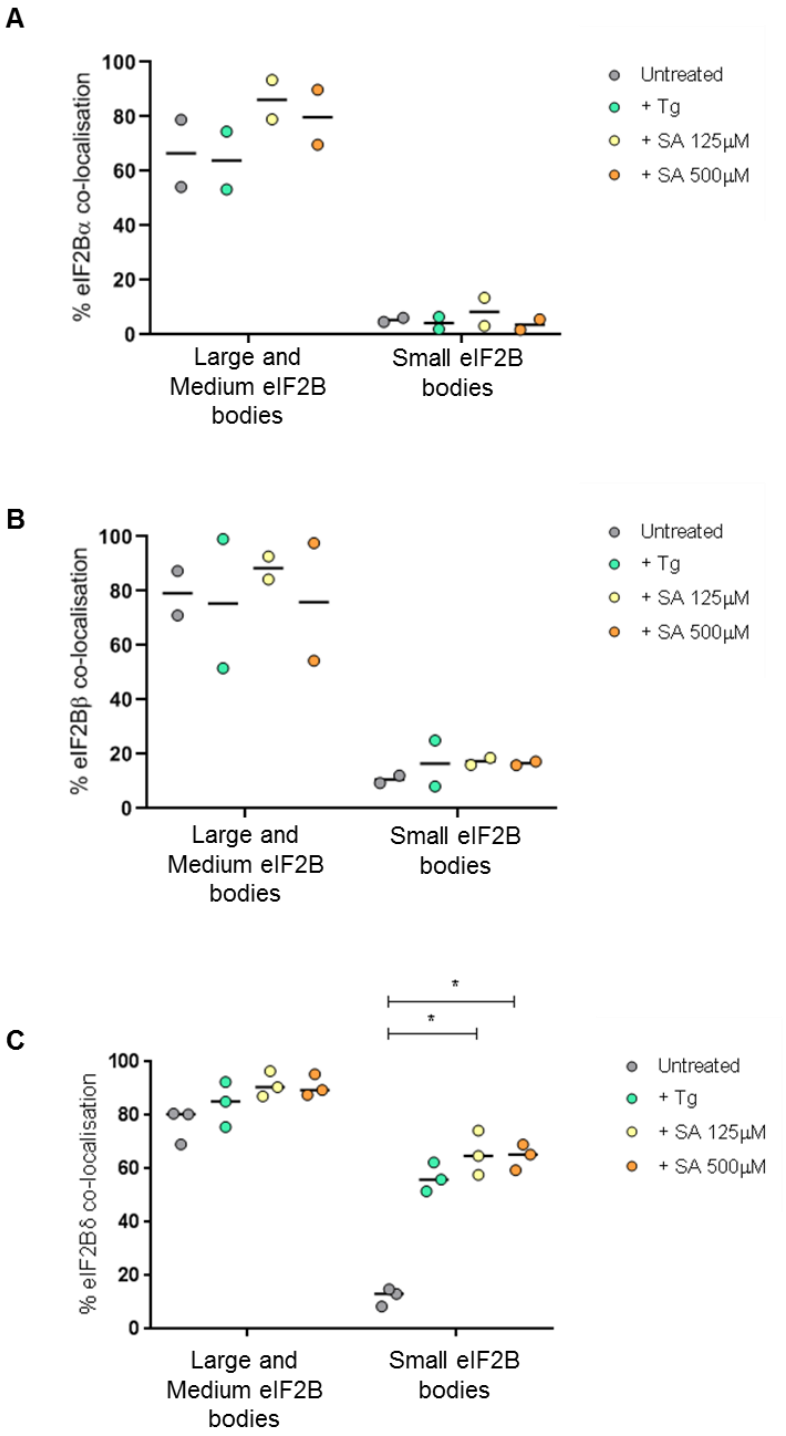

Figure 4.11 eIF2Bδ localises to an increased percentage of small eIF2B bodies during cellular stress.

U373 cells were transfected with eIF2Bε-GFP, and treated with 1 µM Tg, 125 µM SA or 500 µM. Cells were fixed in methanol and subject to ICC with primary (A) anti-eIF2Bα, (B) anti-eIF2Bβ or (C) anti-eIF2Bδ antibodies and visualised using an appropriate secondary antibody conjugated to Alexa Fluor 568. Within a population of 50 cells, the median percentage of co-localisation between anti-eIF2Bα, anti-eIF2Bβ or anti-eIF2Bδ and large and medium or small eIF2B bodies was determined (n=2 for eIF2Bα and β; n=3 for eIF2Bδ). P-values were derived from a Kruskal-Wallis test ($p = 0.0434$), followed by a Conover-Inman analysis; * $p \leq 0.05$.

4.2.7 The size and distribution of eIF2B bodies is altered during cellular stress

Having shown that the subunit composition of small eIF2B bodies is altered during cellular stress, it seemed important to determine if stress also impacted upon the size and distribution of eIF2B bodies. Firstly, counts were carried out on U373 cells expressing eIF2Bε-GFP to determine the number of large and medium, and small eIF2B bodies during cellular stress (Tg 1 μM, SA 125 μM or SA 500 μM). The number of small eIF2B bodies was found to increase for Tg (1 μM) and SA (125 μM and 500 μM) induced cellular stress, however the number of large and medium sized bodies was not changed (Figure 4.12A). Under Tg treatment the average number of small bodies per cell increased by 14, and for treatment with the two concentrations of SA, the average number of small bodies per cell increased by 7 and 8 respectively. Next the size of large eIF2B bodies was analysed under stress treatments to determine if stress could affect the size of eIF2B bodies. The average size of the large eIF2B bodies was found to significantly increase for all stress treatments (Figure 4.12B).

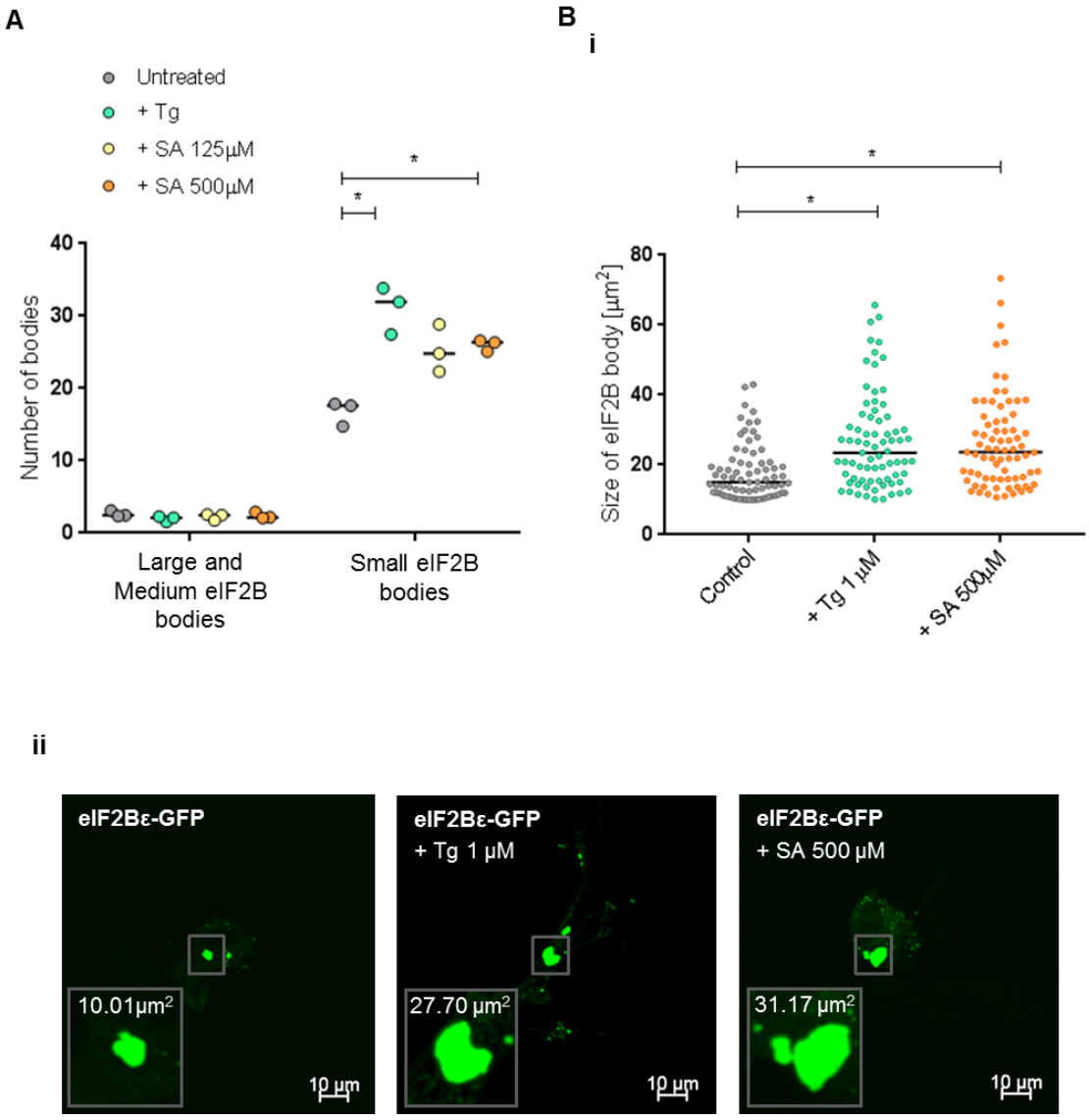

Figure 4.12 During cellular stress the number of small eIF2B bodies increases and the size of large eIF2B bodies increases.

(A) U373 cells were transfected with eIF2Bε-GFP, and treated with 1 µM Tg, 125 µM SA or 500 µM. Counts were performed to determine the median number of large and medium or small eIF2B bodies within a population of 50 cells (n=3). (B) (i) Cells containing large eIF2B bodies were imaged by confocal microscopy and Image J was used to determine the median area of the large eIF2B bodies (25 eIF2B bodies, n=3). (ii) Representative images are shown in the panels. P-values were derived from a Kruskal-Wallis test (A $p = 0.0047$; B $p = < 0.0001$), followed by a Conover-Inman analysis, * $p \leq 0.05$.

4.2.8 The size and distribution of eIF2B bodies in primary astrocytes displays a similar phenotype to stressed U373 cells

The induction of cellular stress in U373 cells correlated with an increase in the number of small eIF2B bodies and an increase in the size of large eIF2B bodies (Figure 4.12). The average number of small eIF2B bodies in primary astrocytes under normal cellular conditions was found to be greater than that of U373 cells; 25 small bodies and 18 small bodies respectively (Figure 3.9). The average number of small eIF2B bodies in primary astrocytes under normal conditions was therefore similar to the average number of small bodies observed in U373 cells experiencing cellular stress (Figure 4.12). In order to determine if the eIF2B body phenotype in primary astrocytes may share other similarities with stressed U373 cells, the size of the large bodies in primary astrocytes was analysed (Figure 4.13). Similar to the trend observed for U373 cells subjected to cellular stress, the size of large bodies in primary astrocytes was significantly increased compared to untreated U373 cells.

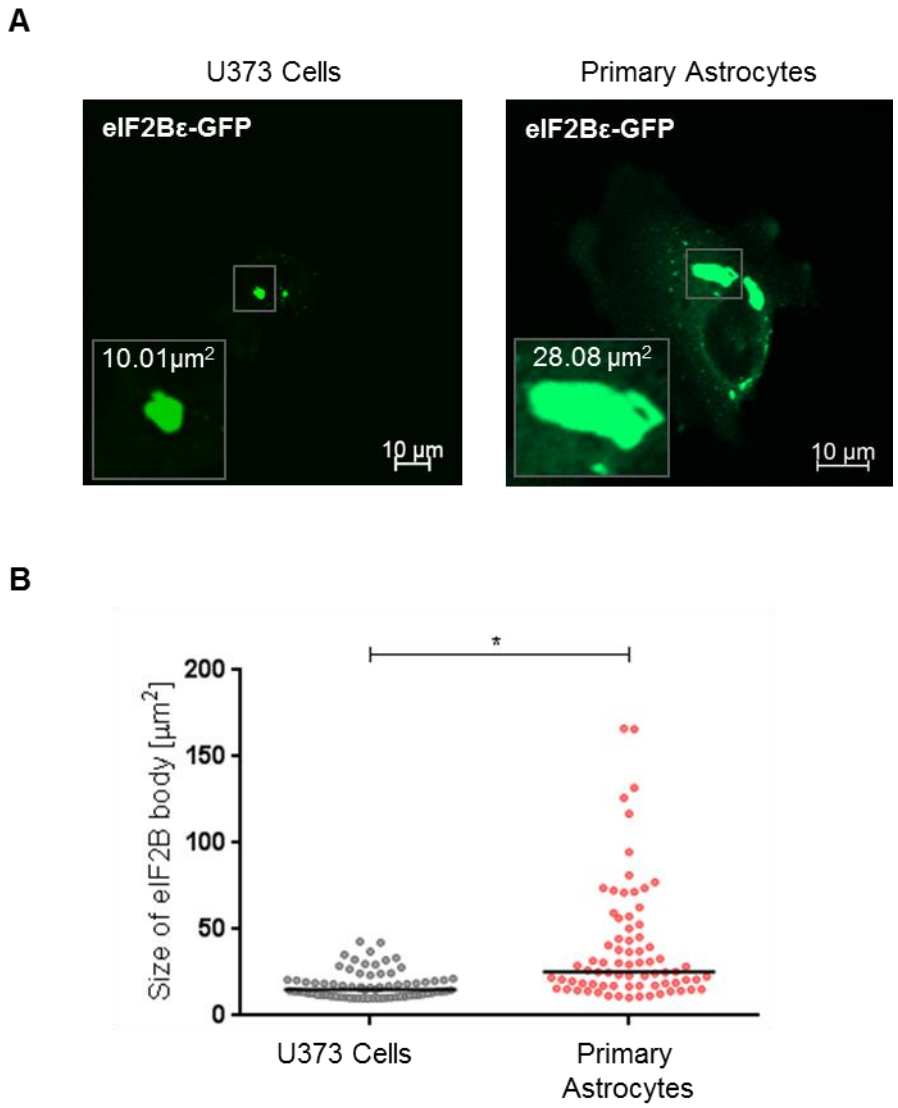

Figure 4.13 The area of large eIF2B bodies is greater in primary human astrocyte cells than in U373 cells.

(A) U373 cells and primary astrocyte cells were transfected with eIF2Bε-GFP, and cells containing large eIF2B bodies were imaged by confocal microscopy. (B) Image J was used to determine the median area of large eIF2B bodies in U373 cells and primary astrocytes (25 eIF2B bodies, n=3). P-values were derived from a Kruskal-Wallis test ($p = < 0.0001$), followed by a Conover-Inman analysis, * $p \leq 0.05$.

From the changes observed in eIF2B body size and distribution in U373 cells treated with Tg and SA (Figure 4.12) it was hypothesised that phosphorylation of eIF2α may impact upon the size and distribution of eIF2B bodies. The levels of phosphorylated eIF2α were therefore analysed in U373 cells and primary astrocytes under normal conditions and during conditions of cellular stress (Figure 4.14). These experiments were only performed once but provide an indication that primary astrocytes may have a higher level of basal eIF2α when compared to U373 cells. Additionally, the induction of cellular stress appeared to induce higher levels of phosphorylated eIF2α in primary human astrocytes, when compared to U373 cells. These experiments should be repeated before conclusions are drawn.

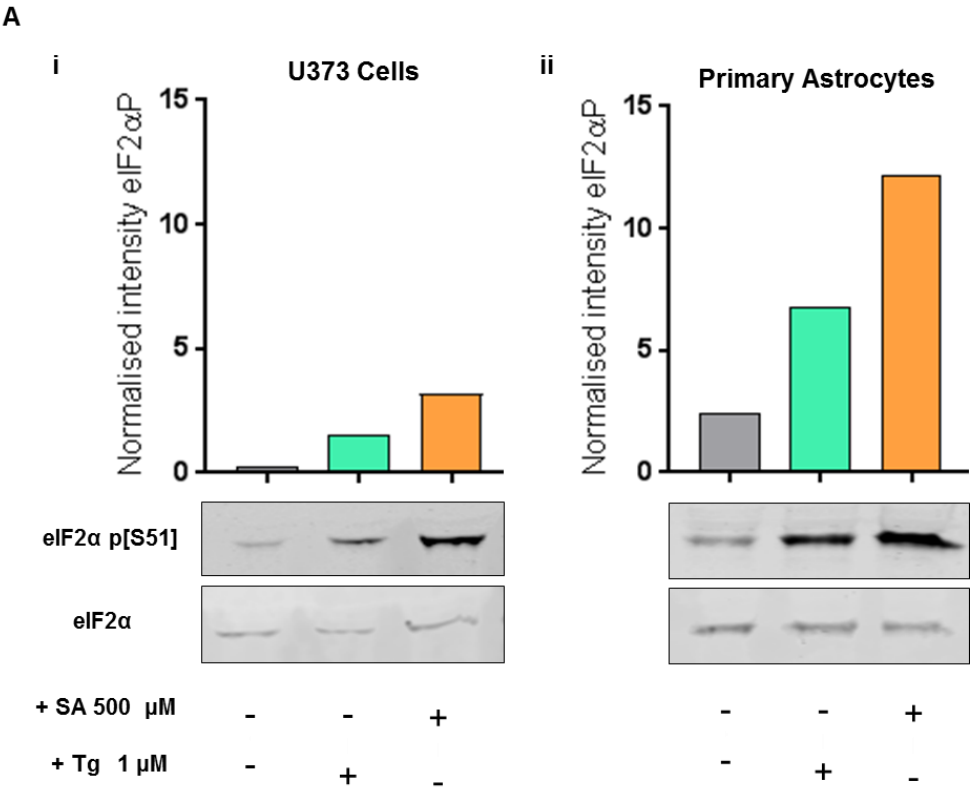

Figure 4.14 Primary human astrocytes appear to express higher levels of phosphorylated eIF2α when compared to U373 cells.
(A) Western blot analysis of the level of eIF2α and eIF2α p[S51] expression in (i) U373 cells and (ii) primary astrocytes either untreated or treated with 1 µM Tg or 500 µM SA to induce cellular stress. Levels of phosphorylated eIF2α were normalised to levels of total eIF2α (n=1).

4.3 Discussion

Previous work in the yeasts *Saccharomyces cerevisiae* and *Candida albicans* has shown that eIF2 localises to eIF2B bodies and is mobile within these bodies. Three different strategies to decrease the GEF activity of eIF2B all inhibited eIF2 movement into the bodies, showing that in yeast, the measurement of eIF2 movement into the eIF2B body correlates precisely with eIF2B GEF activity (Campbell *et al*., 2005). The data presented in this study demonstrates that similarly to yeast, eIF2 localises too and is mobile within mammalian eIF2B bodies.

The functional importance of eIF2 mobility within eIF2B bodies was assessed using cellular stress as a tool to modulate eIF2B activity. Stress-induced phosphorylation of eIF2α converts eIF2 into a competitive inhibitor of eIF2B activity (Rowlands *et al.*, 1988; Dever *et al.*, 1995) and the regulatory subunits of eIF2B (α, β and δ) are essential for mediating this inhibition (Krishnamoorthy *et al*., 2001; Pavitt *et al*., 1997). In chapter 3 of this study the regulatory subunits of eIF2B where found to predominately localise to eIF2B bodies with an area ≥ 3 μm^2; classified as large and medium eIF2B bodies (Figure 3.12). It was therefore hypothesised that the GEF activity of eIF2B localised to large and medium bodies would be downregulated upon the induction of eIF2α phosphorylation. In support of this hypothesis, FRAP analysis revealed that the movement of eIF2 through large and medium eIF2B bodies was attenuated in response to ER and oxidative stress, induced by Tg and SA respectively (Figure 4.8). Furthermore, this decreased movement of eIF2 through the large and medium eIF2B bodies correlated with an increase in the localisation of phosphorylated eIF2 to the eIF2B bodies (Figure 4.5 and 4.7). FRAP analysis with an eIF2α S51A mutant (resistant to stress-induced phosphorylation) confirmed that the movement of eIF2 through large and medium eIF2B bodies is directly influenced by eIF2α-phosphorylation (Figure 4.9). These data therefore provide evidence to suggest that mammalian eIF2B bodies are sites of eIF2B GEF activity.

In addition to the large and medium sized bodies identified in chapter 3, a population of eIF2B bodies with an area of ≤ 2.99 μm^2 were also observed and these were classified as small eIF2B bodies. ICC revealed that these small eIF2B bodies predominately consisted of the catalytic subunits of eIF2B (γ and ε), with the regulatory subunits being either absent or present in a very low percentage of these

bodies (Figure 3.12). *In vitro* GEF assays, in both yeast and mammalian systems, have shown that eIF2Bγε heterodimers exhibit guanine nucleotide exchange activity that is unregulatable by phosphorylated eIF2α (Li *et al*., 2004; Pavitt *et al*., 1998). It was therefore hypothesised that the activity of eIF2B within these bodies would be unaffected upon induction of eIF2α phosphorylation. Intriguingly, the movement of eIF2 through the small eIF2B bodies was in fact significantly increased by cellular stress induced by both Tg, and a low concentration of SA (125 µM) (Figure 4.10). Biochemical assays in yeast have demonstrated that increasing the expression of eIF2B regulatory subunits can enhance the GEF activity of eIF2B (Dev *et al*., 2010; Fabian *et al*., 1997; Liu *et al*., 2011; Williams *et al*., 2001). Interestingly, an increase in the localisation of eIF2Bδ to the small eIF2B bodies under stress treatment was observed (Figure 4.11) and thus may be responsible for the observed increase in movement of eIF2. This increased localisation of eIF2Bδ to small eIF2B bodies during stress is suggestive of the formation of a currently unidentified eIF2B subcomplex, containing eIF2Bδ, γ and ε subunits. This complex may not have been identified in previous studies (which have analysed eIF2B subcomplexes) as such studies did not observe cells under stress conditions (Wortham *et al*., 2014). At higher levels of SA induced cellular stress (500 µM), an increase in the localisation of eIF2Bδ to small bodies was also observed (Figure 4.11), however the movement of eIF2 through these bodies was decreased (Figure 4.10). Phosphorylated eIF2α exhibits a greater affinity for eIF2B than unphosphorylated eIF2α (Rowlands *et al.,* 1988). The favoured explanation for these results is that in the presence of high levels of phosphorylated eIF2α, eIF2B is saturated by phosphorylated eIF2 and thus all eIF2B complexes become inhibited independent of subunit make up.

In recent years, low levels of cellular stress have been shown to induce a protective phenotype. Cells that are preconditioned through the induction of sub-toxic levels of phosphorylated eIF2α have been shown to respond to and overcome episodes of cellular stress more successfully than unconditioned cells (Lewerenz and Maher, 2009; Lu *et al*., 2004a). The data presented here suggests that small eIF2B bodies have increased eIF2B GEF activity in the presence of low levels of phosphorylated eIF2α. A number of recent studies have demonstrated that treatment of cells with activators of eIF2B activity to enhance the GEF activity of eIF2B within a cell can protect the cell

against cellular stress (Sekine *et al*., 2015; Sidrauski *et al*., 2015b). It could therefore be hypothesised that this increase in the GEF activity of small eIF2B bodies may provide a protective phenotype through increasing the overall activity of eIF2B within the cell. Future studies investigating this hypothesis may provide insight into the protective mechanisms of preconditioning cells with low levels of phosphorylated eIF2α. The N-terminus of eIF2Bδ has previously been shown to be important in mediating cellular stress responses (Martin *et al*., 2010). Mutational analysis of this region of eIF2Bδ may provide insight into the mechanisms by which phosphorylated eIF2 modulates small eIF2B body dynamics.

In addition to the changes to the subunit make-up of the small eIF2B bodies observed during cellular stress, the number of small eIF2B bodies was found to increase, and the size of the large eIF2B bodies was also increased (Figure 4.12). Interestingly, primary human astrocytes displayed a similar localisation phenotype for eIF2B under non-stressed conditions (Figure 3.9 and Figure 4.13). Although U373 cells and primary astrocytes are both of astrocytic lineages, immortalisation can alter cell metabolism (Kaur and Dufour, 2012; Mulukutla *et al*., 2010) possibly explaining the differences seen between the cell types. Levels of phosphorylated eIF2α in unstressed primary astrocytes appeared to be similar to levels of phosphorylated eIF2α induced by Tg treatment in U373 cells (Figure 4.14). If this localisation phenotype was found to contribute to a cell's ability to overcome episodes of cellular stress, as hypothesised earlier, studying eIF2B localisation phenotypes could be an interesting avenue to explore. Decreased basal levels of phosphorylated eIF2α have been documented in VWM mouse brain from mice homozygous for eIF2Bδ (R484W) or eIF2Bε (R191H) VWM mutations or heterozygous for eIF2Bδ (R484W) and eIF2Bε (R191H) VWM mutations (Abbink *et al*., 2018). Analysis of the phenotypic distribution of eIF2B bodies within these cells could perhaps provide insight into VWM disease mechanisms and cell-type specificity.

5. The impact of small molecules on eIF2B localisation and functionality

5.1 Introduction

The activation of the ISR in response to conditions of cellular stress can promote cell survival and recovery. Consequently, dysregulation of the ISR has important pathological implications and has been linked to a number of disorders (Bi *et al*., 2005; Chou *et al*., 2017; Eizirik *et al*., 2008; Santos-Ribeiro *et al*., 2018). Neurodegenerative diseases in particular commonly present with impairment of the ISR (Hetz and Saxena, 2017) and thus pharmacological modulation of the ISR is an attractive therapeutic strategy (Chapter 1, Section 1.3.2). PERK is an eIF2α kinase that is activated in response to ER stress, commonly caused by the unfolding or misfolding of proteins (Pavitt and Ron, 2012). It has become a favourable pharmacological target due to an increase in the identification of misfolded proteins in the brains of neurodegenerative disease patients over the last decade (Smith and Mallucci, 2016). GSK2606414 was developed as a small molecule to inhibit PERK activity in cells subject to ER stress (Axten *et al*., 2012), and has been shown to be neuroprotective in mouse models of frontotemporal dementia, Parkinson's disease and prion disease (Mercado *et al*., 2018; Moreno *et al*., 2013; Radford *et al*., 2015). However, in addition to its neuroprotective role, GSK2606414 has been shown to induce pancreatic toxicity (Moreno *et al*., 2013), highlighting that complete ISR inhibition is lethal in specific tissue types; GSK2606414 is therefore not a suitable therapeutic.

Similarly to PERK inhibitors, the small molecule ISRIB reverses stress induced translational repression (Halliday *et al*., 2015; Sidrauski *et al*., 2013; Sidrauski *et al*., 2015a). ISRIB functions downstream of eIF2α kinases and restores translation by enhancing the GEF activity of eIF2B (Sidrauski *et al*., 2015b). Structural studies have revealled that ISRIB interacts with the β and δ subunits of eIF2B, promoting the assembly of two eIF2B(βδγε) tetramers into an octomeric conformation (Tsai *et al*., 2018; Zyryanova *et al*., 2018). In this octomeric conformation, eIF2B has high affinity for eIF2Bα homodimers and in this way, ISRIB favours the formation of decameric eIF2B (Tsai *et al*., 2018). Unlike PERK inhibitors, ISRIB does not cause pancreatic toxicity (Halliday *et al*., 2015). Through increasing eIF2B activity rather than preventing eIF2B

inhibition (through inhibiting eIF2α phosphorylation), ISRIB is only capable of restoring translation below a precise threshold of phosphorylated eIF2α, ensuring that the cytoprotective effects of the ISR are still accessible to the cell during periods of severe stress (Rabouw *et al*., 2019).

ISRIB has emerged as a promising therapeutic that has been shown to promote a neuroprotective phenotype in mouse models of neurodegenerative disease (Chou *et al*., 2017; Halliday *et al*., 2015). Of particular interest is the therapeutic potential of ISRIB for the treatment of VWM. VWM is a leukodystrophy that is directly caused by mutations in eIF2B (Chapter 1, Section 1.5). A number of VWM mutations manifest through structural destabilisation of the decameric eIF2B complex (Li *et al*., 2004; Liu *et al*., 2011; Wortham and Proud, 2015). *In vitro* biochemical assays have confirmed that ISRIB can stabilise decameric eIF2B harbouring these mutations, increasing their GEF activity (Liang Wong *et al*., 2018). Furthermore, ISRIB has been shown to relieve VWM pathology in mouse models of VWM harbouring an eIF2Bδ (R483W) complex destabilising mutation (Abbink *et al*., 2018). The promising effects of ISRIB have led to the development of the molecule 2BAct, a small molecule that like ISRIB activates eIF2B but has improved solubility and pharmacokinetics (Wong *et al*., 2019). Long term treatment with 2BAct has been shown to prevent all pathological signs of VWM in mouse models harbouring an eIF2Bε (R191H) complex destabilising mutation, demonstrating that like ISRIB, 2BAct has potential to be an effective treatment for VWM.

The development of new drugs for the treatment of human disease is a costly and time-consuming process, with only 8 % of drugs that enter clinical trials gaining approval. Drug repurposing is an attractive field. Recently, the currently FDA approved drugs, DBM and trazodone were found to have similar properties to ISRIB (Halliday *et al*., 2017). Both drugs reversed stress-induced translational repression and induced neuroprotective phenotypes in mouse models of neurodegenerative disease (Halliday *et al*., 2017). Although these drugs seem to have similar effects to ISRIB, the mechanisms through which they reverse stress-induced translational repression remain largely unknown. Current evidence suggests that unlike ISRIB, trazodone and DBM do not stabilise eIF2B in its decameric conformation (Halliday *et al*., 2017).

Having shown that the functional and phenotypic localisation of eIF2B is affected by conditions of cellular stress (Chapter 4), it was of interest to determine if small molecules that modulate the cellular stress response would have any impact on eIF2B localisation. This chapter therefore aimed to investigate the phenotypic localisation of eIF2B and the dynamics between eIF2 and eIF2B bodies in the presence of ISRIB, DBM and trazodone, under normal conditions and conditions of cellular stress. It is hypothesised that ISRIB, DBM and Trazodone will reverse the effects that cellular stress was found to have on the movement of eIF2 through eIF2B bodies in Chapter 4. To analyse the impact of the small molecules on the movement of eIF2 through eIF2B bodies, FRAP analysis will be performed on cells expressing eIF2α-GFP and eIF2Bε-RFP. To investigate whether the small molecules have an impact on the phenotypic localisation of eIF2B, eIF2B subunit localisation will be analysed. Cells expressing eIF2Bε-GFP will be fixed and ICC used to detect the presence of the other subunits of eIF2B in relation to the eIF2Bε-GFP bodies.

5.2 Results

5.2.1 ISRIB reverses stress induced translational depression in a manner that is dependent on levels of eIF2α phosphorylation

Recently the small molecule ISRIB has been shown to increase global translation in cells subject to sub-lethal levels of cellular stress (Rabouw *et al*., 2019; Sidrauski *et al*., 2015a). In Chapter 4 of this study Tg and SA treatments were used to induce cellular stress through the phosphorylation of eIF2α. Treatment of cells with 1 µM Tg induced lower levels of eIF2α phosphorylation than treatment with 500 µM SA (Figure 4.4). Both treatments were found to impact upon the functionality of eIF2B bodies in a manner that correlated to levels of phosphorylated eIF2α (Figure 4.8, Figure 4.9 and Figure 4.10). It was therefore of interest to determine if ISRIB affected the functionality of eIF2B bodies in the presence of the different levels of phosphorylated eIF2α induced by Tg and SA treatment. To address this, firstly the ability of ISRIB to restore translation under the conditions of cellular stress induced by Tg and SA treatments was assessed. Puromycin incorporation assays were carried out on U373 cells subject to these stresses in the presence or absence of ISRIB (Figure 5.1). Tg treatment decreased levels of global translation by 65 %, compared to untreated cells, and SA treatment decreased levels of translation by 93 %, compared to untreated cells, reflecting the higher levels of phosphorylated eIF2α induced by the SA treatment (Figure 4.4). The addition of ISRIB to Tg treated cells significantly enhanced translation levels to near normal (92 % of that of untreated cells) (Figure 5.1). In contrast, the addition of ISRIB to SA treated cells did not restore normal levels of translation, although ISRIB did increase levels of translation in SA treated cells by 18 % (Figure 5.1).

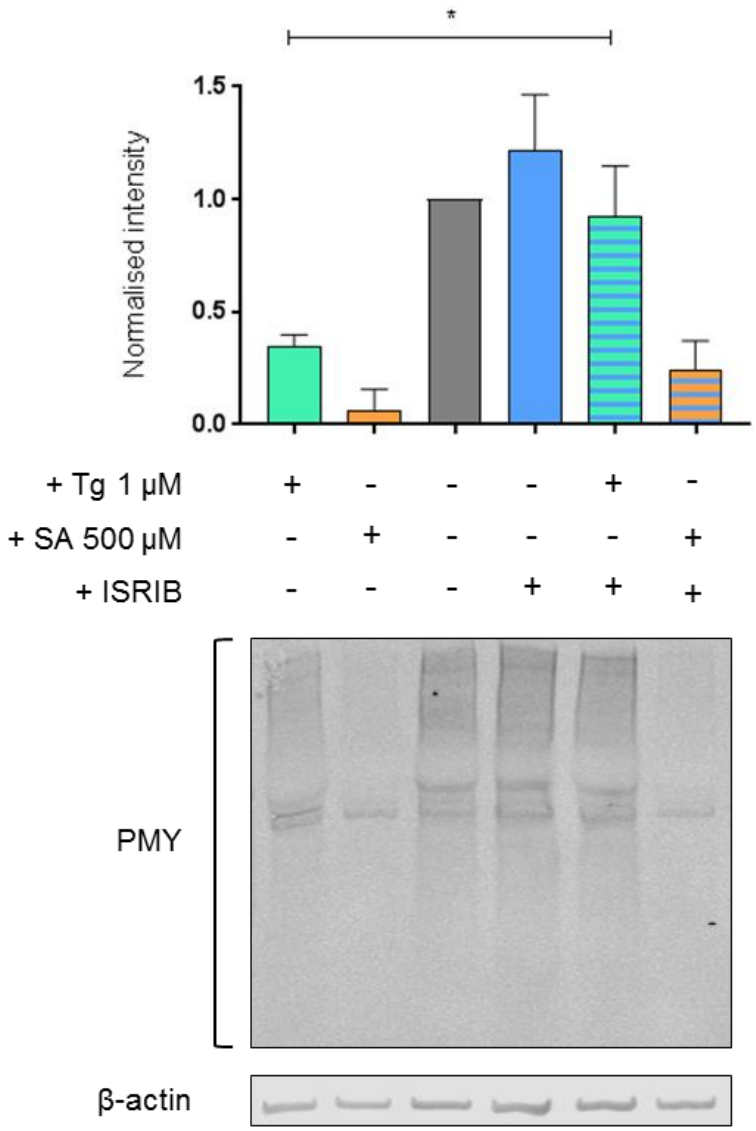

Figure 5.1 ISRIB treatment restores translation in cells treated with 1 µM Tg but not in cells treated with 500 µM SA.

Puromycin incorporation assays were carried out on U373 cells treated with 200 nM ISRIB and 1 µM Tg or 500 µM SA either alone, or in combination with 200 nM ISRIB. Levels of puromycin where normalised to β-actin and are presented as mean ± SD for each treatment normalised to control cells (n=3). P-values were derived from a Kruskal-Wallis test (P = 0.0101), followed by a Conover-Inman analysis, * $p \leq 0.05$.

5.2.2 ISRIB rescues eIF2 mobility within large and medium eIF2B bodies during stress dependent on levels of eIF2α phosphorylation

The decameric eIF2B complex has increased GEF activity compared to eIF2B subcomplexes (Liu *et al*., 2011). ISRIB promotes eIF2B decameric formation, increasing the GEF activity of eIF2B, and enabling cells to overcome low levels of cellular stress (Sidrauski *et al*., 2015b). All subunits of eIF2B localised to some degree with large and medium eIF2B bodies (area of ≥ 3 μm^2) (Figure 3.12), it was therefore hypothesised that ISRIB would affect the GEF activity of these bodies. To investigate this hypothesis, FRAP analysis was used to measure the movement of eIF2 into large and medium eIF2B bodies during stress in the presence and absence of ISRIB, as an indirect measure of eIF2B activity. As shown previously in Figure 4.8, cellular stress induced by treatment with Tg (1 μM) and SA (125 μM and 500 μM), decreased movement of eIF2 into large and medium eIF2B bodies. Treatment of ISRIB alone did not impact upon the movement of eIF2 through these bodies (Figure 5.2). In cells treated with 1 μM Tg, the addition of ISRIB significantly enhanced the movement of eIF2 through the large and medium eIF2B bodies (12 % increase in eIF2 recovery), restoring the percentage recovery of eIF2 to that observed in unstressed cells (Figure 5.2A). A similar trend was observed in cells treated with a low concentration of SA (125 μM) (Figure 5.2B). The addition of ISRIB increased the percentage recovery of eIF2 by 6 %. In contrast ISRIB was not able to rescue the movement of eIF2 through large and medium eIF2B bodies in the presence of a higher concentration of SA (500 μM), with no changes in the percentage recovery of eIF2 observed (Figure 5.2C). A DMSO vehicle control confirmed that these observed changes to the movement of eIF2 through the eIF2B bodies were a direct result of ISRIB (Figure 5.3).

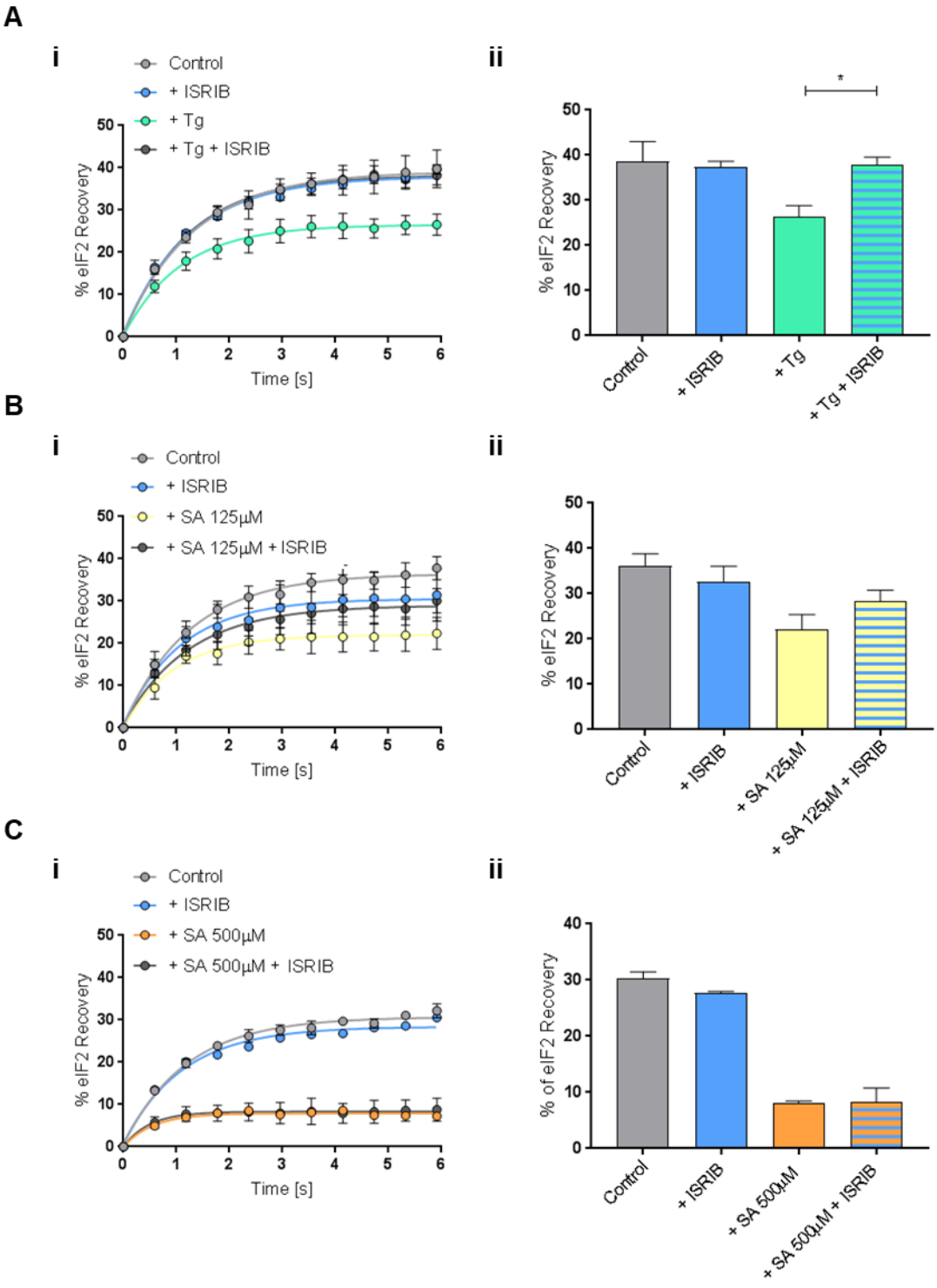

Figure 5.2 ISRIB can reverse the effect that cellular stress has on the movement of eIF2 into large and medium eIF2B bodies dependent on the levels of cellular stress. FRAP analysis was carried out on eIF2α-GFP localised to large and medium eIF2B bodies in U373 cells transfected with eIF2α-GFP and eIF2Bε-RFP to mark the eIF2B bodies. Cells were treated with 200 nM ISRIB alone or in combination with (A) 1 µM Tg, (B) 125 µM SA or (C) 500 µM SA. (i) FRAP recovery curves were plotted and (ii) the mean ± s.e.m percentage of eIF2α-GFP recovery was determined. FRAP analysis was performed on 10 bodies (n=3). P-values were derived from a Kruskal-Wallis test (P = 0.0922), followed by a Conover-Inman analysis * $p \leq 0.05$.

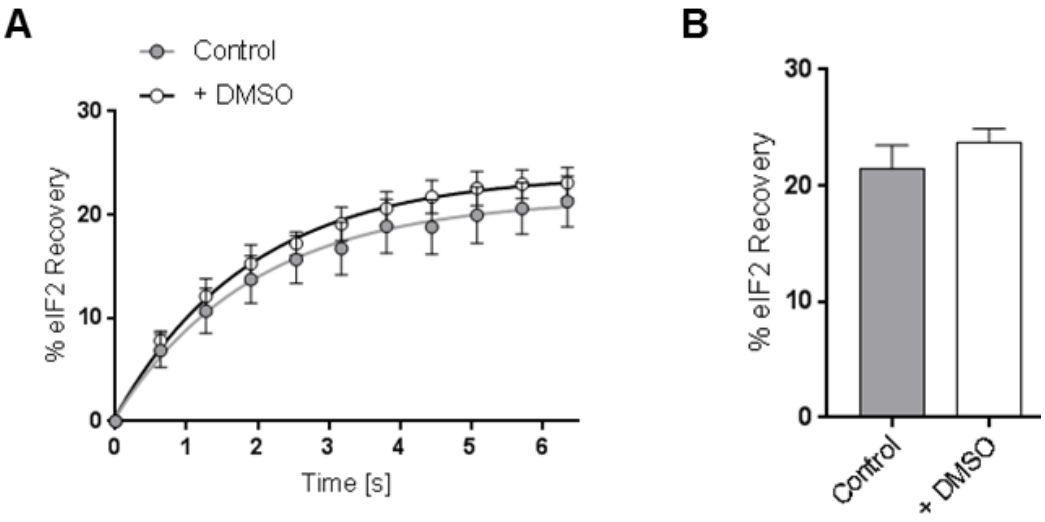

Figure 5.3 DMSO does not influence the movement of eIF2 through large and medium eIF2B bodies.

FRAP analysis was carried out on eIF2α-GFP localised to large and medium eIF2B bodies in U373 cells transfected with eIF2α-GFP and eIF2Bε-RFP to mark the eIF2B bodies. Cells were treated with DMSO as a vehicle control for ISRIB. (A) FRAP recovery curves were plotted and (B) the mean ±s.e.m percentage of eIF2α-GFP recovery was determined. FRAP analysis was performed on 10 bodies (n=3).

5.2.3 Treatment with ISRIB increases the movement of eIF2 into small eIF2B bodies

The mechanism of action of ISRIB relies upon stabilisation of eIF2B in its decameric form to enhance eIF2B GEF activity (Sidrauski *et al*., 2015b; Tsai *et al*., 2018; Zyryanova *et al*., 2018). In Chapter 3, eIF2B bodies with an area ≤ 2.99 μm^2, classified as small eIF2B bodies, primarily presented with only the catalytic subunits of eIF2B (eIF2Bγ and eIF2Bε) localised to them. As all subunits of eIF2B are required to form the decameric conformation, it was hypothesised that ISRIB would not impact upon the GEF activity of eIF2B localised to these bodies. In order to investigate this hypothesis, FRAP analysis was used to measure the movement of eIF2 into small eIF2B bodies as an indirect measure of eIF2B activity. The FRAP analysis was carried out on untreated cells or cells treated with ISRIB (Figure 5.4). Rather surprisingly, the percentage recovery of eIF2 to small eIF2B bodies was found to significantly increase (8 % increase in eIF2 recovery) in the presence of ISRIB (Figure 5.4A). A DMSO vehicle control confirmed that this observed increase in the movement of eIF2 was a direct result of ISRIB (Figure 5.4B).

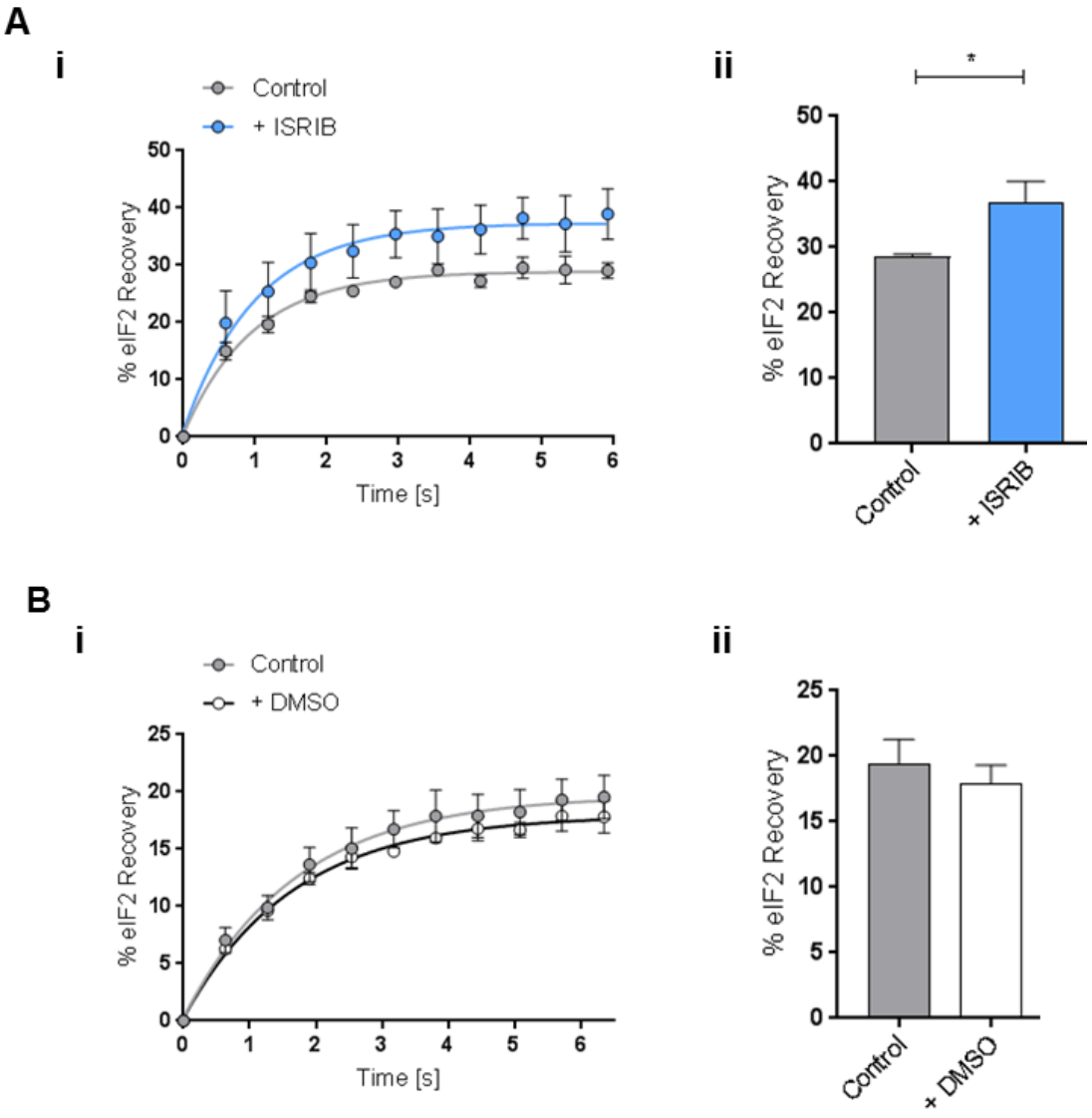

Figure 5.4 The movement of eIF2 into small eIF2B bodies is enhanced during ISRIB treatment.

FRAP analysis was carried out on eIF2α-GFP localised to small eIF2B bodies in U373 cells transfected with eIF2α-GFP and eIF2Bε-RFP to mark the eIF2B bodies. Cells were either untreated or treated with (A) 200 nM ISRIB or (B) a DMSO vehicle control. (i) FRAP recovery curves were plotted and (ii) the mean ± s.e.m percentage of eIF2α-GFP recovery was determined. FRAP analysis was performed on 10 bodies (n=3). P-values were derived from a Kruskal-Wallis test ($p = 0.0495$), followed by a Conover-Inman analysis * $p \leq 0.05$.

5.2.1 The localisation of eIF2Bδ to small eIF2B bodies is increased during ISRIB treatment

Although the γ and ε subunits of eIF2B are sufficient to perform eIF2B GEF activity, eIF2B complexes that contain the regulatory eIF2B subunits display enhanced GEF activity (Dev *et al*., 2010; Fabian *et al*., 1997; Liu *et al*., 2011; Williams *et al*., 2001). Chapter 3 of this study demonstrated that the regulatory subunits of eIF2B predominately localise to large and medium eIF2B bodies with very few small eIF2B bodies co-localising with regulatory subunits (Figure 3.12). To address whether the increased movement of eIF2 into small eIF2B bodies induced by ISRIB could be linked to a change in the subunit composition of these bodies ICC analysis was carried out. Cells transiently expressing eIF2Bε-GFP were either untreated or treated with ISRIB, and then subjected to ICC with primary antibodies to eIF2Bα, eIF2Bβ or eIF2Bδ. Using confocal microscopy counts were carried out across a population of 50 cells to determine the percentage of large and medium or small eIF2B bodies that eIF2Bα, eIF2Bβ or eIF2Bδ localised to. No changes were observed for eIF2Bα or eIF2Bβ upon addition of ISRIB, however a significant increase in the median localisation of eIF2Bδ to small eIF2B bodies (39 %) was observed (Figure 5.5). No significant difference in the percentage of large and medium bodies that eIF2Bδ localised too was observed in the presence of ISRIB (Figure 5.5).

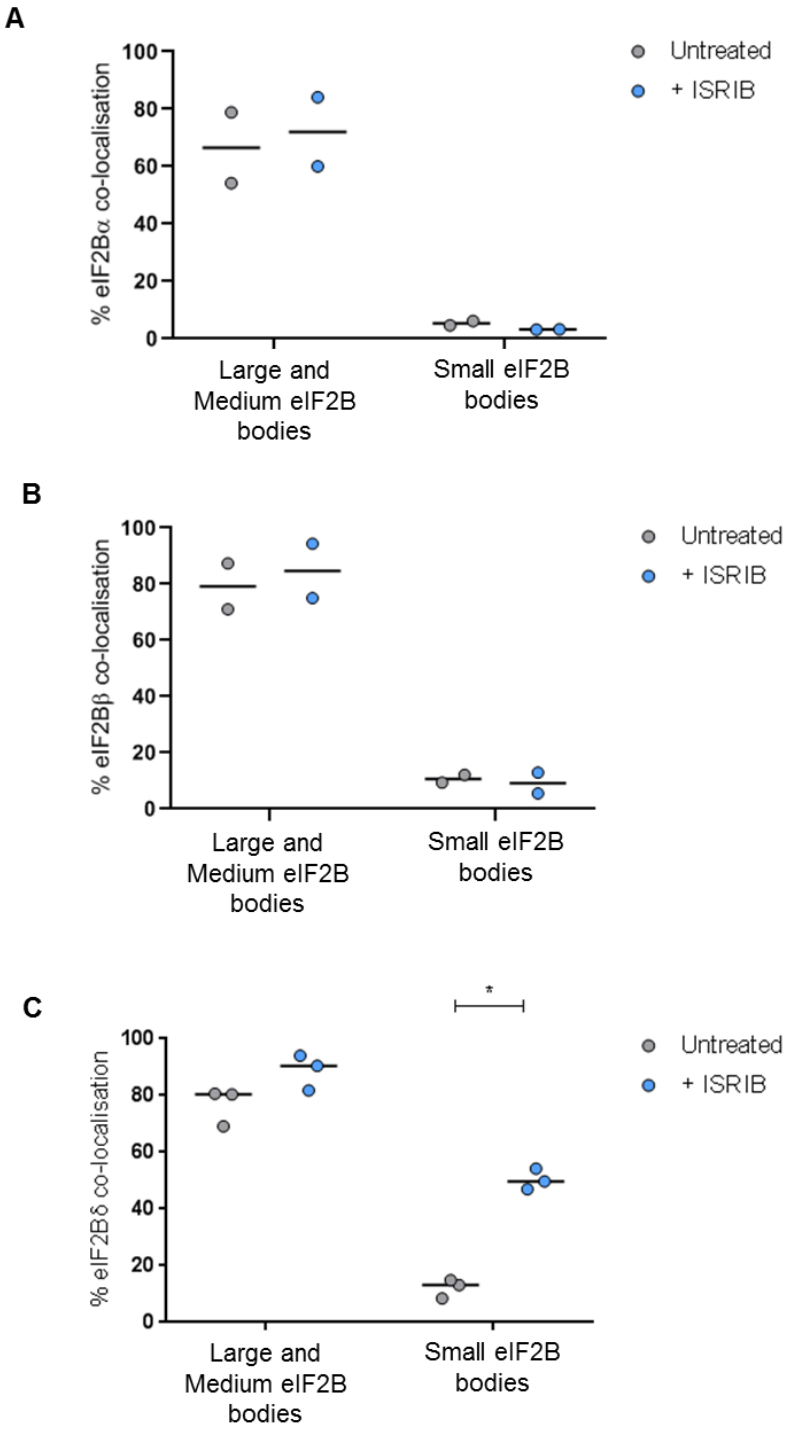

Figure 5.5 eIF2Bδ localises to an increased percentage of small eIF2B bodies following treatment with ISRIB.

U373 cells were transfected with eIF2Bε-GFP and either untreated or treated with 200 nM ISRIB. Cells were fixed in methanol and subject to ICC with a primary (A) eIF2Bα, (B) eIF2Bβ or (C) eIF2Bδ antibodies and visualised using an appropriate secondary antibody conjugated to Alexa Fluor 568. Within a population of 50 cells, the median percentage of co-localisation between anti-eIF2Bα, anti-eIF2Bβ or anti-eIF2Bδ and large and medium or small eIF2Bε-GFP bodies was determined (n=2 for eIF2Bα and eIF2Bβ; n=3 for eIF2Bδ). P-values were derived from a Kruskal-Wallis test ($p = 0.0156$), followed by a Conover-Inman analysis * $p \leq 0.05$.

In order to determine if the increased percentage of small eIF2B bodies with eIF2Bδ co-localised was a direct effect of ISRIB interacting with eIF2Bδ, the localisation of eIF2Bδ was analysed in CHO cells harbouring eIF2Bδ (L180F) mutation. This mutation resides within the ISRIB binding pocket of eIF2B and prevents ISRIB from enhancing eIF2B activity (Sekine *et al*., 2015; Tsai *et al*., 2018; Zyryanova *et al*., 2018). eIF2Bε-RFP was expressed in CHO cells containing wt eIF2Bδ or mutant eIF2Bδ (L180F), cells were either untreated or treated with ISRIB and then subject to ICC with a primary eIF2Bδ antibody (Figure 5.6). To ensure that the eIF2Bδ mutant did not affect antibody recognition, dot blot analysis was carried out (Figure 5.7A). Analysis of extracts prepared from both the wt and the mutant cells showed eIF2Bδ was recognised by the antibody. Using confocal microscopy, counts were performed across a population of 25 cells to determine the percentage of large and medium or small eIF2B bodies that showed eIF2Bδ localisation (Figure 5.7B). Upon ISRIB treatment, an increase in eIF2Bδ localisation to small eIF2B bodies was observed for the wt eIF2Bδ. Interestingly, in the mutant cells, no increase in distribution of mutant eIF2Bδ (L180F) to small bodies was observed.

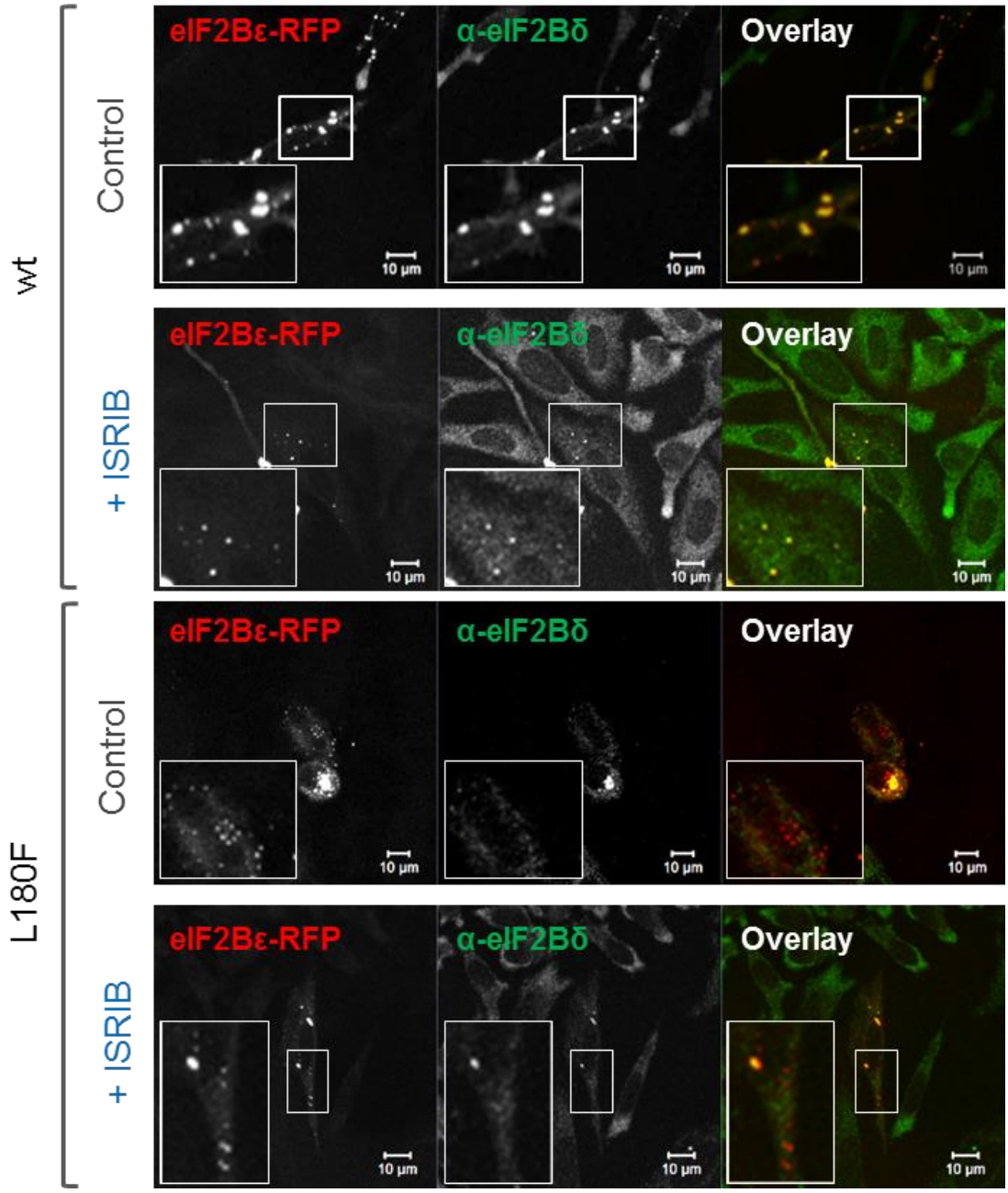

Figure 5.6 Localisation of eIF2Bδ to small eIF2B bodies in the presence of ISRIB is decreased by an eIF2Bδ ISRIB-resistant mutation.
CHO cells harbouring wt eIF2Bδ or mutant eIF2Bδ (L180F) were transfected with eIF2Bε-RFP and treated with 200 nM ISRIB. Cells were fixed in methanol and subject to ICC with a primary anti-eIF2Bδ antibody, detected using an appropriate secondary antibody conjugated to Alexa Fluor 568. The localisation of eIF2Bδ was visualised by confocal microscopy.

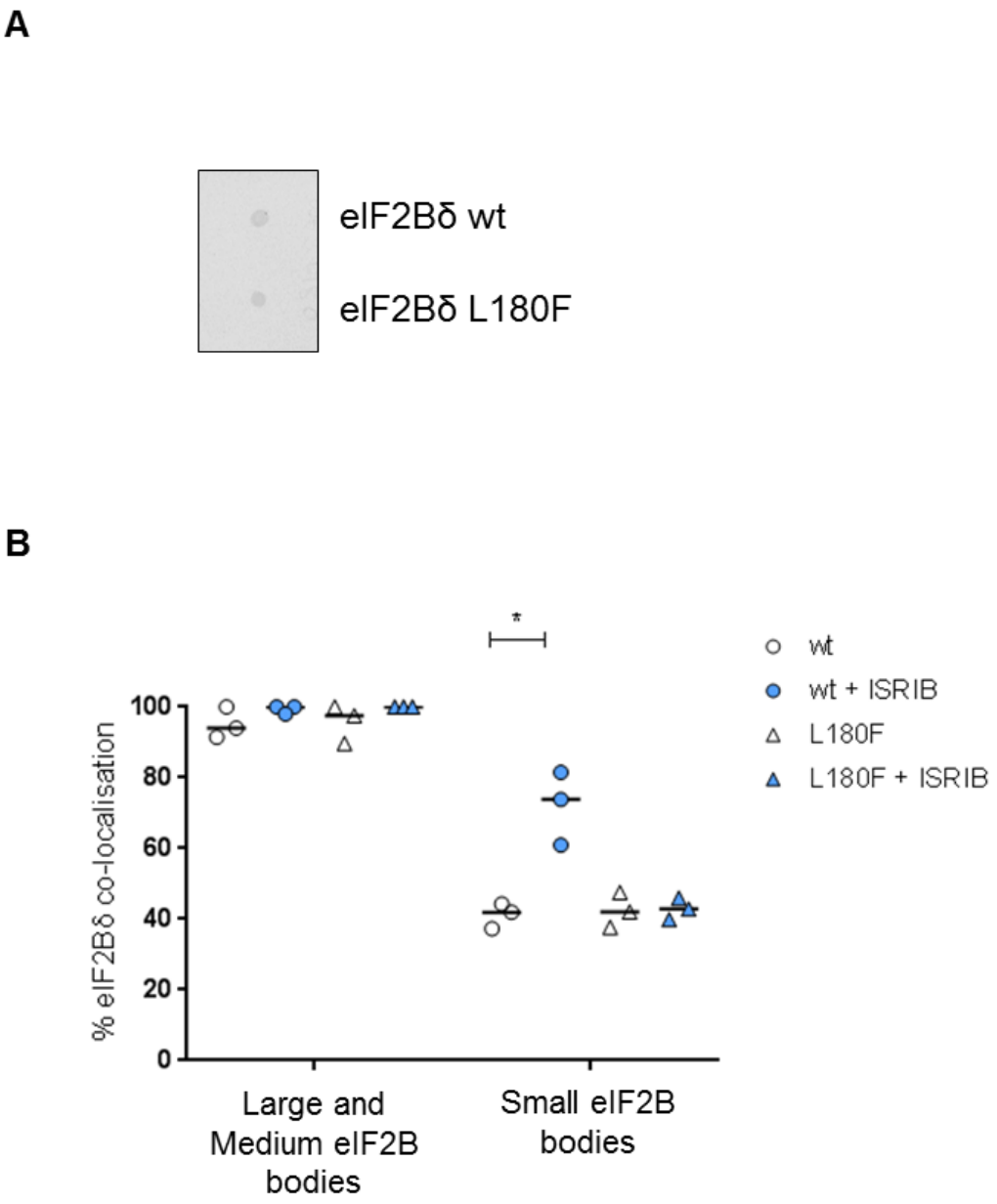

Figure 5.7 Localisation of eIF2Bδ to small eIF2B bodies is a direct consequence of ISRIB interacting with eIF2Bδ.

(A) CHO cells containing wt eIF2Bδ or mutant eIF2Bδ (L180F) were subject to dot blot analysis for anti-eIF2Bδ. (B) CHO cells containing wt eIF2Bδ or mutant eIF2Bδ (L180F) were transfected with eIF2Bε-RFP and either untreated or treated with 200 nM ISRIB. Cells were fixed in methanol and subject to ICC with a primary anti-eIF2Bδ antibody, detected using an appropriate secondary antibody conjugated to Alexa Fluor 568. Using confocal microscopy, the median percentage of co-localisation between anti-eIF2Bδ and large and medium or small eIF2Bε-RFP bodies was determined in the presence or absence of ISRIB treatment (25 cells, n=3). P-values were derived from a Kruskal-Wallis test ($p = 0.4125$), followed by a Conover-Inman analysis, * $p \leq 0.05$.

5.2.2 The size and distribution of eIF2B bodies is altered during ISRIB treatment

The influence of ISRIB on small eIF2B body composition and activity reflects the changes that low levels of cellular stress were observed to have on small eIF2B bodies in Chapter 4 of this study (Figure 4.10 and Figure 4.11). Cellular stress was found to also increase the number of small eIF2B bodies and the size of large eIF2B bodies (Figure 4.12). In order to determine if ISRIB may also affect the number of small eIF2B bodies, U373 cells expressing eIF2Bε-GFP were either untreated or treated with ISRIB and then using confocal microscopy counts were carried out to determine the median number of large and medium or small eIF2B bodies across a population of 50 cells (Figure 5.8A). ISRIB treatment significantly enhanced the median number of small eIF2B bodies (44 % increase) when compared to untreated cells. No significant change to the number of large and medium eIF2B bodies was observed.

In order to determine if ISRIB also influenced the size of large eIF2B bodies, eIF2Bε-GFP was expressed in U373 cells and cells containing large eIF2B bodies were imaged. The area of the large eIF2B bodies were measured using Image J software in both ISRIB treated and untreated cells (Figure 5.8B). ISIRB treatment significantly increased the area of large eIF2B bodies by approximately 2-fold.

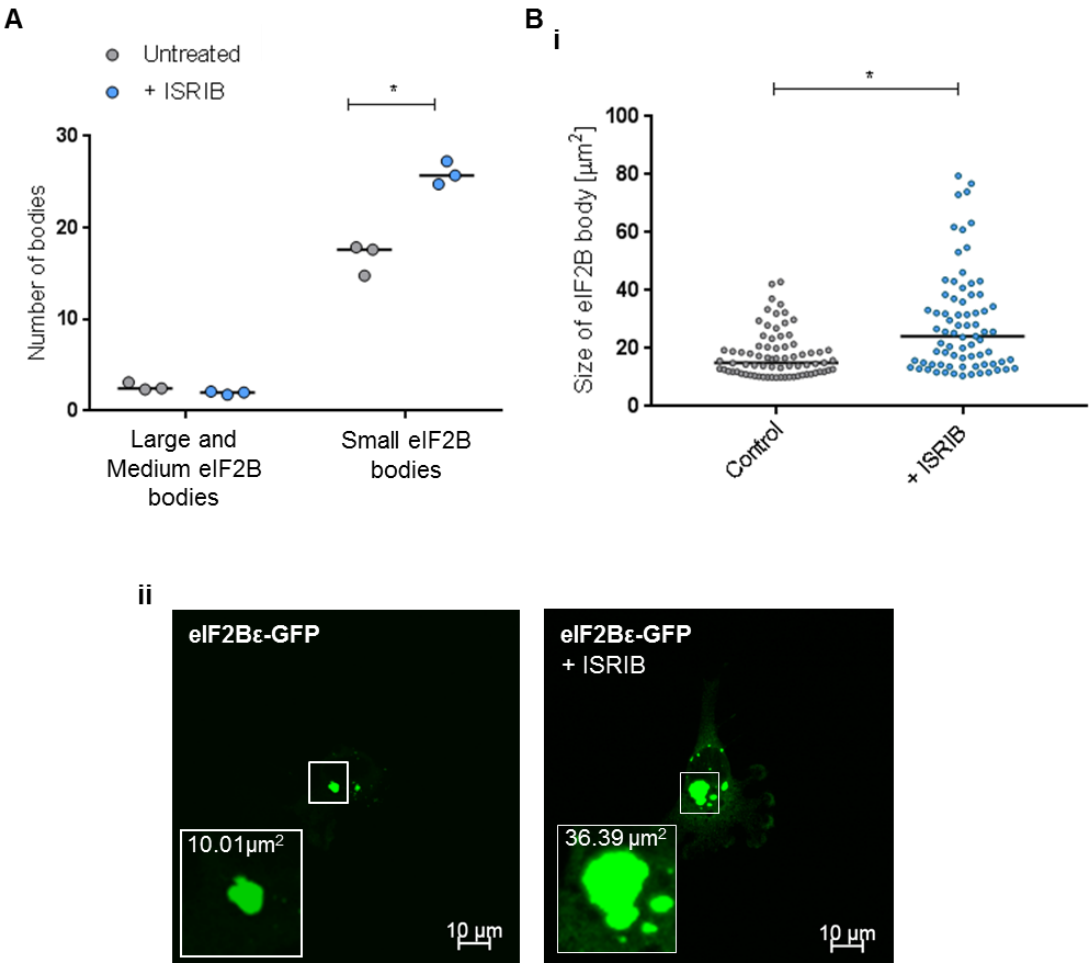

Figure 5.8 Following treatment with ISRIB the number of small eIF2B bodies increased and the size of large eIF2B bodies increased.
U373 cells were transfected with eIF2Bε-GFP and either untreated or treated with 200 nM ISRIB. (A) Using confocal microscopy counts were performed to determine the median number of large and medium or small eIF2B bodies within a population of 50 cells (n=3). (B) (i) Cells containing large eIF2B bodies were imaged by confocal microscopy and image J was used to determine the median area of large eIF2B bodies (25 eIF2B bodies, n=3). (ii) Representative images confocal images are shown. P-values were derived from a Kruskal-Wallis test ((A) $p = 0.0156$; (B) $p = < 0.0001$), followed by a Conover-Inman analysis, * $p \leq 0.05$.

5.2.3 DBM appears to increase translation under normal cellular conditions and during cellular stress

DBM is a naturally occurring structural analogue of curcumin, with widely reported anti-cancer properties (Oo Khor *et al*., 2009) that has recently been shown to also restore translation under conditions of cellular stress induced by Tg (Halliday *et al*., 2017). In order to determine if DBM could enhance translation during the conditions of cellular stress used in this study (specifically Tg treatment) a puromycin incorporation assay was carried out on U373 cells to measure levels of global protein synthesis. Cells were treated with 1 µM Tg, in the presence or absence of 20 µM DBM (Figure 5.9). Tg treatment alone decreased levels of global translation by approximately 45 % while the addition of DBM to the Tg treated cells appeared to enhance translation back to normal levels. Interestingly, in contrast to ISRIB treatment, DBM treatment alone also appeared to increase translation levels (42 % increase in puromycin incorporation). It should be noted this experiment was only performed once and future experiments repeating this should be performed to confirm the trend.

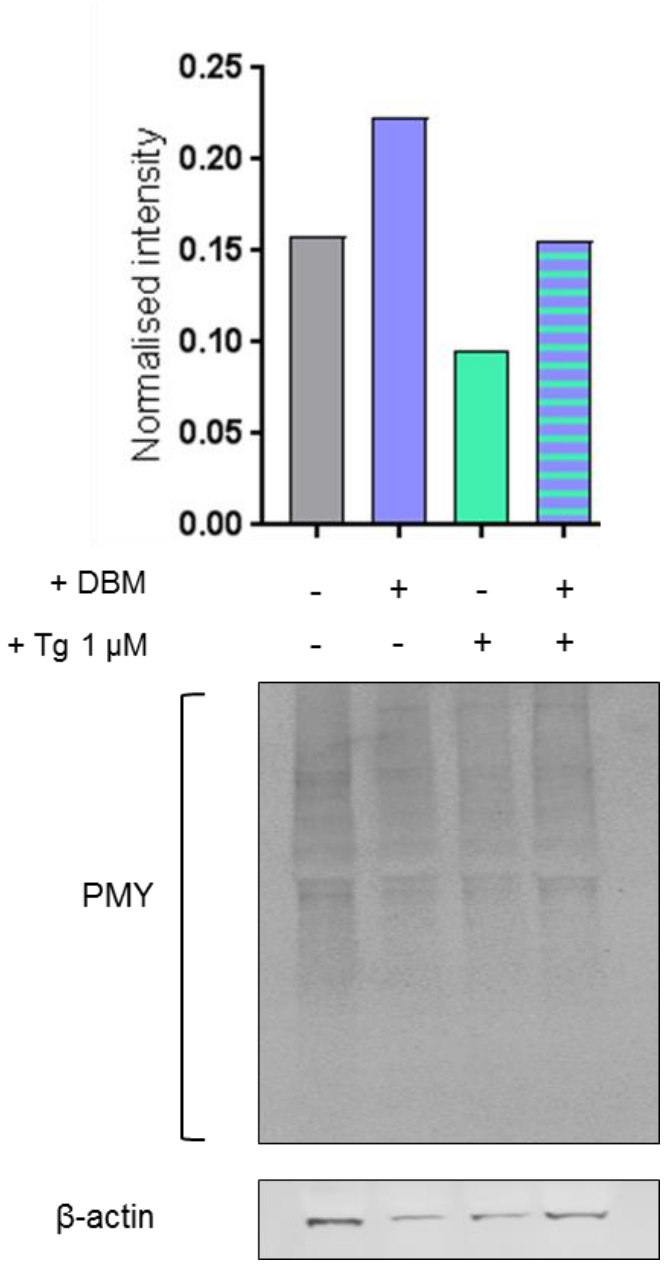

Figure 5.9 DBM treatment increases translation in cells under normal growth conditions and can restore translation rates in cells during Tg induced cellular stress. Puromycin incorporation assays were carried out on U373 cells untreated or treated with 20 µM DBM or 1 µM Tg alone, or in combination. Levels of puromycin where normalised to β-actin and are presented as mean ± SD for each treatment (n=1).

5.2.4 DBM cannot rescue the movement of eIF2 into Large and Medium eIF2B bodies during cellular stress

The mechanism through which DBM restores translation is currently unknown. Unlike ISRIB, DBM does not stabilise eIF2B in its decameric conformation (Halliday *et al*., 2017), however both drugs do share the same downstream effect of restoring translation in stressed cells. Having shown ISRIB modulates eIF2B bodies in a number of different ways (Figure 5.2, Figure 5.4 and Figure 5.5) we were intrigued to determine if DBM may also have an impact upon the properties of eIF2B bodies. Firstly, the effect of DBM on the activity of eIF2B localised to large and medium eIF2B bodies in stressed cells was investigated. FRAP analysis was used as a tool to measure the movement of eIF2 into eIF2B bodies as an indirect measurement of eIF2B activity. Cells were subject to Tg-induced cellular stress either in the presence, or the absence of DBM (Figure 5.10). Similarly to ISRIB, treatment with DBM alone did not impact upon the movement of eIF2 through the large and medium eIF2B bodies in untreated cells (Figure 5.10). However, in contrast to ISRIB, in cells treated with Tg, DBM also had no impact upon the movement of eIF2 through large and medium eIF2B bodies (Figure 5.10). These data suggest that DBM does not restore translation in stressed cells through increasing the activity of eIF2B localised to large and medium eIF2B bodies.

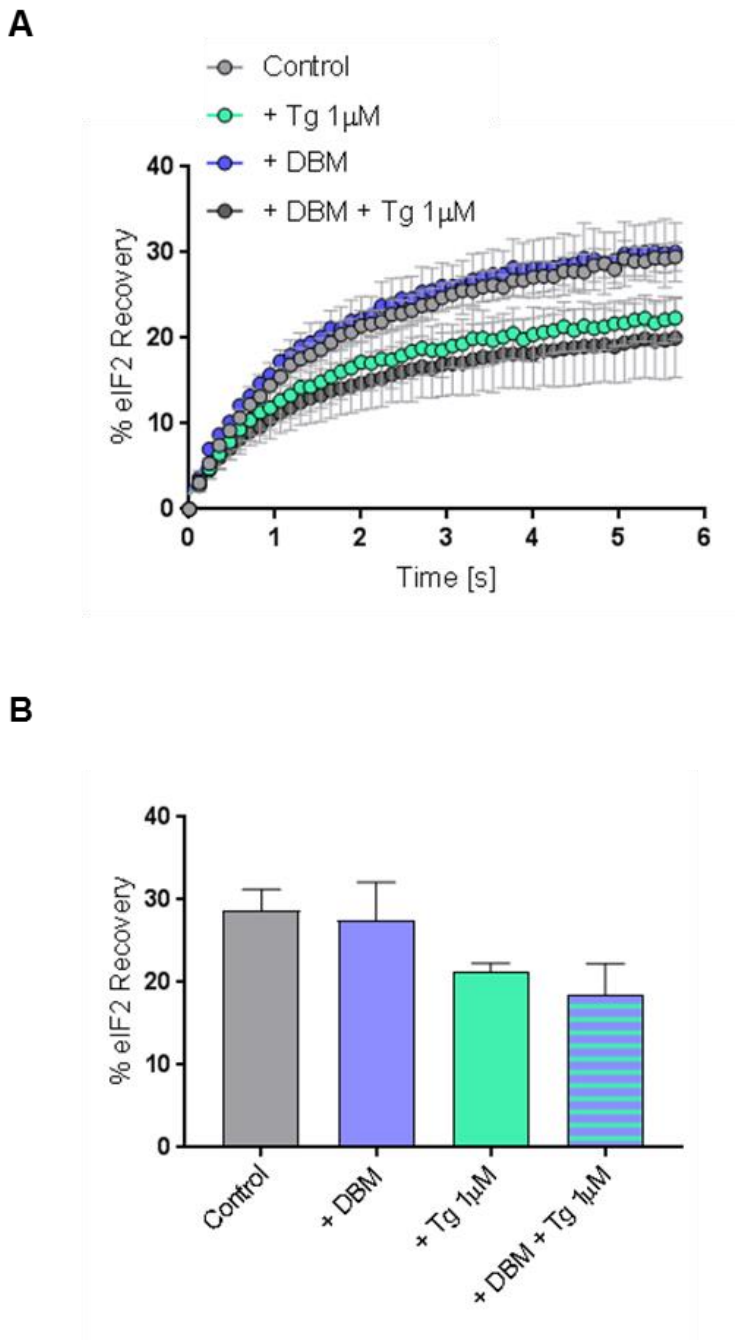

Figure 5.10 DBM cannot rescue the decreased movement of eIF2 through large and medium eIF2B bodies during Tg induced cellular stress.

FRAP analysis was carried out on eIF2α-GFP localised to large and medium eIF2B bodies in U373 cells transfected with eIF2α-GFP, and eIF2Bε-RFP to mark the eIF2B bodies. Cells were either untreated or treated with 20 µM DBM or 1 µM Tg, either alone or in combination (A) FRAP recovery curves were plotted and (B) the mean ± s.e.m percentage of eIF2α-GFP recovery was determined. FRAP analysis was performed on 10 bodies (n=2).

5.2.5 DBM increases the movement of eIF2 into small eIF2B bodies

These data presented in Figure 5.10 suggests that DBM does not restore translation through modulating the activity of eIF2B localised to large and medium eIF2B bodies. The data generated in Figure 5.4 suggests that ISRIB treatment enhances the GEF activity of small eIF2B bodies. In order to determine if DBM had a similar influence on the activity of eIF2B localised to small eIF2B bodies, FRAP analysis was performed as an indirect measure of eIF2B activity. U373 cells expressing eIF2α-GFP were either untreated or treated with DBM and FRAP analysis performed on eIF2α-GFP localised to small eIF2B bodies (eIF2Bε-RFP was also expressed to mark the eIF2B bodies) (Figure 5.11). Interestingly, the percentage recovery of eIF2 to small eIF2B bodies was found to increase by 10 % in the presence of DBM.

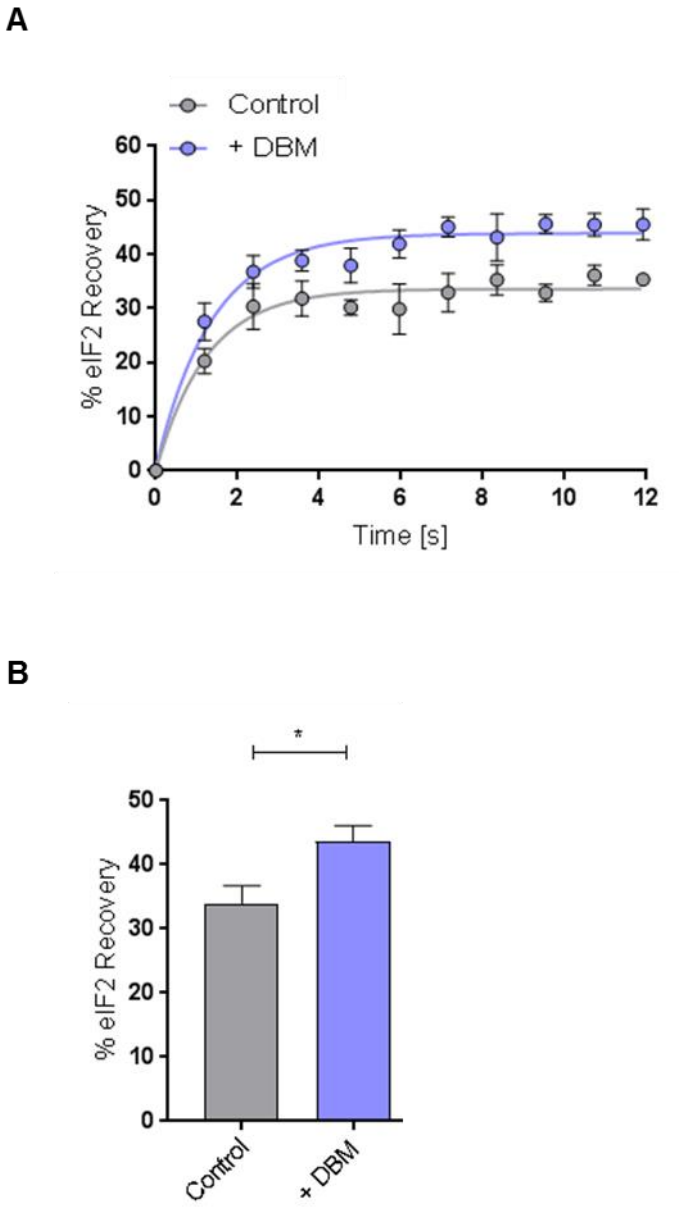

Figure 5.11 The movement of eIF2 through small eIF2B bodies is enhanced during treatment with DBM.

FRAP analysis was carried out on eIF2α-GFP localised to small eIF2B bodies in U373 cells transfected with eIF2α-GFP and eIF2Bε-RFP to mark the eIF2B bodies. Cells were either untreated or treated with 20 µM DBM and FRAP analysis was performed on 10 small bodies (n=3). (A) FRAP recovery curves were plotted and (B) the mean ± s.e.m percentage of eIF2α-GFP recovery was determined. P-values were derived from a Kruskal-Wallis test ($p = 0.0495$), followed by a Conover-Inman analysis, * $p \leq 0.05$.

5.2.6 DBM promotes an increase in the localisation of eIF2Bδ to small eIF2B bodies

The movement of eIF2 into small eIF2B bodies was found to increase in the presence of DBM suggesting that DBM may modulate the GEF activity of eIF2B localised to these eIF2B bodies (Figure 5.11). An increase in the movement of eIF2 into small eIF2B bodies was also observed in stressed cells (Figure 4.10) and cells treated with ISRIB (Figure 5.4). Under these conditions the increased movement of eIF2 correlated with an increase in the percentage of small eIF2B bodies to which eIF2Bδ localised (Figure 4.11 and Figure 5.5). In order to determine if DBM also increased eIF2Bδ localisation to small eIF2B bodies, ICC with primary eIF2Bα, eIF2Bβ or eIF2Bδ antibodies was carried out on U373 cells expressing eIF2Bε-GFP, either in the presence or absence of DBM. Counts were carried out across a population of 50 cells to determine the percentage co-localisation between eIF2Bδ to large and medium or small eIF2Bε-GFP bodies (Figure 5.12). A significant increase in the median localisation of eIF2Bδ to small eIF2B bodies (49 %) was observed in the presence of DBM. Representative images are shown in Figure 5.13. No significant difference in the percentage of large and medium bodies that eIF2Bδ localised to was observed in the presence of DBM (Figure 5.12B).

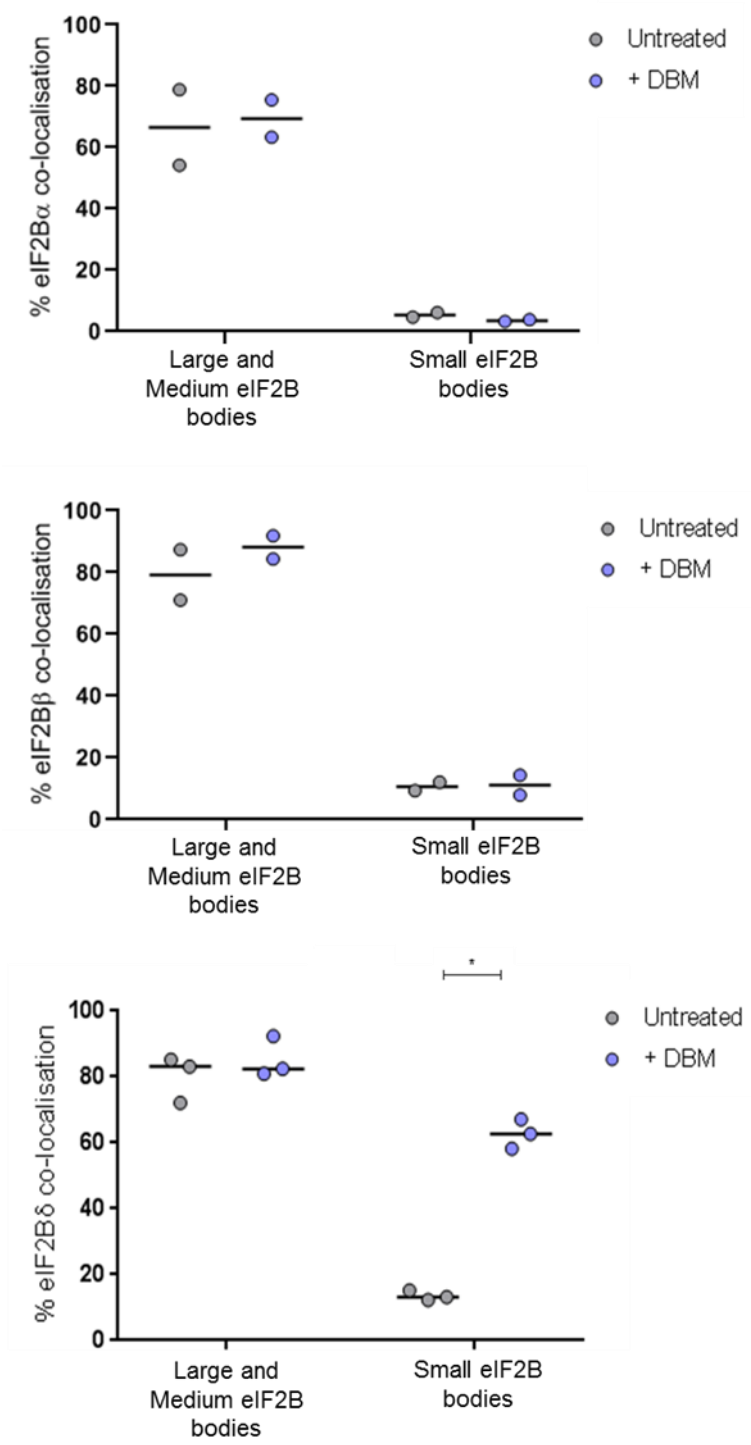

Figure 5.12 eIF2Bδ localises to an increased percentage of small eIF2B bodies following treatment with DBM.

U373 cells were transfected with eIF2Bε-GFP and either untreated or treated with 20 µM DBM. Cells were fixed in methanol and subject to ICC with primary (A) anti-eIF2Bα, (B) anti-eIF2Bβ or (C) anti-eIF2Bδ antibodies, visualised using an appropriate secondary antibody conjugated to Alexa Flour 568. Within a population of 50 cells, the median percentage of co-localisation between anti-eIF2Bδ and large and medium or small eIF2Bε-GFP bodies was determined (n=2 for eIF2Bα and eIF2Bβ; n=3 for eIF2Bδ). P-values were derived from a Kruskal-Wallis test ($p = 0.0495$), followed by a Conover-Inman analysis, * $p \leq 0.05$.

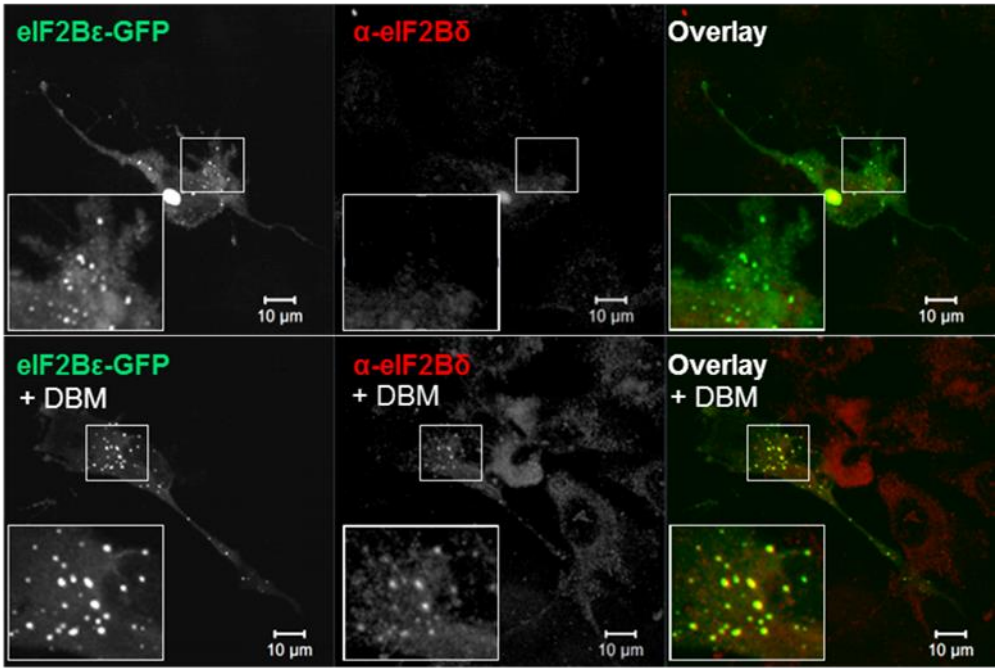

Figure 5.13 eIF2Bδ localises to small eIF2B bodies following treatment with DBM. U373 cells were transfected with eIF2Bε-GFP and either untreated or treated with 20 µM DBM. Cells were fixed in methanol and subject to ICC with a primary anti-eIF2Bδ antibody, visualised using an appropriate secondary antibody conjugated to Alexa Flour 568. Representative confocal images are presented in the panels.

5.2.7 Trazodone partially restores stress induced translational depression.

Similarly to ISRIB and DBM, Trazodone has also been identified as a small molecule that can restore translation in cells subjected to Tg induced cellular stress (Halliday *et al*., 2017). Like DBM, Trazodone is an FDA approved drug. It can modulate the activity of serotonin receptors and thus is currently prescribed as an antidepressant (Maj *et al*., 1979). The mechanism through which trazodone enhances protein synthesis in stressed cells is largely unknown. Having shown that the translation enhancing drugs ISRIB and DBM modulate the properties of eIF2B bodies we were intrigued to determine if trazodone may also have an impact upon the properties of eIF2B bodies. As trazodone has previously been shown to enhance translation in the presence of Tg induced cellular stress (Halliday *et al*., 2017), we focused our study on the impact trazodone has on eIF2B bodies during this type of stress. Firstly, it was important to determine if trazodone could enhance translation under the conditions of Tg induced cellular stress used in this study. Preliminary evidence for this was provided using a puromycin incorporation assay carried out on U373 cells subject to treatment with 1 µM Tg for 1 hour, in the presence or absence of trazodone (Figure 5.14). Tg treatment alone decreased levels of global translation to approximately 44 % of untreated cells levels. The addition of trazodone to Tg treated cells enhanced translation back to 69 % of untreated levels. Interestingly, unlike DBM but similar to ISRIB, trazodone treatment alone did not enhance translation (Figure 5.14). It should be noted this experiment was only performed once and future experiments repeating this should be performed to confirm the trend.

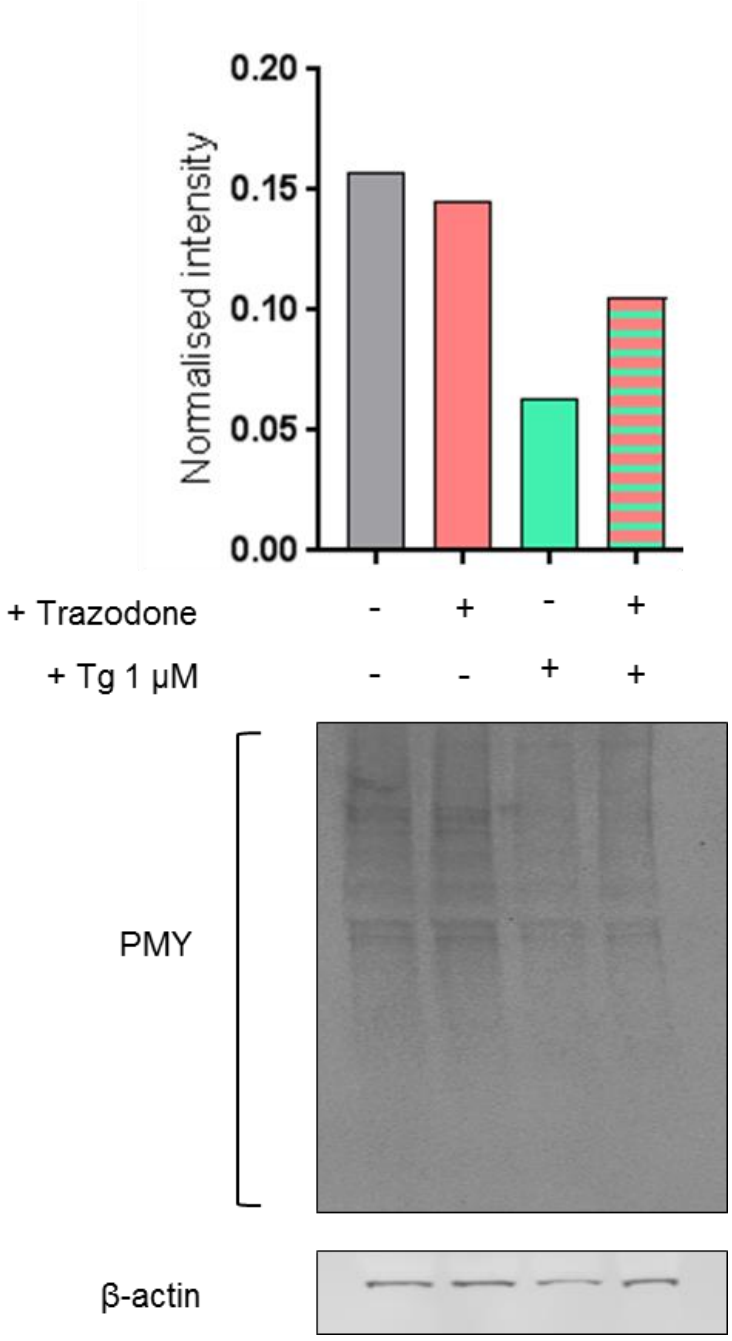

Figure 5.14 Trazodone treatment partially restores translation in cells during Tg induced cellular stress.
Puromycin incorporation assays were carried out on U373 cells untreated or treated with 20 µM trazodone or 1 µM Tg either alone, or in combination. Levels of puromycin where normalised to β-actin and are presented as mean ± SD for each treatment (n=1).

5.2.8 During cellular stress trazodone increases the movement of eIF2 through large and medium eIF2B bodies

Having determined that trazodone enhanced translation in cells subject to Tg induced cellular stress, the effect of trazodone on the GEF activity of large and medium eIF2B bodies was investigated. FRAP analysis was used as a tool to measure the movement of eIF2 into eIF2B bodies as an indirect measurement of eIF2B activity. FRAP analysis was carried out on eIF2α-GFP localised to large and medium eIF2B bodies in cells that were subjected to Tg-induced cellular stress either in the presence, or the absence of trazodone (Figure 5.15). Treatment with trazodone alone did not impact upon the movement of eIF2 through the large and medium eIF2B bodies (Figure 5.15). In cells treated with Tg, the movement of eIF2 was decreased by 7 %. The addition of trazodone to Tg treated cells increased movement of eIF2 through large and medium eIF2B bodies by 2 % (Figure 5.15).

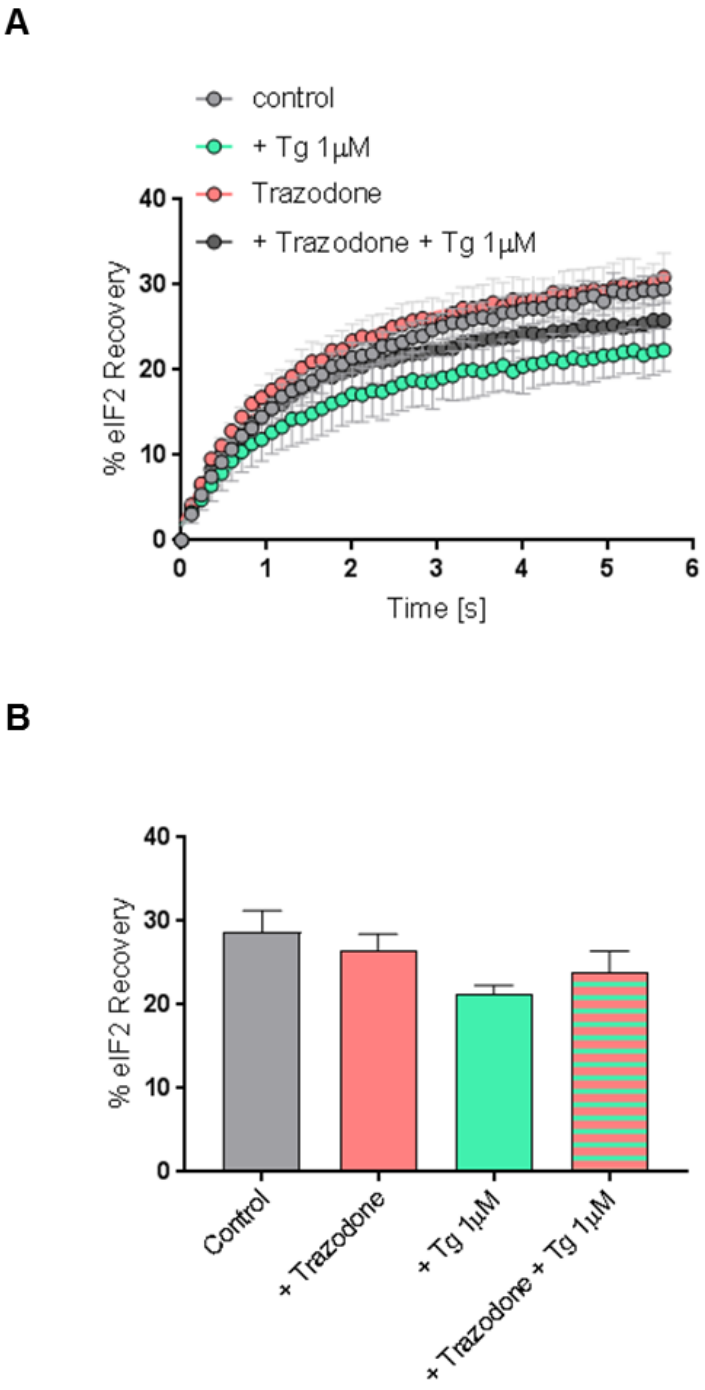

Figure 5.15 Trazodone increases the movement of eIF2 through large and medium eIF2B bodies during Tg induced cellular stress.

FRAP analysis was carried out on eIF2α-GFP localised to large and medium eIF2B bodies in U373 cells transfected with eIF2α-GFP and eIF2Bε-RFP to mark the eIF2B bodies. Cells were treated with 20 μM Trazodone or 1 μM Tg, either alone or in combination. FRAP analysis was performed on 10 bodies (n=2). (i) FRAP recovery curves were plotted and (ii) the mean ± s.e.m percentage of eIF2α-GFP recovery was determined.

5.2.9 Trazodone decreases the movement of eIF2 into small eIF2B bodies

The movement of eIF2 through small eIF2B bodies was increased in the presence of both ISRIB (Figure 5.4) and DBM (Figure 5.11), suggesting that modulating the GEF activity of small eIF2B bodies may be a common trend of translation enhancing drugs. In order to determine if trazodone could modulate the activity of eIF2B localised to small eIF2B bodies FRAP analysis was performed on eIF2α-GFP localised to small eIF2B bodies in untreated cells and cells treated with trazodone (Figure 5.16A). In contrast to the trend observed for ISRIB and DBM treated cells, when cells were treated with trazodone, the percentage recovery of eIF2 to small eIF2B bodies was found to decrease by approximately 10 % (Figure 5.16B).

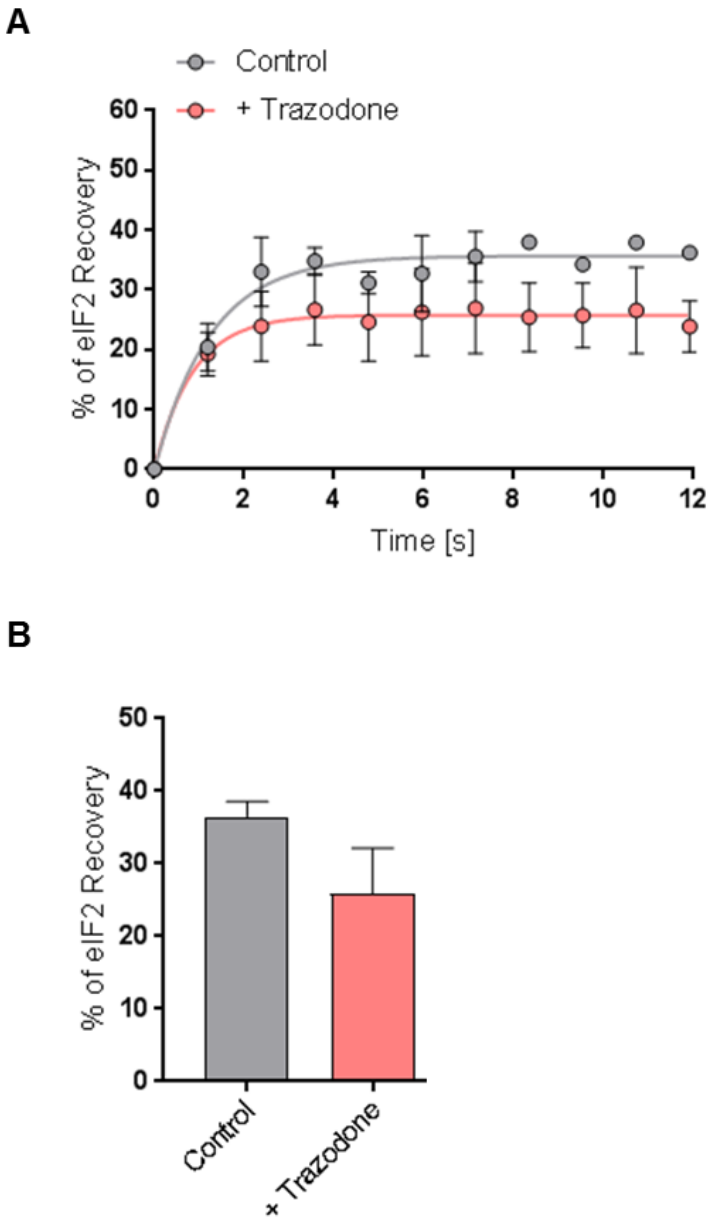

Figure 5.16 The movement of eIF2 through small eIF2B bodies is decreased during treatment with Trazodone.
FRAP analysis was carried out on eIF2α-GFP localised to small eIF2B bodies in U373 cells transfected with eIF2α-GFP and eIF2Bε-RFP to mark the eIF2B bodies. Cells were treated with 20 µM Trazodone and FRAP analysis was performed on 10 bodies (n=2). (A) FRAP recovery curves were plotted and (B) the mean ± s.e.m percentage of eIF2α-GFP recovery was determined.

5.3 Discussion

Pathological disruption of the ISR is common in a number of different diseases including, cancer, diabetes and neurodegenerative diseases (Bi *et al*., 2005; Chou *et al*., 2017; Eizirik *et al*., 2008). Small molecules that regulate the ISR have therefore emerged as promising therapeutic tools and understanding the mechanisms of action of these drugs will enhance the likelihood that they will be used as treatments.

Recently ISRIB was identified as a small molecule that reverses phosphorylated eIF2α induced translational repression (Halliday *et al*., 2015; Sidrauski *et al*., 2013; Sidrauski *et al*., 2015a), through restoration of eIF2B activity (Sekine *et al*., 2015; Sidrauski *et al*., 2015b). It was therefore of interest to investigate if ISRIB may influence the activity of eIF2B localised to eIF2B bodies. ISRIB enhances the GEF activity of eIF2B through promoting the assembly of decameric eIF2B complexes (Sidrauski *et al*., 2015b; Tsai *et al*., 2018; Zyryanova *et al*., 2018). eIF2B subunit co-localisation data presented in Chapter 3 of this study highlighted that all subunits of eIF2B are present to some degree in large and medium sized eIF2B bodies, however small bodies mainly consist of the catalytic eIF2B subunits (Figure 3.12). This led to the hypothesis that ISRIB would increase the GEF activity of eIF2B localised to large and medium bodies during cellular stress. Indeed, in cells treated with 1 µM Tg and 125 µM SA an increase in the movement of eIF2 through large and medium eIF2B bodies was observed in the presence of ISRIB, suggesting that ISRIB increases the GEF actvity of these bodies. ISRIB however had no effect on the movement of eIF2 through large and medium bodies in cells treated with 500 µM SA. These findings suggest that ISRIB increases the GEF activity of large and medium eIF2B bodies when cellular levels of phosphorylated eIF2α are below a certain threshold. This is in concordance with recent studies that have shown ISRIB can only restore translation in cells exposed to SA at a concentration of 100 µM or less (Rabouw *et al*., 2019). The lack of regulatory eIF2B subunits localising to small eIF2B bodies led to the hypothesis that ISRIB would have no effect on the GEF activity of these bodies, as all subunits are required for decameric assembly. Surprisingly, an increase in the movement of eIF2α through these eIF2B bodies was observed during ISRIB treatment, in the absence of cellular stress, suggesting that the GEF activity of these bodies was increased (Figure 5.4). An increase in the localisation of the δ subunit of eIF2B correlated with this increased activity (Figure 5.5). In light of

these observations, it has previously been proposed that in addition to the role of ISRIB in stabilising the eIF2B decamer, ISRIB may also enhance the basal activity of eIF2B by providing a source of eIF2B that is not inhibited by phosphorylated eIF2α (Sidrauski *et al*., 2015b). The data from chapter 4 of this study has highlighted that the activity of small eIF2B bodies is not inhibited by phosphorylated eIF2α when low levels are present (Figure 4.10). In fact, the GEF activity of small eIF2B bodies appears to be increased in the presence of low levels of phosphorylated eIF2, similar to the trend observed here for ISRIB. These findings will be discussed further in Chapter 6.

The drug DBM was recently identified to have similar properties to ISRIB in terms of restoring global translation in stressed cells (Halliday *et al*., 2017). Unlike ISRIB, DBM does not promote the stability of decameric complexes of eIF2B (Halliday *et al*., 2017) and its mechanism of action remains unknown. ISRIB was able to restore the movement of eIF2 into large and medium bodies during cellular stress. It was hypothesised that this was due to all eIF2B subunits localising to these bodies and ISRIBs ability to promote decameric formation of eIF2B. In fitting with this hypothesis DBM was unable to restore the movement of eIF2 into these eIF2B bodies during stress (Figure 5.10). DBM did however modulate the activity of small eIF2B bodies. An increased localisation of eIF2Bδ to small bodies (Figure 5.12), accompanied by an increase in eIF2 movement through these bodies (Figure 5.11), was observed in cells treated with DBM. These data suggest that DBM may share a common mechanism with ISRIB whereby promoting the formation of eIF2Bδγε containing subcomplexes provides a source of eIF2B with increased activity.

Trazodone is another translation enhancing drug that has been shown to restore ISR induced-translation repression and its mechanism of action is also unknown. Trazodone appeared to partially restore the GEF activity of eIF2B localised to large and medium bodies during cellular stress (Figure 5.15); a similar trend to that observed for treatment with ISRIB. In contrast to ISRIB, trazodone does not promote decameric stability of eIF2B (Halliday *et al*., 2017) and therefore is likely to enhance activity of eIF2B localised to these bodies via a different mechanism. In human astrocytes trazodone has been shown to activate protein kinase B (AKT), a kinase involved in cell growth and survival, and it has been proposed that this is via activation of the serotonin 1A receptor (5-HT1A) (Daniele *et al*., 2015). AKT phosphorylates glycogen

synthase kinase 3 (GSK3), inactivating it (Cross *et al*., 1995). Interestingly, in its active form, GSK3 phosphorylates the C-terminal of the ε subunit eIF2B, inhibiting eIF2B activity (Welsh and Proud, 1993; Welsh *et al*., 1998). Investigating the impact of trazodone on GSK3 activity and the phosphorylation status of eIF2Bε could be an interesting avenue to explore in relation to the increased activity of eIF2B that was observed under treatment with trazodone. The effect of trazodone on the GEF activity of small eIF2B bodies was less conclusive. An overall trend suggested that Trazodone in fact decreased activity of eIF2B within these bodies (Figure 5.16); somewhat contradictory to the role of Trazodone in increasing translation. This data however is highly variable and should be repeated before conclusions are drawn.

The three small molecules investigated in this chapter all appear to have an effect on the GEF activity of eIF2B bodies. ISRIB appears to enhance the GEF activity of large and medium eIF2B bodies during acute stress, likely a consequence of its ability to stabilise decameric eIF2B (Sidrauski *et al*., 2015b; Tsai *et al*., 2018; Zyryanova *et al*., 2018). Furthermore, the data presented here point towards a secondary affect of ISRIB, whereby ISRIB can modulate subunit distribution and activity of small eIF2B bodies. DBM appears to also induce these changes to small eIF2B bodies. It could be hypothesised that the enhanced activity of these eIF2B bodies could provide a source of eIF2B to facilitate low levels of translation during episodes of acute cellular stress. Trazodone did not appear to increase the GEF activity of small eIF2B bodies, however it did appear to enhance the activity of large and medium bodies during cellular stress. It should be considered that eIF2B is the target of a number of cellular pathways to allow for tight regulation of translation. The observed effects of these drugs on the GEF activity of eIF2B bodies could therefore be indirect and a result of the drugs acting on different cellular pathways.

6. General Discussion

eIF2B has an important role in facilitating the initiation step of translation within a cell. The loading of the ribosome complex onto a target mRNA transcript requires the hydrolysis of a GTP molecule, carried by eIF2. eIF2B catalyses the recycling of eIF2-GDP into eIF2-GTP allowing for subsequent rounds of translation to occur. Previous work in yeast has shown that eIF2B localises to cytoplasmic foci, termed eIF2B bodies (Campbell *et al*., 2005; Egbe *et al*., 2015) which appear to be sites of GEF activity (Campbell *et al*., 2005). The functional localisation of eIF2B within mammalian cells had not previously been evaluated. Mutations in eIF2B are causative of the neurological disorder, VWM. The pathophysiology of VWM remains somewhat elusive and thus understanding the cellular localisation of mammalian eIF2B could provide insight into the mechanisms of VWM pathology. Although eIF2B is globally expressed, VWM primarily manifests as a leukodystrophy, characterised by defective maturation of astrocytes and oligodendrocytes (Dooves *et al.,* 2016). An astrocytoma cell line, U373, was therefore used in this study as the primary cell type for characterising eIF2B localisation.

The data presented in this study provides the first evidence that eIF2B bodies exist in mammalian cells. Unlike in yeast where cells exhibit a single eIF2B body, mammalian cells exhibited a number of different sized eIF2B bodies. Structural analysis of eIF2B has shown that eIF2B forms a heterodecamer in its native form, comprised of two eIF2B(βδγε) tetramers stabilised by an eIF2Bα homodimer (Gordiyenko *et al*., 2014; Kashiwagi *et al*., 2016; Kashiwagi *et al*., 2017; Wortham *et al*., 2014). In yeast all subunits of eIF2B have been shown to localise to eIF2B bodies and knockdown of eIF2Bα disperses the body, suggesting that decameric conformation of eIF2B is key to this localisation (Campbell *et al*., 2005; Noree *et al*., 2010; Norris *et al.,* 2019). In addition to the decameric eIF2B complex, a number of functional subcomplexes have also been isolated from mammalian cells overexpressing eIF2B subunits (Liu *et al*., 2011; Wortham *et al*., 2014). It could therefore be hypothesised that the increased number of different sized eIF2B bodies observed in mammalian cells could be related to the presence of subcomplexes. In support of this, a correlation between the size of the mammalian eIF2B body and the subunits of eIF2B present was observed (Figure 3.12). All five subunits of eIF2B were found to localise to a percentage of eIF2B bodies

with an area greater than 3 μm^2, referred to as large and medium eIF2B bodies. Whereas eIF2B bodies with an area less than 3 μm^2, termed small bodies, appeared to predominately be formed of only catalytic subunits (γ and ε subunits). A schematic representation of this data is outline in Figure 6.1.

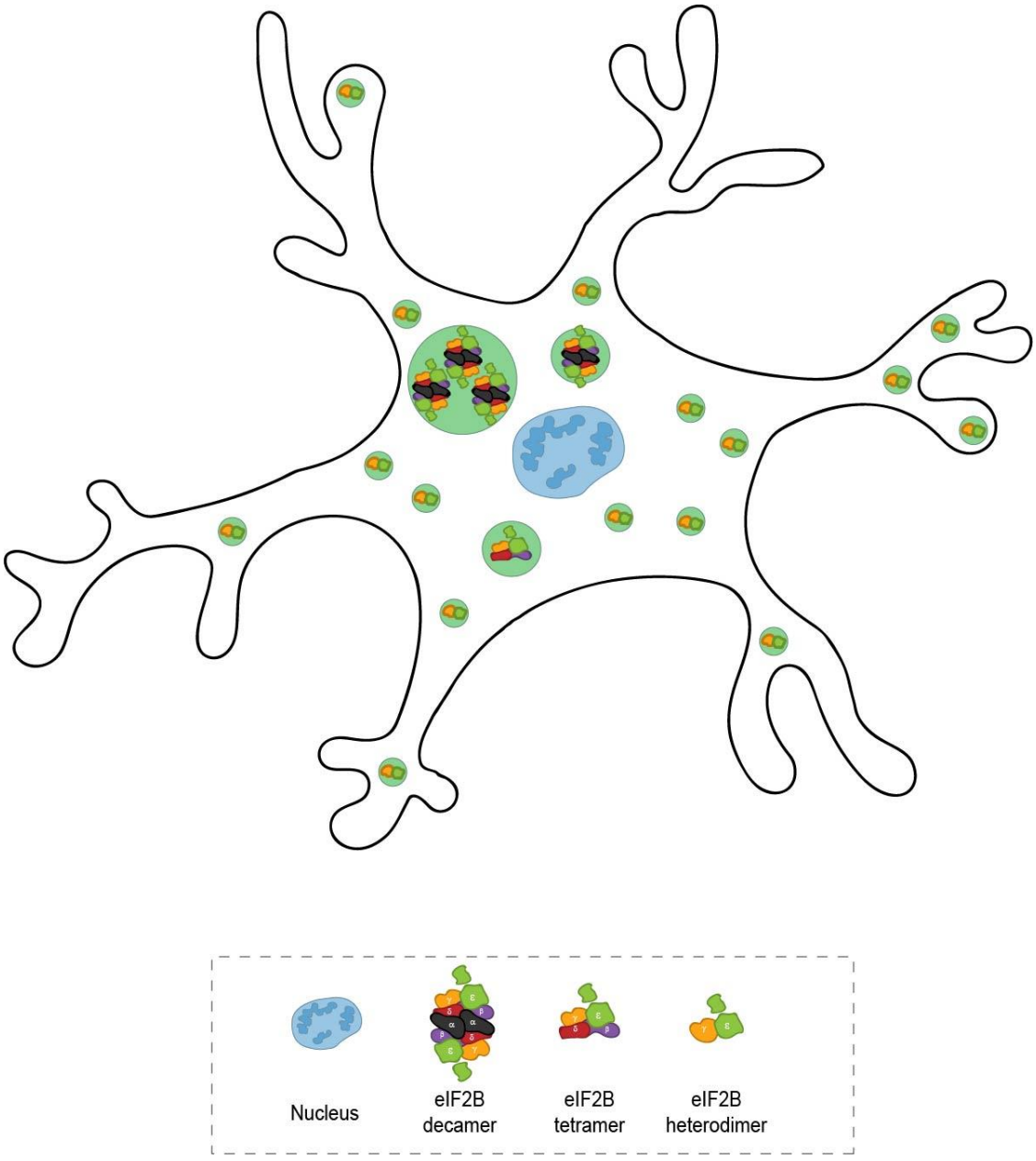

Figure 6.1 Model of eIF2B localisation in mammalian cells.
The eIF2B subunit localisation data presented in this study suggests that eIF2B subcomplexes may localise to different sized eIF2B bodies. All subunits showed a high degree of co-localisation with large eIF2B bodies suggesting eIF2B$(\alpha\beta\delta\gamma\varepsilon)_2$ decameric complexes may reside here. All subunits also showed some degree of co-localisation with medium bodies, however eIF2Bα showed the lowest degree of co-localisation suggesting eIF2B$(\alpha\beta\delta\gamma\varepsilon)_2$ decameric and eIF2B$(\beta\delta\gamma\varepsilon)$ tetrameric complexes may reside within these bodies. Catalytic subunits localised to small eIF2B bodies whereas regulatory subunits showed very low levels of co-localisation suggesting eIF2B$(\gamma\varepsilon)$ heterodimers may localise within these bodies.

To assess the functionality of the mammalian eIF2B bodies identified in this study the relationship between eIF2 and the eIF2B bodies was analysed. Live cell imaging revealed that eIF2 localised to, and was mobile within, eIF2B bodies (Figures 4.1 and 4.3) suggesting that as in yeast, these bodies may be sites of eIF2B GEF activity (Figure 6.2A). In order to investigate this, induction of cellular stress was used as a tool to manipulate eIF2B activity and the movement of eIF2 was monitored. Activation of the ISR by diverse cellular stresses results in the phosphorylation of eIF2α at serine 51. Phosphorylated eIF2 is a competitive inhibitor of eIF2B (Rowlands *et al.*, 1988; Dever *et al.*, 1995) causing the downregulation of global translation initiation. The eIF2B regulatory subunits (α,β and δ) are essential for mediating the control of eIF2B GEF activity under stress (Krishnamoorthy *et al*., 2001; Pavitt *et al*., 1997), and eIF2B complexes containing the regulatory subunits are known to display a higher affinity for eIF2 when present in its phosphorylated form (Kashiwagi *et al*., 2017; Pavitt *et al*., 1998). The effects of stress on the movement of eIF2 within eIF2B bodies was therefore analysed for the eIF2B bodies to which regulatory subunits localised; large and medium eIF2B bodies (Figure 3.12). The movement of eIF2 through large and medium eIF2B bodies was attenuated in response to ER and oxidative stress, induced by Tg and SA respectively (Figure 4.8). Analysis of the cellular localisation of phosphorylated eIF2 under these conditions revealed that phosphorylated eIF2 localised predominately to these bodies (Figure 4.7). Mutational analysis confirmed that the decrease in shuttling of eIF2 through these bodies during stress was directly related to the phosphorylation of eIF2 (Figure 4.9). This evidence supports previous conclusions in yeast where the movement of eIF2 through eIF2B bodies was relative to the GEF activity of eIF2B (Campbell *et al.,* 2005; Taylor *et al.,* 2010). A schematic representation of these results is presented in Figure 6.2A and B.

In vitro GEF assays, in both yeast and mammalian systems, show that eIF2Bγε heterodimers exhibit GEF activity that is unregulatable by phosphorylated eIF2α (Li *et al*., 2004; Pavitt *et al*., 1998). The absence of regulatory eIF2B subunits (α, β and δ) localised to small eIF2B bodies (Figure 3.12) led to the hypothesis that the induction of eIF2α phosphorylation would not impact upon the movement of eIF2 through these bodies. Intriguingly, the movement of eIF2 through small bodies was significantly increased by cellular stress induced by both Tg and a low concentration of SA (125 µM)

(Figure 4.10), suggesting that these bodies have increased GEF activity during stress (Figure 6.2C).

Biochemical assays in yeast have demonstrated that increasing the expression of regulatory eIF2B (α, β and δ) subunits can enhance eIF2B GEF activity (Dev *et al*., 2010; Fabian *et al*., 1997; Liu *et al*., 2011; Williams *et al*., 2001). Interestingly, an increase in the localisation of eIF2Bδ to small bodies was also observed in response to cellular stress (Figure 4.11), perhaps responsible for the observed increase in eIF2 movement. The localisation of eIF2Bδ to the small eIF2B bodies suggests the formation of a currently unidentified eIF2B subcomplex comprised of eIF2Bδ, γ, and ε subunits (Figure 6.2C). This complex may not have been previously identified as characterisation of mammalian eIF2B subcomplexes has not been carried out under stress conditions (Wortham *et al*., 2014). However previous work has demonstrated that the knockdown of eIF2Bβ leads to a reduction in the expression of all eIF2B subunits with eIF2Bδ suffering the greatest reduction (Wortham *et al*., 2016). These data show that eIF2Bβ is required to stabilise the expression of eIF2Bδ and as these subunits are known to heterodimerise it could be expected that eIF2Bβ stabilises eIF2Bδ through binding to it. These conclusions do not support the data presented here whereby an increase in eIF2Bδ localisation was observed in small eIF2B bodies but no change in the localisation of eIF2Bβ was observed. Further experiments should be performed to confirm the existence of an eIF2B(δγε) subcomplex, formed during conditions of cellular stress. Investigation into the expression levels of eIF2B β and δ subunits and pull-down analysis of these subunits under stress conditions may provide further insight.

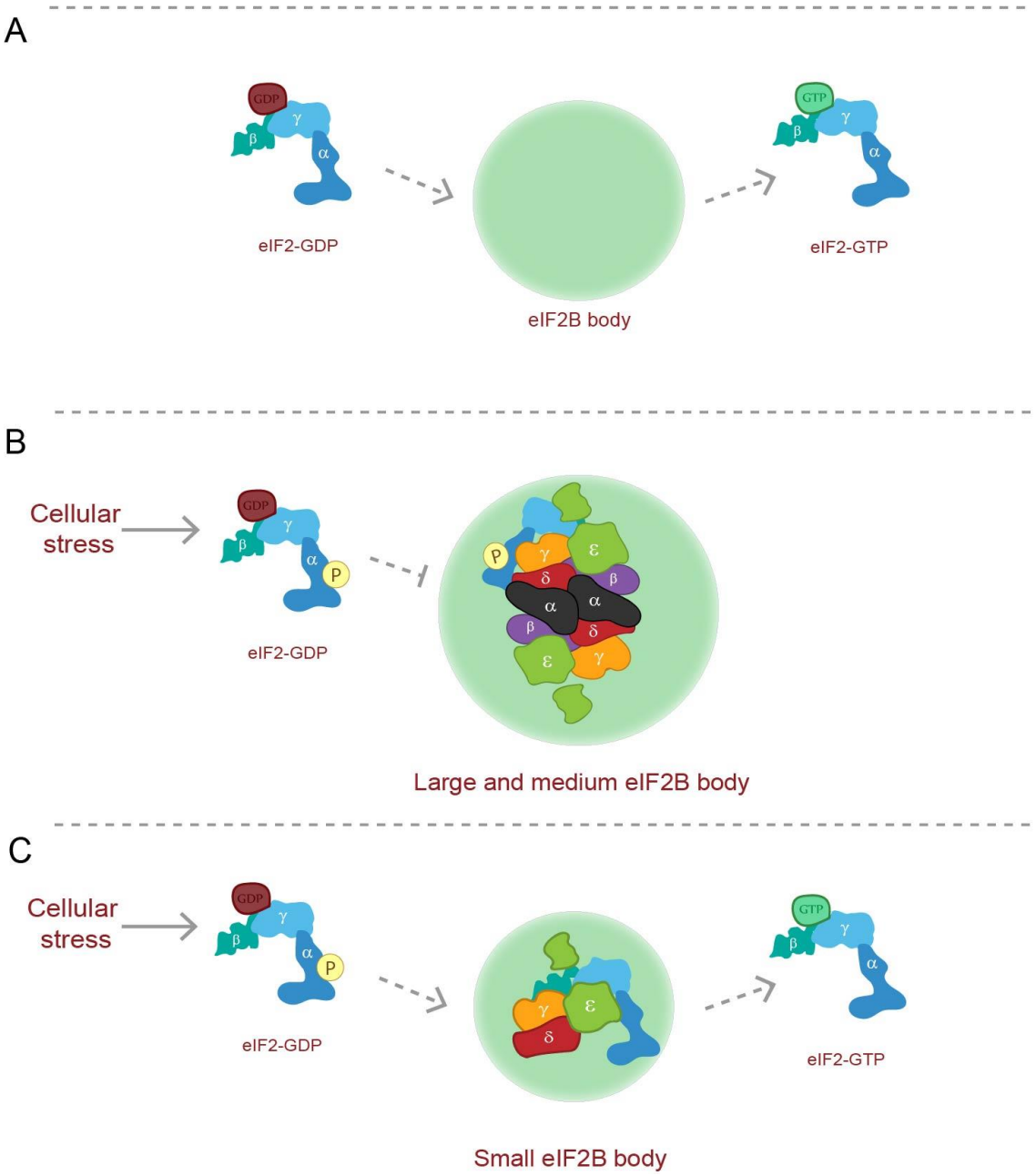

Figure 6.2 Schematic representation of the GEF activity of mammalian eIF2B bodies. (A) eIF2 was found to move through eIF2B bodies suggesting they could be sites of GEF activity. (B) In response to cellular stress, phosphorylation of eIF2 inhibits the movement of eIF2 through large and medium sized eIF2B bodies suggesting a decrease in GEF activity within these bodies. (C) In response to cellular stress the movement of eIF2 through small eIF2B bodies is increased, suggesting that the GEF activity of these bodies is enhanced during cellular stress. This increased movement of eIF2 is accompanied by an increase in the percentage of bodies to which eIF2Bδ localises, suggesting the formation of an eIF2B(δγε) subcomplex.

Low levels of phosphorylated eIF2α have been documented to precondition cells, promoting a stress-resistant phenotype (Lewerenz and Maher, 2009; Lu *et al*., 2004a). It could be hypothesised that the increased activity of the small bodies under low levels of cellular stress may contribute to this stress-induced protective phenotype, through providing a source of eIF2B activity that is not down-regulated during stress. This could allow for a low level of translation to occur during low levels of cellular stress, enabling the cell to respond and survive. The N-terminal of eIF2Bδ has been shown to be required for cells to mediate a response to cellular stress, with the expression of an N-terminal truncated isoform rendering cells insensitive to the effects of phosphorylated eIF2α (Martin *et al*., 2010). Mutational analysis of eIF2Bδ may provide insight into the importance of eIF2Bδ localisation to the increased movement of eIF2 through small bodies and to the cell's ability to respond to stress.

The increased movement of eIF2 through small eIF2B bodies was only observed in the presence of low levels of phosphorylated eIF2. In the presence of high levels of phosphorylated eIF2, eIF2Bδ localised to an increased percentage of small bodies (Figure 4.11) however the movement of eIF2 through these bodies was inhibited (Figure 4.10). This decrease in the mobility of eIF2 correlated with a significant increase in the percentage of small eIF2B bodies to which phosphorylated eIF2 localised. The favoured explanation of these results is that eIF2B regulation is lost above a certain threshold of phosphorylated eIF2, due to eIF2B saturation. In addition to changes in the movement of eIF2 during stress, the number of small eIF2B bodies was found to increase. Recent work in *S. cerevisiae* has observed that induction of stress results in an increase in the number of cells harbouring eIF2B bodies (Moon and Parker, 2018); supporting the hypothesis that cellular stress impacts upon eIF2B localisation. From the data presented here a schematic model of mammalian eIF2B complex formation and regulation during cellular stress is proposed in Figure 6.3.

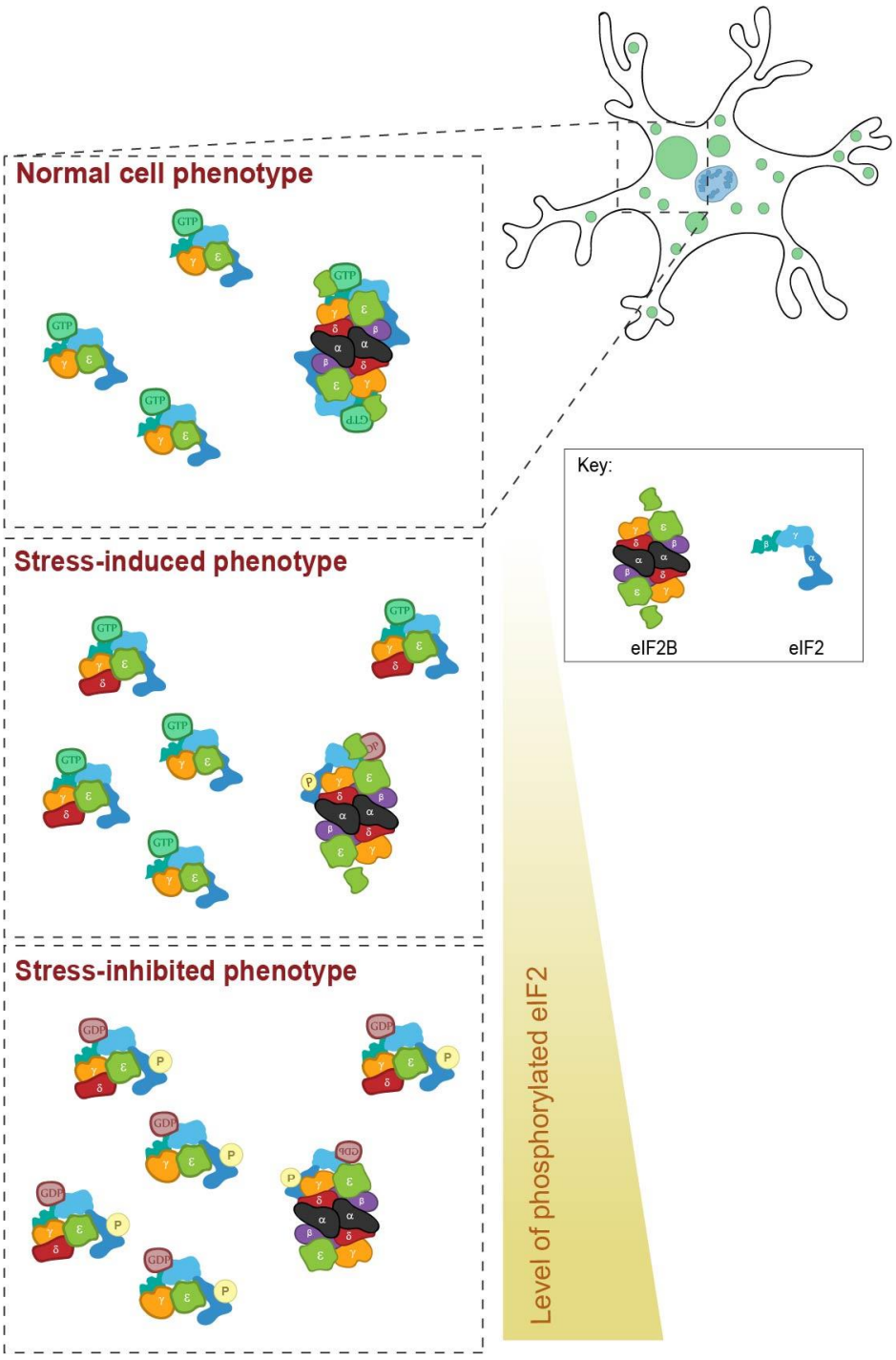

Figure 6.3 Working model for the phenotypic distribution of eIF2B complexes under conditions of cellular stress.

The data presented in this study highlight that under normal cellular conditions eIF2B localises to two distinct populations of eIF2B bodies in mammalian cells; larger bodies containing all subunits and small bodies containing catalytic subunits (γ and ε). In response to low levels of cellular stress larger eIF2B bodies are partially inhibited by phosphorylated eIF2, whereas the GEF activity and number of small eIF2B bodies is increased, accompanied by an increase in the localisation of the eIF2Bδ subunit. It is hypothesised that these changes to small eIF2B body dynamics promote a stress-induced protective phenotype. At high levels of cellular stress all eIF2B complexes are inhibited independent of size or subcomplex make up resulting in a stress-inhibited phenotype.

Having populations of eIF2B bodies where regulatory subunits are either present or absent appears to be linked to eIF2B regulation in U373 cells. If eIF2B bodies share the same properties in other cell types, the size and distribution of eIF2B bodies may provide an indication of a cell's ability to function under conditions of cellular stress. Intriguingly, primary human astrocytes were found to have a significantly increased number of small eIF2B bodies when compared to U373, HepG2, MG-63 and HEK293 cells (Figure 3.2, Figure 3.9 and Figure 3.10). Although U373 cells are also from an astrocytic lineage, these cells are cancerous likely altering their metabolism and perhaps explaining differences observed in eIF2B localisation (Hsu and Sabatini 2008). In U373 cells the induction of cellular stress and thus increased levels of phosphorylated eIF2 correlated to an increase in the number of small eIF2B bodies. The basal level of phosphorylated eIF2 was investigated in primary astrocytes and was found to be heightened in these cells (Figure 4.15). In U373 cells increased levels of phosphorylated eIF2 appeared to correlate with increased GEF activity of small eIF2B bodies. These eIF2B bodies therefore represent a source of eIF2B that is not downregulated during cellular stress. It was therefore hypothesised the presence of these small bodies may be protective through allowing cells to carry out low levels of translation in the presence of cellular stress. Astrocytes have a high metabolic turnover when compared to other cell types (Weber 2015). The high abundance of small bodies in astrocytes could be linked to high levels of translation required by these cells. Additionally, astrocytes require high levels of calcium to facilitate signalling within the brain (Bazargani and Attwell, 2016; Pivneva *et al*., 2008). Disturbances to calcium levels within the cell reduce the protein folding capacity of the ER and result in ER stress (Bahar *et al*., 2016). The ER plays an important role as an intracellular calcium store (Pivneva *et al*., 2008) and it could therefore be hypothesised that astrocytes require the ability to quickly and efficiently respond to ER stress to ensure calcium is readily accessible from ER stores.

Differential localisation and functionality of eIF2B bodies between cell types is of particular interest with respect to VWM. Causative mutations in eIF2B are globally expressed however astrocytes and oligodendrocytes are the main cell types affected in VWM patients. Recent studies have demonstrated that basal levels of phosphorylated eIF2 are reduced in VWM mouse and also patient brain (Abbink *et al*., 2018). Studying

the localisation of VWM mutant eIF2B could provide insight into disease mechanisms. Furthermore, previous studies have demonstrated that although VWM mutant fibroblast cells, like wild-type cells, respond to cellular stress by decreasing global protein synthesis, the downstream transcription factor ATF4 is significantly enhanced suggesting that they suffer a heightened stress response (Kantor *et al*., 2005). Interestingly this hyper-induction of ATF4 expression is not observed for VWM mutant lymphocytes. These data suggest that the impact of VWM disease mutants on the induction of a stress response is cell type dependent (Horzinski *et al*., 2010). Analysing localisation patterns of both wild-type and VWM mutant eIF2B within various cell types could provide insight into VWM tissue specificity.

Biochemically, VWM disease mutations affect eIF2B function in multiple ways (Li *et al*., 2004). Although there is currently no treatment for VWM, the small molecule ISRIB and its derivative 2BAct have emerged as promising therapeutics for VWM mutations that destabilise eIF2B decameric complex formation. ISRIB reverses phosphorylated eIF2α induced translational repression (Sidrauski *et al*., 2013; Halliday *et al*., 2015; Sidrauski *et al*., 2015a), through increasing the activity of eIF2B by promoting decamer formation (Tsai *et al*., 2018; Zyryanova *et al*., 2018). The data presented here suggest that ISRIB promotes decameric stability in large and medium sized eIF2B bodies. Under conditions of cellular stress ISRIB appears to enhance the GEF activity of these eIF2B bodies, and subunit localisation data suggests all eIF2B subunits are present (Figure 5.2 and Figure 3.12).

ISRIB also impacted upon the dynamics of small eIF2B bodies despite not all subunits being present. ISIRB appeared to mimic the effect that low levels of cellular stress had on small eIF2B bodies, with a similar increase in the movement of eIF2 and redistribution of eIF2Bδ to these bodies observed (Figure 5.4 and Figure 5.5). Furthermore, DBM another drug capable of enhancing translation during conditions of cellular stress also induced these changes in small body dynamics. It was hypothesised that under low levels of cellular stress the increased activity of these bodies represents a protective stress-responsive phenotype by providing a source of eIF2B that is not downregulated during exposure to cellular stress (Figure 6.3). The observation of this phenotype under treatment with drugs that are known to reverse stress induced translational depression supports that these bodies may have a role in priming cells to

overcome stress. Further investigation into this phenotype would be an interesting avenue to explore with respect to ISRIB and DBM.

7. Conclusions

The data presented in this thesis demonstrates that like in yeast, eIF2B consolidates into large cytoplasmic bodies. The situation in mammalian cells appears to be more complex. eIF2B bodies of various sizes exist and the size of these bodies correlates with their subunit composition. eIF2B bodies with a surface area ≥ 3μm^2, termed here large and medium eIF2B bodies, harbour regulatory subunits and appear to represent sites of GEF activity vulnerable to stress induced repression. eIF2B bodies with an area ≤ 2.99 μm^2, termed here small eIF2B bodies, are mainly composed of catalytic eIF2B subunits and the GEF activity of these bodies appears to be up-regulated in response to cellular stress. These bodies may therefore provide a level of eIF2B GEF activity during stress, allowing cells to respond and survive. The presence of these diverse bodies in different abundances may allow different cell types to harbour unique stress responses and perhaps contribute to the tissue specificity of VWM; a key area of future research.

8. References

Abbink, T. E. M., Wisse, L. E., Jaku, E., Thiecke, M. J., Voltolini-Gonzalez, D., Fritsen, H., Bobeldijk, S., Braak, T. J. ter, Polder, E., Postma, N. L., *et al*. (2018). Integrated Stress Response Deregulation underlies Vanishing White Matter and is a target for therapy. *bioRxiv* 460840.

Acker, M. G., Shin, B.-S., Dever, T. E. and Lorsch, J. R. (2006). Interaction between Eukaryotic Initiation Factors 1A and 5B Is Required for Efficient Ribosomal Subunit Joining. *J. Biol. Chem.* **281**, 8469–8475.

Adomavicius, T., Guaita, M., Zhou, Y., Jennings, M. D., Latif, Z., Roseman, A. M. and Pavitt, G. D. (2019). The structural basis of translational control by eIF2 phosphorylation. *Nat. Commun.* **10**, 2136.

Algire, M. A., Maag, D. and Lorsch, J. R. (2005). Pi Release from eIF2, Not GTP Hydrolysis, Is the Step Controlled by Start-Site Selection during Eukaryotic Translation Initiation. *Mol. Cell* **20**, 251–262.

Alkalaeva, E. Z., Pisarev, A. V., Frolova, L. Y., Kisselev, L. L. and Pestova, T. V. (2006). In Vitro Reconstitution of Eukaryotic Translation Reveals Cooperativity between Release Factors eRF1 and eRF3. *Cell* **125**, 1125–1136.

Ameri, K. and Harris, A. L. (2008). Activating transcription factor 4. *Int. J. Biochem. Cell Biol.* **40**, 14–21.

Anderson, P. and Kedersha, N. (2006). RNA granules. *J. Cell Biol.* **172**, 803–808.

Asano, K., Clayton, J., Shalev, A. and Hinnebusch, A. G. (2000). A multifactor complex of eukaryotic initiation factors, eIF1, eIF2, eIF3, eIF5, and initiator tRNA(Met) is an important translation initiation intermediate in vivo. *Genes Dev.* **14**, 2534–2546.

Axten, J. M., Medina, J. R., Feng, Y., Shu, A., Romeril, S. P., Grant, S. W., Li, W. H. H., Heerding, D. A., Minthorn, E., Mencken, T., *et al*. (2012). Discovery of 7-Methyl-5-(1-{[3-(trifluoromethyl)phenyl]acetyl}-2,3-dihydro-1 *H* -indol-5-yl)-7 *H* -pyrrolo[2,3- *d*]pyrimidin-4-amine (GSK2606414), a Potent and Selective First-in-Class Inhibitor of Protein Kinase R (PKR)-like Endoplasmic Reticulum Kinase (PERK). *J. Med. Chem.* **55**, 7193–7207.

B'chir, W., Maurin, A.-C., Carraro, V., Averous, J., Jousse, C., Muranishi, Y., Parry, L., Stepien, G., Fafournoux, P. and Bruhat, A. (2013). The eIF2α/ATF4 pathway is essential for stress-induced autophagy gene expression. *Nucleic Acids Res.* **41**, 7683–7699.

Bahar, E., Kim, H. and Yoon, H. (2016). ER Stress-Mediated Signaling: Action Potential and Ca(2+) as Key Players. *Int. J. Mol. Sci.* **17**, 1558.

Barrett, L. W., Fletcher, S. and Wilton, S. D. (2012). Regulation of eukaryotic gene expression by the untranslated gene regions and other non-coding elements. *Cell. Mol. Life Sci.* **69**, 3613.

Barthelme, D., Dinkelaker, S., Albers, S.-V., Londei, P., Ermler, U. and Tampe, R. (2011). Ribosome recycling depends on a mechanistic link between the FeS cluster domain and a conformational switch of the twin-ATPase ABCE1. *Proc. Natl. Acad. Sci.* **108**, 3228–3233.

Bazargani, N. and Attwell, D. (2016). Astrocyte calcium signaling: the third wave. *Nat. Neurosci.* **19**, 182–189.

Ben-Shem, A., Garreau de Loubresse, N., Melnikov, S., Jenner, L., Yusupova, G. and Yusupov, M. (2011). The Structure of the Eukaryotic Ribosome at 3.0 A Resolution. *Science* **334**, 1524–1529.

Beringer, M. and Rodnina, M. V. (2007). The Ribosomal Peptidyl Transferase. *Mol. Cell* **26**, 311–321.

Berlanga, J. J., Herrero, S. and de Haro, C. (1998). Characterization of the hemin-sensitive eukaryotic initiation factor 2alpha kinase from mouse nonerythroid cells. *J. Biol. Chem.* **273**, 32340–32346.

Bertram, G., Bell, H. A., Ritchie, D. W., Fullerton, G. and Stansfield, I. (2000). Terminating eukaryote translation: domain 1 of release factor eRF1 functions in stop codon recognition. *RNA* **6**, 1236–1247.

Bi, M., Naczki, C., Koritzinsky, M., Fels, D., Blais, J., Hu, N., Harding, H., Novoa, I., Varia, M., Raleigh, J., *et al*. (2005). ER stress-regulated translation increases tolerance to extreme hypoxia and promotes tumor growth. *EMBO J.* **24**, 3470–

3481.

Bogorad, A. M., Xia, B., Sandor, D. G., Mamonov, A. B., Cafarella, T. R., Jehle, S., Vajda, S., Kozakov, D. and Marintchev, A. (2014). Insights into the Architecture of the eIF2Bα/β/δ Regulatory Subcomplex. *Biochemistry* **21**, 3432-3445.

Bogorad, A. M., Lin, K. Y. and Marintchev, A. (2017). Novel mechanisms of eIF2B action and regulation by eIF2α phosphorylation. *Nucleic Acids Res.* **45**, 11962–11979.

Bolognesi, B. and Lehner, B. (2018). Reaching the limit. *elife* **7**, e39804.

Boltshauser, E., Barth, P. G., Troost, D., Martin, E. and Stallmach, T. (2002). "Vanishing White Matter" and Ovarian Dysgenesis in an Infant with Cerebro-Oculo-Facio-Skeletal Phenotype. *Neuropediatrics* **33**, 57–62.

Brengues, M., Teixeira, D. and Parker, R. (2005). Movement of Eukaryotic mRNAs Between Polysomes and Cytoplasmic Processing Bodies. *Science* **310**, 486–489.

Brostrom, C. O. and Brostrom, M. A. (1998). Regulation of translational initiation during cellular responses to stress. *Prog. Nucleic Acid Res. Mol. Biol.* **58**, 79–125.

Brush, M. H., Weiser, D. C. and Shenolikar, S. (2003). Growth arrest and DNA damage-inducible protein GADD34 targets protein phosphatase 1 alpha to the endoplasmic reticulum and promotes dephosphorylation of the alpha subunit of eukaryotic translation initiation factor 2. *Mol. Cell. Biol.* **23**, 1292–1303.

Buchan, J. R. (2014). mRNP granules. Assembly, function, and connections with disease. *RNA Biol.* **11**, 1019–1030.

Bugiani, M., Boor, I., Powers, J. M., Scheper, G. C. and van der Knaap, M. S. (2010). Leukoencephalopathy With Vanishing White Matter: A Review. *J. Neuropathol. Exp. Neurol.* **69**, 987–996.

Bugiani, M., Vuong, C., Breur, M. and van der Knaap, M. S. (2018). Vanishing white matter: a leukodystrophy due to astrocytic dysfunction. *Brain Pathol.* **28**, 408–421.

Bushman, J. L., Asuru, A. I., Matts, R. L. and Hinnebuschl, A. G. (1993). Evidence that

GCD6 and GCD7, Translational Regulators of GCN4, Are Subunits of the Guanine Nucleotide Exchange Factor for eIF-2 in Saccharomyces cerevisiae. *Mol. Cell. Biol.* **3**, 1920-1932.

Campbell, S. G. and Ashe, M. P. (2007). An Approach to Studying the Localization and Dynamics of Eukaryotic Translation Factors in Live Yeast Cells. *Methods Enzymol.* **431**, 33-45.

Campbell, S. G., Hoyle, N. P. and Ashe, M. P. (2005). Dynamic cycling of eIF2 through a large eIF2B-containing cytoplasmic body: implications for translation control. *J. Cell Biol.* **170**, 925–934.

Capone, J. P., Sedivy, J. M., Sharp, P. A. and RajBhandary, U. L. (1986). Introduction of UAG, UAA, and UGA nonsense mutations at a specific site in the Escherichia coli chloramphenicol acetyltransferase gene: use in measurement of amber, ochre, and opal suppression in mammalian cells. *Mol. Cell. Biol.* **6**, 3059–3067.

Castilho, B. A., Shanmugam, R., Silva, R. C., Ramesh, R., Himme, B. M. and Sattlegger, E. (2014). Keeping the eIF2 alpha kinase Gcn2 in check. *Biochim. Biophys. Acta - Mol. Cell Res.* **1843**, 1948–1968.

Chen, J. J., Throop, M. S., Gehrke, L., Kuo, I., Pal, J. K., Brodsky, M. and London, I. M. (1991). Cloning of the cDNA of the heme-regulated eukaryotic initiation factor 2 alpha (eIF-2 alpha) kinase of rabbit reticulocytes: homology to yeast GCN2 protein kinase and human double-stranded-RNA-dependent eIF-2 alpha kinase. *Proc. Natl. Acad. Sci. U. S. A.* **88**, 7729–7733.

Chen, Y.-C., Lin-Shiau, S.-Y. and Lin, J.-K. (1998). Involvement of reactive oxygen species and caspase 3 activation in arsenite-induced apoptosis. *J. Cell. Physiol.* **177**, 324–333.

Chen, Y., Podojil, J. R., Kunjamma, R. B., Jones, J., Weiner, M., Lin, W., Miller, S. D. and Popko, B. (2019). Sephin1, which prolongs the integrated stress response, is a promising therapeutic for multiple sclerosis. *Brain* **142**, 344–361.

Chou, A., Krukowski, K., Jopson, T., Zhu, P. J., Costa-Mattioli, M., Walter, P. and Rosi, S. (2017). Inhibition of the integrated stress response reverses cognitive deficits

after traumatic brain injury. *Proc. Natl. Acad. Sci. U. S. A.* **114**, E6420–E6426.

Clemens, M. J. and Elia, A. (1997). The Double-Stranded RNA-Dependent Protein Kinase PKR: Structure and Function. *J. Interf. Cytokine Res.* **17**, 503–524.

Cross, D. A. E., Alessi, D. R., Cohen, P., Andjelkovich, M. and Hemmings, B. A. (1995). Inhibition of glycogen synthase kinase-3 by insulin mediated by protein kinase B. *Nature* **378**, 785–789.

Daniele, S., Zappelli, E. and Martini, C. (2015). Trazodone regulates neurotrophic/growth factors, mitogen-activated protein kinases and lactate release in human primary astrocytes. *J. Neuroinflammation* **12**, 225.

Danielson, C. M. and Hope, T. J. (2013). Using antiubiquitin antibodies to probe the ubiquitination state within rhTRIM5α cytoplasmic bodies. *AIDS Res. Hum. Retroviruses* **29**, 1373–1385.

de Almeida, R. A., Fogli, A., Gaillard, M., Scheper, G. C., Boesflug-Tanguy, O. and Pavitt, G. D. (2013). A Yeast Purification System for Human Translation Initiation Factors eIF2 and eIF2Bε and Their Use in the Diagnosis of CACH/VWM Disease. *PLoS One* **8**, e53958.

Decker, C. J., Teixeira, D. and Parker, R. (2007). Edc3p and a glutamine/asparagine-rich domain of Lsm4p function in processing body assembly in Saccharomyces cerevisiae. *J. Cell Biol.* **179**, 437–449.

DeLano, W. L. (2002). Pymol: An open-source molecular graphics tool. *CCP4 Newsletter On Protein Crystallography.* **40**, 82-92.

Dev, K., Qiu, H., Dong, J., Zhang, F., Barthlme, D. and Hinnebusch, A. G. (2010). The beta/Gcd7 subunit of eukaryotic translation initiation factor 2B (eIF2B), a guanine nucleotide exchange factor, is crucial for binding eIF2 in vivo. *Mol. Cell. Biol.* **30**, 5218–5233.

Dever, T. E. and Green, R. (2012). The elongation, termination, and recycling phases of translation in eukaryotes. *Cold Spring Harb. Perspect. Biol.* **4**, a013706.

Dever, T. E., Feng, L., Wek, R. C., Cigan, A. M., Donahue, T. F. and Hinnebusch, A. G.

(1992). Phosphorylation of initiation factor 2 alpha by protein kinase GCN2 mediates gene-specific translational control of GCN4 in yeast. *Cell* **68**, 585–596.

Dever, T. E., Chent, J.-J., Barbert, G. N., Cigan, A. M., Feng, L., Donahue, T. F., Londontl, I. M., Katzet, M. G. and Hinnebusch, A. G. (1993). Mammalian eukaryotic initiation factor 2a kinases functionally substitute for GCN2 protein kinase in the GCN4 translational control mechanism of yeast (phosphorylation/initiation factors/double-stranded RNA-dependent eIF-2a kinase/p68 kinase/heme-regulate. *Biochemistry* **90**, 4616–4620.

Dever, T. E., Yang, W., Aström, S., Byström, A. S. and Hinnebusch, A. G. (1995). Modulation of tRNA(iMet), eIF-2, and eIF-2B expression shows that GCN4 translation is inversely coupled to the level of eIF-2.GTP.Met-tRNA(iMet) ternary complexes. *Mol. Cell. Biol.* **15**, 6351–6363.

Dmitriev, S. E., Terenin, I. M., Dunaevsky, Y. E., Merrick, W. C. and Shatsky, I. N. (2003). Assembly of 48S translation initiation complexes from purified components with mRNAs that have some base pairing within their 5' untranslated regions. *Mol. Cell. Biol.* **23**, 8925–8933.

Donnelly, N., Gorman, A. M., Gupta, S. and Samali, A. (2013). The eIF2α kinases: their structures and functions. *Cell. Mol. Life Sci.* **70**, 3493–3511.

Dooves, S., Bugiani, M., Postma, N. L., Polder, E., Land, N., Horan, S. T., van Deijk, A.-L. F., van de Kreeke, A., Jacobs, G., Vuong, C., *et al*. (2016). Astrocytes are central in the pathomechanisms of vanishing white matter. *J. Clin. Invest.* **126**, 1512–1524.

Doudna, J. A. and Rath, V. L. (2002). Structure and function of the eukaryotic ribosome: the next frontier. *Cell* **109**, 153–156.

Dreyfus, M. and Régnier, P. (2002). The poly(A) tail of mRNAs: bodyguard in eukaryotes, scavenger in bacteria. *Cell* **111**, 611–613.

Egbe, N. E., Paget, C. M., Wang, H. and Ashe, M. P. (2015). Alcohols inhibit translation to regulate morphogenesis in C. albicans. *Fungal Genet. Biol.* **77**, 50–60.

Eizirik, D. L., Cardozo, A. K. and Cnop, M. (2008). The Role for Endoplasmic Reticulum

Stress in Diabetes Mellitus. *Endocr. Rev.* **29**, 42–61.

Elsby, R., Heiber, J. F., Reid, P., Kimball, S. R., Pavitt, G. D. and Barber, G. N. (2011). The Alpha Subunit of Eukaryotic Initiation Factor 2B (eIF2B) Is Required for eIF2-Mediated Translational Suppression of Vesicular Stomatitis Virus. *J. Virol.* **85**, 9716–9725.

Erickson, F. L. and Hannig, E. M. (1996). Ligand interactions with eukaryotic translation initiation factor 2: role of the gamma-subunit. *EMBO J.* **15**, 6311–6320.

Eulalio, A., Behm-Ansmant, I., Schweizer, D. and Izaurralde, E. (2007). P-Body Formation Is a Consequence, Not the Cause, of RNA-Mediated Gene Silencing. *Mol. Cell. Biol.* **27**, 3970–3981.

Fabian, J. R., Kimball, S. R., Heinzinger, N. K. and Jefferson, L. S. (1997). Subunit assembly and guanine nucleotide exchange activity of eukaryotic initiation factor-2B expressed in Sf9 cells. *J. Biol. Chem.* **272**, 12359–12365.

Fan-Minogue, H., Du, M., Pisarev, A. V., Kallmeyer, A. K., Salas-Marco, J., Keeling, K. M., Thompson, S. R., Pestova, T. V. and Bedwell, D. M. (2008). Distinct eRF3 Requirements Suggest Alternate eRF1 Conformations Mediate Peptide Release during Eukaryotic Translation Termination. *Mol. Cell* **30**, 599–609.

Fogli, A. and Boespflug-Tanguy, O. (2006). The large spectrum of eIF2B-related diseases. *Biochem. Soc. Trans.* **34**, 22.

Francalanci, P., Eymard-Pierre, E., Dionisi-Vici, C., Boldrini, R., Piemonte, F., Virgili, R., Fariello, G., Bosman, C., Santorelli, F. M., Boespflug-Tanguy, O., *et al*. (2001). Fatal infantile leukodystrophy: a severe variant of CACH/VWM syndrome, allelic to chromosome 3q27. *Neurology* **57**, 265–270.

Frank, J. and Agrawal, R. K. (2000). A ratchet-like inter-subunit reorganization of the ribosome during translocation. *Nature* **406**, 318–322.

Fringer, J. M., Acker, M. G., Fekete, C. A., Lorsch, J. R. and Dever, T. E. (2007). Coupled Release of Eukaryotic Translation Initiation Factors 5B and 1A from 80S Ribosomes following Subunit Joining. *Mol. Cell. Biol.* **27**, 2384–2397.

Frolova, L., Le Goff, X., Zhouravleva, G., Davydova, E., Philippe, M. and Kisselev, L. (1996). Eukaryotic polypeptide chain release factor eRF3 is an eRF1- and ribosome-dependent guanosine triphosphatase. *RNA* **2**, 334–341.

Gilks, N., Kedersha, N., Ayodele, M., Shen, L., Stoecklin, G., Dember, L. M. and Anderson, P. (2004). Stress Granule Assembly Is Mediated by Prion-like Aggregation of TIA-1. *Mol. Biol. Cell* **15**, 5383–5398.

Gomez, E. and Pavitt, G. D. (2000). Identification of domains and residues within the epsilon subunit of eukaryotic translation initiation factor 2B (eIF2Bepsilon) required for guanine nucleotide exchange reveals a novel activation function promoted by eIF2B complex formation. *Mol. Cell. Biol.* **20**, 3965–3976.

Gomez, E., Mohammad, S. S. and Pavitt, G. D. (2002). Characterization of the minimal catalytic domain within eIF2B: the guanine-nucleotide exchange factor for translation initiation. *EMBO J.* **21**, 5292.

Gordiyenko, Y., Schmidt, C., Jennings, M. D., Matak-Vinkovic, D., Pavitt, G. D. and Robinson, C. V. (2014). eIF2B is a decameric guanine nucleotide exchange factor with a γ2ε2 tetrameric core. *Nat. Commun.* **5**, 3902.

Gordiyenko, Y., Llácer, J. L. and Ramakrishnan, V. (2018). Structural basis for the inhibition of translation through eIF2α phosphorylation. *bioRxiv* 503979.

Gradi, A., Svitkin, Y. V, Imataka, H. and Sonenberg, N. (1998). Proteolysis of human eukaryotic translation initiation factor eIF4GII, but not eIF4GI, coincides with the shutoff of host protein synthesis after poliovirus infection. *Proc. Natl. Acad. Sci. U. S. A.* **95**, 11089–11094.

Grande, V., Ornaghi, F., Comerio, L., Restelli, E., Masone, A., Corbelli, A., Tolomeo, D., Capone, V., Axten, J. M., Laping, N. J., *et al*. (2018). PERK inhibition delays neurodegeneration and improves motor function in a mouse model of Marinesco-Sjögren syndrome. *Hum. Mol. Genet.* **27**, 2477–2489.

Gross, J. D., Moerke, N. J., von der Haar, T., Lugovskoy, A. A., Sachs, A. B., McCarthy, J. E. G. and Wagner, G. (2003). Ribosome loading onto the mRNA cap is driven by conformational coupling between eIF4G and eIF4E. *Cell* **115**, 739–750.

Gunišová, S., Hronová, V., Mohammad, M. P., Hinnebusch, A. G. and Valášek, L. S. (2018). Please do not recycle! Translation reinitiation in microbes and higher eukaryotes. *FEMS Microbiol. Rev.* **42**, 165–192.

Halliday, M., Radford, H., Sekine, Y., Moreno, J., Verity, N., le Quesne, J., Ortori, C. A., Barrett, D. A., Fromont, C., Fischer, P. M., *et al*. (2015). Partial restoration of protein synthesis rates by the small molecule ISRIB prevents neurodegeneration without pancreatic toxicity. *Cell Death Dis.* **6**, e1672.

Halliday, M., Radford, H., Zents, K. A. M., Molloy, C., Moreno, J. A., Verity, N. C., Smith, E., Ortori, C. A., Barrett, D. A., Bushell, M., *et al*. (2017). Repurposed drugs targeting eIF2α-P-mediated translational repression prevent neurodegeneration in mice. *Brain* **140**, 1768–1783.

Hamilton, E. M. C., van der Lei, H. D. W., Vermeulen, G., Gerver, J. A. M., Lourenço, C. M., Naidu, S., Mierzewska, H., Gemke, R. J. B. J., de Vet, H. C. W., Uitdehaag, B. M. J., *et al*. (2018). Natural History of Vanishing White Matter. *Ann. Neurol.* **84**, 274–288.

Han, A. P., Yu, C., Lu, L., Fujiwara, Y., Browne, C., Chin, G., Fleming, M., Leboulch, P., Orkin, S. H. and Chen, J. J. (2001). Heme-regulated eIF2alpha kinase (HRI) is required for translational regulation and survival of erythroid precursors in iron deficiency. *EMBO J.* **20**, 6909–6918.

Hanefeld, F., Holzbach, U., Kruse, B., Wilichowski, E., Christen, H. and Frahm, J. (1993). Diffuse White Matter Disease in Three Children: An Encephalopathy with Unique Features on Magnetic Resonance Imaging and Proton Magnetic Resonance Spectroscopy. *Neuropediatrics* **24**, 244–248.

Hannig, E. M., Williams, N. P., Wek, R. C. and Hinnebusch, A. G. (1990). The translational activator GCN3 functions downstream from GCN1 and GCN2 in the regulatory pathway that couples GCN4 expression to amino acid availability in Saccharomyces cerevisiae. *Genetics* **126**, 549–562.

Harding, H. P., Zhang, Y. and Ron, D. (1999). Protein translation and folding are coupled by an endoplasmic-reticulum-resident kinase. *Nature* **397**, 271–274.

Harding, H. P., Novoa, I., Zhang, Y., Zeng, H., Wek, R., Schapira, M. and Ron, D. (2000). Regulated translation initiation controls stress-induced gene expression in mammalian cells. *Mol. Cell* **6**, 1099–1108.

Hebert, D. N. and Molinari, M. (2007). In and Out of the ER: Protein Folding, Quality Control, Degradation, and Related Human Diseases. *Physiol. Rev.* **87**, 1377–1408.

Hetz, C. and Saxena, S. (2017). ER stress and the unfolded protein response in neurodegeneration. *Nat. Rev. Neurol.* **13**, 477–491.

Hilbert, M., Kebbel, F., Gubaev, A. and Klostermeier, D. (2011). eIF4G stimulates the activity of the DEAD box protein eIF4A by a conformational guidance mechanism. *Nucleic Acids Res.* **39**, 2260–2270.

Hinnebusch, A. G. and Lorsch, J. R. (2012). The mechanism of eukaryotic translation initiation: new insights and challenges. *Cold Spring Harb. Perspect. Biol.* **4**, a011544.

Hoozemans, J. J. M., van Haastert, E. S., Eikelenboom, P., de Vos, R. A. I., Rozemuller, J. M. and Scheper, W. (2007). Activation of the unfolded protein response in Parkinson's disease. *Biochem. Biophys. Res. Commun.* **354**, 707–711.

Horzinski, L., Kantor, L., Huyghe, A., Schiffmann, R., Elroy-Stein, O., Boespflug-Tanguy, O. and Fogli, A. (2010). Evaluation of the endoplasmic reticulum-stress response in eIF2B-mutated lymphocytes and lymphoblasts from CACH/VWM patients. *BMC Neurol.* **10**, 94.

Huang, H. K., Yoon, H., Hannig, E. M. and Donahue, T. F. (1997). GTP hydrolysis controls stringent selection of the AUG start codon during translation initiation in Saccharomyces cerevisiae. *Genes Dev.* **11**, 2396–2413.

Jackson, R. J. (1991). The ATP requirement for initiation of eukaryotic translation varies according to the mRNA species. *Eur. J. Biochem.* **200**, 285–294.

Jain, S., Wheeler, J. R., Walters, R. W., Agrawal, A., Barsic, A. and Parker, R. (2016). ATPase modulated stress granules contain a diverse proteome and substructure. *Cell* **164**, 487.

Jennings, M. D. and Pavitt, G. D. (2010). eIF5 has GDI activity necessary for translational control by eIF2 phosphorylation. *Nature* **465**, 378–381.

Jennings, M. D. and Pavitt, G. D. (2014). A new function and complexity for protein translation initiation factor eIF2B. *Cell Cycle* **13**, 2660–2665.

Jennings, M. D., Zhou, Y., Mohammad-Qureshi, S. S., Bennett, D. and Pavitt, G. D. (2013). eIF2B promotes eIF5 dissociation from eIF2*GDP to facilitate guanine nucleotide exchange for translation initiation. *Genes Dev.* **27**, 2696–2707.

Kantor, L., Harding, H. P., Ron, D., Schiffmann, R., Kaneski, C. R., Kimball, S. R. and Elroy-Stein, O. (2005). Heightened stress response in primary fibroblasts expressing mutant eIF2B genes from CACH/VWM leukodystrophy patients. *Hum. Genet.* **118**, 99–106.

Kapp, L. D. and Lorsch, J. R. (2004). GTP-dependent Recognition of the Methionine Moiety on Initiator tRNA by Translation Factor eIF2. *J. Mol. Biol.* **335**, 923–936.

Kashiwagi, K., Takahashi, M., Nishimoto, M., Hiyama, T. B., Higo, T., Umehara, T., Sakamoto, K., Ito, T. and Yokoyama, S. (2016). Crystal structure of eukaryotic translation initiation factor 2B. *Nature* **531**, 122–125.

Kashiwagi, K., Ito, T. and Yokoyama, S. (2017). Crystal structure of eIF2B and insights into eIF2-eIF2B interactions. *FEBS J.* **284**, 868–874.

Kashiwagi, K., Yokoyama, T., Nishimoto, M., Takahashi, M., Sakamoto, A., Yonemochi, M., Shirouzu, M. and Ito, T. (2019). Structural basis for eIF2B inhibition in integrated stress response. *Science* **364**, 495–499.

Kaur, G. and Dufour, J. M. (2012). Cell lines: Valuable tools or useless artifacts. *Spermatogenesis* **2**, 1–5.

Kedersha, N. and Anderson, P. (2002). Stress granules: sites of mRNA triage that regulate mRNA stability and translatability. *Biochem. Soc. Trans.* **30**, 963–969.

Kedersha, N. L., Gupta, M., Li, W., Miller, I. and Anderson, P. (1999). RNA-binding proteins TIA-1 and TIAR link the phosphorylation of eIF-2 alpha to the assembly of mammalian stress granules. *J. Cell Biol.* **147**, 1431–1442.

Kedersha, N., Cho, M. R., Li, W., Yacono, P. W., Chen, S., Gilks, N., Golan, D. E. and Anderson, P. (2000). Dynamic Shuttling of Tia-1 Accompanies the Recruitment of mRNA to Mammalian Stress Granules. *J. Cell Biol.* **151**, 1257–1268.

Kedersha, N., Chen, S., Gilks, N., Li, W., Miller, I. J., Stahl, J. and Anderson, P. (2002). Evidence that ternary complex (eIF2-GTP-tRNA(i)(Met))-deficient preinitiation complexes are core constituents of mammalian stress granules. *Mol. Biol. Cell* **13**, 195–210.

Kedersha, N., Stoecklin, G., Ayodele, M., Yacono, P., Lykke-Andersen, J., Fritzler, M. J., Scheuner, D., Kaufman, R. J., Golan, D. E. and Anderson, P. (2005). Stress granules and processing bodies are dynamically linked sites of mRNP remodeling. *J. Cell Biol.* **169**, 871–884.

Kenner, L. R., Anand, A. A., Nguyen, H. C., Myasnikov, A. G., Klose, C. J., McGeever, L. A., Tsai, J. C., Miller-Vedam, L. E., Walter, P. and Frost, A. (2019). eIF2B-catalyzed nucleotide exchange and phosphoregulation by the integrated stress response. *Science* **364**, 491–495.

Kim, H.-J., Raphael, A. R., LaDow, E. S., McGurk, L., Weber, R. A., Trojanowski, J. Q., Lee, V. M.-Y., Finkbeiner, S., Gitler, A. D. and Bonini, N. M. (2014). Therapeutic modulation of eIF2α phosphorylation rescues TDP-43 toxicity in amyotrophic lateral sclerosis disease models. *Nat. Genet.* **46**, 152–160.

Kimball, S. R., Fabian, J. R., Pavitt, G. D., Hinnebusch, A. G. and Jefferson, L. S. (1998). Regulation of guanine nucleotide exchange through phosphorylation of eukaryotic initiation factor eIF2alpha. Role of the alpha- and delta-subunits of eiF2b. *J. Biol. Chem.* **273**, 12841–12845.

Kimball, S. R., Horetsky, R. L., Ron, D., Jefferson, L. S. and Harding, H. P. (2003). Mammalian stress granules represent sites of accumulation of stalled translation initiation complexes. *AJP Cell Physiol.* **284**, C273–C284.

Koonin, E. V. (1995). Multidomain organization of eukaryotic guanine nucleotide exchange translation initiation factor eIF-2B subunits revealed by analysis of conserved sequence motifs. *Protein Sci.* **4**, 1608–1617.

Kozak, M. (1986). Point mutations define a sequence flanking the AUG initiator codon that modulates translation by eukaryotic ribosomes. *Cell* **44**, 283–92.

Krishnamoorthy, T., Pavitt, G. D., Zhang, F., Dever, T. E. and Hinnebusch, A. G. (2001). Tight binding of the phosphorylated alpha subunit of initiation factor 2 (eIF2alpha) to the regulatory subunits of guanine nucleotide exchange factor eIF2B is required for inhibition of translation initiation. *Mol. Cell. Biol.* **21**, 5018–5030.

Kuhle, B., Eulig, N. K. and Ficner, R. (2015). Architecture of the eIF2B regulatory subcomplex and its implications for the regulation of guanine nucleotide exchange on eIF2. *Nucleic Acids Res.* **43**, 9994-10014.

Labauge, P., Horzinski, L., Ayrignac, X., Blanc, P., Vukusic, S., Rodriguez, D., Mauguiere, F., Peter, L., Goizet, C., Bouhour, F., *et al*. (2009). Natural history of adult-onset eIF2B-related disorders: a multi-centric survey of 16 cases. *Brain* **132**, 2161–2169.

Leegwater, P. A. J., Vermeulen, G., Könst, A. A. M., Naidu, S., Mulders, J., Visser, A., Kersbergen, P., Mobach, D., Fonds, D., van Berkel, C. G. M., *et al*. (2001). Subunits of the translation initiation factor eIF2B are mutant in leukoencephalopathy with vanishing white matter. *Nat. Genet.* **29**, 383–388.

Lemaire, P. A., Anderson, E., Lary, J. and Cole, J. L. (2008). Mechanism of PKR Activation by dsRNA. *J. Mol. Biol.* **381**, 351–360.

Levin, D. H., Kyner, D. and Acs, G. (1973). Protein initiation in eukaryotes: formation and function of a ternary complex composed of a partially purified ribosomal factor, methionyl transfer RNA, and guanosine triphosphate. *Proc. Natl. Acad. Sci. U. S. A.* **70**, 41–45.

Lewerenz, J. and Maher, P. (2009). Basal levels of eIF2alpha phosphorylation determine cellular antioxidant status by regulating ATF4 and xCT expression. *J. Biol. Chem.* **284**, 1106–1115.

Li, W., Wang, X., Van Der Knaap, M. S. and Proud, C. G. (2004). Mutations linked to leukoencephalopathy with vanishing white matter impair the function of the eukaryotic initiation factor 2B complex in diverse ways. *Mol. Cell. Biol.* **24**, 3295–

3306.

Wong, YL., LeBon, L., Edalji, R., Ben Lim, H., Sun, C. and Sidrauski, C. (2018). The small molecule ISRIB rescues the stability and activity of Vanishing White Matter Disease eIF2B mutant complexes. *Elife* **7**, e32733.

Lin, W., Bailey, S. L., Ho, H., Harding, H. P., Ron, D., Miller, S. D. and Popko, B. (2007). The integrated stress response prevents demyelination by protecting oligodendrocytes against immune-mediated damage. *J. Clin. Invest.* **117**, 448–456.

Lin, Y., Pang, X., Huang, G., Jamison, S., Fang, J., Harding, H. P., Ron, D. and Lin, W. (2014). Impaired Eukaryotic Translation Initiation Factor 2B Activity Specifically in Oligodendrocytes Reproduces the Pathology of Vanishing White Matter Disease in Mice. *J. Neurosci.* **34**, 12182–12191.

Liu, R., van der Lei, H. D. W., Wang, X., Wortham, N. C., Tang, H., van Berkel, C. G. M., Mufunde, T. A., Huang, W., van der Knaap, M. S., Scheper, G. C., *et al*. (2011). Severity of vanishing white matter disease does not correlate with deficits in eIF2B activity or the integrity of eIF2B complexes. *Hum. Mutat.* **32**, 1036–1045.

Lorsch, J. R. and Herschlag, D. (1998). The DEAD box protein eIF4A. 1. a minimal kinetic and thermodynamic framework reveals coupled binding of RNA and nucleotide. *Biochemistry* **37**, 2180–2193.

Lu, P. D., Jousse, C., Marciniak, S. J., Zhang, Y., Novoa, I., Scheuner, D., Kaufman, R. J., Ron, D. and Harding, H. P. (2004a). Cytoprotection by pre-emptive conditional phosphorylation of translation initiation factor 2. *EMBO J.* **23**, 169–179.

Lu, P. D., Harding, H. P. and Ron, D. (2004b). Translation reinitiation at alternative open reading frames regulates gene expression in an integrated stress response. *J. Cell Biol.* **167**, 27–33.

Luo, Y., Na, Z. and Slavoff, S. A. (2018). P-Bodies: Composition, Properties, and Functions. *Biochemistry* **57**, 2424–2431.

Ma, T., Trinh, M. A., Wexler, A. J., Bourbon, C., Gatti, E., Pierre, P., Cavener, D. R. and Klann, E. (2013). Suppression of eIF2α kinases alleviates Alzheimer's disease–related plasticity and memory deficits. *Nat. Neurosci.* **16**, 1299–1305.

Maag, D., Fekete, C. A., Gryczynski, Z. and Lorsch, J. R. (2005). A Conformational Change in the Eukaryotic Translation Preinitiation Complex and Release of eIF1 Signal Recognition of the Start Codon. *Mol. Cell* **17**, 265–275.

Maj, J., Palider, W. and Rawłów (1979). Trazodone, a central serotonin antagonist and agonist. *J. Neural Transm.* **44**, 237–248.

Majumdar, R., Bandyopadhyay, A. and Maitra, U. (2003). Mammalian Translation Initiation Factor eIF1 Functions with eIF1A and eIF3 in the Formation of a Stable 40 S Preinitiation Complex. *J. Biol. Chem.* **278**, 6580–6587.

Maletkovic, J., Schiffmann, R., Gorospe, J. R., Gordon, E. S., Mintz, M., Hoffman, E. P., Alper, G., Lynch, D. R., Singhal, B. S., Harding, C., *et al*. (2008). Genetic and Clinical Heterogeneity in eIF2B-Related Disorder. *J. Child Neurol.* **23**, 205–215.

Marintchev, A., Kolupaeva, V. G., Pestova, T. V. and Wagner, G. (2003). Mapping the binding interface between human eukaryotic initiation factors 1A and 5B: A new interaction between old partners. *Proc. Natl. Acad. Sci.* **100**, 1535–1540.

Martin, L., Kimball, S. R. and Gardner, L. B. (2010). Regulation of the unfolded protein response by eif2Bdelta isoforms. *J. Biol. Chem.* **285**, 31944–31953.

McCullough, K. D., Martindale, J. L., Klotz, L.-O., Aw, T.-Y. and Holbrook, N. J. (2001). Gadd153 Sensitizes Cells to Endoplasmic Reticulum Stress by Down-Regulating Bcl2 and Perturbing the Cellular Redox State. *Mol. Cell. Biol.* **21**, 1249–1259.

McEwen, E., Kedersha, N., Song, B., Scheuner, D., Gilks, N., Han, A., Chen, J.-J., Anderson, P. and Kaufman, R. J. (2005). Heme-regulated inhibitor kinase-mediated phosphorylation of eukaryotic translation initiation factor 2 inhibits translation, induces stress granule formation, and mediates survival upon arsenite exposure. *J. Biol. Chem.* **280**, 16925–16933.

Mercado, G., Castillo, V., Soto, P., López, N., Axten, J. M., Sardi, S. P., Hoozemans, J. J. M. and Hetz, C. (2018). Targeting PERK signaling with the small molecule GSK2606414 prevents neurodegeneration in a model of Parkinson's disease. *Neurobiol. Dis.* **112**, 136–148.

Merrick, W. C. (2004). Cap-dependent and cap-independent translation in eukaryotic

systems. *Gene* **332**, 1–11.

Meurs, E., Chong, K., Galabru, J., Thomas, N. S., Kerr, I. M., Williams, B. R. and Hovanessian, A. G. (1990). Molecular cloning and characterization of the human double-stranded RNA-activated protein kinase induced by interferon. *Cell* **62**, 379–390.

Michel, Y. M., Poncet, D., Piron, M., Kean, K. M. and Borman, A. M. (2000). Cap-Poly(A) synergy in mammalian cell-free extracts. Investigation of the requirements for poly(A)-mediated stimulation of translation initiation. *J. Biol. Chem.* **275**, 32268–32276.

Mizushima, N. and Komatsu, M. (2011). Autophagy: Renovation of Cells and Tissues. *Cell* **147**, 728–741.

Moazed, D. and Noller, H. F. (1989). Intermediate states in the movement of transfer RNA in the ribosome. *Nature* **342**, 142–148.

Moon, S. L. and Parker, R. (2018). Analysis of eIF2B bodies and their relationships with stress granules and P-bodies. *Sci. Rep.* **8**, 12264.

Moreno, J. A., Halliday, M., Molloy, C., Radford, H., Verity, N., Axten, J. M., Ortori, C. A., Willis, A. E., Fischer, P. M., Barrett, D. A., *et al*. (2013). Oral Treatment Targeting the Unfolded Protein Response Prevents Neurodegeneration and Clinical Disease in Prion-Infected Mice. *Sci. Transl. Med.* **5**, 206ra138.

Mueller, P. P. and Hinnebusch, A. G. (1986). Multiple upstream AUG codons mediate translational control of GCN4. *Cell* **45**, 201–207.

Mulukutla, B. C., Khan, S., Lange, A. and Hu, W.-S. (2010). Glucose metabolism in mammalian cell culture: new insights for tweaking vintage pathways. *Trends Biotechnol.* **28**, 476–484.

Munro, J. B., Altman, R. B., O'Connor, N. and Blanchard, S. C. (2007). Identification of Two Distinct Hybrid State Intermediates on the Ribosome. *Mol. Cell* **25**, 505–517.

Nanda, J. S., Cheung, Y.-N., Takacs, J. E., Martin-Marcos, P., Saini, A. K., Hinnebusch, A. G. and Lorsch, J. R. (2009). eIF1 Controls Multiple Steps in Start Codon

Recognition during Eukaryotic Translation Initiation. *J. Mol. Biol.* **394**, 268–285.

Naveau, M., Lazennec-Schurdevin, C., Panvert, M., Mechulam, Y. and Schmitt, E. (2010). tRNA Binding Properties of Eukaryotic Translation Initiation Factor 2 from *Encephalitozoon cuniculi*. *Biochemistry* **49**, 8680–8688.

Nika, J., Rippel, S. and Hannig, E. M. (2001). Biochemical Analysis of the eIF2βγ Complex Reveals a Structural Function for eIF2α in Catalyzed Nucleotide Exchange. *J. Biol. Chem.* **276**, 1051–1056.

Noree, C., Sato, B. K., Broyer, R. M. and Wilhelm, J. E. (2010). Identification of novel filament-forming proteins in Saccharomyces cerevisiae and Drosophila melanogaster. *J. Cell Biol.* **190**, 541–551.

Noree, C., Monfort, E., Shiau, A. K. and Wilhelm, J. E. (2014). Common regulatory control of CTP synthase enzyme activity and filament formation. *Mol. Biol. Cell* **25**, 2282–2290.

Norris, K., Abell, B., Ashe, M. P. and Campbell, S. G. (2019). The alpha subunit of eIF2B; a key component in the integrity of eIF2B bodies. *Manuscript in preparation.*

Oberer, M., Marintchev, A. and Wagner, G. (2005). Structural basis for the enhancement of eIF4A helicase activity by eIF4G. *Genes Dev.* **19**, 2212–2223.

Oo Khor, T., Yu, S., Barve, A., Hao, X., Hong, J.-L., Lin, W., Foster, B., Huang, M.-T., Newmark, H. L. and Kong, A.-N. (2009). Dietary Feeding of Dibenzoylmethane Inhibits Prostate Cancer in Transgenic Adenocarcinoma of the Mouse Prostate Model. *Cancer Res.* **69**, 7096–7102.

Oslowski, C. M. and Urano, F. (2011). Measuring ER stress and the unfolded protein response using mammalian tissue culture system. *Methods Enzymol.* **490**, 71–92.

Özeş, A. R., Feoktistova, K., Avanzino, B. C. and Fraser, C. S. (2011). Duplex unwinding and ATPase activities of the DEAD-box helicase eIF4A are coupled by eIF4G and eIF4B. *J. Mol. Biol.* **412**, 674–687.

Paddon, C. J., Hannig, E. M. and Hinnebusch, A. G. (1989). Amino Acid Sequence

Similarity Between GCNS and GCD2, Positive and Negative Translational Regulators of GCN4: Evidence for Antagonism by Competition. *Geetics* **122**, 551-559.

Pakos-Zebrucka, K., Koryga, I., Mnich, K., Ljujic, M., Samali, A. and Gorman, A. M. (2016). The integrated stress response. *EMBO Rep.* **17**, 1374–1395.

Palam, L. R., Baird, T. D. and Wek, R. C. (2011). Phosphorylation of eIF2 Facilitates Ribosomal Bypass of an Inhibitory Upstream ORF to Enhance *CHOP* Translation. *J. Biol. Chem.* **286**, 10939–10949.

Panniers, R. and Henshaw, E. C. (1983). A GDP/GTP Exchange Factor Essential for Eukaryotic Initiation Factor 2 Cycling in Ehrlich Ascites Tumor Cells and Its Regulation by Eukaryotic Initiation Factor 2 Phosphorylation. *J. Biol. Chem.* **258**, 7928-7934.

Passmore, L. A., Schmeing, T. M., Maag, D., Applefield, D. J., Acker, M. G., Algire, M. A., Lorsch, J. R. and Ramakrishnan, V. (2007). The Eukaryotic Translation Initiation Factors eIF1 and eIF1A Induce an Open Conformation of the 40S Ribosome. *Mol. Cell* **26**, 41–50.

Patel, J., McLeod, L. E., Vries, R. G. J., Flynn, A., Wang, X. and Proud, C. G. (2002). Cellular stresses profoundly inhibit protein synthesis and modulate the states of phosphorylation of multiple translation factors. *Eur. J. Biochem.* **269**, 3076–3085.

Patil, C. and Walter, P. (2001). Intracellular signaling from the endoplasmic reticulum to the nucleus: the unfolded protein response in yeast and mammals. *Curr. Opin. Cell Biol.* **13**, 349–355.

Pavitt, G. D. and Proud, C. G. (2009). Protein synthesis and its control in neuronal cells with a focus on vanishing white matter disease. *Biochem. Soc. Trans.* **37**, 1298–1310.

Pavitt, G. D. and Ron, D. (2012). New insights into translational regulation in the endoplasmic reticulum unfolded protein response. *Cold Spring Harb. Perspect. Biol.* **4**, a012278.

Pavitt, G. D., Yang, W. and Hinnebusch, A. G. (1997). Homologous segments in three

subunits of the guanine nucleotide exchange factor eIF2B mediate translational regulation by phosphorylation of eIF2. *Mol. Cell. Biol.* **17**, 1298–1313.

Pavitt, G. D., Ramaiah, K. V, Kimball, S. R. and Hinnebusch, A. G. (1998). eIF2 independently binds two distinct eIF2B subcomplexes that catalyze and regulate guanine-nucleotide exchange. *Genes Dev.* **12**, 514–526.

Petrovska, I., Nüske, E., Munder, M. C., Kulasegaran, G., Malinovska, L., Kroschwald, S., Richter, D., Fahmy, K., Gibson, K., Verbavatz, J.-M., *et al*. (2014). Filament formation by metabolic enzymes is a specific adaptation to an advanced state of cellular starvation. *Elife* **3**, e02409.

Pisarev, A. V., Shirokikh, N. E. and Hellen, C. U. T. (2005). Translation initiation by factor-independent binding of eukaryotic ribosomes to internal ribosomal entry sites. *C. R. Biol.* **328**, 589–605.

Pisarev, A. V, Kolupaeva, V. G., Pisareva, V. P., Merrick, W. C., Hellen, C. U. T. and Pestova, T. V (2006). Specific functional interactions of nucleotides at key -3 and +4 positions flanking the initiation codon with components of the mammalian 48S translation initiation complex. *Genes Dev.* **20**, 624–636.

Pisarev, A. V, Hellen, C. U. T. and Pestova, T. V (2007). Recycling of eukaryotic posttermination ribosomal complexes. *Cell* **131**, 286–299.

Pisarev, A. V., Skabkin, M. A., Pisareva, V. P., Skabkina, O. V., Rakotondrafara, A. M., Hentze, M. W., Hellen, C. U. T. and Pestova, T. V. (2010). The Role of ABCE1 in Eukaryotic Posttermination Ribosomal Recycling. *Mol. Cell* **37**, 196–210.

Pisareva, V. P., Pisarev, A. V., Komar, A. A., Hellen, C. U. T. and Pestova, T. V. (2008). Translation initiation on mammalian mRNAs with structured 5′-UTRs requires DExH-box protein DHX29. *Cell* **135**, 1237.

Pivneva, T., Haas, B., Reyes-Haro, D., Laube, G., Veh, R. W., Nolte, C., Skibo, G. and Kettenmann, H. (2008). Store-operated Ca2+ entry in astrocytes: Different spatial arrangement of endoplasmic reticulum explains functional diversity in vitro and in situ. *Cell Calcium* **43**, 591–601.

Power, J. H. T., Barnes, O. L. and Chegini, F. (2017). Lewy Bodies and the Mechanisms

of Neuronal Cell Death in Parkinson's Disease and Dementia with Lewy Bodies. *Brain Pathol.* **27**, 3–12.

Prahlad, V. and Morimoto, R. I. (2009). Integrating the stress response: lessons for neurodegenerative diseases from C. elegans. *Trends Cell Biol.* **19**, 52–61.

Price, N. T., Mellor, H., Craddock, B. L., Flowers, K. M., Kimball, S. R., Wilmer, T., Jefferson, L. S. and Proud, C. G. (1996). eIF2B, the guanine nucleotide-exchange factor for eukaryotic initiation factor 2 Sequence conservation between the α, β and δ subunits of eIF2B from mammals and yeast. *Biochem. J.* **318**, 637–643.

Rabouw, H. H., Langereis, M. A., Anand, A. A., Visser, L. J., de Groot, R. J., Walter, P. and van Kuppeveld, F. J. M. (2019). Small molecule ISRIB suppresses the integrated stress response within a defined window of activation. *Proc. Natl. Acad. Sci.* **116**, 2097–2102.

Radford, H., Moreno, J. A., Verity, N., Halliday, M. and Mallucci, G. R. (2015). PERK inhibition prevents tau-mediated neurodegeneration in a mouse model of frontotemporal dementia. *Acta Neuropathol.* **130**, 633–642.

Ramaiah, K. V. A., Davies, M. V, Chen, J.-J., Kaufman2, R. J., Davies, V., Scherer, J. B., Choi, S. Y., Hershey, J. W. B. and Kaufman, R. J. (1994). Expression of Mutant Eukaryotic Initiation Factor 2 cx Subunit (eIF-2ox) Reduces Inhibition of Guanine Nucleotide Exchange Activity of eIF-2B Mediated by eIF-2o Phosphorylation. *Mol. Cell. Biol.* 4546–4553.

Ramakrishnan, V. (2011). The Eukaryotic Ribosome. *Science.* **331**, 681–682.

Richardson, J. P., Mohammad, S. S. and Pavitt, G. D. (2004). Mutations causing childhood ataxia with central nervous system hypomyelination reduce eukaryotic initiation factor 2B complex formation and activity. *Mol. Cell. Biol.* **24**, 2352–2363.

Rodnina, M. V and Wintermeyer, W. (2009). Recent mechanistic insights into eukaryotic ribosomes. *Curr. Opin. Cell Biol.* **21**, 435–443.

Rogers, G. W., Richter, N. J. and Merrick, W. C. (1999). Biochemical and kinetic characterization of the RNA helicase activity of eukaryotic initiation factor 4A. *J. Biol. Chem.* **274**, 12236–12244.

Rogers, G. W., Richter, N. J., Lima, W. F. and Merrick, W. C. (2001). Modulation of the Helicase Activity of eIF4A by eIF4B, eIF4H, and eIF4F. *J. Biol. Chem.* **276**, 30914–30922.

Rojas-Rivera, D., Delvaeye, T., Roelandt, R., Nerinckx, W., Augustyns, K., Vandenabeele, P. and Bertrand, M. J. M. (2017). When PERK inhibitors turn out to be new potent RIPK1 inhibitors: critical issues on the specificity and use of GSK2606414 and GSK2656157. *Cell Death Differ.* **24**, 1100–1110.

Ron, D. and Walter, P. (2011). The Unfolded Protein Response: From Stress Pathway to Homeostatic Regulation. *Science* **334**, 1081-1086.

Rowlands, A. G., Panniers, R. and Henshaw, E. C. (1988). The Catalytic Mechanism of Guanine Nucleotide Exchange Factor Action and Competitive Inhibition by Phosphorylated Eukaryotic Initiation Factor 2. *J. Biol. Chem.* **263**, 5526–5533.

Rozovsky, N., Butterworth, A. C. and Moore, M. J. (2008). Interactions between eIF4AI and its accessory factors eIF4B and eIF4H. *RNA* **14**, 2136–2148.

Rutkowski, D. T., Arnold, S. M., Miller, C. N., Wu, J., Li, J., Gunnison, K. M., Mori, K., Sadighi Akha, A. A., Raden, D. and Kaufman, R. J. (2006). Adaptation to ER stress is mediated by differential stabilities of pro-survival and pro-apoptotic mRNAs and proteins. *PLoS Biol.* **4**, e374.

Hsu, P. and Sabatini, D. (2008). Cancer Cell Metabolism: Warburg and Beyond. *Cell* **134**, 703-707.

Safer, B., Adams, S. L., Anderson, W. F. and Merrick, W. C. (1975). Binding of MET-TRNAf and GTP to homogeneous initiation factor MP. *J. Biol. Chem.* **250**, 9076–9082.

Santos-Ribeiro, D., Godinas, L., Pilette, C. and Perros, F. (2018). The integrated stress response system in cardiovascular disease. *Drug Discov. Today* **23**, 920–929.

Scheper, W. and Hoozemans, J. J. M. (2015). The unfolded protein response in neurodegenerative diseases: a neuropathological perspective. *Acta Neuropathol.* **130**, 315–331.

Scheper, G. C., Proud, C. G. and van der Knaap, M. S. (2006). Defective translation initiation causes vanishing of cerebral white matter. *Trends Mol. Med.* **12**, 159–166.

Schiffmann, R., Moller, J. R., Trapp, B. D., Shih, H. H.-L., Farrer, R. G., Katz, D. A., Alger, J. R., Parker, C. C., Hauer, P. E., Kaneski, C. R., *et al*. (1994). Childhood ataxia with diffuse central nervous system hypomyelination. *Ann. Neurol.* **35**, 331–340.

Schutz, P., Bumann, M., Oberholzer, A. E., Bieniossek, C., Trachsel, H., Altmann, M. and Baumann, U. (2008). Crystal structure of the yeast eIF4A-eIF4G complex: An RNA-helicase controlled by protein-protein interactions. *Proc. Natl. Acad. Sci.* **105**, 9564–9569.

Sekar, R. B. and Periasamy, A. (2003). Fluorescence resonance energy transfer (FRET) microscopy imaging of live cell protein localizations. *J. Cell Biol.* **160**, 629–633.

Sekine, Y., Zyryanova, A., Crespillo-Casado, A., Fischer, P. M., Harding, H. P. and Ron, D. (2015). Mutations in a translation initiation factor identify the target of a memory-enhancing compound. *Science* **348**, 1027–1030.

Shatkin, A. J. (1976). Capping of Eucaryotic mRNAs Review. *Cell.* **9**, 645-653.

Sheth, U. and Parker, R. (2003). Decapping and decay of messenger RNA occur in cytoplasmic processing bodies. *Science* **300**, 805–808.

Shi, Y., Vattem, K. M., Sood, R., An, J., Liang, J., Stramm, L. and Wek, R. C. (1998). Identification and characterization of pancreatic eukaryotic initiation factor 2 alpha-subunit kinase, PEK, involved in translational control. *Mol. Cell. Biol.* **18**, 7499–7509.

Shimada, S., Shimojima, K., Sangu, N., Hoshino, A., Hachiya, Y., Ohto, T., Hashi, Y., Nishida, K., Mitani, M., Kinjo, S., *et al*. (2015). Mutations in the genes encoding eukaryotic translation initiation factor 2B in Japanese patients with vanishing white matter disease. *Brain and Development* **37**, 960-966.

Shoemaker, C. J., Eyler, D. E. and Green, R. (2010). Dom34:Hbs1 promotes subunit

dissociation and peptidyl-tRNA drop-off to initiate no-go decay. *Science* **330**, 369–372.

Sidrauski, C., Acosta-Alvear, D., Khoutorsky, A., Vedantham, P., Hearn, B. R., Li, H., Gamache, K., Gallagher, C. M., Ang, K. K.-H., Wilson, C., *et al*. (2013). Pharmacological brake-release of mRNA translation enhances cognitive memory. *Elife* **2**, e00498.

Sidrauski, C., McGeachy, A. M., Ingolia, N. T., Walter, P., Placzek, A., Stoica, L., Zhou, H., Bell, J., Friedlander, M., Krnjević, K., *et al*. (2015a). The small molecule ISRIB reverses the effects of eIF2α phosphorylation on translation and stress granule assembly. *Elife* **4**, 1384–1396.

Sidrauski, C., Tsai, J. C., Kampmann, M., Hearn, B. R., Vedantham, P., Jaishankar, P., Sokabe, M., Mendez, A. S., Newton, B. W., Tang, E. L., *et al*. (2015b). Pharmacological dimerization and activation of the exchange factor eIF2B antagonizes the integrated stress response. *Elife* **4**, e07314.

Siekierka, J., Mauser, L. and Ochoa, S. (1982). Mechanism of polypeptide chain initiation in eukaryotes and its control by phosphorylation of the alpha subunit of initiation factor 2. *Proc. Natl. Acad. Sci. U. S. A.* **79**, 2537–2540.

Singh, C. R., Lee, B., Udagawa, T., Mohammad-Qureshi, S. S., Yamamoto, Y., Pavitt, G. D. and Asano, K. (2006). An eIF5/eIF2 complex antagonizes guanine nucleotide exchange by eIF2B during translation initiation. *EMBO J.* **25**, 4537–4546.

Singh, C. R., Watanabe, R., Zhou, D., Jennings, M. D., Fukao, A., Lee, B., Ikeda, Y., Chiorini, J. A., Campbell, S. G., Ashe, M. P., *et al*. (2011). Mechanisms of translational regulation by a human eIF5-mimic protein. *Nucleic Acids Res.* **39**, 8314–8328.

Siridechadilok, B., Fraser, C. S., Hall, R. J., Doudna, J. A. and Nogales, E. (2005). Structural Roles for Human Translation Factor eIF3 in Initiation of Protein Synthesis. *Science* **310**, 1513–1515.

Smith, H. L. and Mallucci, G. R. (2016). The unfolded protein response: mechanisms and therapy of neurodegeneration. *Brain* **139**, 2113–2121.

Sokabe, M., Fraser, C. S. and Hershey, J. W. B. (2012). The human translation initiation multi-factor complex promotes methionyl-tRNAi binding to the 40S ribosomal subunit. *Nucleic Acids Res.* **40**, 905–913.

Svitkin, Y. V, Gradi, A., Imataka, H., Morino, S. and Sonenberg, N. (1999). Eukaryotic initiation factor 4GII (eIF4GII), but not eIF4GI, cleavage correlates with inhibition of host cell protein synthesis after human rhinovirus infection. *J. Virol.* **73**, 3467–3472.

Svitkin, Y. V, Pause, A., Haghighat, A., Pyronnet, S., Witherell, G., Belsham, G. J. and Sonenberg, N. (2001). The requirement for eukaryotic initiation factor 4A (eIF4A) in translation is in direct proportion to the degree of mRNA 5' secondary structure. *RNA* **7**, 382–394.

Tarun, S. Z. and Sachs, A. B. (1996). Association of the yeast poly(A) tail binding protein with translation initiation factor eIF-4G. *EMBO J.* **15**, 7168–7177.

Taylor, E. J., Campbell, S. G., Griffiths, C. D., Reid, P. J., Slaven, J. W., Harrison, R. J., Sims, P. F. G., Pavitt, G. D., Delneri, D. and Ashe, M. P. (2010). Fusel alcohols regulate translation initiation by inhibiting eIF2B to reduce ternary complex in a mechanism that may involve altering the integrity and dynamics of the eIF2B body. *Mol. Biol. Cell* **21**, 2202–2216.

Tourrière, H., Chebli, K., Zekri, L., Courselaud, B., Blanchard, J. M., Bertrand, E. and Tazi, J. (2003). The RasGAP-associated endoribonuclease G3BP assembles stress granules. *J. Cell Biol.* **160**, 823–831.

Treeck, B. Van, Protter, D. S. W., Matheny, T., Khong, A., Link, C. D. and Parker, R. (2018). RNA self-assembly contributes to stress granule formation and defining the stress granule transcriptome. *Proc. Natl. Acad. Sci. U. S. A.* **115**, 2734-2739.

Trinh, M. A., Kaphzan, H., Wek, R. C., Pierre, P., Cavener, D. R. and Klann, E. (2012). Brain-Specific Disruption of the eIF2α Kinase PERK Decreases ATF4 Expression and Impairs Behavioral Flexibility. *Cell Rep.* **1**, 676–688.

Tsai, J. C., Miller-Vedam, L. E., Anand, A. A., Jaishankar, P., Nguyen, H. C., Renslo, A. R., Frost, A. and Walter, P. (2018). Structure of the nucleotide exchange factor

eIF2B reveals mechanism of memory-enhancing molecule HHS Public Access. *Science* **359**, eaaq0939.

Unbehaun, A., Borukhov, S. I., Hellen, C. U. T. and Pestova, T. V (2004). Release of initiation factors from 48S complexes during ribosomal subunit joining and the link between establishment of codon-anticodon base-pairing and hydrolysis of eIF2-bound GTP. *Genes Dev.* **18**, 3078–3093.

Vallejo, M., Ron, D., Miller, C. P. and Habener, J. F. (1993). C/ATF, a member of the activating transcription factor family of DNA-binding proteins, dimerizes with CAAT/enhancer-binding proteins and directs their binding to cAMP response elements. *Proc. Natl. Acad. Sci. U. S. A.* **90**, 4679–4683.

van der Knaap, M. S., Barth, P. G., Gabreëls, F. J., Franzoni, E., Begeer, J. H., Stroink, H., Rotteveel, J. J. and Valk, J. (1997). A new leukoencephalopathy with vanishing white matter. *Neurology* **48**, 845–855.

van der Knaap, M. S., Kamphorst, W., Barth, P. G., Kraaijeveld, C. L., Gut, E. and Valk, J. (1998). Phenotypic variation in leukoencephalopathy with vanishing white matter. *Neurology* **51**, 540–547.

van der Knaap, M. S., Leegwater, P. A. J., Könst, A. A. M., Visser, A., Naidu, S., Oudejans, C. B. M., Schutgens, R. B. H. and Pronk, J. C. (2002). Mutations in each of the five subunits of translation initiation factor eIF2B can cause leukoencephalopathy with vanishing white matter. *Ann. Neurol.* **51**, 264–270.

van der Knaap, M. S., van Berkel, C. G. M., Herms, J., van Coster, R., Baethmann, M., Naidu, S., Boltshauser, E., Willemsen, M. A. A. P., Plecko, B., Hoffmann, G. F., *et al*. (2003). eIF2B-related disorders: antenatal onset and involvement of multiple organs. *Am. J. Hum. Genet.* **73**, 1199–1207.

van der Knaap, M. S., Pronk, J. C. and Scheper, G. C. (2006). Vanishing white matter disease. *Lancet Neurol.* **5**, 413–423.

van der Knaap, M. S., Leegwater, P. A. J., Van Berkel, C. G. M., Brenner, C., Storey, E., Di Rocco, M., Salvi, F. and Pronk, J. C. (2004). Arg113His mutation in eIF2Bε as cause of leukoencephalopathy in adults. *Neurology* **62**, 1598–1600.

van der Voorn, J. P., van Kollenburg, B., Bertrand, G., Van Haren, K., Scheper, G. C., Powers, J. M. and van der Knaap, M. S. (2005). The unfolded protein response in vanishing white matter disease. *J. Neuropathol. Exp. Neurol.* **64**, 770–775.

Van Eden, M. E., Byrd, M. P., Sherrill, K. W. and Lloyd, R. E. (2004). Demonstrating internal ribosome entry sites in eukaryotic mRNAs using stringent RNA test procedures. *RNA* **10**, 720–730.

van Kollenburg, B., van Dijk, J., Garbern, J., Thomas, A. A. M., Scheper, G. C., Powers, J. M. and van der Knaap, M. S. (2006). Glia-Specific Activation of All Pathways of the Unfolded Protein Response in Vanishing White Matter Disease. *J. Neuropathol. Exp. Neurol.* **65**, 707–715.

Vattem, K. M. and Wek, R. C. (2004). Reinitiation involving upstream ORFs regulates ATF4 mRNA translation in mammalian cells. *Proc. Natl. Acad. Sci.* **101**, 11269–11274.

Vazquez de Aldana, C. R., Wek, R. C., Segundo, P. S., Truesdell, A. G. and Hinnebusch, A. G. (1994). Multicopy tRNA genes functionally suppress mutations in yeast eIF-2 alpha kinase GCN2: evidence for separate pathways coupling GCN4 expression to unchanged tRNA. *Mol. Cell. Biol.* **14**, 7920–7932.

Villa, N., Do, A., Hershey, J. W. B. and Fraser, C. S. (2013). Human eukaryotic initiation factor 4G (eIF4G) protein binds to eIF3c, -d, and -e to promote mRNA recruitment to the ribosome. *J. Biol. Chem.* **288**, 32932–32940.

Wang, X., Wortham, N. C., Liu, R. and Proud, C. G. (2012). Identification of Residues That Underpin Interactions within the Eukaryotic Initiation Factor (eIF2) 2B Complex. *J. Biol. Chem.* **287**, 8263–8274.

Wek, R. C., Jiang, H.-Y. and Anthony, T. G. (2006). Coping with stress: eIF2 kinases and translational control. *Biochem. Soc. Trans.* **34**, 7-11.

Wells, S. E., Hillner, P. E., Vale, R. D. and Sachs, A. B. (1998). Circularization of mRNA by eukaryotic translation initiation factors. *Mol. Cell* **2**, 135–140.

Welsh, G. I. and Proud, C. G. (1993). Glycogen synthase kinase-3 is rapidly inactivated in response to insulin and phosphorylates eukaryotic initiation factor eIF-2B.

Biochem. J. **294**, 625–629.

Welsh, G. I., Miller, C. M., Loughlin, A. J., Price, N. T. and Proud, C. G. (1998). Regulation of eukaryotic initiation factor eIF2B: glycogen synthase kinase-3 phosphorylates a conserved serine which undergoes dephosphorylation in response to insulin. *FEBS Lett.* **421**, 125–130.

Williams, D. D., Price, N. T., Loughlin, A. J. and Proud, C. G. (2001). Characterization of the mammalian initiation factor eIF2B complex as a GDP dissociation stimulator protein. *J. Biol. Chem.* **276**, 24697–24703.

Wong, Y. L., LeBon, L., Basso, A. M., Kohlhaas, K. L., Nikkel, A. L., Robb, H. M., Donnelly-Roberts, D. L., Prakash, J., Swensen, A. M., Rubinstein, N. D., *et al*. (2019). eIF2B activator prevents neurological defects caused by a chronic integrated stress response. *Elife* **8**, e42940.

Wortham, N. C. and Proud, C. G. (2015). Biochemical effects of mutations in the gene encoding the alpha subunit of eukaryotic initiation factor (eIF) 2B associated with Vanishing White Matter disease. *BMC Med. Genet.* **16**, 64.

Wortham, N. C., Martinez, M., Gordiyenko, Y., Robinson, C. V and Proud, C. G. (2014). Analysis of the subunit organization of the eIF2B complex reveals new insights into its structure and regulation. *FASEB J.* **28**, 2225–2237.

Wortham, N. C., Stewart, J. D., Harris, S., Coldwell, M. J. and Proud, C. G. (2016). Stoichiometry of the eIF2B complex is maintained by mutual stabilization of subunits. *Biochem. J.* **473**, 571-580.

Yamaguchi, H. and Wang, H.-G. (2004). CHOP Is Involved in Endoplasmic Reticulum Stress-induced Apoptosis by Enhancing DR5 Expression in Human Carcinoma Cells. *J. Biol. Chem.* **279**, 45495–45502.

Yatime, L., Schmitt, E., Blanquet, S. and Mechulam, Y. (2004). Functional Molecular Mapping of Archaeal Translation Initiation Factor 2. *J. Biol. Chem.* **279**, 15984–15993.

Young, S. K. and Wek, R. C. (2016). Upstream Open Reading Frames Differentially Regulate Gene- specific Translation in the Integrated Stress Response. *J. Biol.*

Chem. **291**, 16927-16935.

Zhang, W., Dunkle, J. A. and Cate, J. H. D. (2009). Structures of the Ribosome in Intermediate States of Ratcheting. *Science* **325**, 1014–1017.

Zhouravleva, G., Frolova, L., Le Goff, X., Le Guellec, R., Inge-Vechtomov, S., Kisselev, L. and Philippe, M. (1995). Termination of translation in eukaryotes is governed by two interacting polypeptide chain release factors, eRF1 and eRF3. *EMBO J.* **14**, 4065–4072.

Zyryanova, A. F., Weis, F., Faille, A., Alard, A. A., Crespillo-Casado, A., Sekine, Y., Harding, H. P., Allen, F., Parts, L., Fromont, C., *et al*. (2018). Binding of ISRIB reveals a regulatory site in the nucleotide exchange factor eIF2B. *Science* **359**, 1533–1536.

9. Communications

9.1 Oral Communications

Hodgson R.E., Allen K.E. and Campbell S.G. eIF2B subunits localise to distinct populations of eIF2B bodies that allow for differential regulation by the ISR. **July 2018**. Translation UK; Manchester, UK.

Hodgson R.E., Allen K.E. and Campbell S.G. eIF2B subcomplexes in cells linked to Vanishing White Matter Disease pathology. **November 2016.** Sheffield Glial Symposium, Sheffield UK.

9.2 Poster Presentations

Hodgson, R.E., Varanda B.A., Ashe M.P., Allen K.E. and Campbell S.G. eIF2B subunits localise to distinct populations of eIF2B bodies that allow for differential regulation by the ISR in cells linked to VWM. September 2018. Translational Control; Cold Spring Harbor Laboratory, New York, USA

Hodgson R.E., Allen K.E. and Campbell S.G. Characterisation of eIF2B bodies in Vanishing White Matter Disease. August 2017. The International Society for Neurochemistry (ISN) and the American Society for Neurochemistry (ASN) Meeting; Paris, France.

Hodgson R.E., Allen K.E. and Campbell S.G. eIF2B subcomplexes display differential control of translation initiation in cells directly affected by VWM. July 2017. Translation UK; Nottingham, UK.

Hodgson R.E., Varanda B.A., Allen K.E. and Campbell S.G. Characterisation of the functional significance of eIF2B bodies in Leukoencephalopathy with Vanishing white matter. July 2016. Translation UK; Surrey, UK.

10. Publications

Hodgson, R.E., Varanda B.A., Ashe M.P., Allen K.E. and Campbell S.G. (2019). Cellular eIF2B subunit localization: implications for the integrated stress response and its control by small molecule drugs. *Mol. Biol Cell* **30**, 942-958.